2007

DETRITAL-ZIRCON GEOCHRONOLOGIC PROVENANCE ANALYSES THAT TEST AND EXPAND THE EAST SIBERIA - WEST LAURENTIA RODINIA RECONSTRUCTION

John Stuart MacLean
The University of Montana

DETRITAL-ZIRCON GEOCHRONOLOGIC PROVENANCE ANALYSES THAT TEST AND EXPAND THE EAST SIBERIA – WEST LAURENTIA RODINIA RECONSTRUCTION

By

John Stuart MacLean

Bachelor of Science in Geology, Furman University, Greenville, SC, 2001
Master of Science in Geology, Syracuse University, Syracuse, NY, 2004

Dissertation

presented in partial fulfillment of the requirements
for the degree of

Doctor of Philosophy
in Geosciences

The University of Montana
Missoula, MT

Spring, 2007

Approved by:

Dr. David A. Strobel, Dean
Graduate School

Dr. James W. Sears, Chair
Department of Geosciences

Dr. Julie A. Baldwin
Department of Geosciences

Dr. Kevin R. Chamberlain
Department of Geology and Geophysics, University of Wyoming

Dr. David B. Friend
Department of Physics and Astronomy

Dr. Marc S. Hendrix
Department of Geosciences

MacLean, John, Ph.D., Spring 2007 Geosciences

Detrital-zircon geochronologic provenance analyses that test and expand the East Siberia – West Laurentia Rodinia reconstruction

Chairperson: Dr. James W. Sears

Laurentia's position in the Neoproterozoic supercontinent Rodinia is a topic of continuing debate. Several reconstructions involving Laurentia and Siberia have been proposed, including the east Siberia-west Laurentia connection. The east Siberia-west Laurentia Rodinia reconstruction includes lithostratigraphic correlations of conjugate rift miogeocline sediments located in SE Siberia and SW Laurentia. To constrain provenance relationships and to quantitatively test correlations, we determined detrital-zircon age spectra from samples from the Sette Daban Range of SE Siberia and the Death Valley and White-Inyo regions of SW Laurentia using SHRIMP and LAICPMS. Data indicate that several Siberian samples contain zircons correlative with Laurentian sources, and several Laurentian samples contain zircons correlative with Siberian sources. The results not only strengthen correlations between the two successions, they also lead to a new tectono-sedimentary evolution model of the restored region. The new model involves thickening of the crust during the southern Laurentian Grenville orogeny, crustal flexure resulting in a foreland basin, and extension sub-perpendicular to the Grenville front resulting in extensional basins within the foreland basin on both cratons. Sediments were transported from the Grenville Orogen across the margin between the two cratons and were preserved in the extensional basins. The Grenville source for SE Siberian sediments was cut off in the latest Proterozoic due to successful continental rifting. Grenville sediments were cut off from SW Laurentia in the latest Proterozoic-Middle Cambrian either due to the development of an impediment between the orogen and the basin, or due to the transgression of the Cambrian Sea from the east. Petrographic analyses corroborate the new tectono-sedimentary model.

My research resulted in other avenues of thought that were not anticipated from the outset. For example, I present a comparison of the age-equivalency of SHRIMP and LAICPMS detrital-zircon analyses obtained by analyzing the same zircon grains with both instruments. Also, I show that a possible extension of the East Siberia – West Laurentia connection could be the Anti-Atlas region of Morocco, based on trilobite evidence and detrital-zircon provenance information. Finally, I demonstrate two ways to involve K-12 students in geoscience research.

ACKNOWLEDGMENTS

Foremost, I thank my wife, Michelle Kotler, for encouraging and supporting me through this process. She inspired me to pursue science with excitement, not just awareness, and she continues to make my life more interesting than I could have ever hoped for. I also thank my entire family for instilling in me a work capacity necessary for such an endeavor as pursuing this degree, and for supporting and loving me constantly. I shouldn't leave out the dogs in my life, The Great Jane, Merlin "Bubba" Kotler, the late Richard Parker (RP) and the late Mr. Wayne. And Macky, I'll never forget that you were perfect. It is a lonelier world without you.

I thank the Missoula ultimate community for providing a much-needed escape from reality. I will always cherish memories of the Mental Toss Flycoons realizing our goals in the Fall of 2006.

I thank my graduate committee and those who influenced my academic experience. Julie Baldwin, Marc Hendrix, and Don Hyndman were available and willing to help whenever needed. Kevin Chamberlain was especially generous with his time, effort, and funding regarding the geochronology aspects of this research. David Friend also generously gave his time to serve on a project somewhat out of his expertise. Carol Brewer, Paul Alaback, and the rest of the ECOS community were instrumental in my development as a science educator.

Finally, I thank Jim Sears. Besides my father, no man has ever positively influenced my life more than Jim. Least importantly, he has shown me new ways to think about how the world works. Most importantly, he has been an example of a husband, father, colleague, and friend that I will always strive to emulate.

PREFACE

The SE Siberian taiga and the SW North American desert represent vastly different environments on opposite sides of the world, yet they may have been joined during Precambrian time. Researchers agree that the Proterozoic supercontinent Rodinia broke up during latest Proterozoic to Cambrian time. However, the positions of the continents within Rodinia are debated. In particular, much disagreement has focused on which continent was opposite the western margin of proto-North America (Laurentia). Likewise, researchers have proposed several models of Siberia's position relative to Laurentia. Sears and Price (1978, 2003) have been the strongest proponents of juxtaposing E Siberia and W Laurentia in the Rodinia reconstruction. Their model is based on several lines of evidence, including the fit of the continents when structurally restored to their Proterozoic nature, numerous magmatic and orogenic belts that seamlessly cross the proposed margin between the two continents, supportive paleomagnetic data, and correlative conjugate rift miogeocline sediments. The details of the reconstruction are described in Chapters 1 and 2 in greater detail.

The focus of my research has concerned the Proterozoic-Cambrian miogeoclinal sedimentary correlations between the Sette Daban region, SE Siberia, and the Great Basin region, SW North America. In a field excursion to SE Siberia during the summer before my program began, Sears and his colleagues identified numerous lithostratigraphic similarities between Siberian sedimentary rocks and their correlatives observed in the White-Inyo, Death Valley, and Grand Canyon regions. My research involved quantitatively testing these comparisons with detrital-zircon geochronology analyses using Sensitive High Resolution Ion Microprobe (SHRIMP) and Laser Ablation Inductively Coupled Plasma (LAICPMS) techniques. In Chapter 1, I report the results of these tests, finding that Siberian samples contain zircons from Laurentian sources, and that Laurentian samples contain zircons from Siberian sources.

By accepting that East Siberia and West Laurentia were likely connected during Proterozoic time, further interpretations involving regional tectonic and sedimentation histories can be made by incorporating both continents' geologic evidence. In Chapter 2, I consider samples collected from Siberia and Laurentia, analyzed by several independent detrital-zircon geochronology laboratories, and reported in the literature over the past ten years. The result is a new tectono-sedimentary model that proposes that the Grenville orogen supplied sediment to the SE Siberia – SW Laurentia region during the Proterozoic, and that subsequently both SE Siberia and SW Laurentia were cut off from the Grenville sediment supply during latest Proterozoic – Middle Cambrian time. In Chapter 3, I add petrographic support to this model and provide an example of how to involve K-12 students in authentic scientific research.

Chapter 4 summarizes the detrital-zircon data supporting the E Siberia – W Laurentia connection and introduces compelling paleontology evidence for Cambrian proximity of the two continents. An unanticipated result of the research postulates a possible addition of the Anti-Atlas region of Morocco to the East Siberia – West Laurentia reconstruction, discussed in Chapter 5. Placing the Anti-Atlas region close to the E Siberia – W Laurentia region in Late Proterozoic – Early Cambrian time clarifies trilobite evolutionary problems and provides a source for an unidentified provenance terrane that supplied zircons to Siberia. Finally, the research produced two additional outcomes. First, in the process of testing the same sample zircon grains with both SHRIMP and LAICPMS detrital-zircon techniques, we developed a comparison of the efficacy of the instruments in determining age-equivalency (Chapter 6). And, second, through the Ecologists, Educators, and Schools Program (National Science Foundation: Graduate Teaching Fellows in K-12 Education – GK-12), we demonstrated two ways to involve K-12 students in geoscience research (Chapters 3 and 7).

I have included three appendices. Appendix A is a short summary of an attempt to perform geochronology analyses on carbonate rocks of the poorly constrained Death Valley sedimentary succession. The analyses did not yield interpretable results, but the methods are recorded for future reference. Appendix B is a data table of the new SHRIMP and LAICPMS results from detrital-zircon analyses. Appendix C includes concordia plots of the new SHRIMP and LAICPMS results.

Most of the chapters were prepared for submission to various peer-reviewed scientific journals and special volumes. They were slightly modified for presentation as one complete and coherent document, but some overlap exists so that each chapter could stand alone. This dissertation is a compilation of my work that was accomplished with the help of several collaborators.

TABLE OF CONTENTS

CHAPTER 1

CHAPTER 2

LIST OF TABLES

LIST OF FIGURES

CHAPTER 1

DETRITAL-ZIRCON GEOCHRONOLOGIC TESTS OF THE SE SIBERIA – SW LAURENTIA PALEOCONTINENTAL CONNECTION

1.1 Introduction

The connections of Laurentia to other cratons within the Neoproterozoic supercontinent Rodinia and its predecessors are a topic of continuing debate (see Meert, 2002). This study tests the Sears and Price (1978) Rodinia reconstruction that proposed a connection between E Siberia and W Laurentia. Partially based on a recently compiled Siberian basement tectonic map (Smelov and Timopheev, 2003), the Sears and Price (1978, 2003) reconstruction predicts piercing points of several orogenic and magmatic belts across the restored boundary (Figure 1.1). Correlative Mesoproterozoic intracratonic basin sequences and Neoproterozoic to Early Cambrian sedimentary sequences deposited along the margins of SE Siberia and SW Laurentia during the break-up of Rodinia now are exposed in the Sette Daban Range of SE Siberia and in the Death Valley and White-Inyo areas of SW United States (Stewart, 1970; Khudoley et al., 2001). Sears et al. (2005) suggested a set of possible stratigraphic correlations based on lithologic similarities between these successions. They suggested that the successions could have been deposited in a single basin that collected sediment from both cratons during Meso-Neoproterozoic and Early Cambrian time.

The stratigraphic correlations proposed by Sears et al. (2005) support the E Siberia – W Laurentia Rodinia reconstruction of Sears and Price (1978, 2003). To further compare the proposed stratigraphic linkages, one field excursion was conducted along the Belaya River in Siberia (JWS, AKK, AVP, AK, GS, and others) and several excursions to the Death Valley and White-Inyo regions of the U.S. to observe

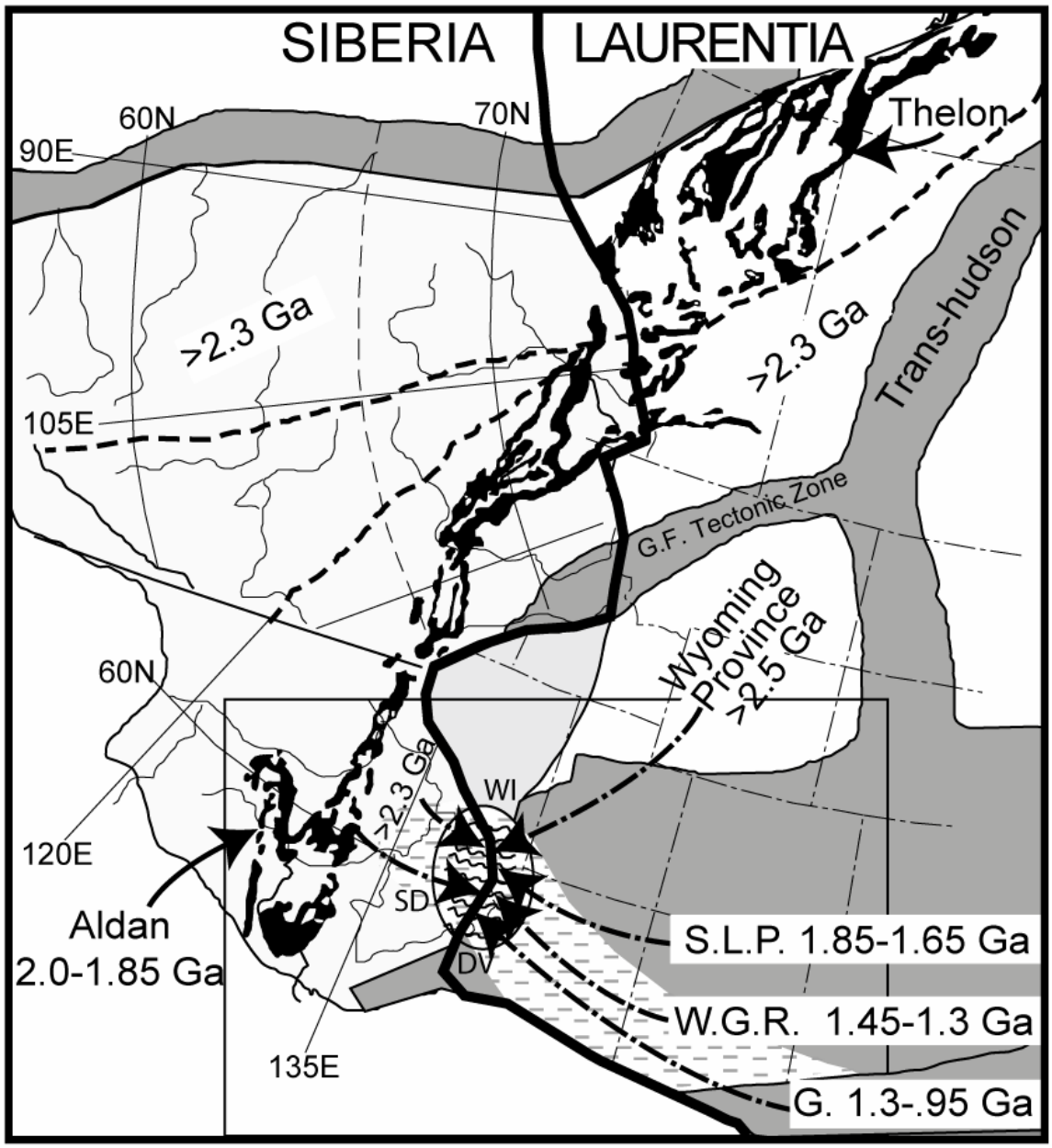

Figure 1.1. Correlations across proposed E Siberia – W Laurentia connection (Meso-Neoproterozoic). Dark solid line = boundary between Siberia and Laurentia. Dashed lines = major faults providing piercing points for connection. Dark shade = magmatic terranes providing piercing points for connection. Light shade = zone of crust that formed Siberian hanging wall and Laurentian footwall wall during low-angle extensional faulting. Black stipple = positive magnetic anomalies marking ~1.9-2.0 Ga Taltson-Thelon magmatic zone (NW Laurentia, labeled as Thelon) and Billyakh, Olenek, Tyrkandin, and Ulkan mélange zones (central and E Siberia, labeled as Aldan Province).

Dashed region = impactogen-related rifts providing avenue for sediment transport, discussed in Chapter 2. Oval = area of samples compared in dissertation. Some samples contain detrital-zircon ages not known on samples' present continent, but found on conjugate continent. SD = Sette Daban Range, Siberia; WI = White-Inyo Range, US; DV = Death Valley, US.: G.F. = Great Falls; S.L.P. = South Laurentian Paleoproterozoic terranes; W.G.R. = West Granite-Rhyolite province; G. = Grenville orogen. Dash/Dot arrows = possible flow paths from source to basin. Box = area for Figure 1.5. Modified from Sears and Price (2003).

stratigraphic relationships and to collect samples for detrital-zircon analyses. We collected samples from sedimentary units that appear to lithologically and stratigraphically match from craton to craton (Sears et al., 2005). We analyzed detrital zircons from stratigraphic units on both margins using SHRIMP and LAICPMS. We report 714 new dates, along with 93 previously reported dates, of detrital zircons from eighteen samples (15 new, three previously reported) from SE Siberia locations and seven samples from SW United States locations (Figures 1.2, 1.3). The sample sites plot within 200 km of one another on the proposed reconstruction (Figure 1.1). We correlate these new geochronologic data, along with existing information, to possible provenance terranes. The data reported here may be useful in testing other proposed connections (e.g. Rainbird et al., 1998) once detrital-zircon spectra are acquired from other Laurentian basins, but other reconstructions are not evaluated here.

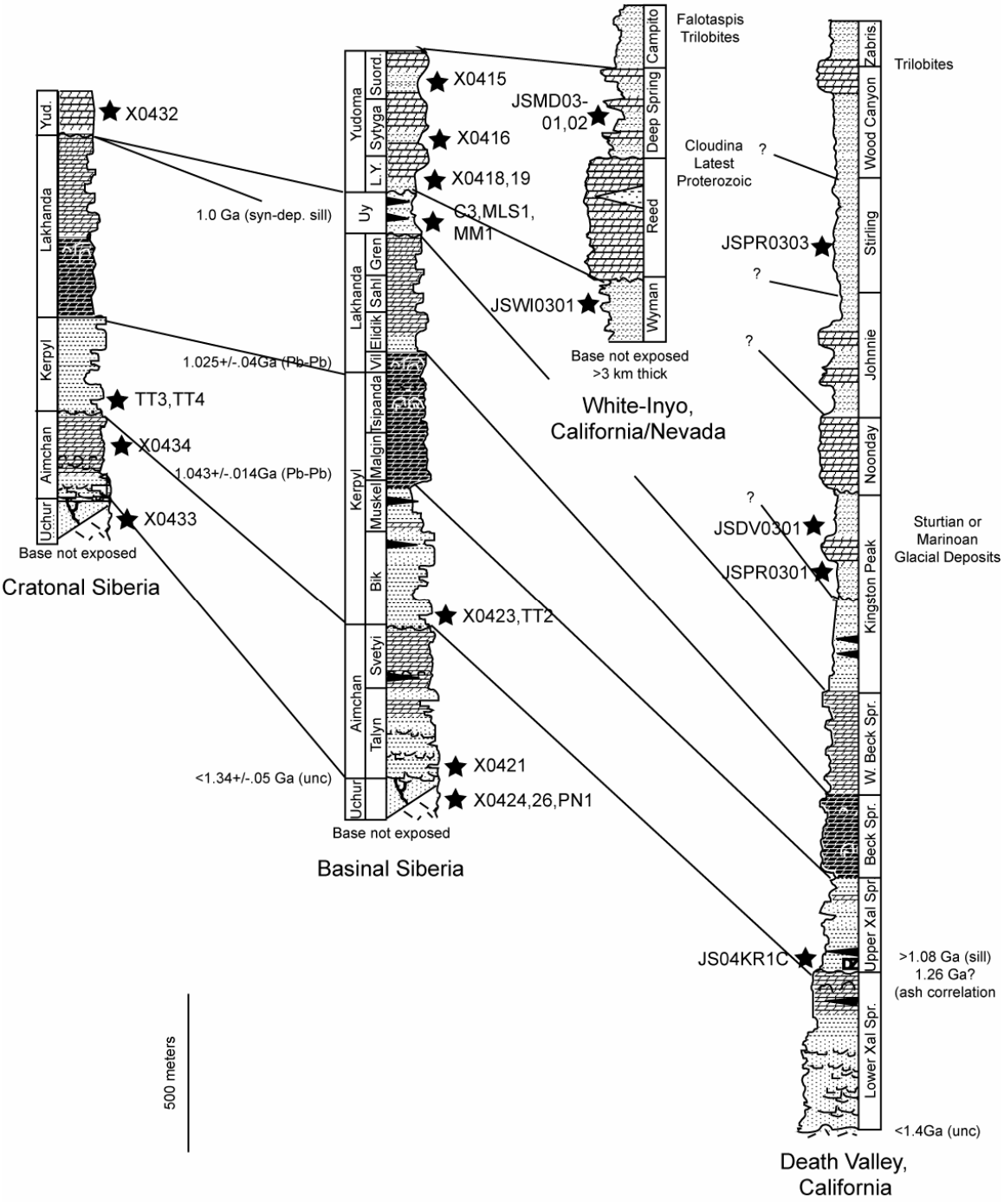

Figure 1.2. Stratigraphic sections across proposed SE Siberia – SW Laurentia connection. Stars show sample locations and numbers. Regions labeled at bottom of each column. Known geochronologic constraints are indicated.

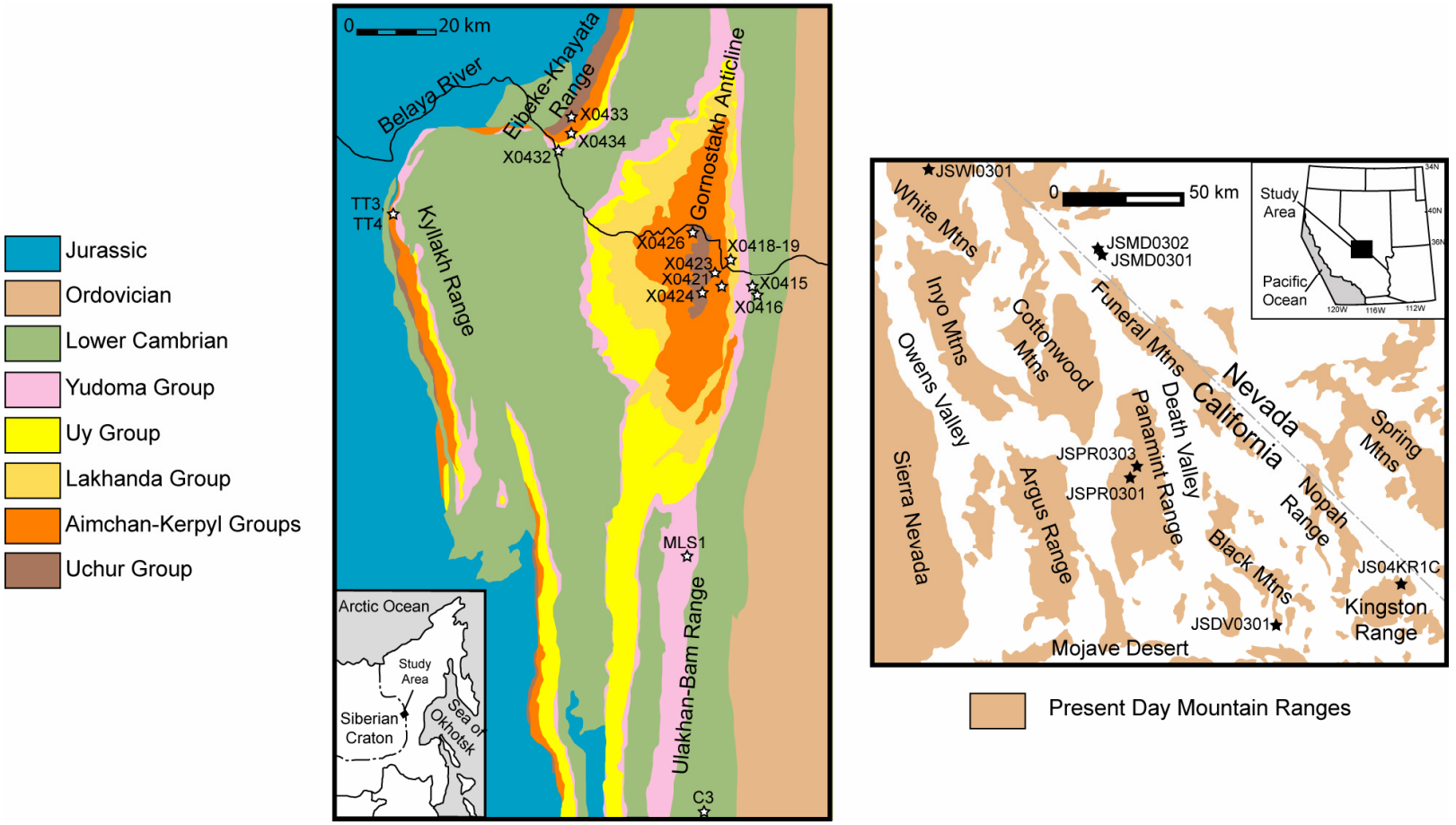

Figure 1.3. Present-day maps of study areas in SE Siberia (left) and SW United States (right). Stars symbolize sample locations. Geology of SE Siberia is provided in legend at left for reference. Valleys and ranges of SW U.S. are provided.

1.2 Stratigraphic overview

Mesoproterozoic intracratonic basin sequences and Neoproterozoic to Early Cambrian sedimentary sequences are exposed on the margins of the Siberian and Laurentian cratons. The sediments of both successions are primarily shallow-water, platform carbonates and fluvial to shallow marine clastic rocks with some turbidites (Corsetti, 1998; Khudoley et al., 2001). Siberia lacks diamictites that are well known in the Death Valley region Kingston Peak Formation (Khudoley et al., 2001). The SE Siberian succession is exposed in the Verkhoyansk thrust and fold belt; the Laurentian succession is exposed in the Basin and Range region in SW United States. In this section, we briefly describe each of the stratigraphic units pertinent to this study. Figures 1.2 and 1.3 show stratigraphic setting and locations of samples taken for geochronologic analyses reported here.

1.2.1 Siberia

The Mesoproterozoic through Early Paleozoic sedimentary succession is well exposed on the margin of the Siberian craton in frontal thrust sheets of the Verkhoyansk belt in the Sette-Daban Range. The following descriptions are modified from Khudoley et al. (2001). In ascending order, the Siberian succession comprises the Uchur Group (~1650-1350 Ma), the Aimchan and Kerpyl groups (~1350-1030 Ma), the Lakhanda and Uy groups (~1030-800 Ma), and the Yudoma Group, including the Sytyga Formation (~620-540 Ma) and the Suordakh Unit (Early Cambrian). The lower part of the succession is primarily composed of shallow-water, platform carbonate and fluvial to shallow marine clastic rocks. The Uchur, Aimchan, and Kerpyl groups represent kilometer-scale siliciclastic-carbonate cycles bounded by unconformities. Smaller-scale transgressive cycles occur within the Aimchan, Lakhanda, and Yudoma groups. The Uy Group is a thick turbidite unit with syn-depositional mafic sills.

Uchur Group The lower part of the Uchur Group comprises 1200 meters of white to gray quartz arenite, gray shale, and sandy stromatolitic dolostone. It grades upward from thinly laminated shales and siltstones with shaly limestone interbeds to sandstone with mud cracks, cross-bedding, and ripple marks. It is interpreted to have been deposited in a fluvial to open marine environment (Khudoley et al., 2001). The upper part of the Uchur Group constitutes 1800 meters of one to eight meter thick cycles of gray, quartzose arenite-shale-dolostone. Dolostone content increases higher in the section. The upper Uchur Group was deposited in lagoonal or lacustrine environments. Paleocurrents indicate that transport was from the Siberian craton (Khudoley et al., 2001). We collected Uchur Group samples from two locations. X0433 is from the Eibeke-Khayata Range and is considered cratonal, or part of the cratonal cover. X0433 was deposited west of the axis of the basin that we suggest may have been shared by Laurentia. X0424 and X0426 are from the Gornostakh anticline and are considered basinal, or deposited in the basin putatively shared by Laurentian sediments. The Gornostakh anticline is the inverted form of the basin. Although nearly two km of section separate the collection sites, we interpret our data for X0424 with data reported by Khudoley et al. (2001) from a sample (PN-1) from the same section (Figure 1.2, Table 1.1).

Aimchan Group The Aimchan Group rests with angular unconformity above the Uchur Group (Figure 1.2). The western side of the basin contains coarser and less mature sediments with more redbeds, representing the landward side of the basin. The lower Aimchan consists of 100-1300 meters of mature gray to reddish-gray quartz arenite with mud cracks, cross-bedding, and ripple marks (Semikhatov and Serebryakov, 1983). It was deposited in fluvial, beach, and supratidal environments (Khudoley et al., 2001). The upper Aimchan consists of 150-600 meters of gray, fine-laminated, sandy stromatolitic dolostone with patches of chert, sandstone, and mud cracked and rippled

Table 1.1. Total number of zircons dated by SHRIMP and LAICPMS in this study, and number of dates within given age ranges. Italics represent zircon dates from similar samples from Khudoley et al. (2001) that fall in given ranges. ba=basinal, cr=cratonal.

	Group Name	Location	Sample name	Total new SHRIMP	Total new LAICPMS	New SHRIMP <10% Discord	New LAICPMS <10% Discord	Intra-cratonic Rift 550-800 Ma	Grenville 950-1300 Ma	West Granite-Rhyolite 1300-1450 Ma	Magmatic Gap (Aus?) 1450-1650 Ma	S Laurentia Paleo–Prot & Ulkan Graben, Siberia 1650-1850 Ma	Aldan Shield 1850-2050 Ma	Unknown Province 2300-2050 Ma	>2300 Ma
Laurentia	Upper Deep Spring	Mt. Dunfee, NV	JSMD0302	-	40	-	19	1	-	3	-	11	1	-	3
	L. Middle Deep Spring	Mt. Dunfee, NV	JSMD0301	15	-	11	-	-	-	1	-	9	-	-	1
	Wyman	White-Inyo Range	JSWI0301	40	20	36	17	-	3	2	-	28	6	-	14
	Stirling Quartzite	Panamint Range	JSPR0303	-	43	-	13	-	1	2	2	5	1	-	2
	KP Wildrose	Black Mountains	JSDV0301	40	10	25	1	-	-	3	-	18	1	-	4
	KP MT Girl	Panamint Range	JSPR0301	-	40	-	23	-	6	3	2	6	1	-	5
	Crystal Spring	Kingston Range	JS04KR1C	40	40	36	11	-	1	-	2	39	2	1	2
Siberia	Suordakh (U. Yudoma, ba)	Gornostakh Anticline	X0415	40	27	33	22	-	2	1	-	2	39	5	6
	Sytyga (U. Yudoma, ba)	Gornostakh Anticline	X0416	35	40	29	21	7	-	-	-	-	25	14	4
	Lower Yudoma (ba)	Gornostakh Anticline	X0418-19	-	81	-	54	-	-	-	-	-	34	20	-
	Upper Yudoma (cr)	Eibeke-Khayata Rnage	X0432	16	-	14	-	-	-	-	-	-	11	-	3
	Uy (ba)	Ulakhan-Bam Range	MLS1 *MM-1*	39	-	35	-	-	9_*17*	8_*6*	10_*7*	3_*1*	2	1_*1*	2_*2*
	Uy (ba)	Ulakhan-Bam Range	C3	-	37	-	17		6	5	2	3	1	-	-
	Kerpyl (ba)	Gornostakh Anticline	X0423_*tt2*	40	40	40	26	-	19_*3*	2_*4*	11_*8*	10_*3*	13_*13*	4_*1*	7_*2*

Kerpyl (cr)	Kyllakh Range	TT3	40	-	39	-	-	-	-	-	30	1	8
Kerpyl (cr)	Kyllakh Range	TT4	-	50	-	31				3	19	1	8
Aimchan (ba)	Gornostakh Anticline	X0421	-	78	-	39	-	-	-	-	3	18	11	7
Aimchan (cr)	Eibeke-Khayata Range	X0434	-	51	-	34	-	-	-	-	-	14	9	11
Uchur (ba)	Gornostakh Anticline	X0424_*PN1*	20	-	17	-	-	-	-	-	*4*	11_*12*	6_*9*	-
Uchur (ba)	Gornostakh Anticline	X0426	-	44	-	24	-	-	-	1	-	5	17	1
Uchur (cr)	Eibeke-Khayata Range	X0433	35	30	27	20	-	-	-	-	-	24	22	1
		Total zircons	400	671	342	372								

shale. It was deposited in a supratidal environment (Khudoley et al., 2001). Paleocurrents indicate that transport was from the Siberian craton (Khudoley et al., 2001). We collected one cratonal Aimchan Group sample (X0434) from the Eibeke-Khayata Range and one basinal sample (X0421) from the Gornostakh anticline.

Kerpyl Group The Kerpyl Group rests unconformably above the Aimchan Group. The base of the Kerpyl Group is characterized by a thin conglomerate. The Kerpyl Group forms an eastward-thickening wedge; it covers a broader area to the west than the Aimchan Group, indicating substantial transgression. The lower Kerpyl constitutes 500-1300 meters of gray shales and calcareous shales with cross-bedding, mud cracks, ripple marks, redbeds, and interbeds of quartz arenite to subarkose. The base of the Kerpyl is defined by the persistent 10-cm thick Bik conglomerate, deposited in a tidal beach environment (Khudoley et al., 2001). The upper Kerpyl consists of 425-700 meters of light-gray dolostone and reddish-brown limestone with laminated and diagenetically-brecciated stromatolites. It was deposited in a shallow marine environment. Some paleocurrent data suggest that transport was from the Siberian craton, but the distribution of redbeds also suggests a local, eastern source (Khudoley et al., 2001). A limestone unit in its upper part yielded a Pb–Pb isochron age of 1043±14 Ma (Ovchinnikova et al. 2001). We analyzed two cratonal Kerpyl Group samples (TT3 and TT4) from the Kyllakh Range and one basinal sample (X0423) from the Gornostakh anticline. We interpret X0423 with with data (TT-2) reported by Khudoley et al. (2001) from the same section (Figure 1.2, Table 1.1).

Lakhanda Group The Lakhanda Group overlies the Kerpyl Group without clear unconformity. Spatially, it is the least variable in terms of thickness and composition. It is composed of 800-1200 meters of stromatolitic gray, orange, and red limestone and dolostone, interbedded with shale. Approximately 100-meter thick cycles contain an upward increase in carbonate content (Khudoley et al., 2001). Superimposed on the

greater cycles are 3-20 meter thick cycles of alternating stromatolitic and shaly carbonate. The section was deposited in a shallow marine environment (Khudoley et al., 2001). A limestone unit in its upper part yielded a Pb–Pb isochron age of 1025±40 Ma (Semikhatov et al. 2000). Sears et al. (2005) suggested that the Lakhanda Group represents a strong correlation with the Beck Spring Formation of the Laurentian succession (discussed below) based on regional and lithologic relationships.

Uy Group The Uy Group conformably overlies the Lakhanda Group. It contains a major component of immature terrigenous sediments, as well as interbedded volcanic rocks. Due to regression and erosion, exposure of the Uy Group is less expansive than the underlying units (Khudoley et al., 2001). The main provenance areas for the Uy Group were from the Siberian craton, as well as from a non-Siberian eastern source. U-Pb analyses of mafic sills intruding the lower and middle Uy Group yielded ages of 1000-940 Ma (Rainbird et al., 1998; Pavlov et al., 2002). Khudoley et al. (2001) interpreted it to have been deposited during active extensional tectonics. The lower Uy consists of 400-1400 meters of coarsening upward cycles (200-400 meter cycles) of gray to green shale, siltstone, and quartz to subarkose, all of which are mud-cracked, ripple-marked, and cross-bedded. It was deposited in subtidal to supratidal, beach, and deltaic environments (Khudoley et al., 2001). The middle Uy consists of 800-3000 meters of gray to green shale, siltstone, and subarkosic arenite and immature greywacke. It contains sediment gravity flows that represent the only deep water sediments in the entire succession. The upper Uy consists of up to 1000 meters of coarsening-upward, pink siltstones and sandstones with interbeds of shale and conglomerate. Cross-bedding and ripple marks are common. It was deposited in fluvial channels and in a shallow marine environment (Khudoley et al., 2001). We analyzed two Uy Group samples (MLS1 and C3) from the Ulakh-Bam Range. We combined our new data from

MLS1 and C3 with data reported by Rainbird et al. (1998) and Khudoley et al. (2001) from the Upper Maya area (MM-1) located southeastward from the study area.

Yudoma Group The Yudoma Group rests unconformably above the Uy Group and older units and marks the beginning of a new depositional cycle (Komar and Rabotnov, 1976; Kornev et al., 1980; Semikhatov and Serebryakov, 1983). The lower Yudoma is only reported in the Gornostakh Anticline where it consists of 200-700 meters of alternating cross-bedded, quartz-rich to immature siliciclastic rocks and stromatolitic carbonate rocks. The upper Yudoma unconformably overlies the lower Yudoma on the Gornostakh Anticline and older units to the west of it. In cratonal sections it consists of 150-200 meters of light-gray dolostone with some shale and quartz-rich sandstone at its base. On the eastern limb of the Gornostakh Anticline (basinal section), the Sytyga Formation of the upper Yudoma consists of 600 meters of interbedded quartz-rich to immature siliciclastic rocks and carbonates. Total eastward thickening of sandstone units along with increasing content of immature sandstones implies an eastern (non-Siberian) source. We analyzed two samples from basinal lower Yudoma (X0418 and X0419), and three samples from upper Yudoma: cratonal section (X0432) and basinal section (Sytyga Formation X0416 and Suordakh Unit X0415, discussed below). We report the data from the lower Yudoma together (Figure 1.2, Table 1.1) because of their spatial and stratigraphic proximity, and we combined our new data with that of Khudoley et al. (2001) from the same section (JD-1).

Suordakh Unit The Suordakh Unit is the uppermost unit of the Yudoma Group, exposed in only the eastern limb of the Gornostakh anticline. It consists of 15-30 meters of quartz-rich to immature siliciclastic rocks with rare interbedded carbonate that grade upward in the succession to shales. This unit contains the first Early Cambrian fauna fossils and is interpreted to be the lowermost Paleozoic unit in the succession. The base of the Suordakh Unit is characterized by a ~2 meter layer of quartzite. We analyzed one

basinal sample (X0415) from the basal quartzite of the Suordakh Unit in the Gornostakh anticline.

1.2.2 Laurentia—Death Valley

The Death Valley succession, exposed in southern California and Nevada, consists of numerous sedimentary formations (Stewart,1970). Those pertinent to this study are described in ascending order.

Crystal Spring Formation Roberts (1974; 1982) provided the most extensive description of the Crystal Spring Formation. He divided the formation into sedimentary members with ~450 meters of diabase sills that have been dated at 1080 Ma (Heaman and Grotzinger, 1992). Members include, in ascending order, arkose, feldspathic sandstone, purple mudstone, dolomite, algal dolomite, hornfels, and the upper member. An unconformity above the algal member is overlain by a 10-cm thick conglomerate, here informally termed the Excelsior Conglomerate from a mine in the Kingston Range, and effectively divides the sequence into upper and lower Crystal Spring Formation. We interpret the Excelsior Conglomerate as equivalent to the Bik Conglomerate of the basal Kerpyl Group of SE Siberia (Sears et al., 2005). We analyzed one sample (JS04KR1C) from the Excelsior Conglomerate in the Kingston Range.

Beck Spring Formation The Beck Spring Formation is typically exposed as a massive dolomite unit dominated by cryptalgal laminites, stromatolites, and grainstones. The contact between the underlying Crystal Spring Formation and the Beck Spring Formation is gradational. Wright et al. (1976) interpreted the transition of alternating shale, siltstone, and dolostone to record a subtidal to supratidal depositional environment in which a shallow carbonate shelf developed. The Beck Spring dolomite contains well-preserved original fabrics, including early fibrous dolomite cements, later sparry dolomite cements, and phases of internal sedimentation (Tucker, 1983). A common feature in the dolomite is widespread syn-depositional or diagenetic

brecciation. At Saratoga Springs, the Beck Spring Formation contains an interesting facies change that involves cycles of stromatolitic gray, orange, and red limestone and dolostone, interbedded with orange and gray beds of shale (Marian and Osborne, 1992). We did not analyze zircons from this formation. However, we interpret the Beck Spring Formation as the lithologic equivalent of the Lakhanda Group of SE Siberia (see Sears et al., 2005).

Kingston Peak Formation The contact between the Beck Spring Formation and the overlying Kingston Peak Formation is a transitional sequence of turbidite beds. The Kingston Peak Formation represents predominantly siliciclastic deposition with rare carbonates and volcanics. It was deposited during active extensional tectonics (Labotka and Albee, 1977; Miller, 1987) and possibly during glacial periods (Miller, 1983; 1985; 1987), although other interpretations are suggested by Eyles and Januszczak (2004). The formation is divided into four members, listed in ascending order: the Limekiln Spring Member composed of arkose, argillite, and quartzite, the Surprise Member composed of diamictite, the Sourdough Limestone Member composed of laminated limestone, and the South Park Member composed of limestone, sandstone, and diamictite (Miller, 1985). The South Park Member is divided into the Middle Park, Mountain Girl, and Wildrose submembers (Miller, 1985). We interpret the Kingston Peak Formation as possibly correlative with part of the Uy Group of SE Siberia. We analyzed one sample (JSPR0301) from the Mountain Girl Submember in the Panamint Range and one sample (JSDV0301) from a quartzite clast in the Wildrose diamictite in the southern Black Mountains.

Stirling Quartzite The Kingston Peak Formation is unconformably overlain by the Noonday Formation, the Johnnie Formation, and the Stirling Quartzite, in ascending order (Stewart, 1970). We focused on the Stirling Quartzite. It is composed of quartzite and siltstone, with minor carbonate. It was deposited in a fluvial to marine setting

(Wertz, 1982). The presence of *Cloudina*-like shelly fossils has led some to place the Stirling Quartzite in the latest Proterozoic (Languille, 1974a and b). Because the upper Yudoma dolomite also contains *Cloudina* fossils, we interpret the Stirling Quartzite as equivalent with part of the Sytyga Formation of SE Siberia. We analyzed one sample (JSPR0303) from the Stirling Quartzite in the Panamint Range.

1.2.3 Laurentia – White-Inyo

The White-Inyo succession, exposed in the White-Inyo Range in California and Nevada, consists of several sedimentary formations. Those pertinent to this study are described below in ascending order.

Wyman Formation The Wyman Formation is over 3000 meters thick, and its base is not exposed. It consists of interbedded mudstone, siltstone, and quartzite, with minor carbonates (Corsetti, 1998). Simple Neoproterozoic trace fossils have been observed (Alpert, 1976). The section appears to have been deposited in a shallow-water environment (Corsetti, 1998). Since the Wyman Formation is unconformably overlain by Reed Dolomite and its base is not exposed, its age of deposition is poorly constrained. The Wyman has been correlated with the Stirling Quartzite in the Death Valley region (Stewart, 1970). We suggest that part of the Wyman Formation is possibly correlative with part of the upper Uy Group of SE Siberia. We analyzed one sample (JSWI0301) from the Wyman Formation in the White-Inyo Range.

Deep Spring Formation The Deep Spring Formation is divided into Lower, Middle, and Upper Members (Gevirtzman, 1986; Dienger, 1986; Greene, 1988). Each member represents a “Grand Cycle,” a cycle that consists of a siliciclastic lower half-cycle and a carbonate upper half-cycle (Gevirtzman et al., 1986). The siliciclastic half-cycles are defined by green siltstones and quartzites with ripple marks and cross-bedding. The carbonate half-cycles are defined by cross-bedded oolitic limestone. Sharp disconformities divide each member (Corsetti, 1998). The Precambrian-Cambrian

boundary lies within this formation. We interpret the Deep Spring Formation as equivalent with the Sytyga Formation and Suordakh unit of SE Siberia, which also contains siliciclastic-carbonate cycles. We analyzed one sample from the Middle Deep Spring Formation (JSMD0302) and one sample from the Upper Deep Spring Formation (JSMD0301) from Mt. Dunfee, NV. These data are reported together due to their spatial and stratigraphic proximity.

1.3 Previous Siberian detrital-zircon geochronology studies

Previous studies of detrital-zircon geochronology in SE Siberia are scarce, but offer important information concerning the provenance and age of sedimentation. Rainbird et al. (1998) and Khudoley et al. (2001) reported U/Pb ages from SHRIMP and ID-TIMS analyses regarding Siberian sedimentary units from several locations. Detrital zircons from the Uchur Group sandstone in the Gornostakh anticline yielded clusters of dates ranging predominantly between 2300-2050 Ma and between 2050-1850 Ma, with one younger date of 1521±31 Ma. Zircons from the Kerpyl Group in the Gornostakh anticline yielded dates ranging primarily between 2050-1850 Ma, and also between 2300-2050 Ma, 1850-1650 Ma, 1650-1450 Ma, and 1450-1300 Ma. Zircons from the Uy Group sandstone in the upper Maya River area yielded dates ranging primarily between 1450-1300 Ma and 1300-950 Ma, with a few dates >2300 Ma, 2300-2050 Ma, and 1850-1650 Ma. Single zircon ID-TIMS analyses from the Yudoma Group sandstone in the Gornostakh anticline yielded dates between 2300-2050 Ma (Khudoley et al., 2001).

1.4 Analytical methods and results

We extracted and separated zircons from fifteen Siberian samples and eight Laurentian samples using standard techniques including crushing, disc milling, density and magnetic separation, and hand picking under a stereoscope. Separation yielded

zircon grains ranging from ~50µm to ~240µm in length. Following standard procedures, we mounted zircons onto pucks for sensitive high resolution ion microprobe-reverse geometry (SHRIMP-RG) analyses and laser ablation inductively coupled plasma mass spectrometer (LAICPMS) analyses. We prepared cathodoluminescence (CL) scanning electron microscope (SEM) images to decipher the internal structures of the sectioned grains.

We performed 400 U-Th-Pb analyses with the SHRIMP-RG in the Stanford – United States Geological Survey cooperative ion microprobe facility. Instrumental conditions and data acquisition followed Williams (1998). Craters produced by the primary O_2^- beam, operated at ~4.8 nA, were ~1 µm deep and ~30µm in diameter. The magnet was cycled through the mass stations six times per analysis, with one standard analysis for every five unknown analyses. We calibrated concentration data against standard CZ3 zircon (550 ppm U), and isotopic ratios against standards R33 zircon (419 Ma, Black et al., 2004) and RG6 zircon. We reduced and plotted raw data using the Squid and Isoplot/Ex programs of Ludwig (1999). All age errors are reported at 2 sigma. We applied a filter so that only data less than 10% discordant were interpreted. Of the SHRIMP 400 analyses, 342 were less than 10% discordant.

We performed 671 U-Th-Pb analyses with the New Wave UP-213 laser ablation system in conjunction with a ThermoFinnigan Element2 single collector double focusing magnetic sector ICP-MS in the GeoAnalytical Lab at Washington State University. We used a fixed diameter spot size of either 16µm or 30µm with a laser frequency of either five Hz or ten Hz, depending on the size of the zircon. Each analysis included six seconds of warm-up, eight seconds of delay, and 35 seconds of rapid scanning (300 sweeps) across the following masses: ^{202}Hg, ^{204}(Hg+Pb), ^{206}Pb, ^{207}Pb, ^{208}Pb, ^{232}Th, ^{235}U, ^{238}U. We corrected for mass and elemental fractionation by calibrating data against standards R33 zircon and FC-1 zircon (Paces and Miller, 1993). The Hg-corrected ^{204}Pb

data was unreliable with both positive and negative values, so the LAICPMS data concerning total Pb values are interpreted without any common Pb correction. Data were reduced off-line using an in-house Excel program supplemented with Visual Basic macros at WSU. We plotted data using the Isoplot program of Ludwig (2001). All age errors are reported at 2 sigma. We applied a filter so that only data less than 10% discordant were interpreted. Of the 671 LAICPMS analyses, 372 were less than 10% discordant.

In order to ensure consistency between data from the two instruments, we analyzed thirty-six grains from three samples (~twelve grains per sample) by both instruments. Measurements were taken from the same spots on twenty-six grains and from different spots on ten grains. Two of the analyses did not yield interpretable results. Thirty-two of the thirty-four $^{207}Pb/^{206}Pb$ dates from comparison analyses are equivalent within 2σ error. Therefore we assume that there is little to no instrument bias between the datasets from the two instruments. A complete discussion of the comparison analyses is given in Chapter 6.

We report our new data, along with previous Siberian detrital-zircon geochronology data from Rainbird et al. (1998) and Khudoley et al. (2001), in Table 1.1, Figure 1.4, and Appendix B. We divided the detrital-zircon dates according to their association with possible provenance terranes, discussed below. Age ranges are >2300 Ma, 2300-2050 Ma, 2050-1850 Ma, 1850-1650 Ma, 1650-1450 Ma, 1450-1300 Ma, 1300-950 Ma, and 800-550 Ma.

1.5 Discussion

Detrital zircons from sedimentary assemblages in SE Siberia point to important contributions from some provenance sources that are not present in Siberia, but are present in SW Laurentia (Figure 1.1). Likewise, SW Laurentian sediments contain

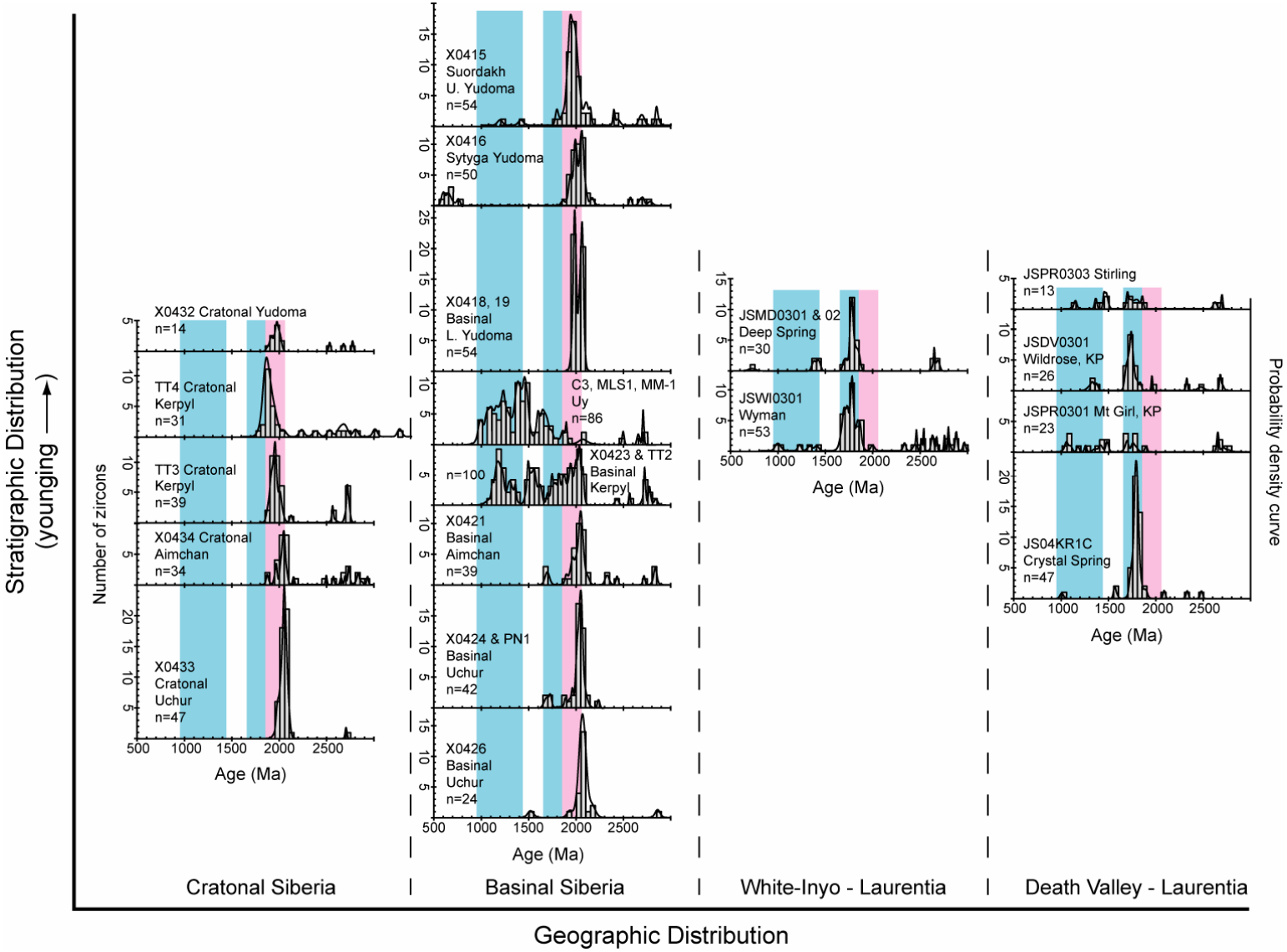
Stratigraphic Distribution
(younging ⟶)
Number of zircons
X0432 Cratonal Yudoma
n=14
TT4 Cratonal
Kerpyl
n=31
TT3 Cratonal
Kerpyl
n=39
X0434 Cratonal
Aimchan
n=34
X0433
Cratonal
Uchur
n=47
Age (Ma)
X0415
Suordakh
U. Yudoma
n=54
X0416
Sytyga Yudoma
n=50
X0418, 19
Basinal
L. Yudoma
n=54
C3, MLS1, MM-1
Uy
n=86
n=100
X0423 & TT2
Basinal
Kerpyl
X0421
Basinal
Aimchan
n=39
X0424 & PN1
Basinal
Uchur
n=42
X0426
Basinal
Uchur
n=24
Age (Ma)
JSMD0301 & 02
Deep Spring
n=30
JSWI0301
Wyman
n=53
Age (Ma)
JSPR0303 Stirling
n=13
JSDV0301
Wildrose, KP
n=26
JSPR0301 Mt Girl, KP
n=23
JS04KR1C
Crystal Spring
n=47
Age (Ma)
Probability density curve
Cratonal Siberia
Basinal Siberia
White-Inyo - Laurentia
Death Valley - Laurentia
Geographic Distribution

Figure 1.4. Detrital zircon ^{207}Pb-^{206}Pb age histograms and associated probability curves for samples from Siberian cratonal and basinal sediments, and from Laurentian sediments from Death Valley and White-Inyo areas. The histograms are arranged along the horizontal axis based on the sample locations, and along the vertical axis based on their stratigraphic position. Blue=Laurentian provenance terranes; red=Siberian provenance terranes.

zircons from sources absent in SW Laurentia, but present in SE Siberia (Figure 1.1). The following discussion evaluates the provenance terranes of detrital zircons found in SE Siberia and SW Laurentia in light of the SE Siberia – SW Laurentia connection proposed by Sears and Price (1978, 2003).

The sedimentary successions in SE Siberia and SW Laurentia may have developed in a single basin that collected sediments during multiple stages of extension and rifting. Sediments may have been shed from numerous terranes from Siberia, Laurentia, and an unknown source (possibly Australia), defined below by their respective age ranges. The focus of this study was to identify the source terranes accessible to the basin based on age populations. Therefore, comparisons with source terranes were based primarily on the presence of zircons within certain age groups.

1.5.1 >2300 Ma provenance terranes

All but three samples (basinal lower Yudoma X0418, X0419, and basinal Uy C3) contained at least one zircon older than 2300 Ma. Since both SE Siberia and SW Laurentia have such basement terranes, these data neither support nor refute the SE Siberia – SW Laurentia connection. However, the proposed reconstruction places >2300 Ma Siberian sources closer to the basin than the Wyoming Province, indicating

that most >2300 Ma zircons could have been derived from Siberia (Figure 1.1). The >2300 Ma zircons also could have been inherited as xenocrysts into S Laurentian Paleoproterozoic magmatism or Aldan Shield magmatism, and then eroded and deposited into SE Siberian and SW Laurentian basins.

1.5.2 2300-2050 Ma provenance terranes

All Siberian samples except the cratonal Yudoma Group (X0432) and the basinal Uy (C3), and one Laurentian sample (Crystal Spring Formation JS04KR1C) contain zircons between 2300-2050 Ma. No known provenance terranes of this age range occur in SE Siberia or SW Laurentia adjacent to the sedimentary basin. Moreover, terranes of this age range are rare in both Siberian (Khudoley et al., 2007) and Laurentian (Karlstrom and Humphreys, 1998) basement and are unlikely to provide sufficient source for numerous detrital zircon grains in Siberian samples with extensive peaks at ca. 2050 Ma on the age probability plots (Figure 1.4). The presence of zircons with this age range in both Siberia and Laurentia suggests that an additional unknown terrane could have supplied zircons of these ages.

1.5.3 2050-1850 Ma provenance terranes

The SE Siberian-SW Laurentian reconstruction relies partly on the correlation of the Taltson-Thelon magmatic zone (NW Laurentia) with the Billyakh, Olenek, Tyrkandin, and Ulkan mélange zones followed by magnetic anomalies from the Anabar to Aldan shield (central and E Siberia) (Parfenov, Kuzmin 2001). Taken together, they form a continuous ca. 1.9-2.0 Ga belt that was capable of shedding zircons that range in age between 2050-1850 Ma. All but one sample (Middle Deep Spring JSMD0301; but Upper Deep Spring sample contained zircons of this age) contained at least one zircon in this age range. It is much more likely that these zircons were derived from the Aldan Province in Siberia (hundreds of kilometers away) than from the Taltson-Thelon magmatic zone in Canada (thousands of kilometers away). Therefore, we interpret that

the presence of zircons of this range in Laurentian sediments supports the SE Siberia – SW Laurentia connection.

1.5.4 1850-1650 Ma provenance terranes

The Colorado, Yavapai, and Mazatzal provinces in SW Laurentia make up a significant 1850-1650 Ma provenance source. We refer to these provinces as the S Laurentian Paleoproterozoic terranes. The Ulkan graben of Siberia contains 1.74-1.7 Ga volcanic rocks. All Laurentian samples contain zircons of this age range. Seven Siberian samples contain zircons of this range: the basinal Uchur Group sample (X0424), the basinal Aimchan Group sample (X0421), the cratonal and basinal Kerpyl Group samples (TT4 and X0423), the Uy Group samples (C3 and MLS1), and the Suordakh sample from the upper Yudoma Group (X0415). The presence of zircons of this range in Siberian sediments suggests possible close proximity to the S Laurentian Paleoproterozoic terranes indicated in the SE Siberia – SW Laurentia connection. Zircons of this range are absent in the cratonal Uchur Group sample (X0433) and the cratonal Aimchan Group sample (X0434), indicating that S Laurentian Paleoproterozoic zircons may not have been transported across Siberia, but just into the basin. The absence of these zircons in the middle and lower Yudoma Group samples (X0432, X0418-19 and X0416) may suggest that tectonic processes involved during rifting possibly blocked sediment transport.

1.5.5 1650-1450 Ma provenance terranes

Four Siberian and three Laurentian samples yielded zircons with ages between 1650-1450 Ma. Of these seven samples, the basinal Kerpyl Group sample (X0423) and the Uy Group samples (MLS1 and C3) may correlate with the Crystal Spring Formation sample (JS04KR1C) and the KP Mountain Girl sample (JSPR0301), respectively. No known provenance terrane of this age range is present on either craton, indicating that sediment transport from an unknown craton (possibly Australia, see Blewett et al., 1998)

occurred. The fact that the Kerpyl and Uy groups and their putatively correlative Crystal Spring and Kingston Peak formations all contain zircons of this age range agrees with the SE Siberia – SW Laurentia connection.

1.5.6 1450-1300 Ma provenance terranes

Numerous igneous bodies referred to here as the West Granite-Rhyolite province ranging in age from 1450-1300 Ma (Karlstrom and Humphries, 1998) are found in the subsurface (dated from drill cores) in SW United States and were available for sediment supply during deposition of part of the SE Siberian and SW Laurentian successions. There is no known provenance terrane of this age range in Siberia. Four Siberian samples (basinal Kerpyl Group X0423, Uy Group MLS1 and C3, and Suordakh Unit X0415) and all Laurentian samples except the Crystal Spring Formation sample (JS04KR1C) yielded zircons of this age range; note that Fletcher et al. (2004) reported zircons of this age range in the Crystal Spring Formation. The presence of zircons of these ages in the basinal Kerpyl and Uy groups and the Suordakh Unit in SE Siberia indicates that the West Rhyolite-Granite province may have been accessible during the time of deposition.

1.5.7 1300-950 Ma provenance terranes

The Grenville orogen, broadly defined as 1300-950 Ma, often has been used as a piercing-point for continental reconstructions. Although SE Siberia lacks Grenville-age exposures, there is abundant detrital-zircon evidence of the Grenville orogen sources in Siberia. Four Siberian samples (basinal Kerpyl X0423, Uy MLS1 and C3, and Suordakh Unit X0415) and four Laurentian samples (Crystal Spring JS04KR1C, KP Mountain Girl JSPR0303, Stirling Quartzite JSPR0301, and Wyman JSWI0301) yielded zircons of this age range. Close proximity of SE Siberia and the Grenville orogen during Proterozoic sedimentation provides the simplest explanation for these data. The presence of Grenville-age zircons in Siberia correlate well with their possible Laurentian

counterparts. For example, the basinal Kerpyl Group is possibly equivalent with part of the Crystal Spring Formation. Although there is no lithofacies correlative to the Kingston Peak diamictite in Siberia, the poorly constrained timing of the lower Kingston Peak Formation, the Wyman Formation, and Siberia's Uy Group allows a tentative correlation between the three.

1.5.8 800-550 Ma provenance terranes

One sample in Siberia (basinal Sytyga Formation X0416) and one in Laurentia (Upper Deep Spring Formation JSMD0302) yielded zircons of ages between 800-550 Ma. We interpret these zircons as being derived from intracratonic rift-related intrusions associated with the final break-up of Siberia and Laurentia.

Figure 1.5 shows an interpretation of the stratigraphic correlations across the SE Siberia – SW Laurentia connection in the form of a fence diagram. We have included the provenance terranes to demonstrate their proximity to the basin. It is clear that Siberian units requiring provenance terranes of 1850-1650 Ma, 1450-1300 Ma, and 950-1300 Ma could have collected sediments from the Grenville, West Granite-Rhyolite, and S. Laurentian Paleoproterozoic terranes. Likewise, the Laurentian units requiring a provenance terrane of 2050-1850 Ma could have collected sediment from the Aldan Province of Siberia. These results provide good support for previous lithologic correlations (Sears et al., 2005).

1.6 Conclusions

Mesoproterozoic to Early Cambrian sedimentary successions deposited in intracratonic basins and along the margins of SE Siberia and SW Laurentia during continental rifting and subsequent passive margin development now are exposed in the Sette Daban Range of SE Siberia and in the Death Valley and White-Inyo areas of SW United States. Our results indicate reasonable detrital-zircon correlations between

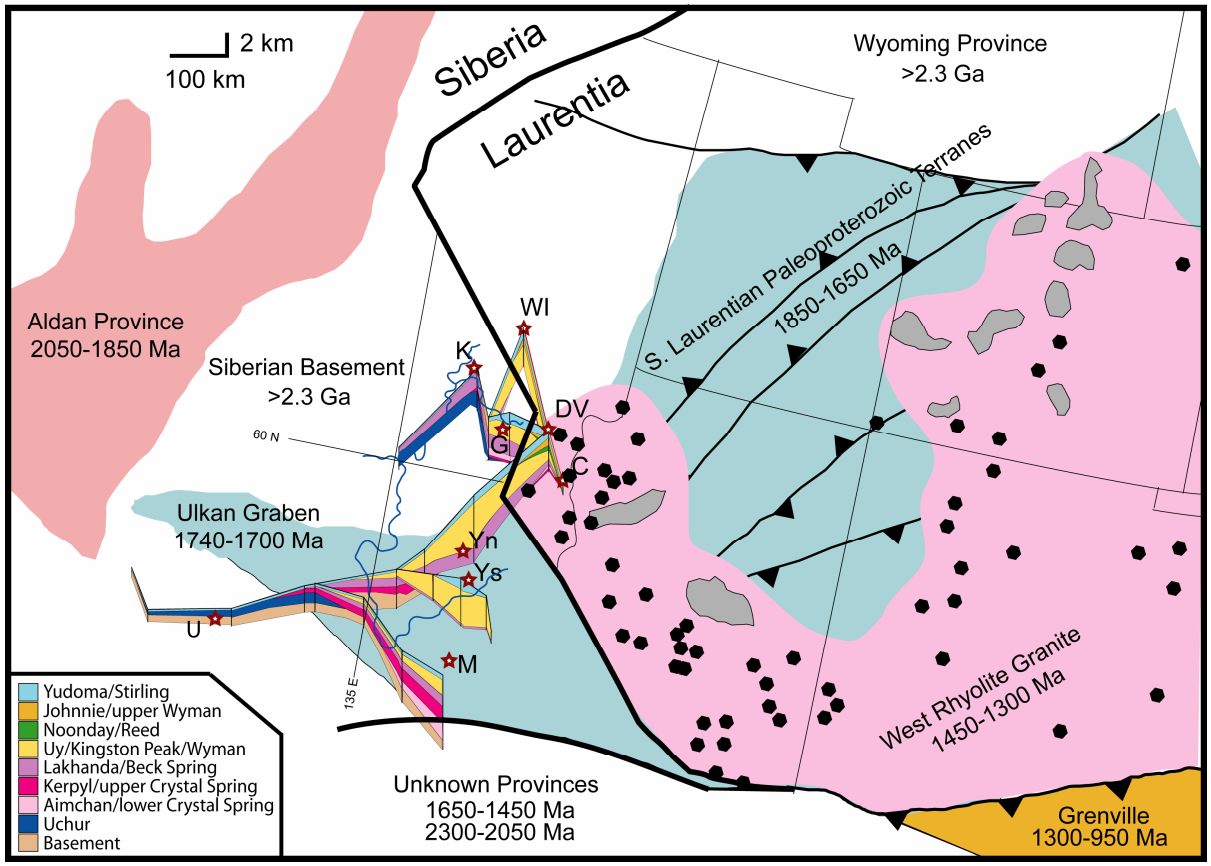

Figure 1.5. Map of possible source terranes accessible to shared basin between SE Siberia and SW Laurentia. Terranes are partially based on Karlstrom and Humphreys (1998) and Sears and Price (2003). Fence diagram constructed from cross-sections reported in Khudoley et al. (2001), Corsetti (1998). Solid black line = boundary between Siberia and Laurentia. Color scheme is same as Table 1.1. Key at lower left is for lithostratigraphic relationships in fence diagram.

stratigraphic units in SE Siberia and SW Laurentia. Several units in SE Siberia suggest close proximity to provenance terranes present in SW Laurentia, including the S. Laurentian Paleoproterozoic terranes (1850-1650 Ma), West Granite-Rhyolite Province (1450-1300 Ma), and Grenville orogen (1300-950 Ma). Likewise, SW Laurentian units could indicate close proximity to the Aldan Province (2050-1850 Ma) of SE Siberia. Correlations based on lithology and detrital-zircon provenance data agree with the SE Siberia – SW Laurentia connection. The 2300-2050 Ma source region has not been identified, but could be a key for further paleocontinental reconstructions. Furthermore, units on each craton require accessibility to an additional provenance terrane (1650-1450 Ma) that has yet to be defined. Blewett et al. (1998) found that a range of geological provinces in N Queensland contain ages between 1600-1450 Ma. Based on these results, Sears and Price (2000) proposed that the N Queensland terrane possibly contributed the zircon grains of this age range to the shared basin of the SE Siberia – SW Laurentia connection.

Similarities of detrital-zircon provenance relationships are best in the basinal units of the Kerpyl and Uy groups, and the proposed correlative Crystal Spring and Kingston Peak formations. Similarities of certain provenance terranes are also evident between the Yudoma Group and the Deep Spring Formation. Starting at the deposition of the Yudoma Group, the Sette Daban linkages seem to transition from the Death Valley region to the White-Inyo region. Yudoma-Deep Spring correlation may indicate that transtensional separation of the two cratons had proceeded enough to inhibit transport of detrital zircons between Siberia and Death Valley, but transport was still allowed between Siberia and White-Inyo region. Therefore, our new data are in agreement with SE Siberia – SW Laurentia sedimentary correlations between ~1120-540 Ma. These correlations, combined with correlations of basement terranes, agree with the Sears and Price reconstruction (2003) for a much wider time range.

CHAPTER 2

A MESOPROTEROZOIC-MIDDLE CAMBRIAN TECTONO-SEDIMENTARY MODEL FOR THE SE SIBERIA – SW LAURENTIA REGION: INFLUENCE OF THE GRENVILLE OROGEN

2.1 Introduction

Researchers generally agree that Laurentia occupied a central position in the Proterozoic supercontinent Rodinia. A continuing debate exists, however, concerning which continent rifted away from Laurentia's western margin (Ernst et al., 2000; Meert, 2002). Some well-known reconstructions, such as the SWEAT (Jefferson, 1978; Moores, 1991; Hoffman, 1991; Dalziel, 1991; Borg and Depalo, 1994; Weil et al., 1998), AUSWUS (Brookfield, 1993; Karlstrom et al., 1999; Burret and Berry, 2000), and AUSMEX (Wingate et al., 2002) hypotheses, suggest Australia or Antarctica held the position to the west of Laurentia. These reconstructions are primarily based on paleomagnetic data. However, we contend that plate reconstructions should be based on all sound geological data that may be available.

The first and most geologically detailed reconstruction places the eastern margin of Siberia against Laurentia's western margin (Sears and Price, 1978, 2003; MacLean et al., *in review*). The E Siberia – W Laurentia reconstruction (Figure 2.1) is based on geological, geophysical, and paleomagnetic data (Sears and Price, 2003), and includes the following lines of evidence:

- The ~1070 Ma key paleomagnetic poles (see Buchan et al., 2000) for Proterozoic Laurentia (Elston et al., 2002), Siberia (Gallet et al., 2000), and Australia (Wingate et al., 2002) permit the E Siberia – W Laurentia connection.

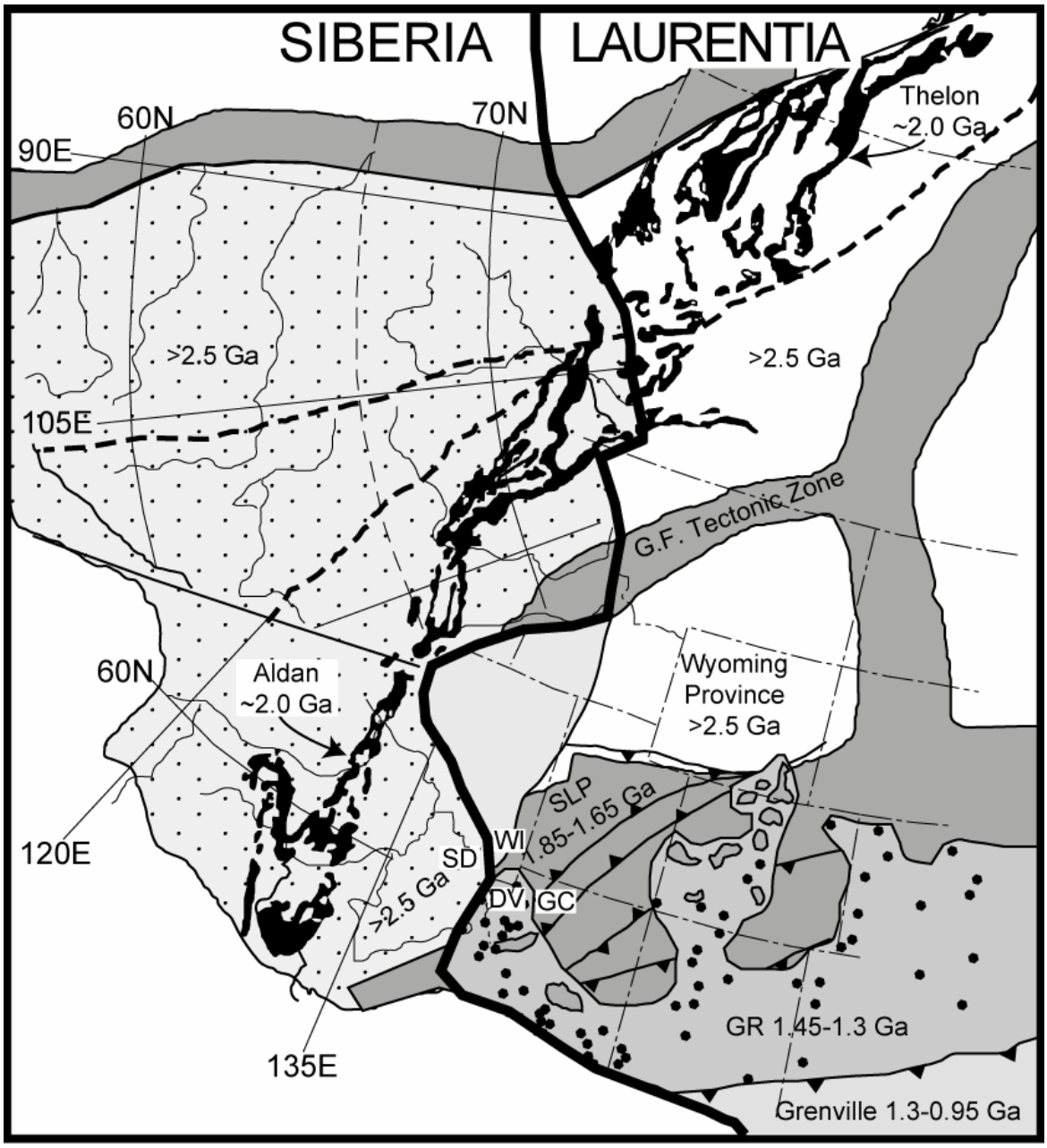

Figure 2.1. Correlations across proposed E Siberia – W Laurentia connection (Meso-Neoproterozoic). See Figure 1.1 caption for description. SD = Sette Daban; WI = White-Inyo; DV = Death Valley; GC = Grand Canyon; S.L.P. = South Laurentian Paleoproterozoic terranes; G.R. = Granite-Rhyolite province. Stipple pattern = Siberian Craton. Modified from Sears and Price (2003).

- Isopach data from Laurentian and Siberian rifted margins indicate that the two cratons can be juxtaposed in a tight fit for a zigzag length greater than 2500 km that includes a Siberian 200 km offset at the Laptev Sea (Rosen et al., 1994) and a Laurentian 200 km offset along the St. Mary-Moyie fault zone (Price and Sears, 2000).
- A reconstructed 4500 km continental collisional belt (2.0-1.8 Ga) forms a piercing point from NW Laurentia through E Siberia and includes the Siberian Hapshan and Aldan provinces (Rosen et al., 1994) and the Laurentian amalgamated domains and the Thelon domain of Gehrels and Ross (1998), and Ross et al. (2000).
- Several Paleo- and Mesoproterozoic orogenic belts and magmatic provinces are present in each craton, are of similar age and geologic character, and may correlate across the restored E Siberia – W Laurentia boundary (Sears and Price, 2003).
- The Siberian Udzha-Taimyr trough contains a thick succession of Mesoproterozoic sedimentary strata and sills that appears to be correlative with the palinspastically restored Mesoproterozoic Belt-Purcell Supergroup of the Cordilleran fold-thrust belt.
- Mesoproterozoic to Early Cambrian sediments preserved in the E Siberian Verkhoyansk fold-and-thrust belt in the Sette Daban region (Khudoley et al., 2001) appear to be correlative with sediments in Laurentia's White-Inyo, Death Valley, and Grand Canyon regions (Sears et al., 2005). Furthermore, detrital-zircon provenance data from E Siberian and W Laurentian sediments indicate strong support for correlations (Chapter 1; MacLean et al., *in review*).
- The first trilobite to appear in North America occurs in W Nevada and closely resembles the SE Siberian trilobite *Repinaella*, which appears 26 m above the first known trilobite *Profallotaspis* (Glaessner, 1984; Palmer et al., 1993; Hollingsworth, 2005). This necessitates a close proximity between Siberia and W Laurentia

because of rapid evolution rates and high endemism of early Cambrian trilobites (Bowring et al., 1993).

Constraining the correct reconstruction will allow researchers to pursue regional geologic problems by using data from multiple cratons in conjunction with each other. Based in part on our results from Chapter 1, we consider the detail of the E Siberia – W Laurentia reconstruction sufficient to begin to use the reconstruction for more detailed investigations of the Proterozoic to Early Cambrian tectono-sedimentary evolution of Siberia and Laurentia, timing and evolution of Rodinian rifting, the long-term behavior of the magnetic field (Kirshvink et al., 1997; Gallet et al., 2000), and the origin and dispersal of metazoans (Bowring et al., 1993).

In this chapter, we present a Proterozoic to Early Cambrian tectono-sedimentary evolutionary model of the strata exposed in SE Siberia's Sette Daban region, and in SW Laurentia's White-Inyo, Death Valley, and Grand Canyon regions. Our model is based on the E Siberia – W Laurentia connection and considers detrital-zircon geochronology data from the four regions of interest. We compiled data from numerous sources, referenced below. The model focuses on the temporal, stratigraphic, and geographic distribution of Grenville-age zircons and other age domains.

2.2 Regional Geology

2.2.1 Surrounding provenance terranes

Several provenance terranes that contributed sediment to the SE Siberia – SW Laurentia basin during Mesoproterozoic-Early Cambrian time were presented in Chapter 1 (and MacLean et al., *in review*). Provenance terranes include the Siberian Aldan Shield (>2300 Ma, 2050-1850 Ma, and 1740-1700 Ma), and the Laurentian Wyoming Province (>2300 Ma), SW Laurentian Paleoproterozoic terranes (1850-1650 Ma), Granite-Rhyolite Province (1450-1300 Ma), and Grenville orogen (1300-950 Ma). Also,

two unknown provenance terranes contributed zircons formed between 2300-2050 Ma and between 1650-1450 Ma. The Laurentian provenance relationships are consistent with several other SW Laurentian detrital-zircon studies (e.g. Timmons et al., 2005; Vogel, 2004; Stewart et al., 2001).

2.2.2 Sette Daban region

Proterozoic to Early Cambrian evolution of the E Siberia succession began with a failed rift that resulted in the 1650-1350 Ma Uchur Group (Khudoley et al., 2001). Thermal subsidence followed the failed rift, resulting in a broad and shallow intracratonic basin, represented by the shallow marine siliciclastic-carbonate cycles of the Aimchan (~1300 Ma), Kerpyl (~1100 Ma), and Lakhanda (~1000 Ma) Groups (Khudoley et al., 2001). A second phase of extension occurred at ~900 Ma, resulting in deeper water deposition and mafic eruptions preserved in the Uy Group. Large gaps in the geologic record are present within the Uy Group, between the Uy Group and the overlying Yudoma Group, or both. The marine transgression sediments of the Yudoma Group (~640-535 Ma) mark the beginning of E Siberia passive margin development (Khudoley et al., 2001). Figure 2.2 and the Table 2.1 summarize the Sette Daban stratigraphy.

2.2.3 White-Inyo region

Proterozoic to Early Cambrian sediments of the White-Inyo region were deposited during extension associated with the rifting of Rodinia and during the initial stages of thermal subsidence and passive margin development. The sediments form the westernmost extension of the Cordilleran miogeocline, a stratigraphic package that extends eastward to the Wasatch Mountains in central Utah, and northward from Sonora, Mexico, to the Canadian Yukon Territory (Stewart, 1970, 1972, Bond et al., 1984). In ascending order, the Proterozoic-Early Cambrian part of the White-Inyo succession includes the Wyman Formation, the Reed Dolomite, the Deep Spring Formation, and the Campito Formation (Figure 2.2 and Table 2.1).

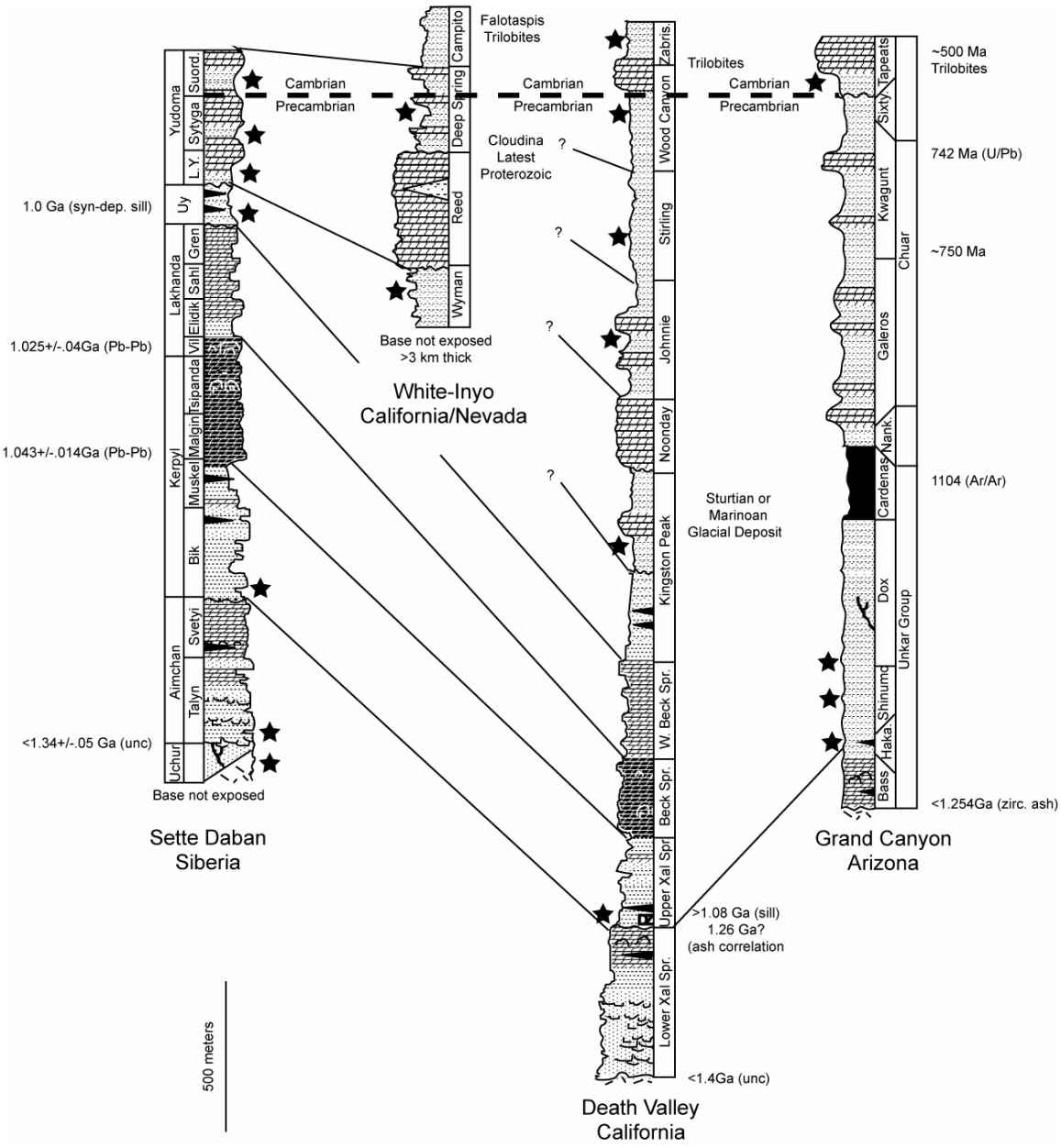

Figure 2.2. Correlation of Meso-Neoproterozoic to Cambrian stratigraphic sections in Sette Daban, White-Inyo, Death Valley, and Grand Canyon. Sample locations used for this study are symbolized with black stars. Note that lithostratigraphic correlations between Siberia and Laurentia are possibly stronger than between different regions within SW Laurentia. Columns are taken from various sources, including Corsetti (1998), Khudoley et al. (2001), and Timmons et al. (2005).

Table 2.1. Stratigraphic descriptions pertinent to this study (primarily from Corsetti, 1998; Khudoley et al., 2001; Timmons et al., 2005).

	Group/ Formation	*Sample Numbers*	*Description*
Sette Daban	Yudoma	lower Yudoma--X0418 & X0419; Sytyga--X0416; Suordakh--X0415	Unconformably above Uy. Alternating siliciclastic rocks and stromatolitic carbonate rocks; Suordakh is only exposed in eastern limb of Gornostakh anticline and contains first Cambrian fossils.
	Uy	MLS1, C3, MM-1	Conformably above Lakhanda. Lower: siliciclastics deposited in subtidal to supratidal, beach, and deltaic environments; middle: siliciclastics deposited in deep water gravity flows during active extension; upper: siliciclastics deposited in fluvial channels and shallow marine environment. U-Pb dates of mafic sills intruding lower and middle Uy yielded ages of 1000-940 Ma (Rainbird et al., 1998; Pavlov et al., 2002).
	Lakhanda	n/a	Conformably above Kerpyl. Predominantly carbonate with shale interbeds deposited in shallow marine environment.
	Kerpyl	X0423, TT2, TT3, TT4	Unconformably above Aimchan, atop a 10cm conglomerate marker bed. Forms an eastward-thickening wedge indicative of transgression from the east. Lower: shales interbedded with quartz arenite; upper: stromatolitic carbonates deposited in shallow marine environment. Presence of redbeds suggests local or eastern source. Limestone in upper Kerpyl yielded Pb-Pb isochron age of 1043±14 Ma (Ovchinnikova et al., 2001).
	Aimchan	X0421, X0434	Angular unconformably above Uchur. Thickens from west to east. Lower: quartz arenite deposited in fluvial, beach, and supratidal environments; upper: sandy stromatolitic dolomite deposited in supratidal environment. Paleocurrents from Siberian craton.
	Uchur	X0424, X0426, X0433, PN-1	Nonconformably above basement. Lower: quartz arenite, shale, and sandy dolomite deposited in a fluvial to open marine environment; upper: 1-8m thick quartzose arenite-shale-dolostone cycles deposited in lagoonal or lacustrine environment.
White-Inyo	Campito	n/a	Unconformably above Deep Spring. Lower: Andrews Mountain Member contains olenellid trilobites that closely resemble SE Siberian trilobite *Repinaella* (Hollingsworth, 2005); upper: Montenegro Member contains first occurrence of Laurentian archeocyathids (Corsetti, 1998).
	Deep Spring	DSM, JSMD0301, JSMD0302	Formally divided into Lower, Middle, and Upper Members (Dienger, 1986; Gevirtzman and Mount, 1986; Greene, 1988), each representing a "Grand Cycle" of siliciclastic lower half-cycle and carbonate upper half-cycle. Precambrian-Cambrian boundary lies within this formation.

White-Inyo	Reed	n/a	Unconformably above Wyman. Lower: subtidal to intertidal layers of oolitic and stromatolitic pink dolomite; Hines Tongue: cross-bedded sandstone and siltstone; upper: massive dolomite with minor karstification and cloudinids (Grant, 1990).
	Wyman	WYSS, JSWI0301	Base not exposed. Predominantly siliciclastics deposited in shallow marine environment. Timing of deposition poorly constrained to probably Neoproterozoic based on simple trace fossils (Alpert, 1976).
Death Valley	Zabriskie	ZQ	Conformably above Wood Canyon. Deposited in a near-shore environment with braidplain deposits and lagoonal/tidal flat deposits.
	Wood Canyon	WC1, WC2	Conformably above Stirling. Lower: intertidal to subtidal siliciclastic and carbonate units with Ediacaran fossils; middle: deposited in terrestrial braidplain setting (Diehl, 1974); upper: siliciclastics and carbonates that contain first definite Cambrian fossils, including trilobites *Fallotaspis, Nevadella,* and *Bonnia-Olenellus* (Corsetti, 1998).
	Stirling	JSPR0303	Quartzite and siltstone with minor carbonates, deposited in a fluvial to marine setting (Wertz, 1992). Contains Neoproterozoic *Cloudina*-like shelly fossils (Languille, 1974a and b).
	Johnnie	Jojo	Unconformably above Noonday. Consists of several siliciclastic and carbonate members.
	Noonday	n/a	Conformably and unconformably above Kingston Peak. Interpreted as post-glacial cap-carbonate, but its age and tectonic setting are poorly constrained between 1080 Ma mafic sills in Crystal Spring Formation and Precambrian-Cambrian boundary in Wood Canyon Formation.
	Kingston Peak	KP, JSPR0301, JSDV0301	Transitional sequence of turbidite beds forms the contact between Kingston Peak and Beck Spring. Kingston Peak contains siliciclastics with rare carbonates and volcanics deposited during active extensional tectonics (Labotka and Albee, 1977; Miller, 1987), and possibly during glacial periods (Miller, 1983, 1985, 1987). Age of deposition is poorly constrained by lithostratigraphic correlation of diamictite units with Sturtian (~750 Ma) and Marinoan (~635 Ma) glacial events (Hoffman, 1998, 2004).
	Beck Spring	n/a	Gradational contact between Beck Spring and Crystal Spring. Beck Spring is a massive dolomite dominated by cryptalgal laminites, stromatolites, and grainstones. Transition of alternating shale, siltstone, and dolostone records a subtidal to supratidal depositional environment in which a shallow carbonate shelf developed (Wright et al., 1976).

D.V.	Crystal Spring	JS04KR1C	Nonconformably above basement. Roberts (1974; 1982) divided the Crystal Spring Formation into seven sedimentary members with ~450 meters of diabase sills, two of which have been dated at 1087±3 and 1069±3 Ma (Heaman and Grotzinger, 1992). The age of deposition is between the underlying 1400 Ma basement and ~1087 Ma. An unconformity above the algal member is overlain by a 10cm thick conglomerate, informally termed the Excelsior Conglomerate (Sears et al., 2005; MacLean et al., in review), from a mine in the Kingston Range.
Grand Canyon	Tapeats	TS	Unconformably above Sixtymile. Precambrian-Cambrian boundary lies within unconformity. Tapeats Sandstone consists of sand and conglomerate deposited in a shallow marine environment, and it contains Middle Cambrian trilobites.
	Sixtymile	n/a	Contains siltstone and sandstone. It has been interpreted as being associated with Neoproterozoic glacial sequences (Levy et al., 1994), and has been correlated with glaciogenic rocks of the Death Valley succession and the Windermere Supergroup (Link et al., 1993).
	Chuar	n/a	Unconformably above Nankoweap. Deposited in an intracratonic basin associated with extension related to the breakup of Rodinia. It consists of alternating siliciclastic and carbonate units of the Galeros and Kwagunt Formations. Its age of deposition is constrained by the Cardenas Basalt below and an ash bed (742±6 Ma) from the upper Kwagunt Formation (Karlstrom et al., 2000).
	Nankoweap	K00-53-3 Nankoweap	Unconformably above Unkar. Quartzitic sandstones and mudstones deposited in a moderate- to low-energy, shallow-water environment (Elston and Scott, 1976; Gebel, 1978). It separates the underlying Unkar Group from the overlying Chuar Group.
	Unkar	LC-02-81-2 Hakatai, T01-75-4 Shinumo, T02-75-1z Dox	Nonconformably above basement. Contains in ascending order: 1) the Bass Formation, deposited during repeated subaerial exposure and flooding in a low-energy transgressive environment (Dalton, 1972; Beus et al., 1974; Hendricks and Stevenson, 1990); 2) the Hakatai Shale, deposited in a marginal-marine/tidal-flat environment (Reed, 1976); 3) the Shinumo Sandstone, deposited in a nearshore, marginal marine, and/or fluvial/deltaic environment (Daneker, 1975); 4) the Dox Formation, deposited in a marginal marine deltaic to tidal flat sequence (Timmons et al., 2005); and 5) the Cardenas Basalt, a ~300 meter thick igneous unit dated by Larson et al. (1994) to 1103±66 Ma based on Rb/Sr data.

2.2.4 Death Valley region

The Proterozoic to Early Cambrian Death Valley succession is exposed in isolated ranges in SE California. In ascending order, it consists of the Crystal Spring Formation, Beck Spring Formation, and Kingston Peak Formation of the Pahrump Group, and the overlying Noonday Dolomite, Johnnie, the Stirling Quartzite, and Wood Canyon formations (Figure 2.2 and Table 2.1). Ages of deposition are poorly constrained. The Crystal Spring and Beck Spring formations represent a cratonic cover sequence that was dismembered during extensional tectonism associated with the deposition of the middle to upper Kingston Peak Formation (Wernicke et al., 1988; Levy and Christie-Blick, 1989). The Kingston Peak Formation has been the subject of recent research with regard to the Snowball Earth hypothesis (e.g. Hoffman, 1989). Units overlying the Kingston Peak Formation represent the rift-to-drift phase of deposition.

2.2.5 Grand Canyon region

The Grand Canyon Supergroup, exposed in fault-bounded remnants in the Grand Canyon region of Arizona, rests on basement metamorphic and igneous rocks. It consists of the Mesoproterozoic Unkar Group, the Nankoweap Formation, the Neoproterozoic Chuar Group, and the Sixtymile Formation. These sediments are unconformably overlain by the Middle Cambrian Tapeats Sandstone (Figure 2.2 and Table 2.1). The Unkar Group and lower Nankoweap Formation were deposited in an environment affected by far-field stresses related to Grenville-age orogenesis, including NW shortening and orthogonal NE-SW extension (Timmons et al., 2005). Subsequent deposition occurred in an intracratonic extensional basin associated with the breakup of Rodinia (Weil et al., 2003).

2.3 Analytical Methods

Our interpretations are based on detrital-zircon geochronology studies reported by several independent research groups, including Rainbird et al. (1998), Khudoley et al. (2001), Stewart et al. (2001), Vogel (2004), Timmons et al. (2005), and MacLean et al. (*in review*). All U-Pb isotopic analyses were performed using standard ID-TIMS, SHRIMP, or LAICPMS techniques explained in detail within each respective article. Table 2.2 shows which samples from each location were analyzed by each research group, and which methods were used. By convention, all detrital-zircon ages are reported here at a 1σ confidence level.

Recent articles (e.g. Cawood et al., 2003; Andersen, 2005; Moecher and Samson, 2006) have discussed limitations concerning the assumptions that detrital-zircon modes accurately discriminate provenance terranes and that the relative proportion of modes accurately reproduces mass balance of sediment from source to basin. These limitations are important to consider when determining which sources contributed to the basin. However, our model is based on the proportion of Grenville-age zircons through space and time. It is therefore not necessary that the detrital-zircon modes accurately reflect the proportion of mass balance from all potential source terranes. It is only necessary that all source terranes were already in place at the time of deposition, and that we are comparing the percentage of Grenville-age zircons in each location at different stratigraphic levels. The possibility that the Grenville orogeny resulted in anomalously different zircon content in comparison to other potential source terranes is not relevant to our comparisons.

2.4 Results

It has been customary in recent literature to report detrital-zircon geochronology data with histograms and/or probability density distributions (see Fedo et al., 2003). We

Table 2.2. List of samples, instruments, and sources used in this chapter.

SETTE DABAN	*icp*	*shrimp*
Yudoma (172)		
X0415 *a*	22	32
X0416 *a*	21	29
X0418 *a*	29	
X0419 *a*	25	
X0432 *a*		14
Uy (82)		
C3 *a*	17	
MLS1 *a*		31
MM1 *f*		34
basinal Kerpyl (100)		
TT2 *d*		34
X0423 *a*	26	40
rest of Kerpyl (170)		
TT3 *a*		43
TT4 *a*	27	
Aimchan (73)		
X0421 *a*		39
X0434 *a*		34
Uchur (113)		
PN1 *d*		25
X0426 *a*	24	
X0433 *a*	20	27
X0424 *a*		17

WHITE-INYO	*icp*	*shrimp*
Deep Spring (127)		
DSM *c*		61
JSMD0301 *a*		11
JSMD0302 *a*	19	
Wyman (78)		
JSWI0301 *a*	17	36
WYSS *c*	61	

DEATH VALLEY	*icp*	*shrimp*	*tims*
Zabriskie (22)			
ZQ *e*			22
Wood Canyon (44)			
WC1 *e*			22
WC2 *e*			22
Stirling (13)			
JSPR0303 *a*	13		
Johnnie (60)			
Jojo *c*	60		
Kingston Peak (85)			
KP *c*	62		
JSPR0301 *a*	23		
JSDV0301 *a*		25	
Crystal Spring (73)			
JS04KR1C *a*	12	36	

GRAND CANYON	*icp*	*tims*
Tapeats (22)		
TS *e*		22
Nankoweap (85)		
K00-53-3 Nankoweap *b*	85	
Unkar (276)		
LC-02-81-2 Hakatai *b*	85	
T01-75-4 Shinuma *b*	89	
T02-75-1Z Dox *b*	93	

a - MacLean et al., *in review*
b - Timmons et al., 2005
c - Vogel, 2004
d - Khudoley et al., 2001
e - Stewart et al., 2001
f - Rainbird et al., 1998

present data from relevant samples in the form of cumulative percent distributions to show more clearly temporal relationships concerning certain provenance fluxes. The general cumulative percent distribution trends of samples from each formation are approximately equivalent, so in some cases we have combined data from multiple samples from a particular sedimentary formation for display simplicity. One graph is provided for each geographic region, with several stratigraphic levels represented in each graph. Data are organized according to three general periods of deposition: Early Mesoproterozoic through Middle Mesoproterozoic (~1600-1200 Ma), Late Mesoproterozoic through Middle Neoproterozoic (~1200-630 Ma), and Late Neoproterozoic through Middle Cambrian (~630-500 Ma). Table 2.2 and the following sections describe the number of zircon grains per sample used for each cumulative percent distribution.

2.4.1 Sette Daban samples

We plotted data from four Uchur samples, two Aimchan samples, two Kerpyl samples, three Uy samples, and five Yudoma samples (Table 2.2). Figure 2.3A shows cumulative percent distributions for the five stratigraphic levels from the Sette Daban region. The Uchur and Aimchan Groups were deposited during Early Mesoproterozoic through Middle Mesoproterozoic (~1600-1200 Ma). Although this time period overlaps slightly with the Grenville orogeny (~1300-950 Ma) as determined by zircon provenance relationships, Grenville-age zircons do not occur. The Uchur and Aimchan Groups exhibit detrital-zircon patterns indicative of exclusively Siberian or unknown provenance. The Kerpyl and Uy Groups were deposited during Late Mesoproterozoic through Middle Neoproterozoic (~1200-630 Ma), and they both contain Grenville-age zircons. The Uy Group has a greater proportion of Grenville-age zircons than the Kerpyl Group, indicating an increase of Grenvillian input through time. The Uy Group contains zircons dominated by Laurentian sources. The Yudoma Group was deposited during Late

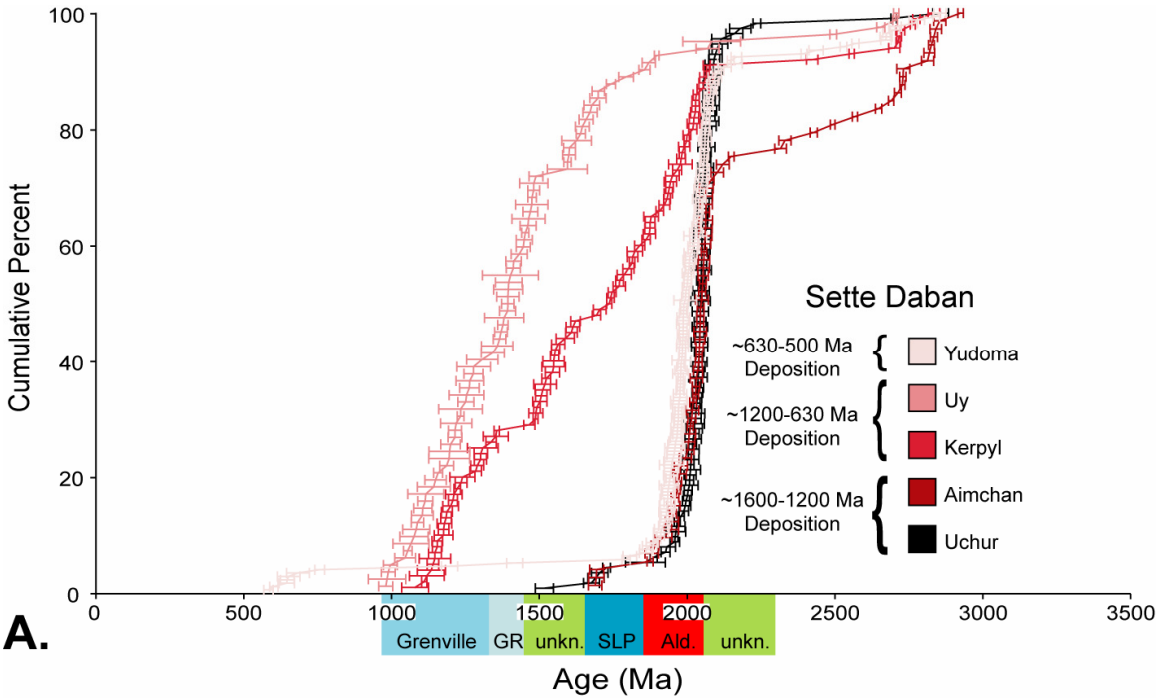
A.
Cumulative Percent
Age (Ma)
Sette Daban
~630-500 Ma Deposition
Yudoma
~1200-630 Ma Deposition
Uy
Kerpyl
~1600-1200 Ma Deposition
Aimchan
Uchur
Grenville
GR
unkn.
SLP
Ald.
unkn.

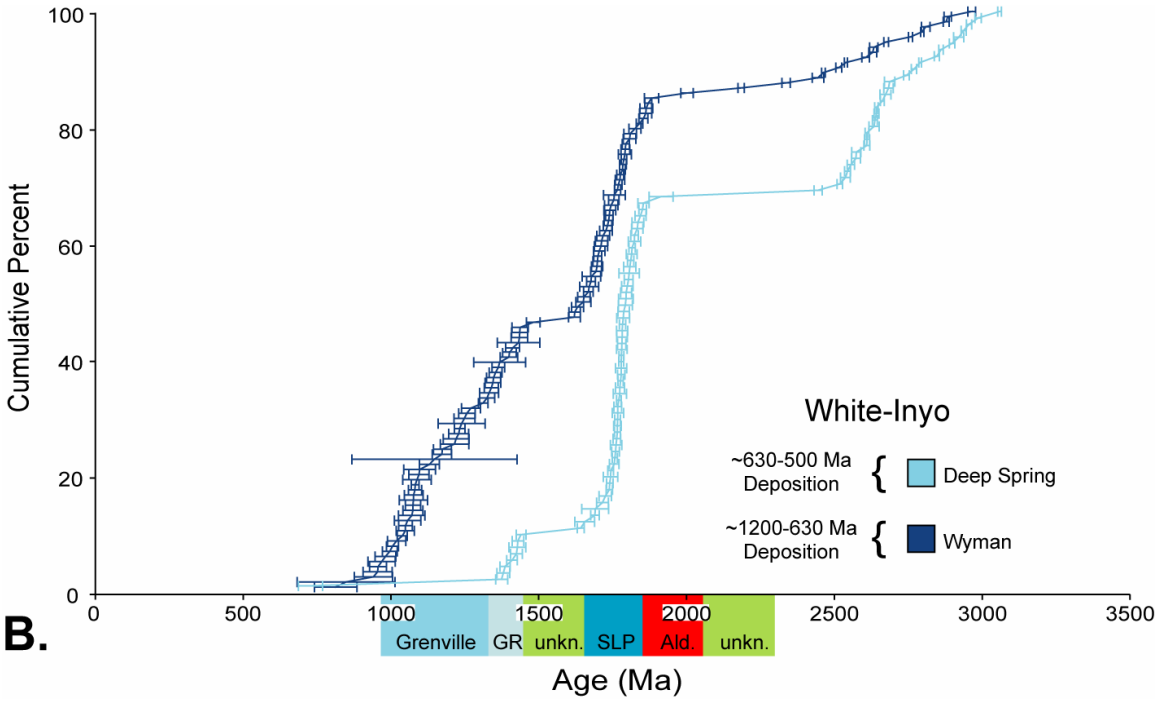
B.
Cumulative Percent
Age (Ma)
White-Inyo
~630-500 Ma Deposition
Deep Spring
~1200-630 Ma Deposition
Wyman
Grenville
GR
unkn.
SLP
Ald.
unkn.

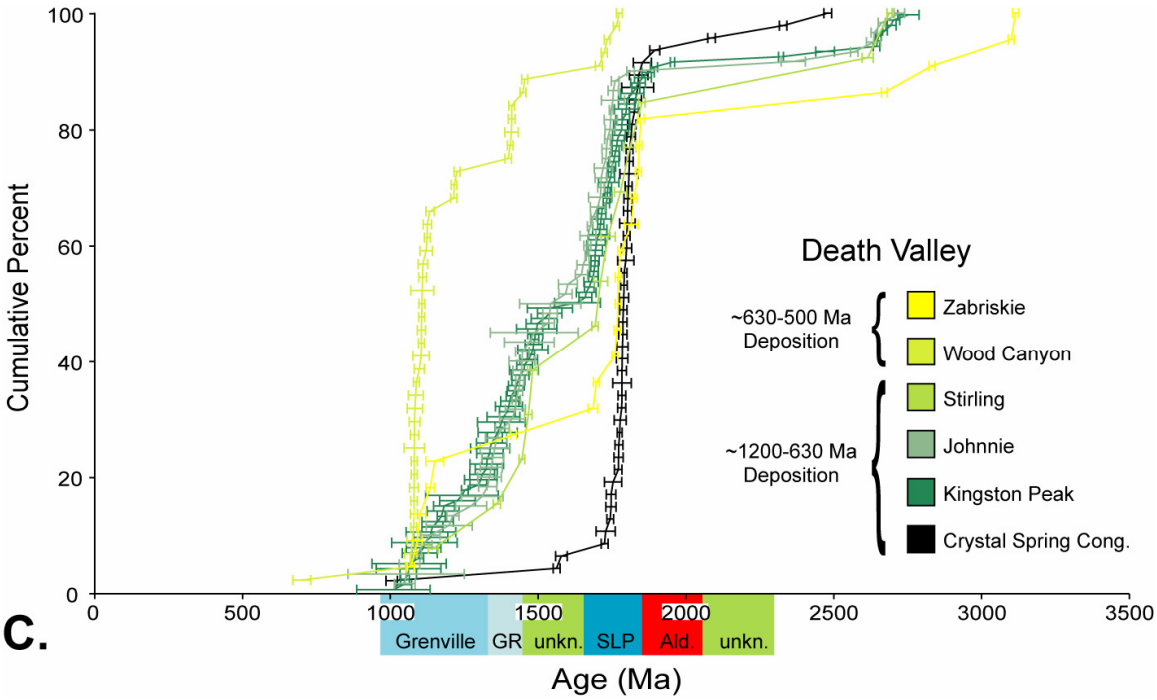
Cumulative Percent
100
80
60
40
20
0
0
500
1000
1500
2000
2500
3000
3500
Grenville
GR
unkn.
SLP
Ald.
unkn.
Age (Ma)
Death Valley
~630-500 Ma Deposition
Zabriskie
Wood Canyon
~1200-630 Ma Deposition
Stirling
Johnnie
Kingston Peak
Crystal Spring Cong.

C.

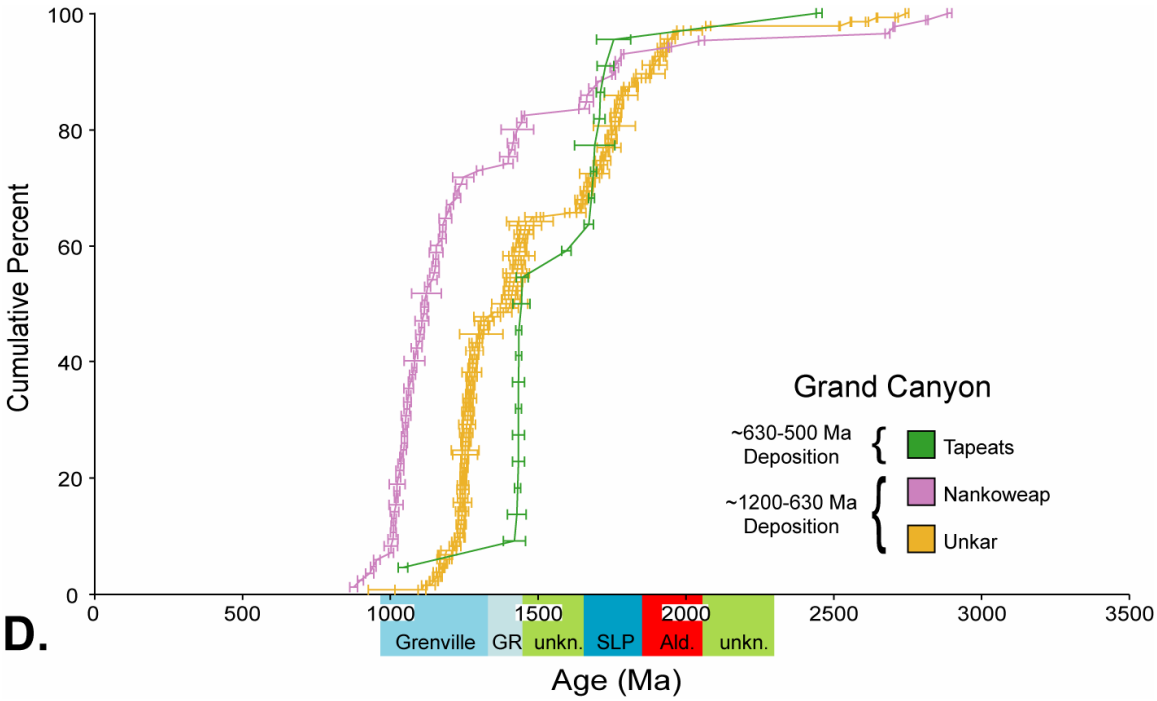
Cumulative Percent
100
80
60
40
20
0
0
500
1000
1500
2000
2500
3000
3500
Grenville
GR
unkn.
SLP
Ald.
unkn.
Age (Ma)
Grand Canyon
~630-500 Ma Deposition
Tapeats
~1200-630 Ma Deposition
Nankoweap
Unkar

D.

Figure 2.3. Cumulative percent distributions of detrital-zircon ages from four regions. Colors differentiate periods of deposition. Probable provenance terranes discussed in Chapter 1 are shown on x-axis. A) Sette Daban distribution showing distinct Siberian distributions for pre-, syn-, and post-Grenvillian influence; B) White-Inyo distribution showing two distinct patterns for Grenvillian influence and post-Grenvillian influence, respectively; C) Death Valley distribution showing more complicated pattern in which Grenvillian input generally increases until Zabriskie deposition; D) Grand Canyon distribution showing increase in Grenvillian input until Tapeats deposition. All data is reported in Rainbird et al. (1998), Khudoley et al. (2001), Stewart et al. (2001), Vogel (2004), Timmons et al. (2005), and MacLean et al. (Chapter 1 and *in review*).

Neoproterozoic through Early Cambrian (~630-530 Ma). It contains zircons almost exclusively from Siberian sources, suggesting that rifting had progressed to the point that non-Siberian sediment did not cross the axis of the basin.

2.4.2 White-Inyo samples

We plotted data from two Wyman Formation samples and from three Deep Spring Formation samples (Table 2.2). Figure 2.3b shows cumulative percent distributions for each stratigraphic level from the White-Inyo region. The Wyman Formation, deposited during Late Mesoproterozoic to Middle Neoproterozoic, exhibits a high percentage of Grenville-age zircons. This indicates that at the poorly constrained time of Wyman deposition, a major source of zircon input was from the Grenville orogen. The Deep Spring Formation was deposited during the Late Neoproterozoic to Early Cambrian. Contrary to the Wyman, the Deep Spring contains remarkably few Grenville-age zircons, but does contain zircons from other common Laurentian sources, such as

the Granite-Rhyolite and the SW Laurentian Paleoproterozoic terranes. The shift away from Grenvillian influence is remarkably similar to that of the Siberian samples.

2.4.3 Death Valley samples

We plotted data from two Crystal Spring samples, two Kingston Peak samples, and two Wood Canyon samples, and we used one sample for the Johnnie Formation, the Stirling Quartzite, and the Zabriskie Quartzite (Table 2.2). Figure 2.3c shows cumulative percent distributions for the six stratigraphic levels from the Death Valley region. The upper Crystal Spring, the Kingston Peak, Johnnie, and Stirling Formations were deposited during Late Mesoproterozoic to Middle Neoproterozoic. Grenville-age zircons are sparse in our Crystal Spring samples, but others have found Grenville-age zircons in Crystal Spring samples (Karl Karlstrom, personal communication of unpublished data). The lack of Grenville abundance in our Crystal Spring sample may be due to the provenance of the Excelsior Conglomerate, which requires further study. The distributions of the Kingston Peak, Johnnie, and Stirling data are basically identical, with a large percentage of Grenville-age zircons, Granite-Rhyolite zircons, and zircons from an unknown source. The Wood Canyon and Zabriskie Formations were deposited during the Late Neoproterozoic to Early Cambrian. The Wood Canyon analyses yielded an anomalously high percentage of Grenville-age zircons, indicating a noteworthy flux of sediment from Grenville sources. The distribution of Zabriskie section most closely resembles that of the Crystal Spring Formation, with zircons primarily from the SW Paleoproterozoic terranes, and few Grenville-age and Granite-Rhyolite-age zircons. These six zircon distributions reveal a relative increase in Grenville input through time until the deposition of the Zabriskie, at which time the SW Paleoproterozoic terranes dominated zircon input. Again, this pattern is strikingly similar to Figures 2.3A and 2.3B.

2.4.4 Grand Canyon samples

We plotted data from three Unkar Group samples, and we usedonesample for the Nankoweap Formation and for the Tapeats Sandstone (Table 2.2). Figure 2.3D shows cumulative percent distributions for the three stratigraphic levels from the Grand Canyon region. The Unkar and Nankoweap were deposited during Late Mesoproterozoic to Middle Neoproterozoic time. The Unkar Group distribution reveals a major proportion of Grenville-age zircons, probably related to the Grand Canyon's close proximity to the Grenville orogen. The Nankoweap analyses yielded a distribution of ages nearly identical to the anomalous distribution of Death Valley's Wood Canyon Formation. This could indicate a similar, albeit older, flux of sediment from Grenville sources. The Tapeats Sandstone was deposited during Middle Cambrian time. There is a significant gap in time between the Nankoweap Formation and the Tapeats Sandstone for which we have no detrital-zircon data. Despite this lack of data, it is apparent that the Grenville input increased through time from the Unkar Group to the Nankoweap Formation, but basically ceased by the deposition of the Tapeats Sandstone. The pattern follows that of the other three sites (Figures 2.3A, 2.3B, and 2.3C).

2.5 Discussion

An important outcome of this study concerns the influx of Grenville-age (~1300-950 Ma) zircons, and to a lesser extent Granite-Rhyolite-age (~1450-1300 Ma) zircons, through time and space. Sette Daban's Uchur and Aimchan Groups did not collect Grenville-age zircons. Death Valley's Crystal Spring Formation (pre-Late Mesoproterozoic deposition) may have collected Grenville-age zircons, and did collect 1650-1450 Ma zircons that came from a foreign craton, possibly Australia (Sears and Price, 2003; Sears, 2007). All four regions experienced an influx of Grenville- and Granite-Rhyolite-age zircons during Late Mesoproterozoic through Middle

Neoproterozoic sedimentation. Then they all experienced a significant decline in Grenville-age zircon input in the Latest Neoproterozoic to Middle Cambrian.

These observations lead to a new tectono-sedimentary evolution model of the SE Siberia – SW Laurentia region during Proterozoic through Middle Cambrian time. The model involves major control of the Grenville orogenic belt over the evolution of the sedimentary basin centered on the margin between the two cratons. The Grenville orogenic belt records over 300 million years of orogenic activity. A series of tectonic events occurred along the southern margin of Laurentia, beginning with ~1400-1350 Ma continental rifting that resulted in rhyolite flows, welded ash-flow tuffs, and shallow sea clastic sedimentation (Mosher, 1998). Continued extension and an encroaching island arc with northward-dipping subduction contributed to a ~1350-1300 Ma backarc basin consisting of diabase and granodiorite intrusions, felsic volcanism, and shallow-marine sedimentation. The formation of the island arc occurred at ~1326-1275 Ma (Mosher, 1998). A north-dipping continental margin arc produced magmatism at ~1260-1232 Ma as a second island arc and a postulated but unknown continental landmass encroached from the south (Mosher, 1998). Collision of the unknown continent with Laurentia occurred at ~1150-1120 Ma, resulting in polyphase deformation and metamorphism. Thrusting continued from ~1120 to ~1080 Ma, greatly thickening the crust (Mosher, 1998).

Middle Proterozoic igneous activity was prevalent in California, Arizona, Colorado, New Mexico, and Texas (~1250-1075 Ma). These events were approximately synchronous with the Grenville orogeny and the formation of the Midcontinent Rift System (1109-1086 Ma) (Adams and Keller, 1994). The early Phanerozoic experienced the formation of the south-southwestern-trending backbone of the Transcontinental Arch (Carlson, 1999), possibly along tectonic zones produced in the Proterozoic. Cather et al. (2006) discussed the prolonged tectonic history of the Picuris-Pecos fault, a prominent

north-south trending strike-slip feature in central New Mexico and southern Colorado that was repeatedly reactivated from Mesoproterozoic to Cenozoic time, including during Grenville time, ~700 Ma rifting, and ~550 Ma rifting. We suggest that the Grenville orogen and the extensional basins are related, and that they both played key roles in the sedimentation history in SW Laurentia and SE Siberia.

2.5.1 Early-Middle Mesoproterozoic (~1600-1200 Ma)

This study addresses two sedimentary sections deposited during the Early and Middle Mesoproterozoic—the Uchur and Aimchan Groups of the Sette Daban region. The Uchur Group was deposited as cratonal cover in Siberia, perhaps equivalent to Arizona's Mazatzal Quartzite. During Uchur and Aimchan deposition, sediments may have been transported from Australia (SW of our study area), along the intracratonic rift, and into the Belt-Purcell basin (Sears, 2007). The Uchur and Aimchan Groups were deposited before the Grenville orogeny, so they collected sediment primarily from the Siberian Craton, with very minor input from other sources (Figure 2.4A).

2.5.2 Late Mesoproterozoic through Middle Neoproterozoic (~1200-630 Ma)

All four regions discussed in this text contain sediments deposited during Late Mesoproterozoic through Middle Neoproterozoic time. All sedimentary sections, including the Sette Daban section of Siberia, contain Grenville-age zircons. Grenville input appears to proportionally increase through time in the Sette Daban, Death Valley, and Grand Canyon regions.

In light of the severe crustal thickening during the late stages of S Laurentian Grenville orogenesis, we interpret the sediments to have been deposited in a foreland basin that encompassed the entire SE Siberia – SW Laurentia region (Figure 2.4B). The foreland basin represented the base of a pediment surface—a vast, low-relief plain that descended exponentially from the tectonic highlands of the Grenville front to sea level. Pediment surfaces appear to have been characteristic features prior to the colonization

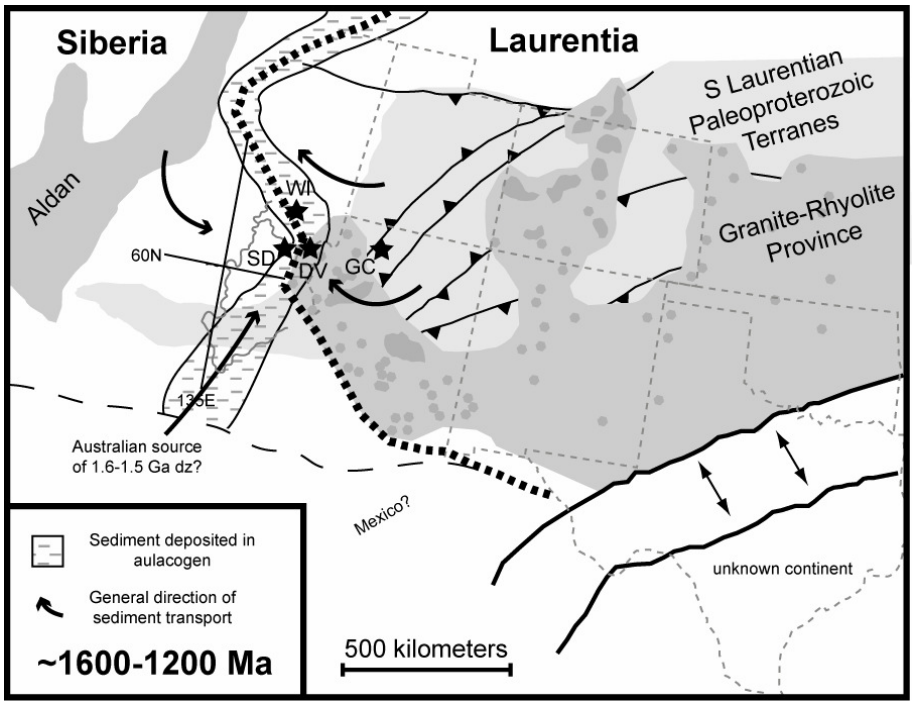
Siberia
Laurentia
S Laurentian
Paleoproterozoic
Terranes
Granite-Rhyolite
Province
Aldan
WI
SD
DV
GC
60N
135E
Australian source
of 1.6-1.5 Ga dz?
Mexico?
unknown continent
Sediment deposited in
aulacogen
General direction of
sediment transport
~1600-1200 Ma
500 kilometers

A.

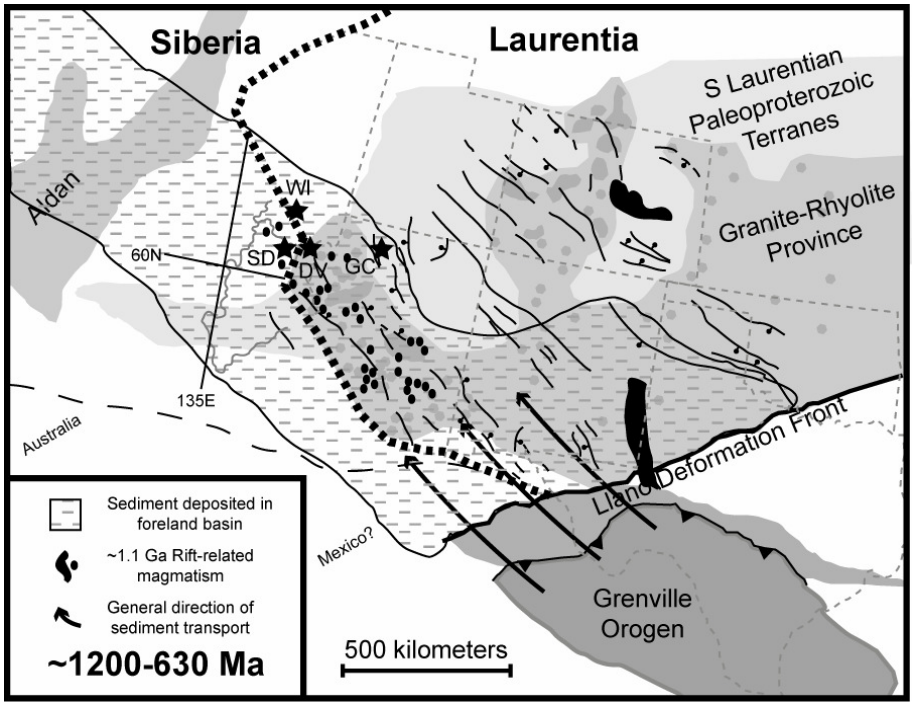
Siberia
Laurentia
S Laurentian
Paleoproterozoic
Terranes
Granite-Rhyolite
Province
Aldan
WI
SD
DV
GC
60N
135E
Australia
Llano Deformation Front
Mexico?
Grenville
Orogen
Sediment deposited in
foreland basin
~1.1 Ga Rift-related
magmatism
General direction of
sediment transport
~1200-630 Ma
500 kilometers

B.

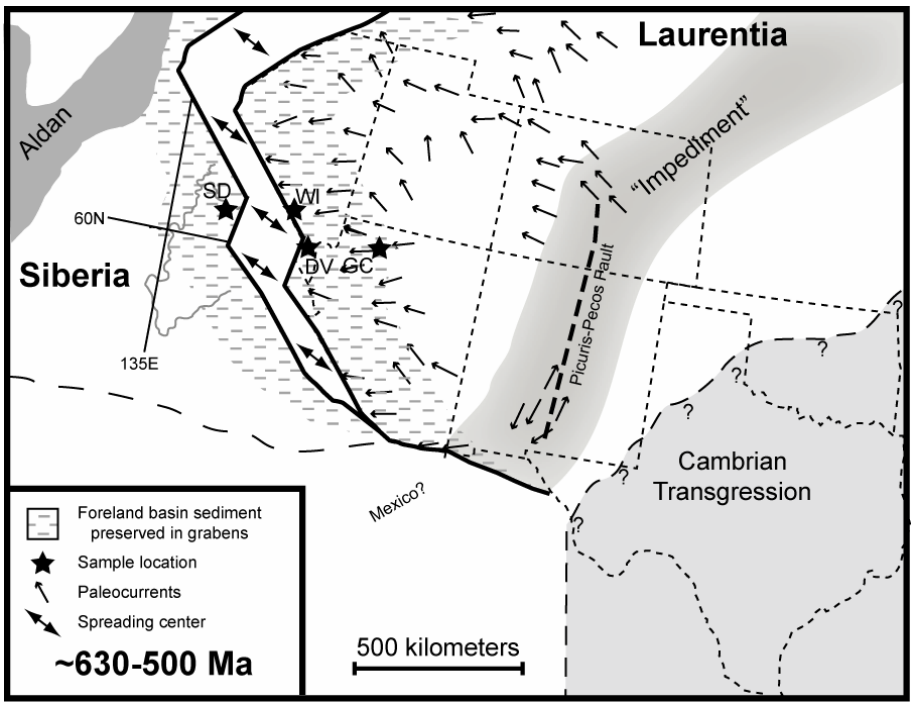

C.

Figure 2.4. SE Siberia – SW Laurentia tectono-sedimentary model at three time periods. A) ~1600-1200 Ma: Intracratonic rift along future Siberia – Laurentia margin funneled sediments possibly from Australia (Sears and Price, 2003; Sears, 2007). Uchur and Aimchan groups were deposited before Grenville orogeny. Sediment was not allowed to cross axis of basin. S Laurentian Paleoproterozoic Terranes and Granite-Rhyolite Province locations from Karlstrom and Humphries (1998); southern margin rift from Mosher (1998); intracratonic rift from Sears (2007). B) ~1200-630 Ma: Grenville orogenic belt thickened crust during continent-continent collision. Grenville foreland basin formed across SE Siberia – SW Laurentia region. Entire region experienced sedimentation directed from Grenville orogen. Extensional environments perpendicular to Llano deformation front augmented sediment transport to west and later preserved foreland basin sediments. Grenville orogen locations from Mosher (1998); extension-related faults and magmatism from Timmons et al. (2005). C) ~630-500 Ma: Rift between E Siberia and W Laurentia succeeded. Transportation of sediments across margin and into Siberia ceased. Termination of Grenvillian input in SW Laurentia could be due to: "impediment" associated with Picuris-Pecos Fault (Cather et al., 2006), Transcontinental Arch (Carlson, 1999), or W Texas segment of Midcontinent rift system (Adams and Miller, 1995) blocked sediment transport, or could be due to Cambrian Sea transgression over Grenville orogen. Generalized paleocurrents from Seeland (1968).

of land by Devonian plants (Sears, 2007). The flexure of the crust in response to Grenville thickening was such that Siberian paleocurrent directions were reversed, allowing sediments to travel across the pediment surface, down the axis of the rift basin, and into Siberia. The fact that almost all sediment deposited in the Sette Daban region during Uy Group deposition had Laurentian provenance leads to our interpretation.

The Neoproterozoic foreland basin sediments, typically susceptible to future erosion, were preserved in the SE Siberia – SW Laurentia basin because extension during Uy and Kingston Peak deposition changed the architecture of the basin. Figure 2.4B shows significant NW-SE oriented normal faults and sill swarms (~1250-1075 Ma) that were likely caused during extension perpendicular to the Grenville deformation front. The extension-related magmatism has been interpreted as a splay off the Midcontinent Rift System (Adams and Keller, 1994), which also could have resulted from Grenville compression as an impactogen. The extension could have augmented the foreland basin sediment transport by funneling sediment to the NW. Such extension perpendicular to continent-continent collisional stress is a common occurrence in Phanerozoic tectonic environments such as the Ouachita-Marathon orogen and their respective Anadarko and Delaware extensional basins in SW USA (Kluth and Coney, 1981), the China-Mongolia Late Mesozoic rift system (Meng et al., 2003), and the European Cenozoic rift system (Dèzes et al., 2004).

2.5.3 Late Neoproterozoic through Early Cambrian (~630-500 Ma)

In all regions, Grenville input greatly decreased or completely ceased near the Precambrian-Cambrian boundary. In the Sette Daban region of Siberia, the distribution of zircon ages of the Yudoma Group returned to its pre-foreland basin character, absent of Laurentian provenance. The distribution of the White-Inyo section's Deep Spring Formation is dominated by SW Paleoproterozoic Terrane provenance, with a minor signal of Granite-Rhyolite source. Grenville-age zircons are virtually absent. The Wood

Canyon Formation of the Death Valley region includes the Precambrian-Cambrian boundary and contains a flux of Grenville-age zircons, with minor input from other Laurentian sources. The Zabriskie Quartzite, however, lies conformably above the Wood Canyon Formation and contains a much smaller distribution of Grenville-age zircons. In the Grand Canyon section, the Middle Cambrian Tapeats Sandstone is virtually absent of Grenville-age zircons.

We interpret Siberia's late Neoproterozoic absence of all Laurentian sources to indicate post-rift sedimentation (Figure 2.4C-D). A new mid-ocean ridge between Siberia and Laurentia prevented sediment transport across the basin axis. Thermal subsidence of Siberia's rifted margin resulted in paleocurrent direction reversal such that the Yudoma Group received sediment strictly from the west and possibly southwest.

Two possible scenarios could explain the absence of Grenville-age zircons in the three Laurentian regions. The first scenario involves a disturbance in the pediment surface funneling Grenville sediment into the foreland basin (Figure 2.4C). Among the possible geologic features that could have served as the "impediment" are: the raised rift shoulders of the W Texas segment of the Midcontinent rift system (Adams and Keller, 1994); the repeatedly reactivated Picuris-Pecos fault in New Mexico and southern Colorado (Cather et al., 2006); and the early Phanerozoic initiation of the Transcontinental Arch (Carlson, 1999).

The second scenario involves thermal subsidence of the Grenville front and flooding from the east by the transgressing Cambrian intercontinental seaway (Figure 2.4D). Thomas et al. (1991) reported that East Laurentia also experienced rifting during Early Cambrian time, leading to thermal subsidence and westward transgression. Such flooding would terminate Grenville erosion, thereby ceasing deposition of Grenville-age zircons. The rate of transgression was high both on a global scale due to increased rates of seafloor spreading associated with the breakup of Rodinia, and on a regional

scale due to thermal subsidence of the rifted margins of Siberia and Laurentia. Basement uplifts north of the Llano Front could have allowed erosion of the S Laurentian Paleoproterozoic terranes and the Granite-Rhyolite Province to provide the dominant sediment source for the SW Laurentian region.

2.6 Conclusions

An accurate plate reconstruction allows additional interpretations to be made by combining data from two or more cratons. In this study, we propose a new tectono-sedimentary evolution for the SE Siberia – SW Laurentia region based on detrital-zircon geochronology data from Siberia's Sette Daban region and Laurentia's White-Inyo, Death Valley, and Grand Canyon regions. The model includes three periods of distinct sedimentation controlled by tectonic activity during the Grenville orogeny and the breakup of Rodinia. The stages of sedimentation are: 1) intracratonic rift sedimentation during Early and Middle Mesoproterozoic time; 2) foreland basin sedimentation in a rift basin resulting from severe thickening of the crust and impactogen-related extension sub-perpendicular to thrusting during continent-continent collision of the Grenville orogeny during Late Mesoproterozoic and Early Neoproterozoic time; and 3) post Rodinia-breakup passive margin sedimentation devoid of Grenville-sourced sediment in Siberia due to continental separation, and in Laurentia due to either an "impediment" or the transgression of the Cambrian Intercontinental Sea over the southern Grenville province near the Precambrian-Cambrian boundary. The pattern observed in this study of 1) pre-orogen sedimentation dominated by local basement sources; 2) syn-orogen sedimentation dominated by orogenic sources; and 3) post-orogen sedimentation dominated once again by local basement sources, may be characteristic of other sedimentary settings associated with nearby orogenic activity.

CHAPTER 3

SANDSTONE FRAMEWORK COMPOSITION ANALYSES THAT STRENGTHEN DETRITAL-ZIRCON PROVENANCE INTERPRETATIONS OF THE SE SIBERIA – SW LAURENTIA REGION DURING RODINIA BREAKUP: A MENTORSHIP PROJECT BETWEEN UM GEOSCIENCE DEPARTMENT AND BIG SKY HIGH SCHOOL

3.1 Introduction

In Chapters 1 and 2, detrital-zircon geochronology data were used to test lithostratigraphic correlations between Sette Daban sediments and Death Valley/White-Inyo sediments pertinent to the E Siberia – W Laurentia Rodinia reconstruction (Sears et al., 2005). We have found that provenance information garnered from SE Siberian and SW Laurentian detrital zircons not only support the Rodinia reconstruction, but also strengthen details of the region's tectono-sedimentary evolution.

Dickinson and Gehrels (2000) combined detrital-zircon geochronology analyses with petrographic analyses of sandstones from Paleozoic and Triassic strata in an effort to characterize provenance relationships and revise paleotectonic hypotheses in a region of severe structural deformation. They found that combining the two types of analyses clarified information provided by each dataset. When considered together, the two techniques allow a greater scope for interpretation than either considered alone. In a comprehensive study of Proterozoic sediments in SE Siberia, Khudoley et al. (2001) combined preliminary detrital-zircon data with petrographic analyses to better understand provenance relationships. They reported ternary diagrams (Dickinson and Suczek, 1979) showing composition of Proterozoic sandstones based on quantitative estimation of detrital modes. We performed point count analyses on Laurentian sediments that are thought to correlate with Siberian units (Sears et al., 2005), to further

test correlations and provenance relationships. This chapter presents our new petrographic results under the lens of the detrital-zircon geochronology data presented in Chapters 1 and 2.

3.2 Geologic setting

In the E Siberia – W Laurentia reconstruction (see Sears and Price, 2003), Proterozoic rift-related siliciclastic-carbonate cycles in the Sette Daban region, SE Siberia, are juxtaposed against similar Proterozoic rift-related sediments in the White-Inyo and Death Valley regions of SW Laurentia. Strata are listed here in ascending order: Siberia—Uchur Group, Aimchan Group, Kerpyl Group, Uy Group, and Yudoma Group; White-Inyo—Wyman Formation, Reed Dolomite, and Deep Spring Formation; Death Valley—Crystal Spring Formation, Beck Spring Formation, Kingston Peak Formation, Noonday Dolomite, Johnnie Formation, Stirling Quartzite, Wood Canyon Formation, and Zabriskie Quartzite. Detailed descriptions of each unit are provided in Chapters 1 and 2 of this dissertation.

A Proterozoic through Middle Cambrian tectono-sedimentary evolution model for the SE Siberia – SW Laurentia region is presented in Chapter 2. The model, based on detrital-zircon geochronology data from samples collected from the Sette Daban, White-Inyo, Death Valley, and Grand Canyon regions, describes a flux of Grenville-age and Granite-Rhyolite-age zircons deposited in all regions during foreland basin development. The sediments from this flux were preserved in Siberian and Laurentian extensional basins oriented sub-perpendicular to the Grenville deformation front. Then in the latest Proterozoic, Laurentian sources essentially were cut off from the Sette Daban basins, probably because the rift between Siberia and Laurentia had developed such that sediment transport across the Siberia – Laurentia margin was blocked. Also in the latest Proterozoic to Middle Cambrian, Grenville sourced sediment in SW Laurentian basins

greatly diminished, possibly due to the development of a sediment transport impediment (Transcontinental Arch, Midcontinent Rift, Picuris-Pecos Fault) and/or because transgression of the Cambrian sea from the east drowned the Grenville source.

3.3 Petrographic analyses

Samples selected for analysis were primarily sublithic to lithic sandstones from White-Inyo and Death Valley regions. An effort was made to collect unweathered Laurentian samples that would provide the most useful provenance information for correlations with the Siberian samples analyzed by Khudoley et al. (2001). We collected samples from the basal conglomerate of the Crystal Spring Formation (possible correlation—Aimchan Group), the basal transition turbidites of the Kingston Peak Formation (possible correlation—Uy Group), the Wyman Formation (possible correlation—Uy Group), the Hines Tongue of the Reed Dolomite (possible correlation—lower Yudoma Group), and the Lower, Middle, and Upper Deep Spring Formation (possible correlation—middle and upper Yudoma Group). We also gathered point count data from the Johnnie Formation, Stirling Quartzite, Wood Canyon Formation, and Zabriskie Quartzite previously reported in several dissertations (Benmore, 1978; Diehl, 1979; Wertz, 1983, Prave, 1984).

From the collected samples, slabs were cut perpendicular to bedding, and standard petrographic thin-sections were prepared from the slabs. At least 500 statistical point counts were made per sample. Counts were performed in the sedimentary petrology laboratory at University of Montana under a petrographic microscope equipped with a mechanical stage. Table 3.1 lists the categories of framework grain types used in this study to define compositional components. Matrix components were also recorded, but are not reported here. Instead, data reported here are normalized to consider only framework grain types. To minimize differential effects

Table 3.1.

Categories of Sand Grain Types for QFL Ternary Diagrams

Quartzose grains (Q)	- Monocrystalline quartz mineral grains - Polycrystalline quartz mineral grains
Monocrystalline feldspar grains (F)	- K-feldspar - Plagioclase feldspar
Polycrystalline aphanitic lithic fragments (L)	- Sedimentary-metasedimentary lithic fragments - Volcanic-metavolcanic lithic fragments

of grain size on detrital modes, the Gazzi-Dickinson convention (Ingersoll et al., 1984) was used. This method specifies that points falling within intragrain clastic particles larger than silt size (>0.0625 mm) are assigned to monominerallic grain types (e.g. Q_m).

3.4 Results

We report traditional quartz-feldspar-lithic (QFL) ternary diagrams showing mean framework modes from SE Siberian samples (Figure 3.1A, modified from Khudoley et al., 2001) and from SW Laurentian samples (Figure 3.1B, new data and data from Benmore, 1978; Diehl, 1979; Wertz, 1983). The diagrams also show tectonic setting provenance domains defined by Dickinson and Suczek (1979). These domains include continental block, recycled orogen, and magmatic arc provenances, and reflect parent rock composition, as well as physical and chemical maturity of sediments. For instance, sediments with high proportions of feldspar and lithic fragments are interpreted as

having a magmatic arc provenance due to the nature of the parent rock. Alternatively, physically mature sediments are lacking in lithic fragments, suggesting prolonged sediment transport from a continental block provenance. Finally, recycled orogen provenance yields feldspar-poor sediment due to chemical weathering of feldspar during sediment transport. Figure 3.1C shows a hypothetical situation discussed in section 3.5 of this chapter.

Siberian samples from the Uchur Group and Aimchan Group collected from the Gornostakh Anticline in the Sette Daban region fall in the continental block provenance domain of the QFL diagram. One Kerpyl Group sample falls in the recycled orogen provenance domain, and one falls in the continental block domain. The middle and upper Uy Group samples fall in the recycled orogen provenance domain. The Yudoma Group samples collected from the Gornostakh Anticline fall in the continental block provenance domain. Laurentian samples from the Lower and Upper Deep Spring Formation and the Zabriskie Quartzite fall in the continental block provenance domain. All other Laurentian samples fall in the recycled orogen provenance domain. Figure 3.2 shows photomicrographs of selected samples.

We also present a graph (Figure 3.3) that displays the proportion of quartz normalized to the QFL framework in the thin-sections against the proportion of detrital zircons derived from Grenville and Granite-Rhyolite sources (see Chapter 2). The proportion of quartz indicates each sample's maturity, with the most mature sediment containing the highest proportion of quartz. Such samples also tend to exhibit the lowest proportion of detrital zircons from Grenville and Granite-Rhyolite sources. We present data reported from multiple samples of the following sedimentary units: the Gornostakh Uchur Group (2 samples), the Kerpyl Group (2 samples), the middle and upper Uy Group (8 samples), the Gornostakh Yudoma Group (2 samples), the Johnnie Formation (52 samples), the Stirling Quartzite (79 samples), the Wood Canyon Formation (54

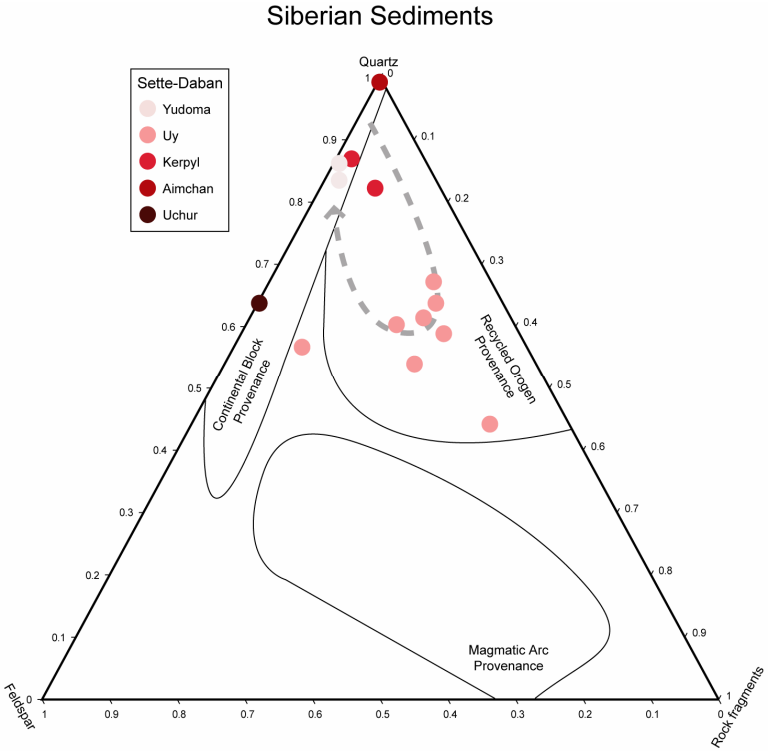
Siberian Sediments
Sette-Daban
Yudoma
Uy
Kerpyl
Aimchan
Uchur
Quartz
Feldspar
Rock fragments
Continental Block Provenance
Recycled Orogen Provenance
Magmatic Arc Provenance

A.

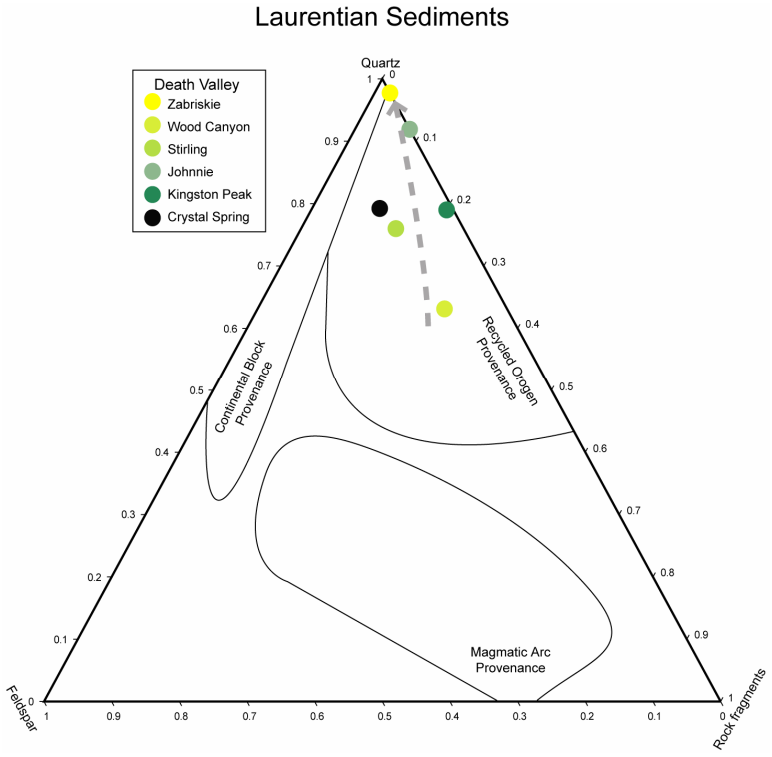
Laurentian Sediments
Death Valley
Zabriskie
Wood Canyon
Stirling
Johnnie
Kingston Peak
Crystal Spring
Quartz
Feldspar
Rock fragments
Continental Block Provenance
Recycled Orogen Provenance
Magmatic Arc Provenance

B.

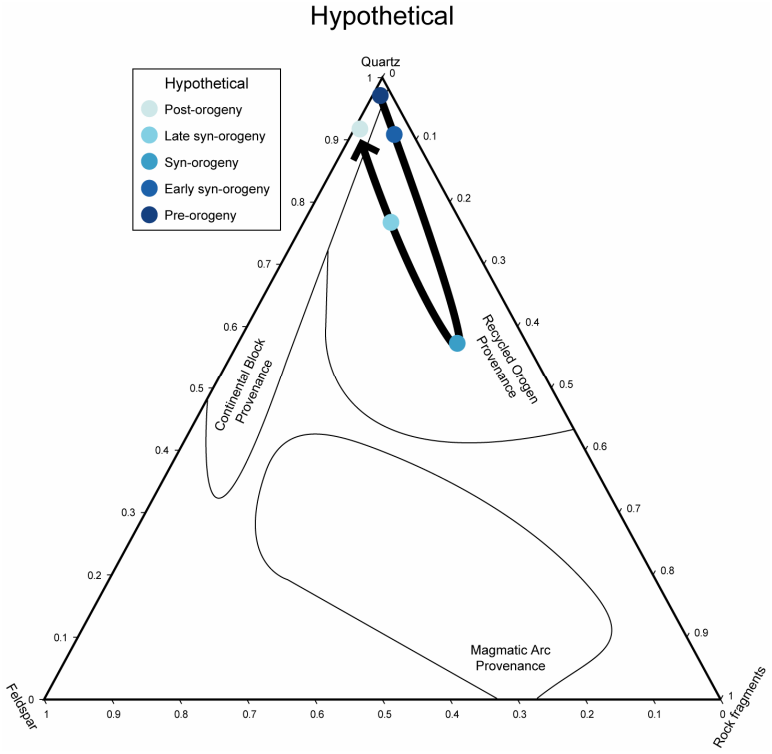

C.

Figure 3.1. Standard QFL ternary diagrams showing framework compositions. A) Samples from Siberia showing evolution from continental block, to recycled orogen, back to continental block provenance. B) Samples from Laurentia showing evolution from recycled orogen to continental block provenance; initial continental block provenance is missing because no pre-orogen samples from Laurentia are present in Death Valley or White-Inyo regions. C) Hypothetical scenario of pre-orogen, syn-orogen, post-orogen sedimentation history, discussed in text. Tectonic provenance interpretations are from Dickinson and Suczek (1979). Siberian data (note only samples from Gornostakh region are reported here) are from Khudoley et al. (2001); Zabriskie, Wood Canyon, Stirling, and Johnnie data are from Prave (1984), Diehl (1979), Wertz (1983), and Benmore (1981), respectively. All other data were collected for this study.

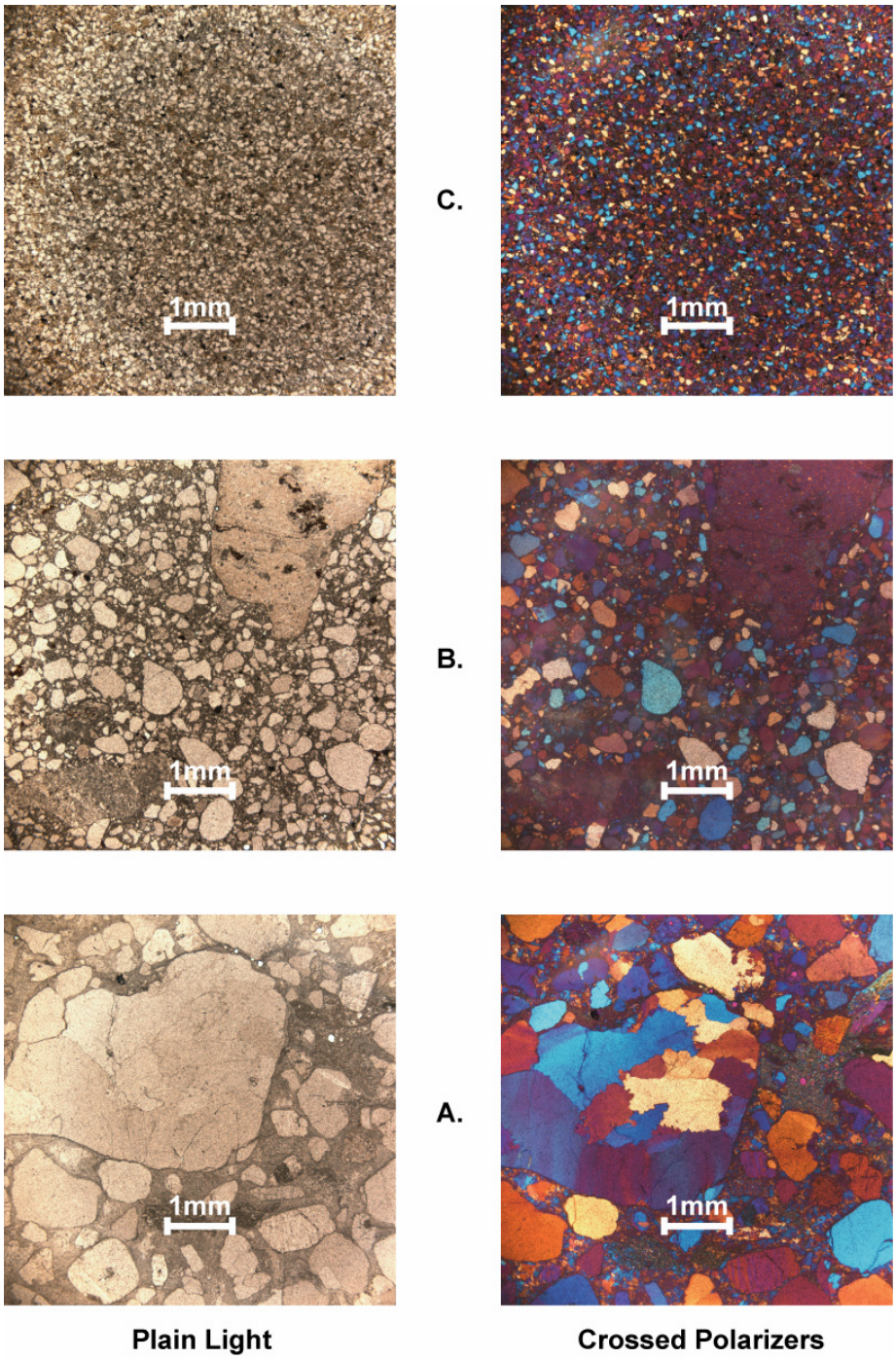

Figure 3.2. Selected photomicrographs displaying similar framework modes and differing degrees of grain sizes. In ascending stratigraphic order: A – basal conglomerate of Crystal Spring Formation; B – basal turbidite of Kingston Peak Formation; C – Upper Deep Spring Formation.

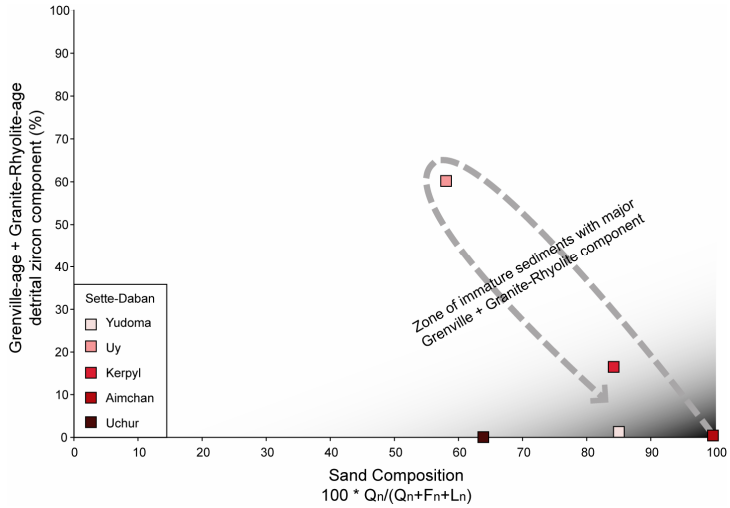
Grenville-age + Granite-Rhyolite-age detrital zircon component (%)
Sand Composition
100 * Qn/(Qn+Fn+Ln)
Zone of immature sediments with major Grenville + Granite-Rhyolite component
Sette-Daban
Yudoma
Uy
Kerpyl
Aimchan
Uchur

A.

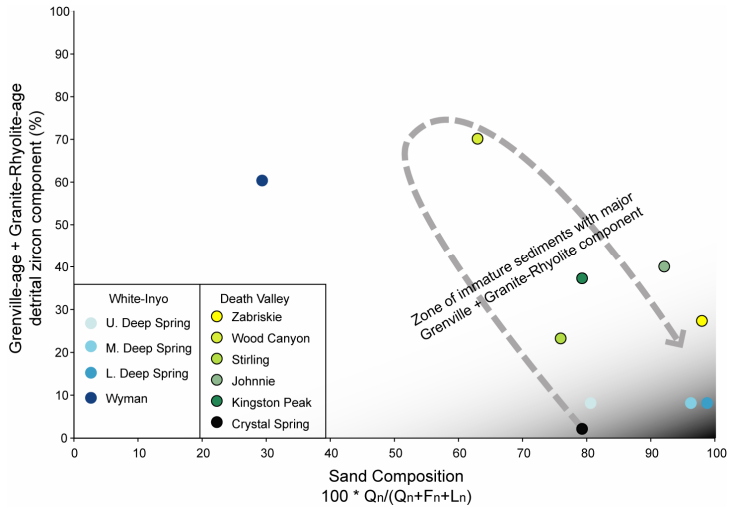
Grenville-age + Granite-Rhyolite-age detrital zircon component (%)
Sand Composition
100 * Qn/(Qn+Fn+Ln)
Zone of immature sediments with major Grenville + Granite-Rhyolite component
White-Inyo
U. Deep Spring
M. Deep Spring
L. Deep Spring
Wyman
Death Valley
Zabriskie
Wood Canyon
Stirling
Johnnie
Kingston Peak
Crystal Spring

B.

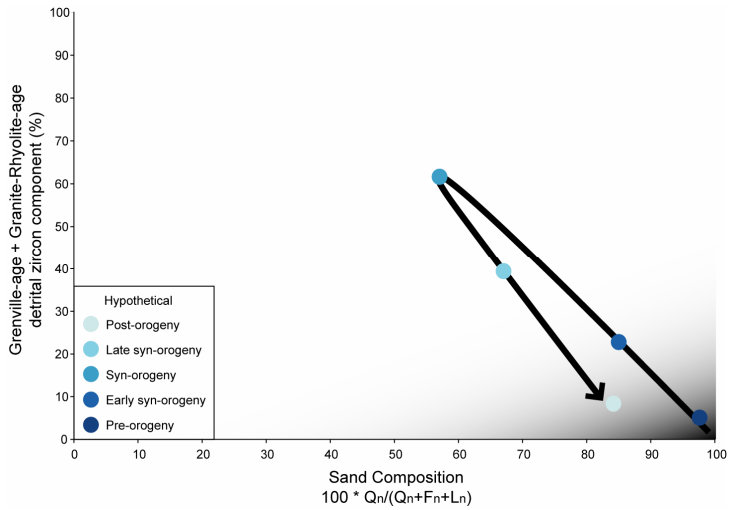
Grenville-age + Granite-Rhyolite-age detrital zircon component (%)
Sand Composition
100 * Qn/(Qn+Fn+Ln)
Hypothetical
Post-orogeny
Late syn-orogeny
Syn-orogeny
Early syn-orogeny
Pre-orogeny

C.

Figure 3.3. Graph showing composition of quartz, normalized against all framework grain types, versus percent of Grenville- and Granite-Rhyolite-age zircons in samples from each stratigraphic level. Some Siberian samples from QFL diagrams were averaged for simplicity; averaging did not alter interpretations. Shaded area of graph represents highly mature sediments from continental block provenance that did not receive large quantities of Grenville or Granite-Rhyolite zircons. Samples in this region were deposited before Grenville orogeny, after rift completion, and after formation of impediment (e.g. Transcontinental Arch, Midcontinent Rift, or Picuris-Pecos Fault). A) Siberian samples; B) Laurentian samples; C) Hypothetical scenario based on tectono-sedimentary model of Chapter 2.

samples), and the Zabriskie Quartzite (55 samples). Because samples from each sedimentary unit were collected from geographically and stratigraphically similar locations, the graph displays their average composition values. Figure 3.3C shows a hypothetical situation, discussed below.

3.5 Discussion

The overall trend observed in the QFL diagrams (Figure 3.1) indicates a close match between recycled orogen provenance sediment compositions of Siberia's Kerpyl and middle and upper Uy groups with essentially all Laurentian units. The continental block provenance of the Gornostakh Uchur, Aimchan, and Yudoma samples indicates that their source was predominantly from non-Laurentian regions. This is a similar pattern as reported in Chapter 1 of this dissertation, based on detrital-zircon data. Additionally, Figure 3 shows a hypothetical prediction of the sediment composition collected in a region that experiences a similar evolution to that described in Chapter 2.

Initially, the region collects primarily mature sediment from the interior of the craton (pre-orogen). Then, the region experiences a local orogenic event, resulting in more local and immature sedimentation (syn-orogen). Finally, the orogenic source is blocked, and the region returns to mature, basement-related sedimentation (post-orogen).

Figure 3.3 further illustrates this relationship by showing detrital zircon information with sandstone composition information. During Uchur and Aimchan deposition, the Gornostakh region collected primarily mature sediment from the continental block of the Siberian Craton. During Kerpyl and Uy deposition, sediment from the young Grenville orogen and other exclusively Laurentian sources were transported across the Grenville foreland basin and down extensional basin corridors oriented sub-perpendicular to the Grenville deformation front. The sediments were preserved in extensional basins in SE Siberia and SW Laurentia. Sediment supply from Laurentia into Siberia diminished during Yudoma deposition, as the Siberian sediment composition returned to quartz-rich sand that was poor in Laurentian-sourced zircons.

Sediments deposited in SW Laurentia essentially mimic this sedimentary history, except that the majority of Laurentian sediments analyzed for this study were deposited after the onset of the Grenville orogeny. Only three units contain a continental block provenance character: the basal conglomerate of the Crystal Spring Formation possibly was deposited before Grenville-age sediments reached Death Valley; the Zabriskie Quartzite and the Deep Spring Formation also contain a diminished proportion of Grenville- and Granite-Rhyolite-age zircons. As described in Chapter 2, this could be due to the development of a sediment transport impediment (Transcontinental Arch, Midcontinent Rift, Picuris-Pecos Fault), and/or it could be due to transgression of the Cambrian Sea over the Grenville source during latest Neoproterozoic to Middle Cambrian. Figure 3.3C predicts a pattern based on this model. As in Figure 3.1, our data closely resemble the prediction.

Our results support the claim of Dickinson and Gehrels (2000) that petrography and detrital-zircon geochronology analyses considered together can offer a greater scope for interpretation. An additional observation from this study is the possible relationship between sediment modal compositions and detrital-zircon age heterogeneity (Figure 3.4). Samples that fall in the recycled orogen domain of the QFL diagram exhibit greater Proterozoic age heterogeneity than samples that fall in the continental block domain, reflecting greater influence from Proterozoic orogenic and magmatic events. Samples that fall in the continental block domain exhibit somewhat greater Archean age heterogeneity, reflecting more pronounced influence of Archean basement sources.

Detrital-zircon geochronology is a relatively expensive and specialized procedure compared to point count analyses. Therefore, point counting may be an inexpensive and informative method of screening sandstone samples that are candidates for future detrital-zircon investigations. Such relationships may be restricted to specific tectonic settings. More research is needed to establish definite relationships.

3.6 Geoscience education

There has been a recent surge of interest in improving science education at the secondary level (NRC, 1996). For instance, the National Science Foundation is promoting projects wherein the students are immersed in current scientific research.

This study was part of a mentorship program between the University of Montana Geosciences Department and Big Sky High School. Chris Casas, a senior at Big Sky High School, served a vital role in the analytical process (Figure 3.5). Each week throughout the school year, he spent time at the UM Geosciences Department learning petrography techniques such as thin-section preparation, mineral identification, and statistical sampling. Over the course of the school year, he participated in most aspects of the research including, under my supervision, the characterization of some of the

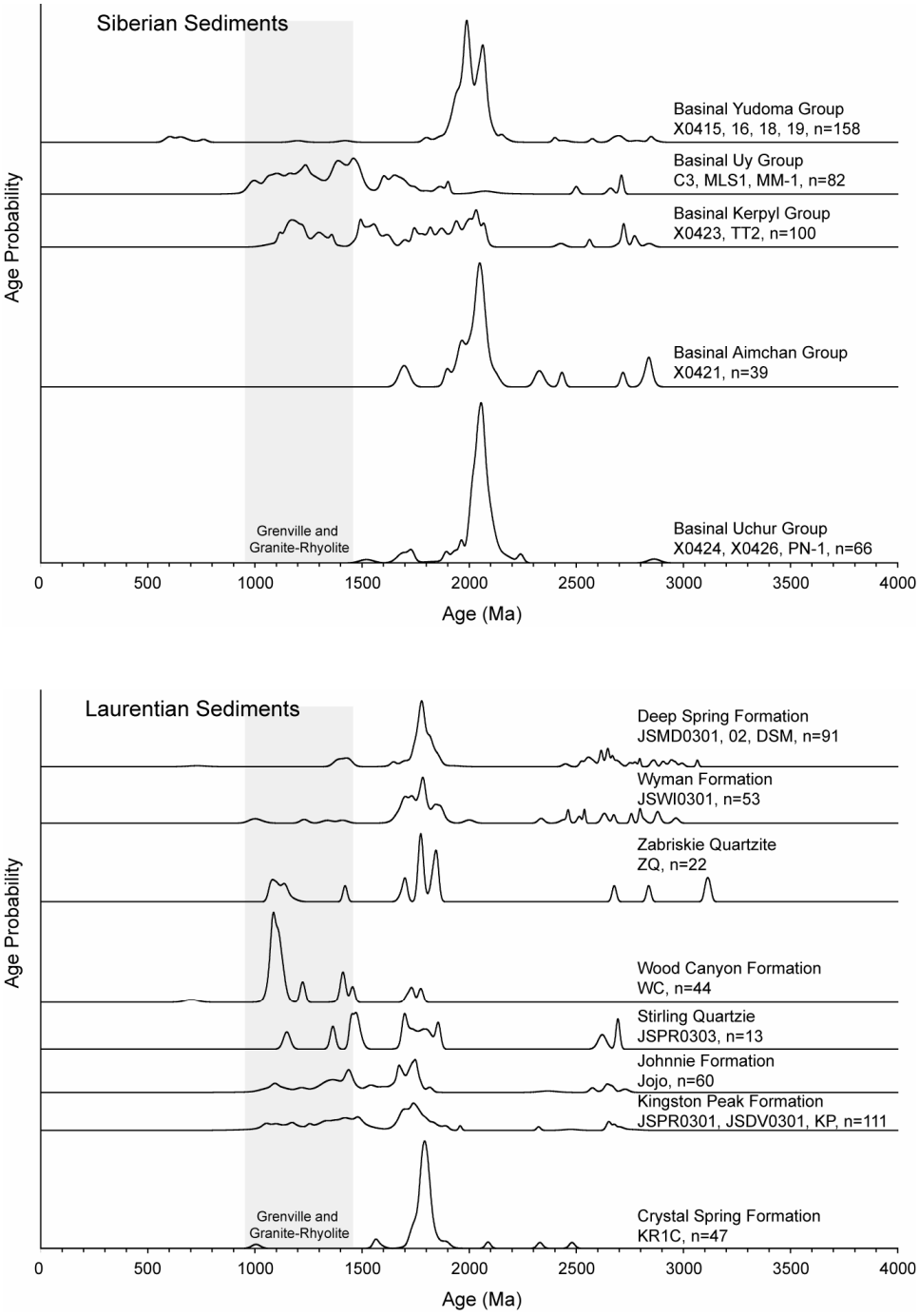

Figure 3.4. Normalized probability curves of detrital-zircon geochronology analyses used for this study. Notice greater Proterozoic age heterogeneity of samples that also plot in Recycled Orogen domain of Figure 3.1.

samples and the interpretation process. Possibly the most important aspect of his experience was his participation in multiple science fairs where he communicated these new scientific findings. After a second place finish at the 2007 Montana Tech Regional Science and Engineering Fair, he was chosen as a student finalist for the 2007 Intel International Science and Engineering Fair in Albuquerque, NM, where he will compete with 1,500 student finalists from 47 countries for a grand prize college scholarship of $50,000.

Our sediment provenance investigation illustrates a successful mentorship program between a high school student and a Ph.D. candidate. The partnership between University of Montana Geosciences Department and Big Sky High School can serve as a model for involving young people in geologic research.

3.7 Conclusions

Our results support lithostratigraphic correlations proposed by Sears et al. (2005). The correlations best supported are those involving the Kerpyl and Uy Groups, both of which exhibit a recycled orogen provenance similar to most SW Laurentian samples analyzed in this study. Furthermore, the tectono-sedimentary model described in Chapter 2 is strengthened for the SE Siberia – SW Laurentia region during Proterozoic through Middle Cambrian time. Finally, our study is an example of how high school students can participate in authentic research in the geosciences.

Figure 3.5. Chris Casas, senior at Big Sky High School, using University of Montana Geosciences Department rock saw to prepare samples for thin section analysis.

CHAPTER 4

DETRITAL-ZIRCON LINKAGES BETWEEN SIBERIA AND NORTH AMERICA IN THE CRADLE OF CAMBRIAN LIFE

4.1 Introduction

Geologists generally agree that the Siberian and North American cratons occupied contiguous parts of a Proterozoic supercontinent before the Siberian craton rifted away and became embedded in the Eurasian landmass (Hoffman, 1991). However, for nearly 30 years researchers have disagreed on the exact linkages of these ancient crustal fragments and have published a bewildering array of Proterozoic continental reconstructions (Ernst et al., 2000). The correct reconstruction would constrain significant geological problems ranging from the long-term behavior of the magnetic field (Kirshvink et al., 1997; Gallet et al., 2000) to the origin and dispersal of metazoans (Bowring et al., 1993). Here we show that closely similar sequences of Mesoproterozoic strata connect the Sette Daban region of SE Siberia and the Death Valley region of California at a unique geological “golden spike” (Figure 4.1A). Our U-Pb detrital-zircon data show that the strata occupied one intracratonic basin that was fed by erosion of basement age-provinces in SE Siberia and SW North America. Our data further show that late Neoproterozoic continental rifting split this basin into conjugate halves. The ocean basin that opened between the cratons has unique significance to Earth history because it may have nurtured the cradle of Cambrian life.

4.2 Interpretations from detrital-zircon data

We separated detrital grains of zircon from Proterozoic sandstones of the Sette Daban and Death Valley regions and used standard techniques to U-Pb date them at the

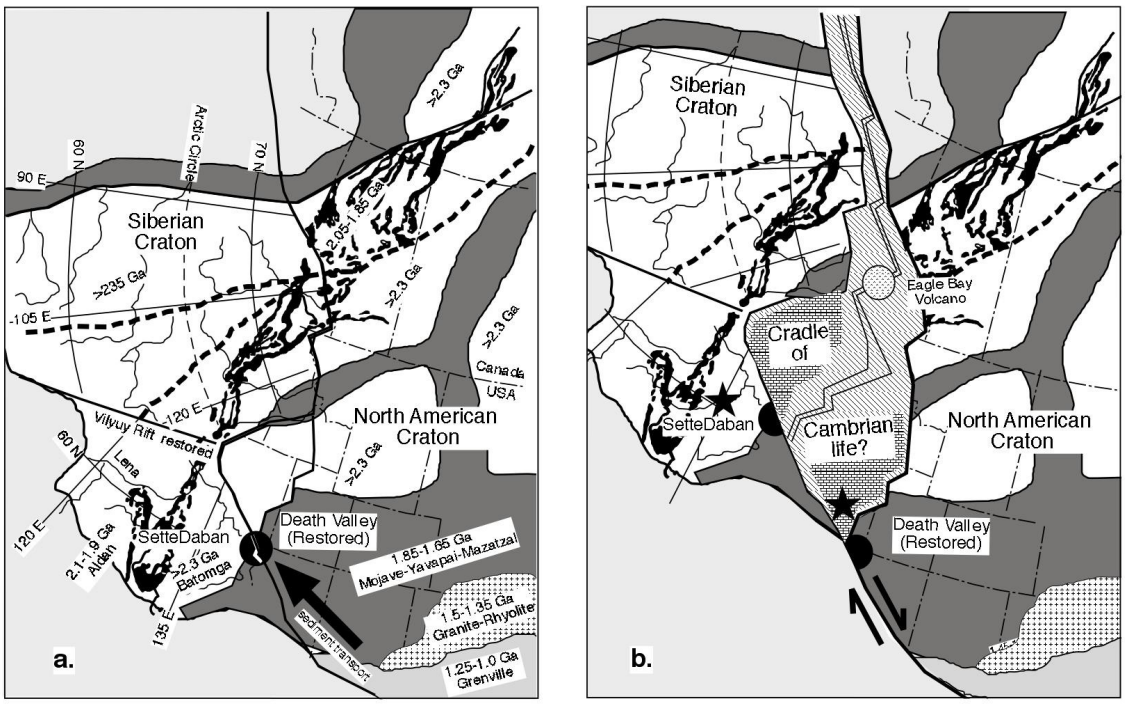

Figure 4.1A. Siberia – North America Proterozoic reconstruction. See Sears and Price (2003) for more details. Black circle - location of Sette Daban-Death Valley "golden spike". Large black arrow shows transport direction to transfer North American zircons to Siberian craton before continental breakup. Devonian Vilyuy rift restored on Siberian craton. Black – positive aeromagnetic anomalies of 2100-1900 Ma tectonic belt. Dark grey – 1850-1650 Ma tectonic belts. Unpatterned - >2300 Ma terranes. Crosses – 1500-1350 Ma Granite-Rhyolite belt. Medium grey – 1250-1000 Ma Grenville tectonic belt. Light grey – unmapped. Dashed black lines – major shear zones in basement.

Figure 4.1B. Suggested Early Cambrian (530 Ma) positions of Siberian and North American cratons. Shifting of cratons along transform faults split Sette Daban-Death Valley "golden spike" (black half-circles), inhibited exchange of detrital zircons between North America and Sette Daban, and opened ocean basin in which Early Cambrian fauna first appeared. Black stars – *Repinaella* trilobite localities in Siberia and Nevada. Circle– Early Cambrian Eagle Bay mid-ocean-ridge volcano that may have shed clasts to Siberia and Canada (Sears and Price, 2003).

Stanford University-US Geological Survey SHRIMP facility, and at the LAICPMS facility at Washington State University. We analyzed 34 of the grains at both facilities and found that the two techniques gave equivalent U-Pb ages at the 2-sigma confidence level. Our conclusions are based on detrital-zircon grains with Pb-Pb ages that were < 10% discordant.

The SE Siberian and SW North American cratons comprise amalgamations of tectonic terranes with specific crystallization ages (Figure 4.1A). Erosion of these terranes cast age-distinctive detrital-zircon grains into neighboring sedimentary basins. Pb-Pb dates of detrital-zircon grains therefore link the sedimentary rocks to basement source-rocks in their drainage basins. SE Siberian basement terranes include the 2050-1850 Ma Aldan and >2300 Ma Batomga provinces (Frost et al., 1998; Khudoley et al., 2007). SW North American basement age-provinces include the 1300-950 Ma Grenville, 1450-1300 Ma West Granite-Rhyolite, and 1850-1650 Ma Mojave, Yavapai, and Mazatzal provinces (Farmer et al., 2005). Mojave province granites also contain >2300 Ma zircon xenocrysts (Farmer et al., 2005) that are not distinguishable in age from those of the Batomga province.

Late Neoproterozoic continental rifting established both the E Siberian and W North American margins (Link et al., 1993; Khudoley et al., 2001). We found that post-rifting sandstones in the Sette Daban and Death Valley regions contain mutually exclusive detrital-zircon age suites that correlate with basement sources on their respective cratons (Figure 4.2A). This indicates that the cratons were too isolated for sedimentary processes to transfer zircon-bearing sand between them (Figure 4.1B). Three prominent peaks for the Death Valley region histogram correspond to nearby Grenville, West Granite-Rhyolite, and Mojave-Yavapai-Mazatzal sources. These three peaks are characteristic of post-rifting Neoproterozoic and Early Paleozoic sandstones of W North America (Farmer et al., 2005). A peak corresponding to the Aldan province

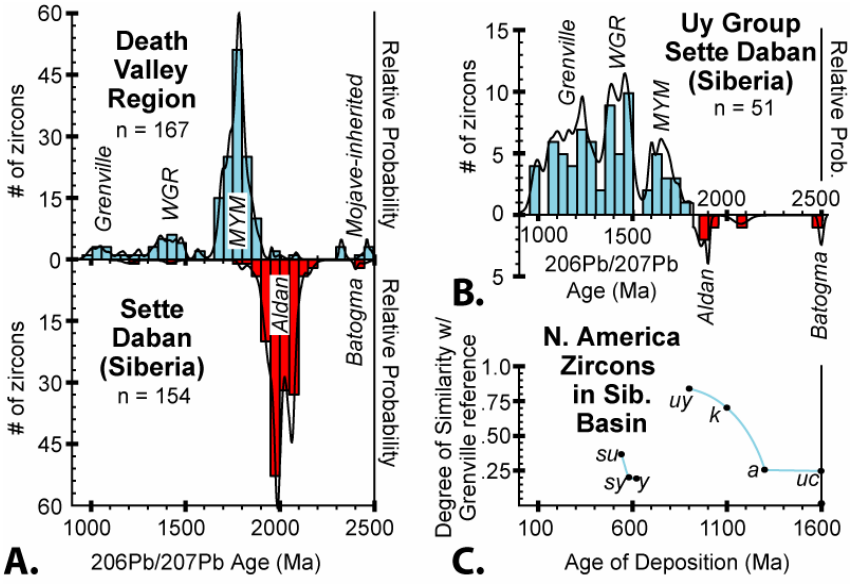

Figure 4.2A. Paleo- and Mesoproterozoic detrital-zircon age spectra from Neoproterozoic and Cambrian sandstones from Death Valley (upper) and Sette Daban, Siberia (lower). These samples were deposited after rifting had isolated North American and Siberian cratons. Diagnostic age groups from Death Valley correlate with Grenville, West Granite Rhyolite (WGR), and Mojave-Yavapai-Mazatzal (MYM) crystalline source provinces in SW North America (Farmer et al., 2005), and Sette Daban samples correlate with Aldan source province in SE Siberia (Frost et al., 1998).

Figure 4.2B. Detrital-zircon age distribution for Uy Group, a pre-rift Mesoproterozoic sandstone from Sette Daban, Siberia. Note high proportion of distinctly SW North America ages with Grenville, West Granite Rhyolite (WGR), and Mojave-Yavapai-Mazatzal (MYM) sources. See Figure 4.1A for sediment transport direction.

Figure 4.2C. Variation of similarity (Gehrels, 2007) between North American detrital-zircon component defined by Grenville sediments (Stewart, 2001) and Siberian detrital-zircon component, plotted according to age of deposition for Sette Daban basin. Distinct North American components appear at ca. 1300 Ma, and increase to a similarity level of 0.835 by 900 Ma, reflecting erosion of Grenville mountain belt. North American components drop radically after 640 Ma, reflecting rift-separation of Siberia from North American zircon sources. uc – Uchur Group, n=113, a – Aimchan Group, n=73, k – Kerpyl Group, n=100, uy – Uy Group, n=82, y – lower Yudoma Group, n=68, sy – Sytyga Formation, n=50, su – Suordakh Formation, n=54.

dominates the post-rift Sette Daban detrital-zircon histogram.

By contrast, pre-rift Mesoproterozoic Siberian sandstones contain large percentages of detrital-zircon grains with distinct North American affinities. The characteristic Grenville, West Granite-Rhyolite, and Mojave-Yavapai-Mazatzal zircon peaks are well represented in Uy Group sandstone that was deposited in the Sette Daban intra-cratonic basin before rifting (Figure 4.2B). Furthermore, gaps in Uy Group detrital-zircon ages coincide with age gaps in SW North American source rocks (Farmer et al., 2005). Paleocurrents indicate that the Uy Group sandstones were derived from outboard of the Siberian craton to the southeast (Khudoley et al., 2001), consistent with sediment sources in SW North America shown on the reconstructed map (arrow in Figure 4.1A). Less abundant SW North American grains occur in the underlying Kerpyl and Aimchan groups of the Sette Daban basin (Figure 4.2C). The increase in North American detrital-zircon components with time correlates with subsidence of the Sette Daban basin into a deep-water turbidite trough from ca. 1200 to 900 Ma (Khudoley et al., 2001). The subsidence may record collapse of the Siberian crust under the load of the Grenville orogen, which crossed North America to within a few hundred km of the basin on the reconstructed map (Figure 4.1A).

The Mesoproterozoic section of the Sette Daban basin (Link et al., 1993; Khudoley et al., 2001) exhibits strikingly similar stratigraphy to the Mesoproterozoic section of Death Valley (Figure 4.3). The Aimchan Group matches the lower Crystal Spring Formation. Both rest on angular unconformities that truncate intrusive rocks as young as1400-1350 Ma and basement gneisses dated to 1700 Ma, and comprise fluvial-braidplain sandstone and conglomerate overlain by pink and yellow stromatolitic dolomite. A karst surface cuts the top of both dolomite sections. The overlying Bik and Muskel formations of the Kerpyl Group match the upper Crystal Spring Formation. Each locally includes a dm-thick bed of distinctive quartz-pebble conglomerate at the base,

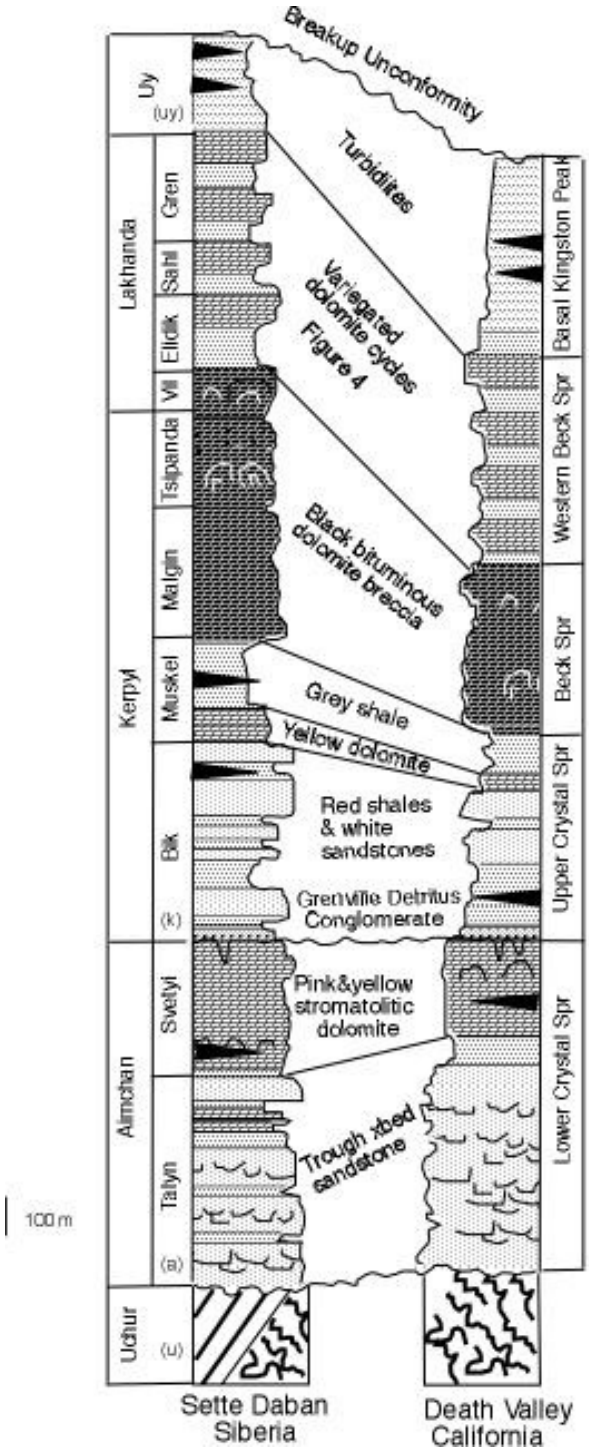

Figure 4.3. Comparative pre-breakup stratigraphy of Sette Daban, Siberia (Khudoley et al., 2001), and Death Valley, California (Link et al., 1993). a,k,uy correspond to detrital-zircon samples of Figure 4.2C.

succeeded in order by red shales and trough-crossbedded white sandstone, yellow dolomite, and grey shale. Both sections contain diabase sills with wide hornfelsic contacts.

The sections pass upward into nearly identical microlaminated black bituminous dolomite and solution-collapse dolomite-breccia, - the upper Kerpyl Group, and the Beck Spring Formation. These formations include distinctive 2-3m tall microbial mounds with flanking roll-up structures and breccias. Variegated sandstone-dolomite cycles of the Lakhanda Group and western Beck Spring Formation match bed-for-bed (Figure 4.4). The Lakhanda Group grades upward into the Uy Group, a kms-thick turbidite succession. Similarly, the Beck Spring Formation passes up into turbidites of the basal Kingston Peak Formation. The Uy Group contains basic sills or flows as does basal Kingston Peak Formation in the western Panamint Range of Death Valley (Link et al., 1993). The Siberian section lacks diamictites that are typical of the upper Kingston Peak Formation (Link et al., 1993). Our correlation predicts that the basal Kingston Peak turbidites are significantly older than the diamictites, which may record the initiation of continental breakup at 700-600 Ma (Link et al., 1993).

In Siberia, a >200 m.y. hiatus followed deposition of the Uy Group. A new depositional cycle then occurred in response to continental rifting, which also isolated Sette Daban from North American sources. We found virtually no North American detrital-zircon component in Siberian sandstone of the late Neoproterozoic (Vendian) Yudoma Group (Figure 4.2A, C). The Yudoma Group rests on an unconformity that cuts the 640 Ma alkaline ultramafic Ingli stock. The Yudoma Group is in part older than a 553±23 Ma Pb-Pb carbonate date, and passes upward into the Early Cambrian (Khudoley et al., 2007). Correlative strata exposed in SW North America bear lithologic and faunal similarities to the Yudoma Group, including oncolites, Boxonia, Ediacaran fauna, and cloudinids (Signor et al., 1987; Fedonkin, 1992; Link et al., 1993). Both

Figure 4.4. Bed-for-bed matching of clastic-dolomite cycles from Sette Daban, Siberia (left, Lakhanda Group) and western Death Valley (right, Beck Spring Formation, Saratoga Spring area). Photographs by J.W. Sears.

sections are characterized by several “grand cycles” from clastic to carbonate sedimentary rocks; the two basal cycles have massive dolomite members, and the upper ones have distinctive cross-bedded sandy dolomite and feldspathic sandstone. Carbon isotope patterns support correlations of the sections (Corsetti and Kaufman, 1994). The SE Siberian and SW North American grand cycles evidently record correlative Neoproterozoic and Cambrian eustatic sea level changes phased with passive continental-shelf subsidence.

We conclude that by Early Cambrian time, separation of the SE Siberian and SW North American cratons along a rift-transform system was sufficient to isolate segments of their rift margins from intercontinental sediment mixing. Clastic sediment eroded from North America was trapped in kms-thick deposits on its new western continental shelf, but the Siberian shelf was largely covered with carbonate and received only limited sand from its interior (Sears and Price, 2003). Some sand may have passed from Canada to northern Siberia where the Cambrian ocean basin may have been narrower (Sears and Price, 2003). The Eagle Bay mid-ocean-ridge volcano of British Columbia may help

delineate the Early Cambrian configuration of the basin (Figure 4.1B) because it may have shed volcanic boulders into NE Siberia formations (Sears and Price, 2003). The orientations of faults shown in Figure 4.1B would allow Siberia to rotate clockwise around Canada on margin-parallel transform faults toward its late Paleozoic collision with the Ural Mountains (Sears and Wright, 2005).

4.3 Implications regarding trilobite evolution

The ocean basin that opened between the diverging continents may have cradled explosive Early Cambrian metazoan evolution. Fossil evidence indicates that the Siberian side of the reconstructed basin was teeming with Early Cambrian organisms, including the first occurrences of numerous animal groups (Rosanov and Zhuravlev, 1992). A highly diverse early Tommotian fauna (ca. 530 Ma, Bowring et al., 1993), with 11 major skeletal animal groups, includes the earliest brachiopods, gastropods, mollusks, porifera, crustaceans, arthropods, and archeocyathids, among others (Briggs and Fortey, 1992; Rosanov and Zhuravlev, 1992). An Early Cambrian archeocyathid reef originated in SE Siberia in the Tommotian stage and crossed to the rifted western margin of North America by the Atdabanian stage (ca. 527 Ma, Bowring et al., 1993; Sears and Price, 2003). The world's earliest trilobite occurrence, *Profallotaspis*, is found at the base of the Atdabanian stage in SE Siberia (Glaessner, 1984; Palmer and Repina, 1993). The first trilobite to appear in North America occurs in western Nevada and closely resembles the SE Siberian trilobite *Repinaella*, which appears 26 m above *Profallotaspis* (Hollingsworth, 2005). The median generic longevity for Cambrian trilobites was just over one m.y. (Bowring et al., 1993). Trilobites might therefore have originated in Siberia and migrated to nearby North America within two m.y. Widening of the ocean basin may have increased evolutionary branching rates as animal populations

became isolated on the diverging continents and Early Cambrian transgressions across the broad continental shelves created more faunal habitat (Briggs and Fortey, 1992).

CHAPTER 5

SIBERIA – LAURENTIA – MOROCCO: THE TRILOBITE GARDEN OF EDEN?

5.1 Introduction

The Siberia – Laurentia connection of Sears and Price (1978, 2003) is permissive with regard to fit of the continents, structural and magmatic piercing points, conjugate rift-margin lithostratigraphic correlations, and paleomagnetism data. Furthermore, detrital-zircon populations from Siberia correlate closely with several SW Laurentian basement provinces, permitting provenance linkages (Khudoley et al., 2001; MacLean et al., *in review*). Paleobiogeographic data provide additional and useful perspectives for continental reconstructions (e.g. Williams, 1973; Burrett and Richardson, 1980; Cocks and Fortey, 1982; Cocks and Scotese, 1991; Fortey and Cocks, 1992; Lieberman and Eldredge, 1996; Rushton and Hughes, 1996; Lees et al., 2002). Several researchers have suggested paleobiogeographic ties between SE Siberia, SW Laurentia, and Morocco (e.g. Lieberman, 2002; Meert and Lieberman, 2004).

In this chapter, we propose a Neoproterozoic-Early Cambrian reconstruction that places Morocco against the Siberia – Laurentia connection (Figure 5.1). The reconstruction satisfies detrital-zircon provenance data from Laurentia and Siberia, and embraces structural, magmatic, sedimentary, and faunal correlations. We propose that the Anti-Atlas region of Morocco linked Early Cambrian archeocyathid communities of SE Siberia and SW Laurentia at the onset of dispersal of the rifted fragments of Rodinia, and that the widening rift system provided the habitat in which the earliest trilobites evolved. The reconstruction implies that the Anti-Atlas terrane accreted to Africa during late Paleozoic Appalachian-Variscan-Hercynian collisions.

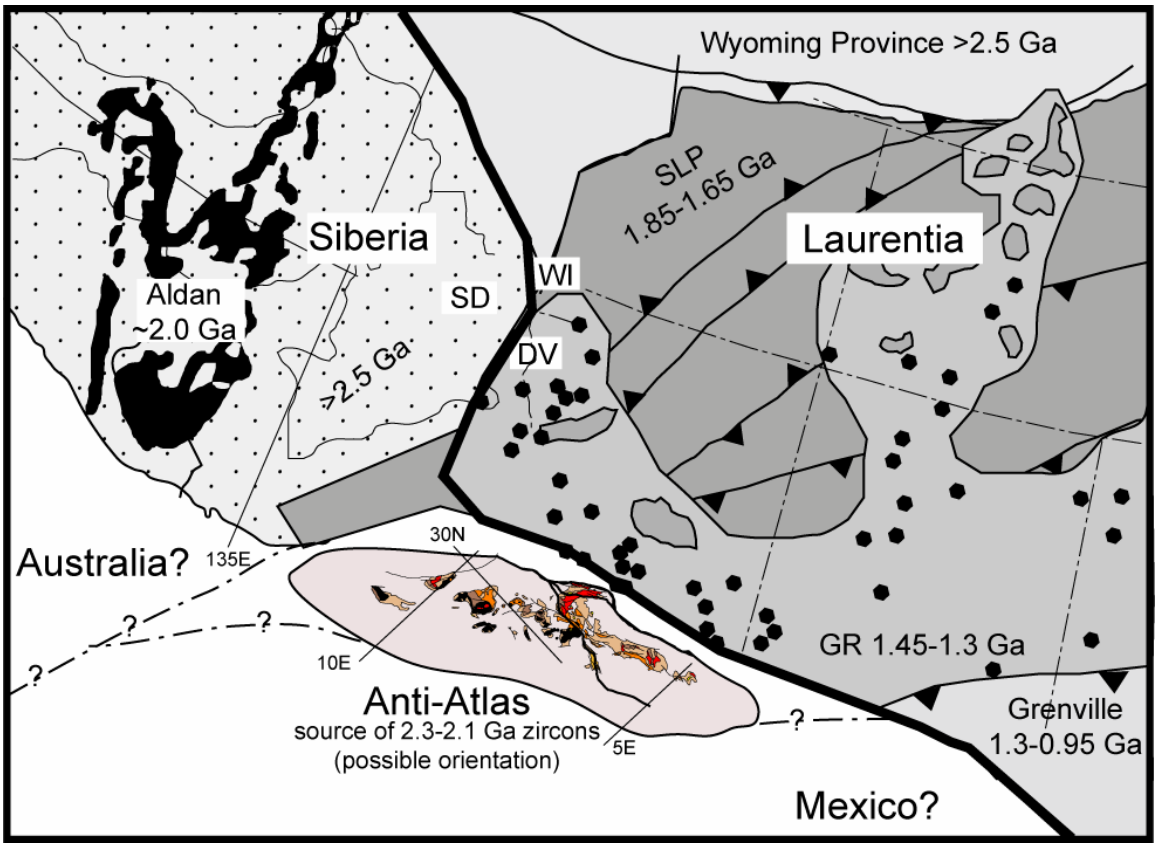

Figure 5.1. Proposed Neoproterozoic-Early Cambrian Anti-Atlas—Siberia—Laurentia connection. See Figure 1.1 for descriptions. Shaded regions in Anti-Atlas terrane are Precambrian outcrops from Thomas et al. (2004).

5.2 Detrital-zircon provenance

Chapters 1 and 2 presented detrital-zircon geochronology data that support the SE Siberia – SW Laurentia connection of Sears and Price (2003). Specifically, Meso-Neoproterozoic strata of the Sette-Daban region of SE Siberia contain detrital-zircon assemblages that correlate with the S Laurentian Paleoproterozoic terranes, Granite-Rhyolite province, and Grenville province (Figure 5.2). Similarly, Meso-Neoproterozoic

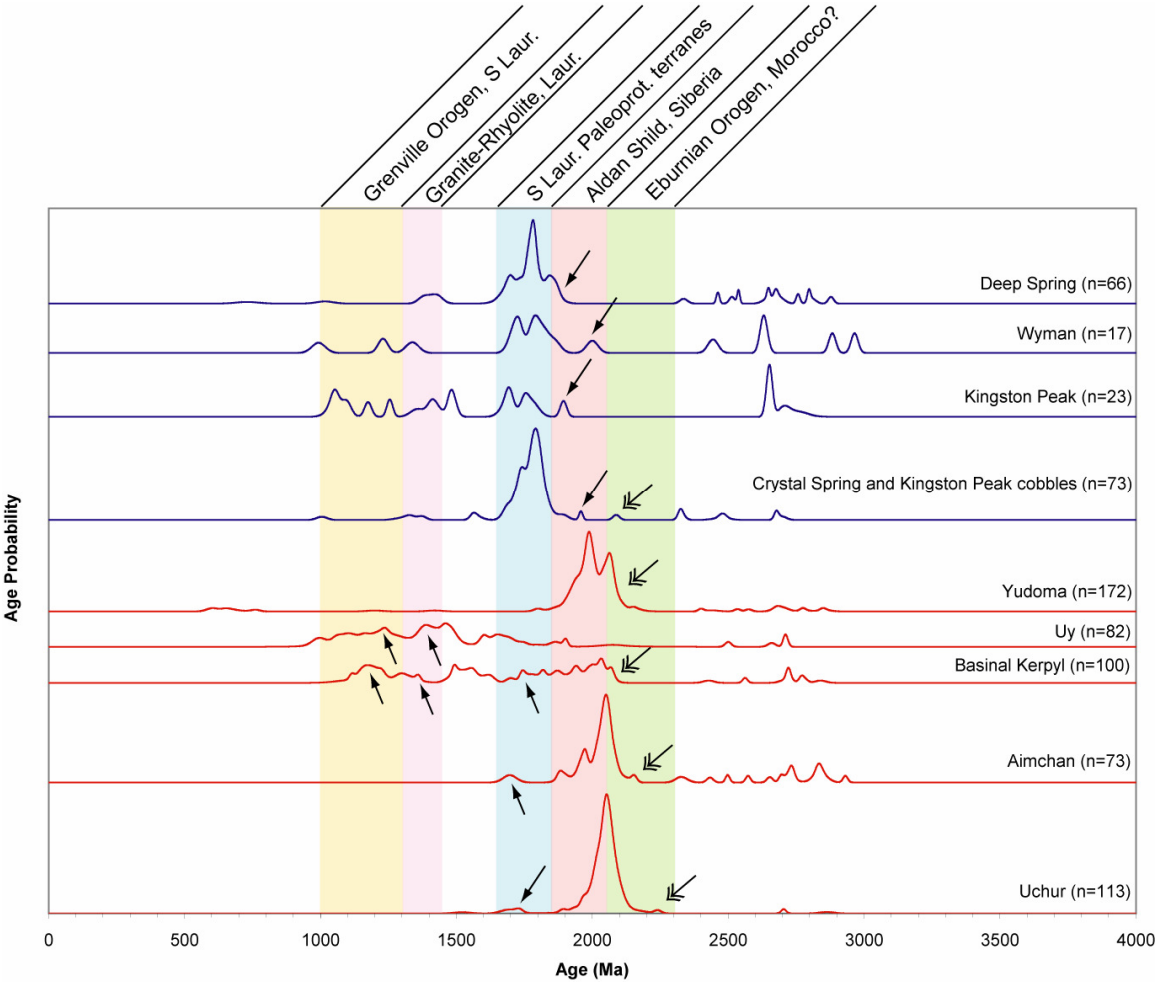

Figure 5.2. Detrital-zircon ^{207}Pb-^{206}Pb age histograms and associated probability curves for samples from Siberian cratonal and basinal sediments, and from Laurentian sediments from Death Valley and White-Inyo areas (from Chapter 1 and MacLean et al., *in review*). Colored backgrounds distinguish interpreted provenance domains. Red probability curves = Siberian samples; blue curves = Laurentian samples. Laurentian sediments contain some zircons that likely originated from Siberian craton, and Siberian sediments contain some zircons that likely originated from Laurentian craton (signified by single arrows). Sediments on both cratons contain zircons that could have originated from Eburnian orogen of Morocco (signified by double arrows).

strata of the Death Valley region contain detrital-zircon populations that correlate with the Aldan province of Siberia. However, abundant 2200-2050 Ma detrital zircons that occur both in Siberian and Laurentian sandstone samples do not match known source regions in either Siberia or Laurentia; these zircons indicate exotic source terranes. The age of the Eburnian basement province of the Anti-Atlas region of S Morocco (Thomas et al., 2004) is approximately concurrent with the exotic zircon ages in Siberia and Laurentia. We propose that the Eburnian basement province could represent a missing detrital-zircon source terrane.

Soulaimani and Piqué (2004) reported several ^{40}K-^{40}Ar muscovite dates ranging between 1389 and 989 Ma from Tasrirt orthogneisses and migmatites in the SW Anti-Atlas region. These dates record a thermal event in the Anti-Atlas that could be associated with the Grenville orogen present in S Laurentia. Grenville detrital zircons are abundant in Siberian and Laurentian samples.

5.3 Structural, magmatic, and sedimentary relationships

Several sedimentary units were deposited in intracratonic extensional basins in SE Siberia and SW Laurentia during Mesoproterozoic and Neoproterozoic time, including the Crystal Spring, Beck Spring, and Kingston Peak formations of the Death Valley region (Wright and Troxel, 1966), the Wyman Formation of the White-Inyo region (Stewart, 1970), and the Uchur, Aimchan, Kerpyl, and Uy groups of Siberia (Khudoley et al., 2001). Intracratonic rifting also affected the Anti-Atlas region during this time, with deposition of the Anti-Atlas Supergroup (Thomas et al., 2004). In the Anti-Atlas region, extension produced oceanic crust in Middle Neoproterozoic (Admou et al., 2000). This may correlate with MORB basalts reported from the Middle Neoproterozoic Kingston Peak Formation in the Panamint Range of Death Valley region (Prave, 1999), and Middle Neoproterozoic MORB and gabbro reported from the Middle Neoproterozoic Uy

Group in the S Siberian Platform (Khudoley et al., 2001). Anti-Atlas and S Siberian margins also experienced collisional island arc tectonics in Middle Neoproterozoic time (Khudoley et al., 2001; Thomas et al., 2002), as if the rifted margin was quickly converted into a collisional margin.

Numerous authors have recognized Late Neoproterozoic to Early Cambrian rift margins associated with the break-up of Rodinia in SE Siberia and SW Laurentia (e.g. Stewart, 1972; Hoffman, 1989, 1991; Dalziel, 1991; Khudoley et al., 2001; Sears and Price, 2003). The following lines of evidence reported by Piqué (2003), Soulaimani and Piqué (2004), and Burkhard et al. (2006) indicate that a rift margin developed in the Anti-Atlas region during Neoproterozoic and Early Cambrian as well: 1) structural extension and transtension resulting in fault-limited basins and pull-apart basins, 2) marine transgression resulting in Early Cambrian carbonate deposition, 3) mostly alkaline magma intrusion associated with extensional faulting, 4) hydrothermal activity accompanying faulting and magma emplacement, and 5) a rift-related sediment accumulation curve beginning in latest Neoproterozoic. Similar sediment-accumulation curves were determined in SW Laurentia by Levy and Christie-Blick (1989) and in SE Siberia by Khudoley and Serkina, (2002).

We suggest that final rifting of Rodinia involved SE Siberia, SW Laurentia, and the Anti-Atlas region. Sinistral transtensional faulting resulted in the deposition of the volcano-sedimentary Ouarzazate Supergroup (Soulaimani and Piqué, 2004; Thomas et al., 2004). Such faulting could have provided an escape route for the Anti-Atlas terrane away from the SE Siberia – SW Laurentia region.

5.4 Early-Middle Cambrian trilobite distribution

Lieberman's (1997, 1999, 2002) phylogenetic analyses of early trilobites (Figure 5.3) indicate "a uniform trilobite fauna was once distributed across SW Laurentia, the

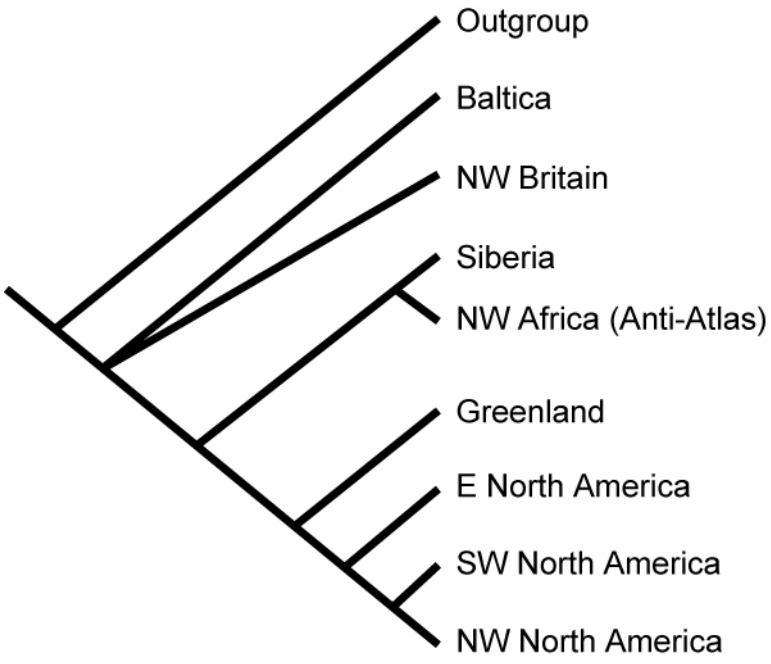

Figure 5.3. Best-supported vicariance tree showing biogeographic relationships based on Early Cambrian trilobite analyses (from Lieberman, 1997). Trees are interpreted as displaying relative timing of separation of respective regions by rifting, emergence of barriers, or sea level fall. Close regions on vicariance tree indicate more recent separation. Tree shows closest relationship of Siberia and Anti-Atlas region, as well as their close relationship to Laurentia. Tree is rooted by using outgroup, discussed in Lieberman and Eldredge (1996).

margins of Gondwana [Anti-Atlas], and Siberia." The oldest trilobite groups, "fallotaspidoids," Olenellids, and Redlichiids, are found in these three locations (Sdzuy, 1978; Repina, 1981; Hollingsworth, 2005). The initial distribution of the "fallotaspidoids" was restricted to Siberia. Range expansion of "fallotaspidoids" first entailed migration from Siberia into northern Africa (Anti-Atlas), and then into SW Laurentia. For Olenellids, range expansion involved migration from Siberia into SW Laurentia. The

ancestral biogeographic state of the Redlichiid faunal province, derived from the Olenellid faunal province, is Siberia and northern Africa (Lieberman, 1999; 2002).

The median generic longevity for Cambrian trilobites was just over one m.y. (Bowring et al., 1993). It appears that the rate of evolution was faster than the rate of geographic dispersal, requiring a close proximity of these three closely related trilobite species. Our reconstruction places the three locations in close proximity, allowing range expansions and vicariance events to occur during break-up of Rodinia and subsequent tectonic development. This could be the simplest explanation for trilobite radiation in which long-term cryptic divergence (100's of My) of Metazoan radiation is not necessary (c.f. Fortey et al., 1996).

5.5 Early-Middle Cambrian archeocyathid distribution

Archeocyathids originated during the Tommotian Stage in the Anabar-Sinyaya Basin of the Siberian Platform and were extant only from 530-510 Ma (Zhuravlev, 1986; Riding and Zhuravlev, 1995; Rowland and Shapiro, 2002). Archeocyathids spread first to the margin of Gondwana during the Atdabanian Stage (Rowland and Shapiro, 2002). By late Atdabanian-early Botomian time, they had spread to Laurentia and other parts of the world. Distribution patterns have been suggested involving dispersal from Siberia through the Far East to Australia, and from Siberia through Iran and central Europe to W Europe and N Africa (Zhuravlev, 1986; Debrenne, 1992). However, these distribution patterns are based on previous continental reconstructions that do not consider Siberia, Laurentia, and the Anti-Atlas in close proximity.

The early distribution of archeocyathids from Siberia into northern Gondwana and Laurentia provides yet another line of support for the proximity of these three regions during Neoproterozoic and Early Cambrian time. Our reconstruction traces a possible route of expansion from the Siberian Platform, through the Anti-Atlas region,

along the western margin of Laurentia, across the Eagle Bay volcanics that may represent a spreading ridge associated with the break-up of Rodinia, and back into NE Siberia (see Sears and Price, 2003).

5.6 Implications for plate tectonics and paleontology

Our Neoproterozoic Anti-Atlas – SE Siberia – SW Laurentia reconstruction implies that either the Anti-Atlas terrane was not attached to the West African Craton (WAC) until the Phanerozoic, or the entirety of Gondwana was close to SE Siberia and SW Laurentia during Neoproterozoic and Early Cambrian. There seems to be a space problem with including all of Gondwana with the Siberia – Laurentia connection. While many researchers contend that the Anti-Atlas terrane accreted onto the WAC during Neoproterozoic Pan-African orogeny (e.g. Hefferan et al., 1992; Saquaque et al., 1992; Fekkak et al., 2000; Ennih and Liègois, 2001; Thomas et al., 2002; Walsh et al., 2002), it is conceivable that the Anti-Atlas terrane was separate from the WAC until the Appalachian-Variscan-Hercynian orogeny (c.f. Caritg et al., 2004).

Soulaimani et al. (2003) recognized Proterozoic syn-rift passive margin deposits upwards of 10km-thick in the Anti-Atlas region, indicating a possible association with Rodinia break-up. Following rifting, the Anti-Atlas terrane could have traveled along major strike-slip faults observed in the Anti-Atlas region, SW Laurentia, and the later Appalachian-Variscan-Hercynian orogenic belt. The Tindouf Basin to the south of the present-day Anti-Atlas region forms a 10km-thick succession of Paleozoic sediments deposited in what appears to be the foreland basin of the Appalachian-Variscan-Hercynian orogenic belt to the north. Caritg et al. (2004) describe Late Paleozoic fold-and-thrust structures in the Anti-Atlas rocks that they assign to the Appalachian-Variscan-Hercynian orogeny.

Juxtaposing the Anti-Atlas, SE Siberia, and SW Laurentia simplifies some paleontology problems with other extant plate reconstructions. For instance, some Early Cambrian reconstructions place northern Africa at high latitude (e.g. Dalziel, 1997), an unlikely position for development of the abundant reefs in the Anti-Atlas, especially during "cold house" global climate conditions reported for Early Cambrian time (Trompette, 1996). Our reconstruction places the Anti-Atlas region near the equator along with Siberia and Laurentia, allowing the development of the earliest animals and the archeocyathid reefs in an appropriate environment.

Another paleontological implication of our reconstruction involves the explanation for speciation and range expansion of some of the first Metazoans and archeocyathids. The close proximity of the three regions implies that Metazoan radiation did not necessarily diverge for such a long time to distribute various species to distant parts of the globe. The divergence could have occurred in a spatially confined region in a relatively short period of time, albeit still probably beginning before the Cambrian. The proximity of trilobite and archeocyathid distribution through time also suggests a possible symbiotic relationship between the two organisms, although more analysis is necessary.

5.7 Conclusions and tests

Based on detrital-zircon, structural, magmatic, sedimentologic, and paleontologic data, we suggest that SE Siberia, SW Laurentia, and the Anti-Atlas region were in close proximity during Neoproterozoic time, and that they separated during Neoproterozoic and Early Cambrian rifting. Our reconstruction raises questions regarding the tectonic evolution of the Anti-Atlas region and the speciation and range expansion of Earth's first animals.

We offer the following tests for our hypothesis: 1) detrital-zircon provenance analyses from Anti-Atlas sedimentary units such as the Anti-Atlas Supergroup and the

Ouarzazate Supergroup, with respect to Laurentian and Siberian source terranes; 2) structural analyses of compressional events in Neoproterozoic and older sediments in SE Siberia and SW Laurentia that could be associated with compressional events in the Anti-Atlas region; 3) paleomagnetic analyses of Proterozoic rocks within the Anti-Atlas, Siberian, and Laurentian regions; 4) structural analyses concerning suturing of the Anti-Atlas terrane to the WAC during the Appalachian-Variscan-Hercynian orogeny.

CHAPTER 6

COMMENT ON THE EQUIVALENCY OF SHRIMP-RG VERSUS LAICPMS IN DETRITAL-ZIRCON GEOCHRONOLOGY ANALYSES

6.1 Introduction

In situ U-Th-Pb geochronology is a powerful technique for determining age heterogeneities and concordant sections within single zircon crystals. Two primary *in situ* techniques are sensitive high resolution ion microprobe-reverse geometry (SHRIMP-RG; e.g. Williams, 1998; Compston, 1999) and laser ablation inductively coupled plasma mass spectrometry (LAICPMS; e.g. Feng et al., 1993; Fryer et al., 1993; Chang et al., 2006). Although these techniques yield lower age precision than conventional isotope dilution-thermal ionization mass spectrometry (ID-TIMS), they offer several advantages such as 1) the ability to analyze individual zircon domains, 2) shorter analyzing time, 3) sample preparation without chemical treatment, and 4) only partial sample destruction during analysis.

Among other recent applications, SHRIMP and LAICPMS have been applied heavily to detrital-zircon U-Pb geochronology studies. Several differences exist between the two techniques, so it is important to assess their equivalency to insure that interpretations are based on comparable data. We compared ages yielded by SHRIMP analyses to ages yielded by LAICPMS analyses on the same zircons.

This comment is an outcome of an extensive study that included 1130 detrital-zircon U-Pb geochronology analyses from 28 different samples taken from two different continents (see Chapter 1, MacLean et al., *in review*). We obtained our data from the LAICPMS laboratory at Washington State University (WSU), and from the SHRIMP laboratory at Stanford University. To test the equivalency of the two techniques, we

analyzed 36 zircons with both SHRIMP and LAICPMS. The study was part of a larger project involving a Precambrian plate reconstruction that juxtaposes E Siberia with W Laurentia (see Sears and Price, 1978; 2003; MacLean et al., *in review*). We also analyzed additional zircons for another project not discussed here.

6.2 Experimental and Analytical Techniques

We extracted and separated zircons from 15 Siberian samples and 13 Laurentian samples using standard techniques including crushing, density and magnetic separation, and hand picking under a stereoscope. Separation yielded zircon grains ranging from ~50µm to ~240µm in length. Following standard procedures, we mounted zircons onto pucks for analysis. We prepared cathodoluminescence scanning electron microscope images to decipher the internal structures of the sectioned grains.

In four consecutive 24-hour days, we performed 427 U-Th-Pb analyses with the SHRIMP-RG in the Stanford-United States Geological Survey cooperative ion microprobe facility. Instrumental conditions and data acquisition followed Williams (1998). Craters produced by the primary O_2^- beam, operated at ~4.8 nA, were ~1 µm deep and ~30µm in diameter. The magnet was cycled through the mass stations six times per analysis, with one standard analysis for every five unknown analyses. We calibrated concentration data against standard CZ3 zircon (550 ppm U), and isotopic ratios against standards R33 (419 Ma, Black et al., 2004) and RG6. Raw data were reduced and plotted by the SHRIMP-RG research staff at Stanford University using the Squid and Isoplot/Ex programs of Ludwig (1999, 2003).

In four consecutive ~16 hour days, we performed 703 U-Th-Pb analyses with the New Wave UP-213 laser ablation system in conjunction with a ThermoFinnigan Element2 single collector double focusing magnetic sector ICP-MS in the GeoAnalytical Lab at WSU. We used a fixed diameter spot size of either 16µm or 30µm with a laser

frequency of either five Hz or ten Hz, depending on the sizes and Pb concentrations of the zircons. Each analysis included six seconds of warm-up, eight seconds of delay, and 35 seconds of rapid scanning (300 sweeps) across the following masses: ^{202}Hg, ^{204}(Hg+Pb), ^{206}Pb, ^{207}Pb, ^{208}Pb, ^{232}Th, ^{235}U, ^{238}U. We corrected for mass and elemental fractionation by calibrating data against standards R33 zircon (Black et al., 2004) and FC-1 zircon (Paces and Miller, 1993). The Hg-corrected ^{204}Pb data fluctuated between ±1500 cps and were deemed to be unreliable so the U-Th-Pb data were interpreted without any common Pb correction. Some LAICPMS laboratories, such as the University of Arizona Laser Chron center (see Stewart et al., 2001), claim to reliably measure common ^{204}Pb and can interpret radiogenic Pb data rather than total Pb. Reliable ^{204}Pb measurements will be a significant improvement in ICP geochronological techniques, but we restrict our comment to our results from the LAICPMS laboratory at WSU. We reduced raw data off-line using an in-house Excel spreadsheet supplemented with Visual Basic macros at WSU. We then processed and plotted data using the Isoplot program of Ludwig (2003) at the University of Montana.

In order to ensure consistency between data from the two instruments, we analyzed 36 grains from three samples (~twelve grains per sample) by both instruments. SHRIMP-RG analyses were performed first and the gold coating was dissolved by potassium iodide vapors in preparation for ICP analysis. The pucks were not repolished between the two analytical sessions. SHRIMP ion beam pits were located and laser ablated for ICP analysis on twenty-six grains, although the laser pits were generally 20 to 30 microns deeper than the ion beam pit. For ten grains, we analyzed different spots in the same CL domains.

6.3 Results

Figures 6.1 and 6.2 show results from zircons analyzed by both instruments. Two of the 36 LAICPMS analyses did not yield interpretable results, probably because the grain was smaller than the ablation pit. Thirty-two of the 34 remaining zircons yielded SHRIMP and LAICPMS $^{207}Pb/^{206}Pb$ dates that are equivalent within 2σ error despite the lack of a common Pb correction to the LAICPMS data (Figure 6.1A). Thirty of the 34 zircons yielded $^{206}Pb/^{238}U$ dates that are equivalent within 2σ error despite the lack of a LAICPMS common Pb correction (Figure 6.1B). Figure 6.2B illustrates a slight shift towards younger LAICPMS $^{206}Pb/^{238}U$ dates relative to SHRIMP (line runs through ages without considering errors; slope = 0.93). Ages ranged from ~958 Ma to ~2881 Ma. LAICPMS analyses yielded an average $^{207}Pb/^{206}Pb$ error of 2.9% at 2σ and an average $^{206}Pb/^{238}U$ error of 9.1% at 2σ. SHRIMP analyses yielded an average $^{207}Pb/^{206}Pb$ error of 2.5% at 2σ and an average $^{206}Pb/^{238}U$ error of 1.9% at 2σ.

One commonly discussed disadvantage to LAICPMS is its lower precision compared to the SHRIMP technique ($^{207}Pb/^{206}Pb$ 2σ error of 2.9% vs 2.5%, and $^{206}Pb/^{238}U$ 2σ error of 9.1% vs 1.9%, respectively). Although this is evident in our study, a more noticeable outcome involves the proportion of analyses that yielded dates <10% discordant. 85% of SHRIMP-RG analyses were <10% discordant (361 of 427), compared to only 56% of LAICPMS analyses (395 of 703). Therefore, while we were able to analyze almost twice as many zircons with the LAICPMS in the same number of days, the two instruments yielded similar numbers of useable data. Pretreatment of detrital-zircon samples by the annealing and partial dissolution technique of Mattinson (2005) can greatly decrease the number of discordant LAICPMS (as well as SHRIMP and ID-TIMS) dates by removing discordant domains (personal comm., Randy Parrish, 2006). However, pretreatment complicates the sample preparation and requires clean chemistry laboratories.

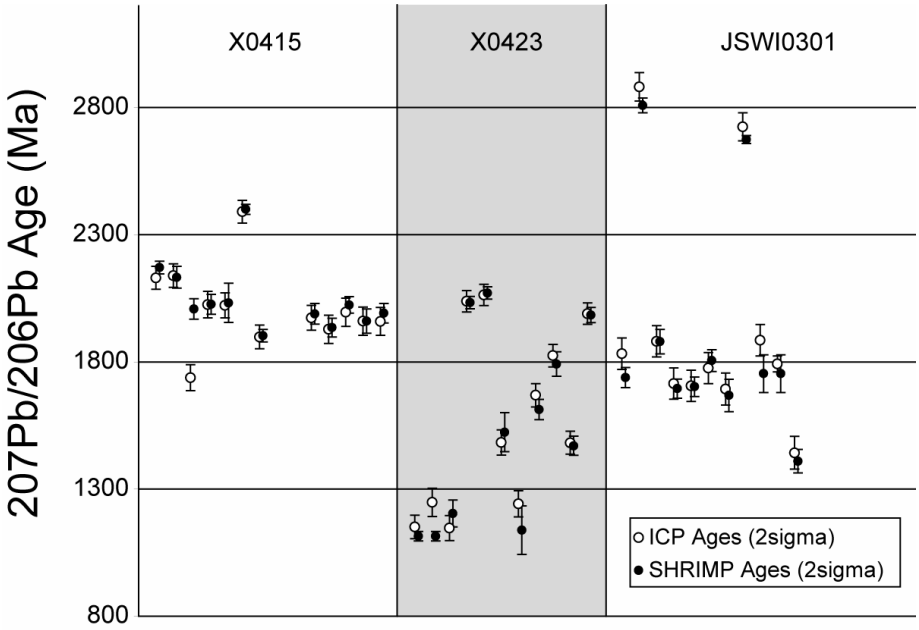

A.

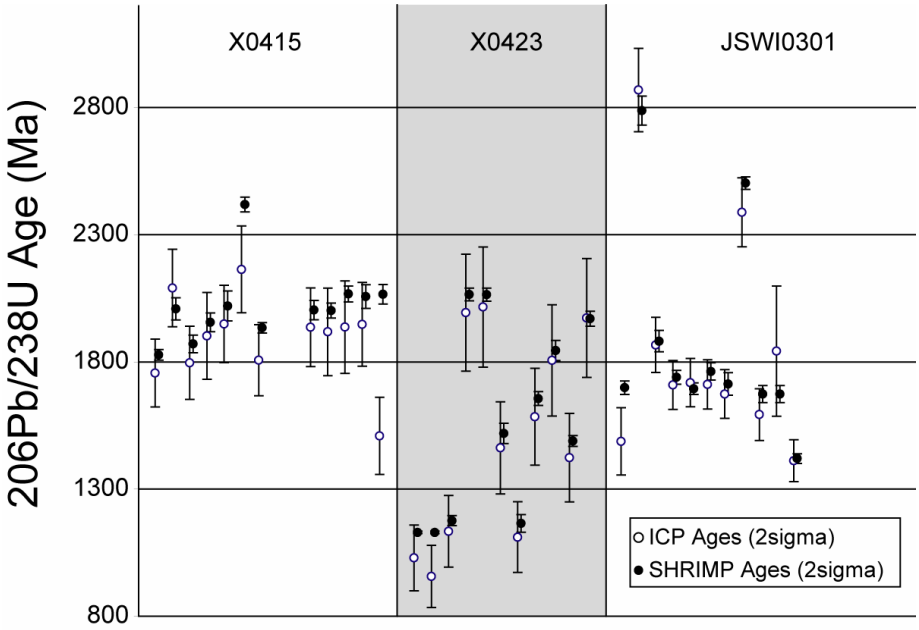

B.

Figure 6.1. Comparison of SHRIMP and LAICPMS $^{207}Pb/^{206}Pb$ dates (A.) and $^{206}Pb/^{238}U$ dates (B.). Dates with 2σ error ranges are presented as couplets. Each couplet represents one zircon that was analyzed by each method. Open circle in each couplet represents LAICPMS age; closed circle represents SHRIMP age. X0415, X0423, and JSWI0301 are sample names.

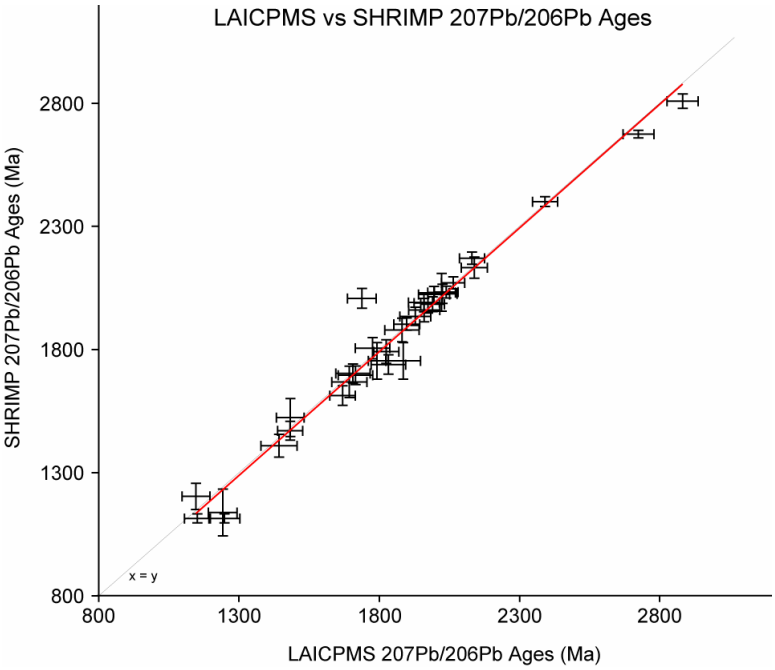

A.

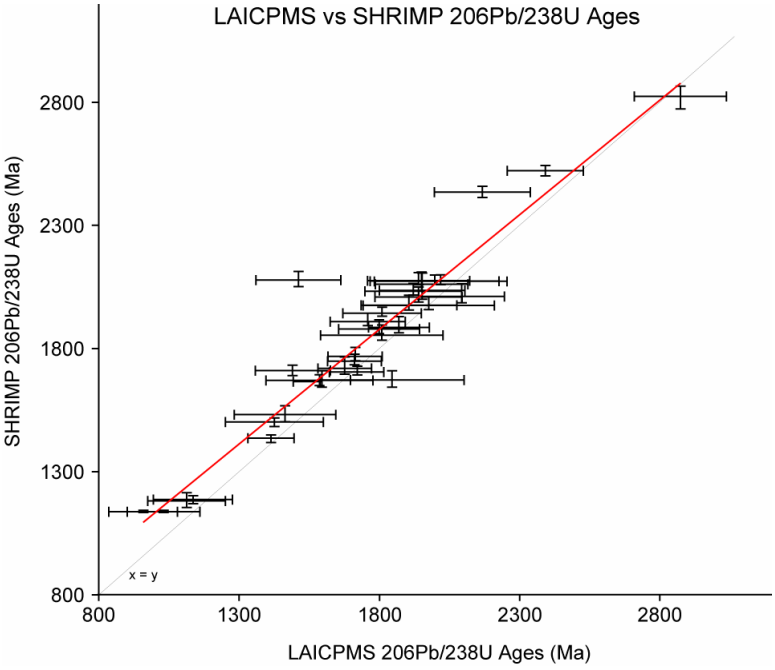

B.

Figure 6.2. Comparison of SHRIMP and LAICPMS $^{207}Pb/^{206}Pb$ dates (A.) and $^{206}Pb/^{238}U$ dates (B.). Dates with 2σ error ranges are presented together, with each point representing one grain analyzed be each method. Red line represents best-fit line through mid-points of each grain. Faint black line represents hypothetical 1:1 ratio.

The SHRIMP-RG laboratory at Stanford University is set up for 24-hour per day operation. Analysis times of ~12 minutes per spot allow a single user to operate the instrument efficiently. With two users working alternating 12-hour shifts for four days, we analyzed 427 unknown zircon grains and 93 standards. The SHRIMP-RG laboratory has automated most data processing subsequent to the actual analyses, thus additional processing time is relatively short and often performed by the laboratory staff. By contrast, the system at WSU's LAICPMS laboratory is relatively complicated for first-time users, partially due to the rapid ~3 minute analysis time, as well as less-automated data filing. We found that three users working in two-person shifts could efficiently work for ~16 hours per day. In four days, we analyzed 703 unknown zircon grains and 271 standards. We then processed the raw data from the LAICPMS at the University of Montana over the course of six weeks. Approximately 100 hours of processing and file-sorting time was required after raw data acquisition. The post-analysis data processing time may become shorter as LAICPMS techniques are refined. The University of Arizona Laser Chron laboratory, for example, already employs a series of macros and flags to assist users in assessing the quality of the analyses. Nevertheless, in general, more post-analysis data processing time is required to finalize LAICPMS dates than SHRIMP dates.

6.4 Discussion

The purpose of this chapter is to evaluate current advantages and limitations of the two common detrital-zircon U-Pb geochronology techniques. The following sections discuss our comparisons from an age-equivalency perspective and from a practical perspective (see Table 6.1).

Table 6.1. SHRIMP-RG versus LAICPMS comparison of practical considerations.

	SHRIMP-RG	LAICPMS
Number of analyses	427	703
Number of analyses <10% discordant	361	395
Percent of analyses <10% discordant	85%	56%
Analysis time	2 people, 24 hours/day, 1-person shifts, 4 days	3 people, ~16 hours/day, 2-person shifts, 4 days
Post-data acquisition processing time	minimal	~100 hours
Total person-hours	96 hours	~164 hours
Person-minutes per useable zircon date	~16 minutes	~25 minutes
Cost	$1500/day	$750/day
Cost per usable zircon date	$16.62	$7.59
Instrument availability	~1 year wait list	< 2 month wait
Destruction	~1 µm deep by ~30µm in diameter	up to ~30µm deep by ~30µm in diameter

6.4.1 Age equivalency

A few studies have compared LAICPMS to SHRIMP and ID-TIMS methods with the general conclusion that the lower precision LAICPMS dates are acceptable for detrital-zircon studies (e.g. Scott and Gauthier, 1996; Horn et al., 2000; Ballard et al.,

2001; Košler et al., 2002; Black et al., 2004; Weislogel et al., 2004; Chang et al., 2006). Our results show that SHRIMP-RG analyses at Stanford University and LAICPMS analyses at WSU generally yielded equivalent results within 2σ error, despite the lack of a common Pb correction with LAICPMS (discussed below). LAICPMS analyses yielded $^{206}Pb/^{238}U$ dates that were slightly younger than SHRIMP analyses yielded on the same zircons; however, the vast majority of comparison analyses were identical within 2σ error. Chang et al. (2006) contend that the accuracy and precision of individual zircon analyses at WSU's LAICPMS are better than 4% (2σ error), based on their comparison study of five zircon samples dated both by LAICPMS at WSU and by ID-TIMS.

Most zircon grains likely contain small amounts of common Pb from sample preparation contamination or from the zircon grain itself. One challenge for LAICPMS Pb isotopic analyses is to monitor accurately the common Pb component by measuring ^{204}Pb. The ^{204}Pb signal has low intensity and is masked by trace levels of ^{204}Hg in the argon gas at WSU. The abundance of ^{204}Hg can be estimated by measuring ^{202}Hg and using the natural $^{202}Hg/^{204}Hg$ ratio. This value can then be subtracted from the measured ^{204}mass peak to obtain ^{204}Pb. Due to the high variation in the calculated ^{204}Pb values, we interpreted our data without a common Pb correction (also see Chang et al., 2006).

Other laboratories use different types of mass spectrometers, collectors, and lasers, and their analytical and data reduction techniques differ slightly. Some laboratories claim to be capable of accurately measuring common Pb (e.g. Stewart et al., 2001). The discrepancies in laboratory procedures are partially due to the relatively inexpensive nature of ICP mass spectrometers and the recent explosion in application of ICP geochronology. With time, these differences may diminish as successful strategies are developed and shared. Thus, refinements in common Pb corrections may be forthcoming.

Our LAICPMS analyses that were not corrected for common Pb yielded generally equivalent results to our SHRIMP analyses that were corrected for common Pb. Our mean measured common ^{206}Pb value from SHRIMP analyses was only 0.07%. The equivalency in calculated dates despite a common Pb correction and the low common ^{206}Pb percentage indicate that the interiors of our grains did not contain significant amounts of common Pb, and that a common Pb correction may not always be necessary.

6.4.2 Practical considerations

Detrital-zircon U-Pb geochronology requires 117 analyses per sample to achieve 95% confidence of dating at least one grain of an age range that represents 5% of the total population (Vermeesch, 2004). Therefore time, cost, availability, and useable sample output constraints are important considerations in designing experiments. Our results show that SHRIMP and LAICPMS each have practical advantages. LAICPMS has the capability of yielding ~60% more total zircon analyses at half the cost. Also, the wait for LAICPMS availability is much shorter than that for SHRIMP availability. However, SHRIMP yields a much higher proportion of nearly concordant (<10% discordant) analyses, and the user does not have to process the data post-acquisition. Furthermore, the minimal destruction caused by SHRIMP permits future analyses on small individual grains. This could be important in a detrital-zircon study where more precise ID-TIMS dates are desired for certain zircons. Note that numerous variations of LAICPMS laboratory procedures are continually being developed as the scientific community continues to refine the method.

One important consideration regarding the number of discordant grains involves the sizes of the error ellipses. The 10% discordant cut-off was applied to the center of the error ellipse, but some ellipses, especially in the LAICPMS data, are large enough that they intersect concordia. It may be useful to consider the edges instead of the

centers of the error ellipses when determining which data to cull. If we were to use the edges, we would retain many more data, especially from LAICPMS analyses, and the advantage of SHRIMP would be diminished. This research is ongoing.

6.5 Conclusions

We analyzed 36 detrital zircons with the SHRIMP-RG at Stanford University, and then we analyzed the same zircons with the LAICPMS at WSU. In four days at each instrument, we found that the two laboratories yielded 32 of 34 equivalent $^{207}Pb/^{206}Pb$ dates and 29 of 34 equivalent $^{206}Pb/^{238}U$ dates within 2σ error (2 LAICPMS analyses yielded results that were not interpretable). Our results show that the interiors of the zircon grains in our study did not exhibit significant amounts of common Pb, and that a common Pb correction is not always necessary.

We also found that each instrument has practical advantages and limitations. The SHRIMP-RG yields more precise and less discordant data, produces a smaller amount of destruction, and requires fewer total person-hours (including post-acquisition time) per useable date. The LAICPMS yields many more total zircon dates, and slightly more useable zircon dates for a given amount of instrument time. LAICPMS instrument time is also less expensive and more readily available. Other LAICPMS laboratories may yield different levels of precision, error, time, and cost.

CHAPTER 7

CONNECTING TEXTBOOK FACTS TO GEOLOGIC RESEARCH METHODS IN MIDDLE SCHOOL SCIENCE USING ARC9 GIS, PLATE TECTONICS DATA, AND BEACH SANDS

7.1 Introduction

There has been a recent surge of interest in improving science education at the secondary level (NRC, 1996). For instance, the National Science Foundation is promoting projects wherein the students are immersed in current scientific research. Middle school students rarely have the opportunity to experience actual geologic research methods. Students who learn how geologists use the present to study the past can better understand relationships between modern Earth processes and ancient environments.

Through the Ecologists, Educators, and Schools Program, funded by the NSF – GK-12 program, we developed a four-part inquiry that allows middle school students to perform geologic research using observation, analytic equipment, and quantitative data. Our inquiry combines group participation in constructing students' own categories for beach sand compositions and plate boundary types with geographic information system software (Arc9 GIS). Students answer the question, "How are plate tectonics and sand related?" One of our goals was to integrate many practices used in geologic studies that are consistent with the National Science Education Standards (NRC, 1996). These practices include assessment of quantitative and spatial data, sample categorization, hypothesis generation and testing, sampling strategies, limits of laboratory methods, and comparison of laboratory models to natural and ancient settings.

This inquiry was tested at Hellgate Middle School in Missoula, Montana, as the

first section of an earth science unit for seventh graders that built upon previous Arc9 GIS lessons.

Standard instruction on plate tectonics in middle schools includes the history of plate tectonics theory, the distribution of earthquakes, volcanoes, and fossils, the Pangean fit of the continents, and the age of oceanic crust. By relating analyses of beach sands to standard plate tectonics exercises, our inquiry allows students to discover connections between seemingly unrelated processes (e.g., earthquakes and deposition). Our inquiry focuses on simple observations and assumes no prior geologic knowledge, but introduces multiple disciplines including geography, plate tectonics, sedimentary processes, source rock analysis, and earth history. Students integrate data from earthquakes, volcanoes, topography/bathymetry, and geochronology to discern types of plate boundaries. Then they use observations and analyses of beach sands to relate types of beach sands to types of current plate boundaries and continental margins. Finally, they discern ancient tectonic environments through observations and analyses of ancient sandstones.

Students construct their own categories through observations with Arc9 GIS and stereographic microscopes to 1) become familiar with mapping technology used in scientific research, 2) learn about to plate tectonic processes, 3) recognize connections between current plate boundaries and beach sands, and 4) gain a first-hand look at research methods geologists use to discern Earth's history.

Teachers can refer to the experiences gained by the students in this inquiry during subsequent instruction. The inquiry ties explicitly to content standards for middle school students, such as the nature of science, scientific inquiry, and science technology.

7.2 Beach Sands and Plate Tectonics

7.2.1 Geologic Concepts

Because the concept of plate tectonics is well presented in seventh grade science textbooks, this chapter focuses on the relationship between plate tectonics and beach sands. Sand compositions are influenced by the source rock (the rock that broke down to produce the sand), sedimentary processes, and the paths that link the source rock to the place where the sand is deposited. The primary control on all of these factors, including sand composition, is plate tectonics. Scientists have evaluated the effect of modern tectonic processes on modern sand compositions. They have extrapolated their findings to ancient sandstone compositions in order to determine the tectonic setting necessary to produce those sandstone compositions. For example, Crook (1974), Schwab (1975), and Dickinson and Suczek (1979) showed that careful analyses of the quartz grains, feldspar grains, and rock fragments contained in sand reveal trends that point to possible plate tectonic environments present during the formation of the source rock. Today, researchers routinely plot the proportions of minerals onto triangle diagrams to ascertain trends in the data (see Figure 7.1). A high proportion of quartz and a low proportion of rock fragments signify a "*continental block*" environment; a high proportion of quartz and a low proportion of feldspar signify a "*recycled orogen*" environment; and a low proportion of quartz signifies a "*magmatic arc*" environment (Figure 7.2 and glossary). We use these basic ideas as the foundation for introducing geologic research methods to middle school students.

7.2.2 Learning About Tectonics from Sand Compositions

Teachers will need a variety of sands for this investigation. These samples can be collected during travel or by having students correspond with classes around the world to request sand samples. Also, universities near beaches often are willing to supply a sample of sand. In this example, we used five beach sands from around the

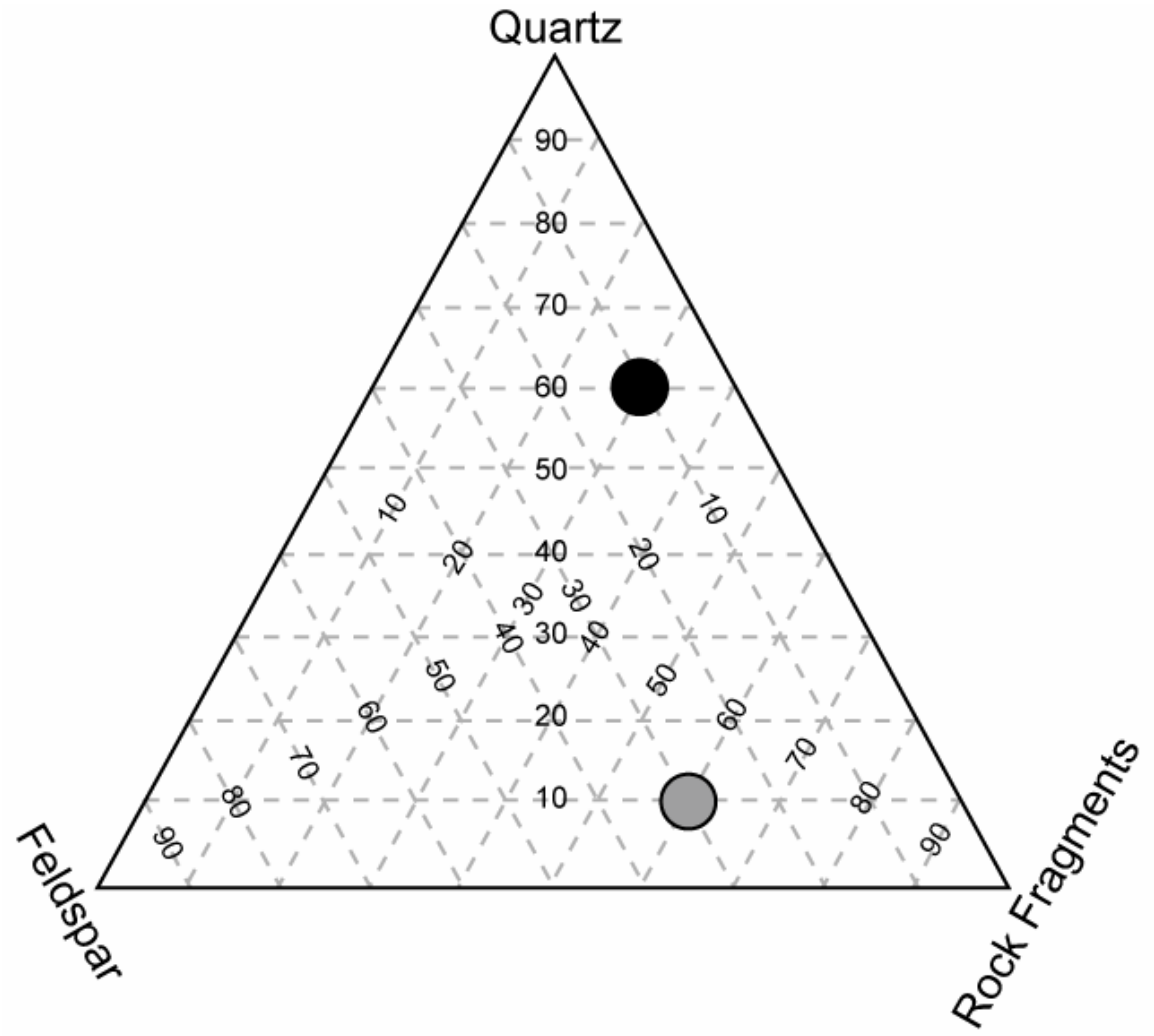

Figure 7.1. Triangle diagram showing constituents of two hypothetical samples (black and gray circles). Black circle contains 60% quartz, 10% feldspar, and 30% rock fragments. Gray circle contains 10% quartz, 30% feldspar, and 60% rock fragments.

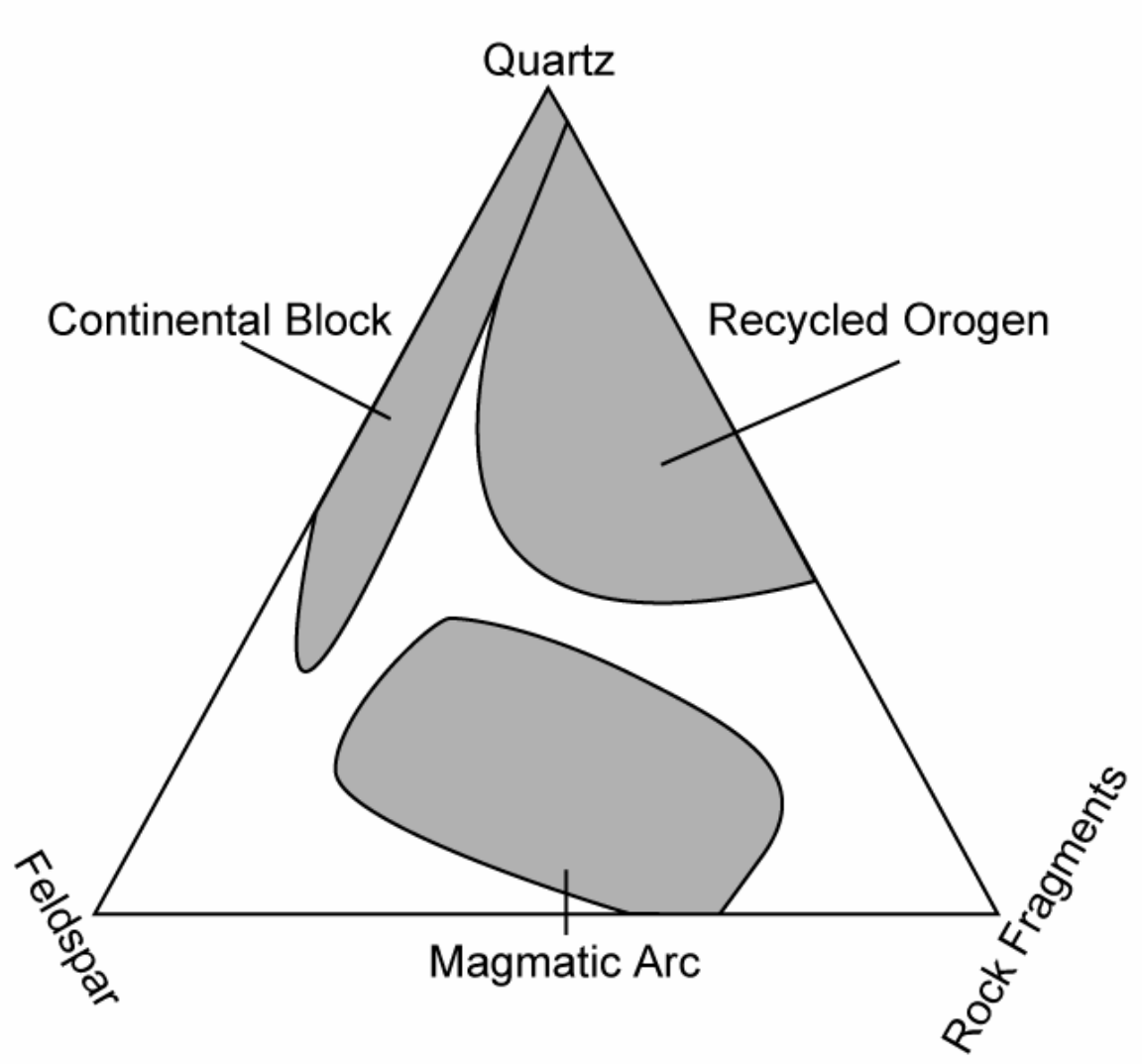

Figure 7.2. Triangle diagram showing geologists' interpretation of which tectonic setting produces particular percentages of mineralogical constituents (Dickinson and Suczek, 1979). Summary of each tectonic setting is provided in glossary.

world to illustrate relationships between tectonic environments and source rocks for sands. These sands came from Florida, Costa Rica, Fiji, Hawaii, and Japan. The students may or may not infer the same geologic interpretations as geologists have, but we include brief and simple descriptions of geologists' current interpretations here for reference.

Our analyses revealed that Florida sand contained a high proportion of quartz and a low proportion of rock fragments because the eastern margin of North America has been tectonically inactive for over 150 million years. The sand that collects on Florida's shores has traveled far enough and has had enough time for most minerals to break down either physically or chemically. Quartz, however, is quite resistant to physical and chemical weathering, so it is abundant in this environment.

Sand from Costa Rica contained a high proportion of rock fragments because Costa Rica sits over an ocean-continent subduction zone that is producing an active continental volcanic arc. Volcanoes such as Arenal are shedding new material onto nearby beaches. The lack of distance and time between the formation of rock and the deposition of sand results in a higher proportion of rock fragments that have yet to break down physically and chemically.

Fiji sand contained a large predominance of volcanic rock fragments. The Fiji islands sit on the tectonically active margin between the Australian and Pacific plates. Ocean-ocean subduction produced volcanic islands that are now undergoing deformation due to the stress of plate interactions. The volcanic rocks are eroding, and the resulting rock fragments are being deposited nearby.

Hawaiian sand had a high proportion of rock fragments because Hawaii was formed due to volcanism from a hot spot, and Hawaiian volcanoes continue to shed new volcanic rock fragments onto nearby beaches. Note that Hawaii is not close to a plate margin, but is the result of a hot spot. The information obtained from beach sands must

be considered with other data such as earthquake activity, volcanism, topography, and geochronology to infer an accurate geologic interpretation.

Sand from Japan was comprised of a high proportion of rock fragments because Japan rests above an active subduction zone. Mount Fuji is a volcano that sheds new volcanic rock fragments onto nearby beaches.

7.2.3 Investigation 1: Beach Sand Characterization

After a brief introduction to the inquiry and discussion of the research instructions, the students break into small groups of three to five students. Each group needs a stereographic microscope, a pair of needle-nose pliers, a small sheet of graph paper, and small samples (~20 grams) of beach sands in plastic containers.

Each group observes the sands through the stereographic microscopes, and constructs three categories of sand grain composition for each sample based on their observations. Students should consider color, size, shape, number, and any other characteristics they observe. Using the needle-nose pliers, they spread the sand grains into one layer on the graph paper so that each category covers a certain number of graph paper squares. The grains should touch each other without overlapping (Figure 7.3). To calculate the percentage of grains per category, students divide the number of covered squares of each category by the total number of covered squares. Then they record the characteristics of each of their categories (color, size, shape, etc.), as well as the percentage of the total sample that each category represents. Students produce a triangle diagram illustrating the percentages of grains per category for each of the five samples (refer to Figure 7.1 for sample of a triangle diagram). The investigation takes between 1 and 1.5 hours.

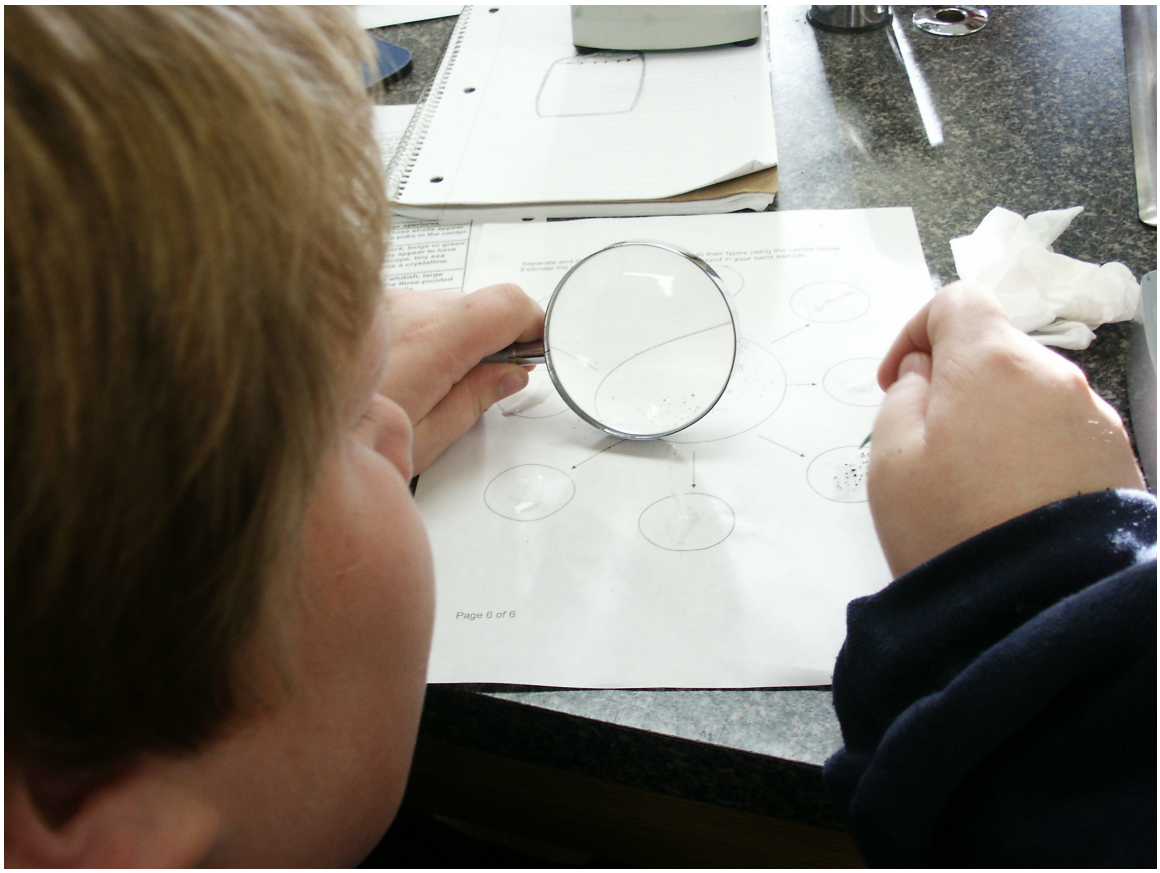

Figure 7.3. Photograph of 7th grade student separating sand grains according to his own classification scheme based on color, size, and shape of sand grains.

7.2.4 Investigation 2: Plate Boundaries Characterization Using Arc9 GIS

The plate boundaries phase of the inquiry is a modified version of *Discovering Plate Boundaries, a Data Rich Classroom Exercise* (Sawyer, 2002) and requires computers with Arc9 GIS software. Software is available through ESRI (Environmental Systems Research Institute) education grants. Datasets may be downloaded from *http://terra.rice.edu/plateboundary/* (website last accessed 5/2006).

In their research groups, students use Arc9 GIS to analyze various types of map data concerning plate boundaries. Map data include seismicity, volcanology, topography/bathymetry, and age of seafloor (Figure 7.4). Each group receives only one of the four map datasets on their computer. We emphasize that each group member must take an active part in the data analysis because they each will teach other students about their dataset in the following section of the investigation (Figure 7.5). After familiarizing themselves with their information, they overlay their map data onto a map of the global plate boundaries saved on each computer. By observing the features that the two maps have in common, the students construct a classification scheme for the world's plate boundaries. They write descriptions for 3-5 different types of plate boundaries and give each a number such as boundary type 1, boundary type 2, and so on. Descriptions are based purely on their observations, and include simple terms such as high or low topography, continuous or discontinuous distribution, clustered or scattered volcanoes, shallow or deep earthquakes, etc. Finally, students create a new plate boundary map on Arc9 GIS containing different classes of lines based on the categories they developed. Students use a different color to represent each boundary type. This section of the investigation takes between 1 and 1.5 hours.

Next, students prepare to share their results with their class members. Each group member receives a digital copy of the group's dataset and the new map that the group created. Students break into new groups so that each group has one member who studies the seismology map, one who studies the volcanology map, one who studies the topography/bathymetry map, and one who studies the geochronology map. Each member of the group becomes the expert on his/her field, but each member studies only one type of data. The group analyzes each of the four map datasets, and each member explains the appropriate features of his/her map, including what the data are, how they are symbolized, and what the most important characteristics are. Then

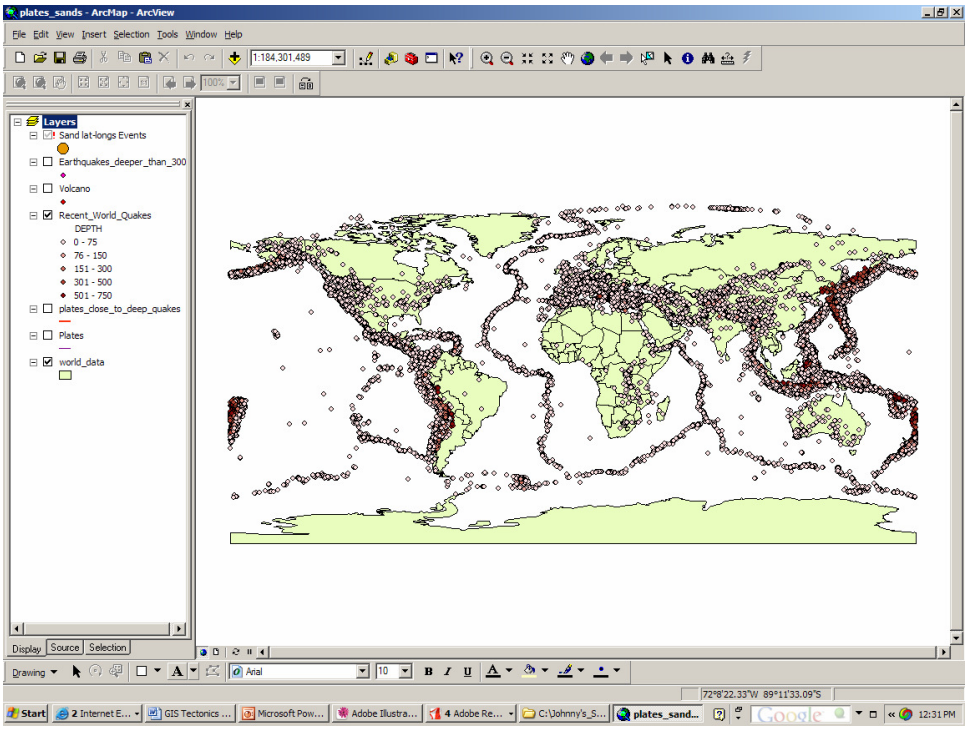

A.

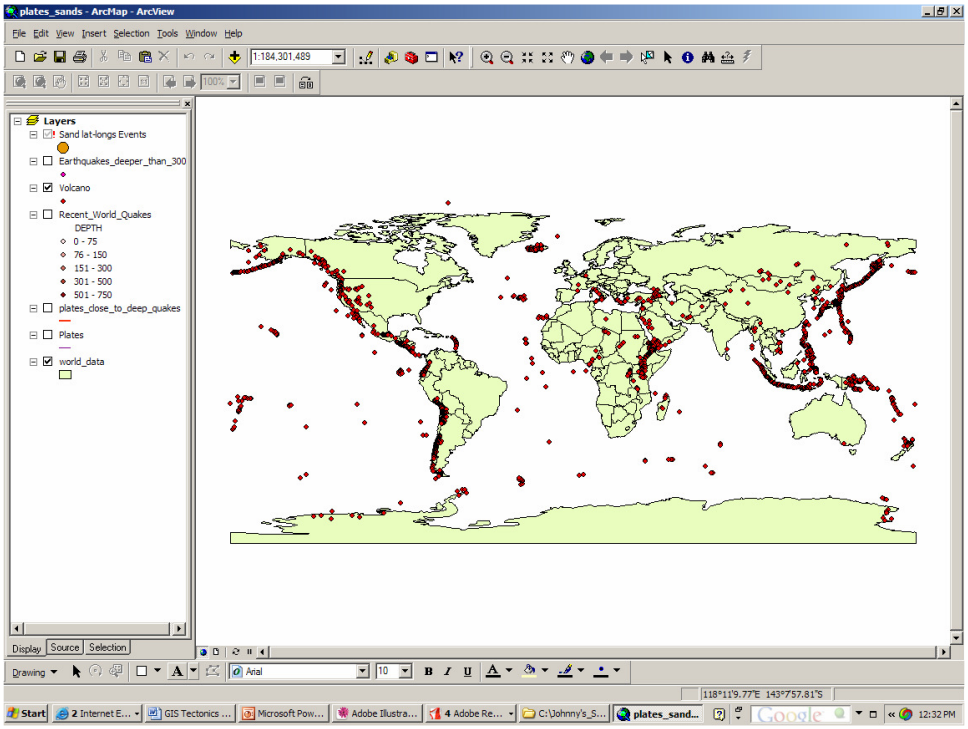

B.

Figure 7.4. Arc9 GIS screenshots of global earthquake (A) and volcano (B) data.

Figure 7.5. Three 7th graders discussing relationships between plate boundaries to create their own classification schemes for plate boundaries, following *Discovering Plate Boundaries* investigation by Sawyer (2002).

they discuss each member's new map based on the categories each previous group developed. Students may be advised to overlay each of the new maps and to perform a query using GIS to discern similarities between the four classification schemes. The goal for the new groups is to create and record a combined classification scheme that considers data from each of the four areas of specialty. For example, students might develop the following description of a plate boundary: plate boundary type A has shallow

earthquakes directly on the plate boundary, has sparse or no volcanoes, lies on a bathymetric high with deeper water to either side, and follows a line of young seafloor. Their analyses result in a final plate boundary map composed of different classes of lines based on their combined classification scheme using a different color for each boundary type (Figure 7.6). This requires between 1 and 1.5 hours.

7.2.5 Investigation 3: Spatial Integration of Beach Sand and Plate Boundary Types Using Arc9 GIS

Once students have categorized the types of beach sands and the types of plate boundaries, they receive digital data on the locations of their beach sand samples. They overlay these data onto their new plate boundary map and perform a distance query using GIS regarding the beach sand location and the nearest plate boundary. Then they infer what type of sand could be expected based on proximity to various plate boundary types. They record their inferences and explanations in their science notebooks. This analysis lasts between 0.5 and 1 hour.

7.2.6 Investigation 4: Extending Source Rock Analyses to Ancient Geologic Environments

Students perform another sand classification using stereographic microscopes on an ancient sandstone rock that has been partially crushed into sand. They use the skills gained through the inquiry to infer what type of plate boundary the sandstone was near at the time of deposition. They present their results, inferences, and explanations to the class. They are assessed based on their ability to support their inferences using their sand and plate boundary classification schemes. This application takes between 0.5 and 1 hour.

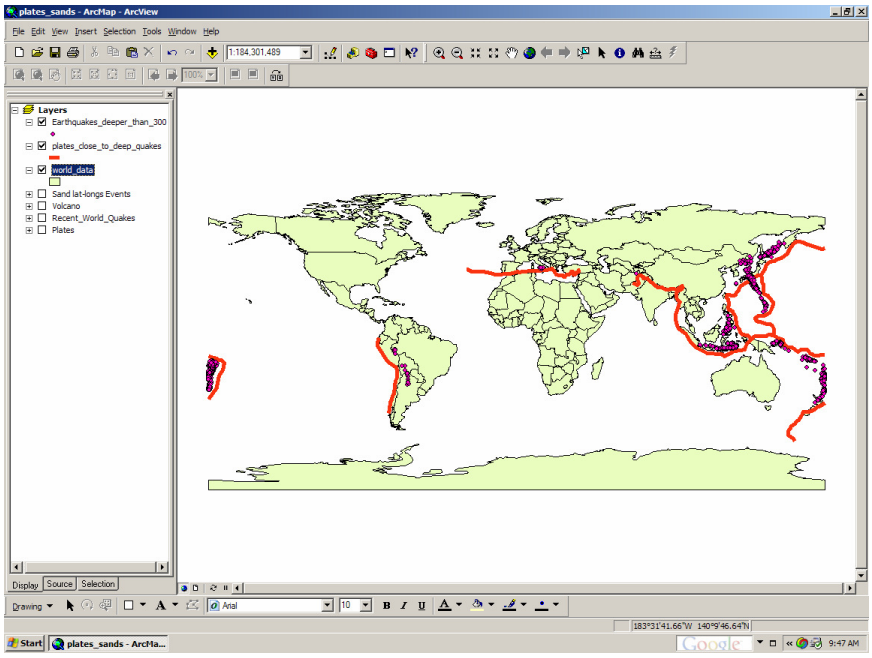

A.

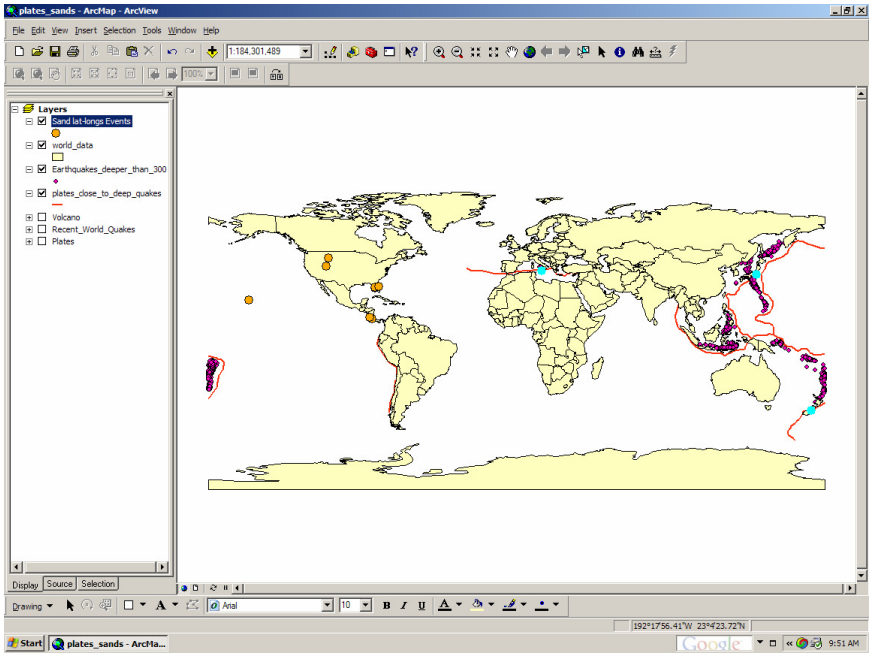

B.

Figure 7.6. Arc9 GIS screenshots of students' queries regarding proximity of plate boundaries to deep earthquakes (A), and regarding proximity of those plate boundaries to specific types of sand compositions shown as blue circles (B).

7.3 Implications and Extensions

Our inquiry introduces students to numerous earth science topics included in the National Science Education Standards. Furthermore, it allows them to employ research methods that geologists use to understand modern and ancient earth processes. Teachers can build the rest of the earth science curriculum around this inquiry by relating it to other topics and processes such as minerals, rocks, earth history, climate change, river processes, and planetary science. We include brief descriptions of possible extensions for teacher reference below.

Minerals—Students can use geologists' categories (as opposed to creating their own categories) to perform source rock analyses. This involves identifying and sorting quartz minerals, feldspar minerals, and rock fragments from sand.

Rocks—Teachers can do a similar inquiry, but with rocks and their locations. Care must be taken to determine whether the rock comes from a modern or an ancient tectonic environment.

Earth history—The ancient sand used for the inquiry assessment can be the cornerstone for introducing deep time, paleontology, and relative and absolute dating.

Climate—Plate location is one of the controlling factors of climate. Students can research how the positions of the continents have affected ocean currents, thereby affecting climate through time. Also, volcanism due to plate tectonics has had local and global effects on climate.

River Processes—The inquiry relates plate tectonic environments to beach sedimentation. River processes are inherent in transporting sediment from the source to the depositional basin. The inquiry can serve as a staging point for discussion and research regarding rivers. Also, students can collect sand from local rivers and compare the sand composition and texture to the surrounding geologic setting.

Planetary Science—Students can compare plate tectonics activity on Earth to that on other planets. Furthermore, students can research new photographs and data from the Mars expeditions (see NASA website) to make correlations with Earth's wind, river, and tectonic processes.

7.4 Conclusions

The students involved with this inquiry performed geologic research analyses to answer a specific question. They were able to extrapolate current processes to ancient environments in the same ways geologists do. They enjoyed the hands-on applications that geologists use, and they were prepared to continue through the rest of the earth science curriculum.

7.5 Glossary

Continental block—This environment includes 1) tectonically inactive mid-continent areas, and 2) uplifted fault blocks containing igneous and metamorphic continental crust (Figure 7.7A). Continental block environments produce sands rich in quartz and poor in rock fragments because the time and distance from the source rock to the point of sedimentation are great enough to break down particles that are more susceptible to weathering than quartz.

Recycled orogen—This environment includes several types of mountain-building settings (Figure 7.7B) that ultimately result in the erosion of sedimentary rocks, hence the *recycling* of sediments. The mountain-building settings include 1) subduction zones where oceanic materials are scraped onto the overriding plate, creating a highland susceptible to weathering and erosion that can shed sediments back into the subduction zone or onto the overriding plate, 2) continental collision zones where sedimentary rock

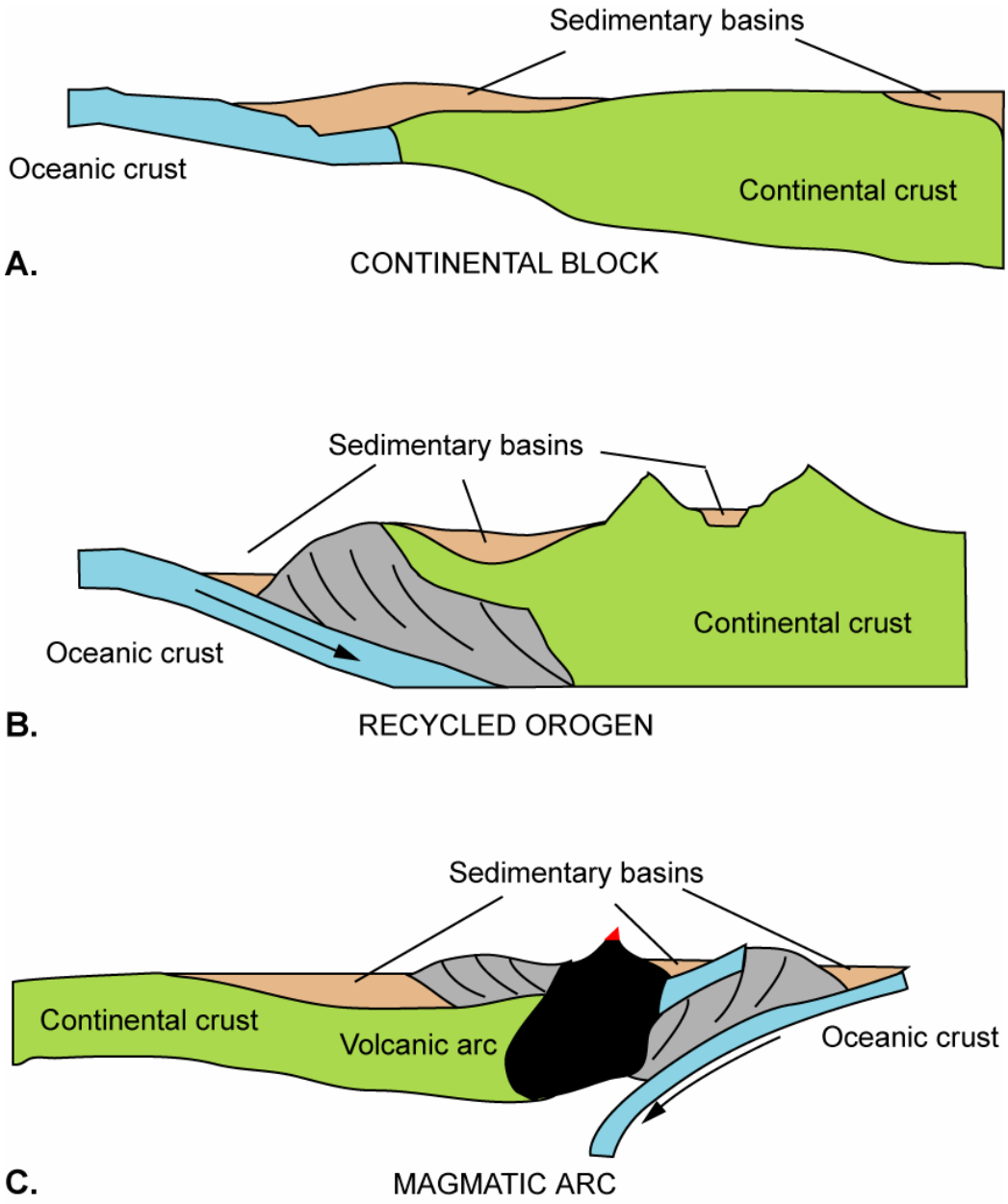

Figure 7.7. Generalized tectonic environments and their sedimentary basins (from Dickinson and Suczek, 1979). Summaries are provided in glossary.

along the margin of one plate is thrust up in a series of folds and faults, creating a structurally high region susceptible to weathering and erosion, and 3) any zone of compression which produces thickened, and therefore uplifted, continental crust, allowing weathering and erosion.

Magmatic Arc—This environment includes volcanic chain settings, including volcanic island chains and volcano chains along continental margins (Figure 7.7C).

REFERENCES

Adams, D.C. and Keller, G.R., 1994, Possible extension of the Midcontinent Rift in West Texas and eastern New Mexico, Canadian Journal of Earth Sciences, 31, 4, 709-720.

Admou, H., 2000, Structuration de la paleosuture ophiolitique panafricaine de Bou Azzer—Siroua (Anti-Atlas Central, Maroc), These Docteur d'Etat es-Sciences, Universite Cadi Ayyad, Marrakech, Morocco, 201 pp.

Alpert, S.P., 1976, Trace fossils of the White-Inyo Mountains: in J.N. Moore and A.E. Fritche, eds., Depositional Environments of the Lower Paleozoic Rocks in the White-Inyo Mountains, Inyo County, California, Pacific Coast Paleogeography Field Guide 1, Pacific Section, Society of Economic Paleontologists and Mineralogists.

Anderson, T., 2005, Detrital zircons as tracers of sedimentary provenance; limiting conditions from statistics and numerical simulation, Chemical Geology, 216, 3-4, 249-270.

Babinski, M., Chemale, F.,Jr., Van Schmus, W.R., 1995, The Pb/Pb age of the Minas Supergroup carbonate rocks, Quadrilatero Ferrifero, Brazil. Precambrian Research, 72, 235-245.

Babinski, M., Van Schums, W.R., Chemale, F., Jr., 1999, Pb-Pb dating and Pb isotope geochemistry of Neoproterozoic carbonate rocks from the São Francisco basin, Brazil: implications for the mobility of Pb isotopes during tectonism and metamorphism. Chemical Geology, 160, 175-199.

Ballard, J.R., Palin, J.M., Williams, I.S., Campbell, I.H., Faunes, A., 2001, Two ages of porphyry intrusion resolved for the super-giant Chuquicamata copper deposit of northern Chile by ELA-ICP-MS and SHRIMP, Geology, 29, 5, 383-386.

Benmore, W.C., 1981, Stratigraphy, sedimentology, and paleoecology of the late Paloephytic or earliest Phanerozoic Johnnie Formation, eastern California and southwestern Nevada [PhD dissertation], University of California Santa Barbara, 243 p.

Beus, S.S., Rawson, R.R., Dalton, R.O., Jr., Stevenson, G.M., Reed, J.C., and Daneker, T.M., 1974, Preliminary report on the Unkar Group (Precambrian) in Grand Canyon, Arizona, in Karlstrom, T.N.V., Swann, G.A., and Eastwood, R.L., eds.,

Geology of Northern Arizona, Part I, Regional Studies: Flagstaff, Arizona, Geological Society of America, Rocky Mountain Section Meeting, 407 p.

Black, Lance P; Kamo, Sandra L; Allen, Charlotte M; Davis, Donald W; Aleinikoff, John N; Valley, John W; Mundil, Roland; Campbell, Ian H; Korsch, Russell J; Williams, Ian S; Foudoulis, Chris, 2004, Improved (super 206) Pb/ (super 238) U microprobe geochronology by the monitoring of a trace-element-related matrix effect; SHRIMP, ID-TIMS, ELA-ICP-MS and oxygen isotope documentation for a series of zircon standards, Chemical Geology, 205, 1-2, 115-140.

Blewett, R.S., Black, L.P., Sun, S.-s., Knutson, J., Hutton, L.J., and Bain, J.H.C. , 1998, U-Pb zircon and Sm-Nd geochronology of the Mesoproterozoic of north Queensland: Implications for a Rodinia connection with the Belt Supergroup of North America, Precambrian Research, 89, 101-127.

Bond, G.C., Nickeson, P.A., and Kominz, M.A., 1984, Breakup of a supercontinent between 625 Ma and 555 Ma: New evidences and implications for continental histories, Earth and Planetary Science Letters, 95, 155-173.

Borg, S.G., and DePaolo, D.J., Laurentia, 1994, Australia and Antarctica as a late Proterozoic supercontinent: Constraints from isotopic mapping, Geology, 22, 307-310.

Bowring, S.A. et al., 1993, Calibrating rates of Early Cambrian evolution, Science, 261, 1293-1298.

Brannon, J.C., Cole, S.C., Podosek, F.A., Ragan, V.M., Coveney, R.M.,Jr., Wallace, M.W., and Bradley, A.J., 1996, Th-Pb and U-Pb dating of ore-stage calcite and Paleozoic fluid flow. Science, 271, 491-493.

Briggs, D.E.G. & Fortey, F.A. , 1992, The Early Cambrian radiation of arthropods, In Lipps, J.H. & Signor, P.W., eds. Origin and early evolution of the metazoa (Plenum Press, New York, 336-374.

Broecker, W.S., Peng, T.-H., 1982, Tracers in the Sea. New York: Eldigio Press.

Brookfield, M.E., Neoproterozoic Laurentia-Australia fit, 1993, Geology, 21, 8, 683-686.

Buchan, K.L., Mertanen, S., Park, R.G., Pesonen, L.J., Elming, S.-A, Abrahamsen, N., and Bylund, G. , 2000, Comparing the drift of Laurentia and Baltica in the Proterozoic: The importance of key palaeomagnetic poles, Tectonophysics, 319, 167-198.

Burkhard, M., Caritg, S., Helg, U., Robert-Charrue, C., Soulaimani, A., 2006, Tectonics of the Anti-Atlas of Morocco, Tectonics, 338, 11-24.

Burret, C., Berry, R., 2000, Proterozoic Australia-Western United States (AUSWUS) fit between Laurentia and Australia, Geology, 28, 2, 103-106.

Burrett, C., Richardson, R., 1980, Trilobite biogeography and Cambrian tectonic models, Tectonophysics, 63, 1-4, 155-192.

Caritg, S., Burkhard, M., Ducommun, R., Helg, H., Kopp, L., Sue, C., 2004, Fold interference patterns in the Late Paleozoic Anti-Atlas of Morocco, Terra Nova, 16, 1, 27-37.

Carlson, M.P., 1999, Transcontinental Arch – a pattern formed by rejuvenation of local features across central North America, Tectonophysics, 205, 225-233.

Cather, S.M., Karlstrom, K.E., Timmons, J.M., Heizler, M.T., 2006, Palinspastic reconstruction of Proterozoic basement-related aeromagnetic features in north-central New Mexico: Implications for Mesoproterozoic to late Cenozoic tectonism, Geosphere, 2, 6, 2999-323.

Cawood, P.A., Nemchin, A.A., Freeman, M., Sicrombe, K., 2003, Linking source and sedimentary basin: Detrital zircon record and sediment flux along a modern river system and implications for provenance studies, Earth and Planetary Science Letters, 210, 259-268.

Chang, Z., Vervoort, J.D., McClelland, W.C., Knaack, C., 2006, U-Pb dating of zircon by LA-ICP-MS, Geochemistry, Geophysics, Geosystems, 7.

Chester, R., 1990, Marine Geochemistry, Unwin Hyman, London, 698 p.

Christie-Blick, N., Levy, M., 1989, Stratigraphic and tectonic framework of the upper Proterozoic and Cambrian rocks in the western United States, in Christie-Blick, N., and Levy, M., eds., Late Proterozoic and Cambrian tectonics, sedimentation and record of metazoan radiation in the western United States, Washington D.C., American Geophysical Union, Fieldtrip Guidebook T221, 7-21.

Cocks, L.R.M., Fortey, R.A., 1982, Faunal evidence for oceanic separations in the Palaeozoic of Britain, Journal of the Geological Society of London, 139, 4, 465-478.

Cocks, L.R.M., Scotese, C.R., 1991, The global biogeography of the Silurian period, Special Papers in Palaeontology, 44, 109-122.

Compston W., 1999, Geological age by instrumental analysis, The 29th Hallimond lecture, Mineral Magazine, 63, 297-311.

Corsetti, F.A., 1998, Regional correlation, age constraints, and geologic history of the Neoproterozoic-Cambrian strata, southern Great Basin, USA; integrated carbon

isotope stratigraphy, biostratigraphy, and lithostratigraphy [Ph.D. dissertation], University of California Santa Barbara, 235 p.

Corsetti, F.A., Grotzinger, J.P., 2005, Origin and significance of tube structures in Neoproterozoic post-glacial cap carbonates: Example from Noonday Dolomite, Death Valley, United States, Palaios, 20, 348-362.

Corsetti, F.A. & Kaufman, A.J., 1994, Chemostratigraphy of Neoproterozoic-Cambrian units, White-Inyo region, Eastern California and western Nevada: Implications for global correlation and faunal distribution. Palaios 9, 211-219.

Crook, K.A.W., 1974, Lithogenesis and geotectonics: the significance of compositional variations in flysch arenites (graywackes), In: Modern and ancient geosynclinals sedimentation, SEPM Special Publication, 19, 304-310.

Dalton, R.O., Jr., 1972, Stratigraphy of the Bass Formation (Late Precambrian, Grand Canyon, Arizona), [M.S. thesis]: Flagstaff, Northern Arizona University, 140 p.

Dalziel, I.W.D., 1997, Neoproterozoic-Paleozoic geography and tectonics; review, hypothesis, environmental speculation, Geological Society of America Bulletin, 109, 1, 16-42.

Dalziel, I.W.D., 1991, Pacific margins of Laurentia and East Antarctic-Australia as a conjugate rift pair: Evidence and implications for an Eocambrian supercontinent, Geology, 19, 598–601.

Daneker, T.M., 1975, Sedimentology of the Precambrian Shinumo Sandstone, Grand Canyon, Arizona [M.S. thesis], Flagstaff, Northern Arizona University, 195 p.

Debrenne, F., 1992, Diversification of the Archaeocyatha, Topics in Geobiology, 10, 425-443.

DeWolf, C.P. and Halliday, A.N., 1991, U-Pb dating of a remagnetized Paleozoic limestone. Geophysical Research Letters, 18, 1445-1448.

Dèzes, P., Schmid, S.M., Ziegler, P.A., 2004, Evolution of the European Cenozoic Rift System: interaction of the Alpine and Pyrenean orogens with their foreland lithosphere, Tectonophysics, 389, 1-33.

Dickinson, W.R., and Gehrels, G.E., 2000, Sandstone petrofacies of detrital zircon samples from Paleozoic and Triassic strata in suspect terranes of northern Nevada and California, Geological Society of America, Special Paper 347, 151-171.

Dickinson, W.R., and Suczek, C.A., 1979, Plate tectonics and sandstone compositions, AAPG Bulletin, 63, 12, 2164-2182.

Diehl, P.E., 1979, The stratigraphy, depositional environments, and quantitative petrography of the Precambrian-Cambrian Wood Canyon formation, Death Valley [PhD dissertation], Pennsylvania State University, 365 p.

Diehl, P.E., 1974, Stratigraphy and sedimentology of the Wood Canyon Formation, Death Valley area, California, in Guidebook: Death Valley Region, California and Nevada (see Geological Society of America), Death Valley Publication Company, Shoshone, California, 37-48.

Dienger, J.L., 1986, Facies modeling of mixed siliciclastic and carbonate sediments in the Lower Cambrian Middle Deep Spring Formation, White-Inyo Mountains, California [Ph.D. dissertation].

Elston, D.P., and Scott, G.R., 1976, Unconformity at the Cardenas-Nankoweap contact (Precambrian), Grand Canyon Supergroup, northern Arizona: Geological Society of America Bulletin, 87, 1763–1772

Elston, D.P., Enkin, R.J., Baker, J., and Kisilevsky, D.K., 2002, Tightening the Belt: Paleomagnetic-stratigraphic constraints on deposition, correlation, and deformation of the Middle Proterozoic (ca. 1.4 Ga) Belt-Purcell Supergroup, United States and Canada: Geological Society of America Bulletin, 114, 619–638.

Ennih, N. and Liègois, J., 2001, The Moroccan Anti-Atlas: the West African craton passive margin with limited Pan-African activity. Implications for the northern limit of the craton, Precambrian Research, 112, 289-302.

Ernst, R.E., Buchan, K.L., Hamilton, M.A., Okrugin, A.V., and Tomshin, M.D., 2000, Integrated paleomagnetism and U-Pb geochronology of mafic dikes of the eastern Anabar Shield region, Siberia: Implications for Mesoproterozoic paleolatitude of Siberia and comparison with Laurentia: Journal of Geology, 108, 381–401.

Eyles, N., Januszczak, N., 2004, 'Zipper-rift': a tectonic model for Neoproterozoic glaciations during the breakup of Rodinia after 750 Ma, Earth-Science Reviews, 65, 1-73.

Farmer G.L. et al., 2005, Paleoproterozoic Mojave province in northwestern Mexico? Isotopic and U-Pb zircon geochronologic studies of Precambrian and Cambrian crystalline and sedimentary rocks, Caborca, Sonora. Geological Society of America Special Paper 393, 183-198.

Fedo, C.M., Sircombe, K.N., Rainbird, R.H., 2003, Detrital Zircon Analysis of the Sedimentary Record, Reviews in Mineralogy and Geochemistry, 53, 277-303.

Fedonkin, M.A.,1992, Vendian Faunas and the early evolution of metazoa, in Lipps, J.H. and Signor, P.W., eds., Origin and early evolution of the metazoa, New York, Plenum Press, 87-129.

Fekkak, A., Boualoul, M., Badra, L., Amenzou, M., Saquaque, A., El-Amrani, I E., 2000, Origine et contexte geotectonique des depots detritiques du groupe neoproterozoique inferieur de Kelaat Mgouna (Anti-Atlas oriental, Maroc). Origin and geotectonic setting of detrital deposits of the lower Neoproterozoic Kelaat Mgouna Group, eastern Anti-Atlas, Morocco, Journal of African Earth Sciences, 30, 2, 295-311.

Feng R., Machado N., Ludden J., 1993, Lead geochronology of zircon by LaserProbe-Inductively coupled plasma mass spectrometry (LP-ICPMS), Geochimica Cosmochimica Acta, 57, 3479-3486.

Fletcher, K.E., Heizler, M.T., Karlstrom, K.E., Timmons, J.M., Crossey, L.J., Bloch, J.D., 2004, Provenance and geochronology of Mesoproterozoic sedimentary rocks from across the Southwest United States revealed by $^{40}Ar/^{39}Ar$ dating of detrital muscovites, Abstracts with Programs - Geological Society of America, 36, 5, 405.

Fortey, R. A., and Cocks, L. R. M., 1992, The early Palaeozoic of the North Atlantic region as a test case for the use of fossils in continental reconstruction, Tectonophysics, 206, 147–158.

Fortey, R. A., Briggs, D. E. G., and Willis, M. A., 1996, The Cambrian evolutionary “explosion”: Decoupling cladogenesis from morphological disparity, Linnaean Society Biological Journal, 57, 13-33.

Frost, B. R., Avchenko, O. V., Chamberlain, K. R. & Frost, C. D., 1998, Evidence for extensive Proterozoic remobilization of the Aldan shield and implications for Proterozoic plate tectonic reconstructions of Siberia and Laurentia, Precambrian Research 89, 1-23.

Fryer B.J., Jackson S.E., Longerich H.P., 1993, The application of laser ablation microprobe-inductively coupled plasma mass spectrometry (LAM-ICPMS) to in situ (U)-Pb geochronology, Chemical Geology, 109, 1-8.

Gallet, Y., Pavlov, V.E., Semikhatov, M.A., and Petrov, P.Y., 2000, Late Mesoproterozoic magnetostratigraphic results from Siberia: Paleogeographic implications and magnetic field behavior: Journal of Geophysical Research, 105, 16, 481-516.

Gebel, D.C., 1978, Stratigraphy of the Nankoweap Formation, eastern Grand Canyon, Arizona [M.S. thesis], Flagstaff, Northern Arizona University, 129 p.

Gehrels, G.E., and Ross, G.M., 1998, Detrital zircon geochronology of Neoproterozoic to Permian miogeoclinal strata in British Columbia and Alberta: Canadian Journal of Earth Sciences, 35, 1380–1401.

Gehrels, G.E., 2000, Introduction to detrital zircon studies of Paleozoic and Triassic strata in western Nevada and northern California. Geological Society of America Special Paper 347, 1-17.

Gevirtzman, D.A., and Mount, J.F., 1986, Paleoenvironments of an Earliest Cambrian (Tommotian) shelly fauna in the southwestern Great Basin, USA, Journal of Sedimentary Petrology, 56, 412-421.

Glaessner, M.F., The dawn of animal life, Cambridge Univ. Press, 1984.

Grant, S.W.F., 1990, Shell structure and distribution of Cloudina, a potential index fossil for the terminal Proterozoic, American Journal of Science, 290-A, 261-294.

Greene, L.R., 1986, Cyclic sedimentation within the upper member of the Deep Spring Formation (Lower Cambrian), eastern California and western Nevada; the anatomy of a Grand Cycle [Ph.D. dissertation].

Heaman, L.M., and Grotzinger, J.P., 1992, 1.08 Ga diabase sills in Pahrump Group, California: Implications for development of the Cordilleran miogeocline, Geology, 20, 637-640.

Hefferan, K., Karson, J., and Saquaque, A., 1992, Proterozoic collisional basins in a Pan-African suture zone, Anti-Atlas Mountains, Morocco, Precambrian Research, 54, 295-319.

Hoff, J.A., Jameson, J., Hanson, G.N., 1995, Application of Pb isotopes to the absolute timing of regional exposure events in carbonate rocks, An example from U-rich dolostones from the Wahoo Formation (Pennsylvanian), Prudhoe Bay, Alaska. Journal of Sedimentary Petrology, A65, p. 225-233.

Hoffman, P.J., 1998, A Neoproterozoic snowball earth, Science, 281, 5381, 1342-1346.

Hoffman, P.J., 1991, Did the breakout of Laurentia turn Gondwanaland inside-out?, Science, 252, 1409-1412.

Hoffman, P.J., 2004, Neoproterozoic snowball earth; exercising the imaginative muscle, Geobulletin, 47, 2, pp. 3, 5, 10-13, 24-25, 33.

Hoffman, P.J., 1989, Speculations on Laurentia's first giga year (2.0-1.0 Ga), Geology, 17, 135-138.

Hollingsworth, J.S., 2005, The earliest occurrence of trilobites and brachiopods in the Cambrian of Laurentia, Palaeogeography, Palaeoclimatology, Palaeoecology, 220, 153-165.

Holt, T.R., 1998, U-Pb ages of Late Paleozoic Carbonate Paleosols: Potential for Directly Dating Sedimentary Sequences [Ph.D. dissertation], SUNY Stony Brook, p. 95.

Horn, I., Rudnick, R.L., McDonough, W.F., 2000, Precise elemental and isotope ratio determination by simultaneous solution nebulization and laser ablation-ICP-MS: application to U-Pb geochronology, Chemical Geology, 164, 281-301.

Ingersoll, R.V., Bullard, T.F., Ford, R.L., Grimm, J.P., Pickle, J.D., and Sares, S.W., 1984, The effect of grain size on detrital modes: A test of the Gazi-Dickinson point-counting method, Journal of Sedimentary Petrology, 54, 103–116.

Israelson, C., Halliday, A.N., and Buchardt, B., 1996, U-Pb dating of calcite concretions from Cambrian black shales and the Phanerozoic time scale. Earth and Planetary Science Letters, 105, 153-159.

Jahn, B. and Cuvellier, H., 1994, Pb-Pb and U-Pb geochronology of carbonate rocks: an assessment, Chemical Geology, 115, 125-151.

Jahn, B., 1988, Pb-Pb dating of young marbles from Taiwan, Nature, 332, 429-432.

Jahn, B., and Simonson, B.M., 1995, Carbonate Pb-Pb ages of the Wittenoom Formation and Carawine Dolomite, Hamersley Basin, Western Australia (with implications for their correlation with the Transvaal Dolomite of South Africa), Precambrian Research, 72, 247-261.

Jahn, B., Bertrand-Sarfati, J., Morin, N., and Mace, J., 1990, Direct dating of stromatolitic carbonates from the Schmidtsdrif Formation (Transvaal Dolomite), South Africa, with implications on the age of the Ventersdorp Supergroup, Geology, 18, 1211-1214.

Jefferson, C.W., Correlation of middle and upper Proterozoicstrata between northwestern Canada and south and central Australia [abs.], 1978, Geological Association of Canada Program with Abstracts, 13, 429.

Karlstrom, K.E., and Humphreys, E.D., 1998, Persistent influence of Proterozoic accretionary boundaries in the tectonic evolution of southwestern North America: Interaction of cratonic grain and mantle modification events, Rocky Mountain Geology, 33; 2, 161-179.

Karlstrom, K.E., Bowring, S.A., Dehler, C.M., Knoll, A.H., Porter, S.M., Des Marais, D.J., Weil, A.B., Sharp, Z.D., Geissman, J.W., Elrick, M.B., Timmons, J.M., Crossey,

L.J., and Davidek, K.L., 2000, Chuar Group of the Grand Canyon: Record of breakup of Rodinia, associated changes in the global carbon cycle, and ecosystem expansion by 740 Ma, Geology, 28, 619–622.

Karlstrom, K.E., Harlan, S.S., Williams, M.L., McLelland, J., Geissman, J.W., and Ahall, K.-I., 1999, Refining Rodinia; geologic evidence for the Australia–Western U.S. Connection in the Proterozoic, GSA Today, 9, 10, 1–7.

Khudoley, A.K., and Serkina, G.G., 2002, Early Paleozoic rifting of the east margin of Siberian craton: Comparison of geological data and subsidence curves, in Karakin, Yu.V., ed., Tectonics and geophysics of lithosphere, Moscow, GEOS, 288–291 (in Russian).

Khudoley, A.K., Kropachev, A.P., Tkachenko, V.I., Rublev, A.G., Sergeev, S.A., Matukov, D.I., Lyahnitskaya, O.Yu., 2007, Meso- to Neoproterozoic evolution of the Siberian craton and adjacent microcontinents: an overview with constraints for Laurentian connection, in SEPM Special Publication 86, Proterozoic Geology of Western North America and Siberia, edited by P.K. Link and R.S. Lewis, *in press.*

Khudoley, A.K., Rainbird, R.H., Stern, R.A., Kropachev, A.P., Heaman, L.M., Zanin, A.M., Podkovyrov, V.N., Belova, V.N., and Sukhorukov, V.I., 2001, Sedimentary evolution of the Riphean-Vendian basin of southeastern Siberia, Precambrian Research, 111, 129-163.

Kirshvink, J.L., Ripperdan, R.L. & Evans, D.A., 1997, Evidence for a large-scale reorganization of Early Cambrian continental masses by inertial interchange true polar wander, Science, 277, 541-545.

Kluth, C.F., Coney, P.J., 1981, Plate tectonics of the ancestral Rocky Mountains, Geology, 9, 10-15.

Komar, V.A., Rabotnov, V.T., 1976, Upper Precambrian of North–East Russia, Izvestiya Soviet Academy of Science, 8, 5–16.

Kornev, B.V., Rabotnov, V.T., Gudzenko, V.T., Nevolin, B.S., Sigaeva, E.N., Mazanov, V.F., Stavtsev, A.L., Kotelnikov, D.D., Potapov, S.V., 1980, Lithology and Oil Resources of Southeastern of Siberian Platform (Upper Precambrian), Nauka Press, Moscow in Russian.

Košler, J., Fonneland, H., Sylvester, P., Tubrett, M., Pedersen, R.B., 2002, U–Pb dating of detrital zircons for sediment provenance studies—a comparison of laser ablation ICPMS and SIMS techniques, Chemical Geology, 182, 2-4, 605-618.

Labotka, T.C., and Albee, A.L., 1977, Late Precambrian depositional environment of the Pahrump Group, Panamint Mountains, California, California Division of Mines and Geology Special Report 129, 93-100.

Lance P.B., Kamo, S.L., Allen, C.M., Davis, D.W., Aleinikoff, J.N., Valley, J.W., Mundil, R., Campbell, I.H., Korsch, R.J., Williams I.S., and Foudoulis, C., 2004, Improved $^{206}Pb/^{238}U$ microprobe geochronology by the monitoring of a trace-element-related matrix effect; SHRIMP, ID–TIMS, ELA–ICP–MS and oxygen isotope documentation for a series of zircon standards, Chemical Geology, 205, 1-2, 30, 115-140.

Languille, G.B., 1974a, Earliest Cambrian-Latest Proterozoic ichnofossils and problematic fossils from Inyo County, California, [Ph.D. Dissertation, State University of New York, Binghamton].

Langille, G.B., 1974b, Problematic calcareous fossils from the Stirling Quartzite, Funeral Mountains, Inyo County, California [abstract], in Cordilleran Section, 70th Annual Meeting, Abstracts with programs-Geological Society of America, 6, 3, 204-205.

Larson, E.E., Patterson, P.E., and Mutschler, F.E., 1994, Lithology, chemistry, age, and origin of the Proterozoic Cardenas Basalt, Grand Canyon, Arizona, Precambrian Research, 65, 1–4, 255–276.

Lees, D.C., Fortey, R.A., Cocks, L., Robin M., 2002, Quantifying paleogeography using biogeography; a test case for the Ordovician and Silurian of Avalonia based on brachiopods and trilobites, Paleobiology, 28, 3, 343-363.

Levy, M., and Christie-Blick, N., 1989, Pre-Mesozoic palinspastic reconstruction of the eastern Great Basin (western United States), Science, 245, 1454-1462.

Levy, M., Christie-Blick, N., and Link, P.K., 1994, Neoproterozoic incised valleys of the eastern Great Basin, Utah and Idaho: Fluvial response to changes in depositional base level, in Dalrymple, R.W., et al., eds., Incised-valley systems: Origin and sedimentary sequences, Society for Sedimentary Geology Special Publication 51, 369–382.

Lieberman B.S., 1997, Early Cambrian paleogeography and tectonic history: a biogeographic approach, Geology, 25, 1039-42.

Lieberman B.S., 2002, Phylogenetic analysis of some basal Early Cambrian trilobites, the biogeographic origins of the Eutrilobita, and the timing of the Cambrian radiation, Journal of Paleontology, 76, 692-708.

Lieberman, B.S., and Eldredge, N., 1996, Trilobite biogeography in the Middle Devonian: Geological processes and analytical methods, Paleobiology, 22, 66–79.

Lieberman, B.S., 1999, Testing the Darwinian legacy of the Cambrian radiation using trilobite phylogeny and biogeography, Journal of Paleontology, 73, 2, 176-181.

Link, P.K., Christie-Blick, N., Devlin, W.J., Elston, D.P., Horodyski, R.J., Levy, M., Miller, J.M.G., Pearson, R.C., Prave, A., Stewart, J.H., Winston, D., Wright, L.A., and Wrucke, C.T., 1993, Middle and late Proterozoic stratified rocks of the western U.S. Cordillera, Colorado Plateau, and Basin and Range Province, in Reed, J.C., Bickford, M.E., Houston, R.S., Link, P.K., Rankin, D.W., Sims, P.K., and Van Schumus, W.R., eds., Decade of North American Geology Precambrian: Conterminous U.S.: Boulder, Geological Society of America, The Geology of North America, C-2, 463–594.

Ludwig K.R., 1999, IsoplotEx v. 2.6. Berkeley Geochronological Center Special Publication 1a.

Ludwig, K.R., 2000, SQUID 1.00, A User's Manual; Berkeley Geochronology Center Special Publication, No. 2, 2455 Ridge Road, Berkeley, CA 94709, USA.

Ludwig, K.R., 2003, Isoplot 3.00. Berkeley Geochronology Center, Special Publication No. 4, 70 p.

MacLean, J.S., Sears, J.W., Chamberlain, K.R., Khudoley, A.K., Prokopiev, A.V., Kropachev, A., Serkina, G., *in review*, Detrital zircon geochronologic tests of the SE Siberia – SW Laurentia paleocontinental connection, in Geology and Tectonic Origins of Northeast Russia: A Tribute to Leonid Parfenov.

Marian, M.L., and Osborne, R.H., 1992, Petrology, petrochemistry, and stromatolites of the middle to late Proterozoic Beck Spring Dolomite, eastern Mojave Desert, California, in Precambrian sedimentation, Rice, R.J., ed., Canadian Journal of Earth Sciences, 29, 12, 2595-2609.

Mattinson, J.M., 2005, Zircon U/Pb chemical abrasion (CA-TIMS) method; combined annealing and multi-step partial dissolution analysis for improved precision and accuracy of zircon ages, Chemical Geology, 220, 1-2, 47-66.

Meert, J.G., Lieberman, B.S., 2004, A palaeomagnetic and palaeobiogeographical perspective on latest Neoproterozoic and early Cambrian tectonic events, Journal of the Geological Society, London, 161, 477-487.

Meert, J.G., 2002, Rodinia: Problems, issues, and acronyms [abs.], Geological Society of America Abstracts with Programs, 34, 6, 558.

Meng, Q, Hu, J., Jin, J., Zhang, Y., Xu, D., 2003, Tectonics of the late Mesozoic wide extensional basin system in the China-Mongolia border region, Basin Research, 15, 397-415.

Miller, J.M.G., 1985, Glacial and syntectonic sedimentation: The upper Proterozoic Kingston Peak Formation, southern Panamint Range, eastern California, Geological Society of America Bulletin, 96, 1537-1553.

Miller, J.M.G., 1987, Paleotectonic and stratigraphic implications of the Kingston Peak-Noonday contact in the Panamint Range, eastern California, Journal of Geology, 95, 1, 75-85.

Miller, J.M.G., 1983, Stratigraphy and sedimentology of the upper Proterozoic Kingston Peak Formation, Panamint Range, eastern California, [Ph.D. dissertation], Santa Barbara, California, University of California, 335.

Moecher, D.P., Samson, S.D., 2006, Differential zircon fertility of source terranes and natural bias in the detrital zircon record: Implications for sedimentary provenance analysis, Earth and Planetary Science Letters, 247, 252-266.

Moorbath, S., Taylor, P.N., Orpen, J.L., Treloar, P., and Wilson, J.F., 1987, First direct radiometric dating of Archaean stromatolitic limestone, Nature, 326, 865-867.

Moores, E.M., 1991, Southwest U.S.—East Antarctic (SWEAT) connection: A hypothesis, Geology, 19, 425-428.

Mosher, S., 1998, Tectonic evolution of the southern Laurentian Grenville orogenic belt, Geological Society of America Bulletin, 110, 1357–1375.

National Research Council, 1996, National Science Education Standards, Washington DC, National Academy Press.

Ovchinnikova, G.V., Semikhatov, M.A., Vasil'eva, I.M., Gorokhov, I.M., Kaurova, O.K., Podkovyrov, V.N., and Gorokhovskii, B.M., 2001, Pb–Pb age of carbonates from the middle Riphean Malga Formation, Uchur-Maya region of east Siberia: Stratigraphy, Geological Correlation, 9, 6, 3–16 (in Russian).

Paces, J. B., Miller, J.D.,Jr., 1993, Precise U-Pb ages of Duluth Complex and related mafic intrusions, northeastern Minnesota; geochronological insights to physical, petrogenetic, paleomagnetic, and tectonomagnetic processes associated with the 1.1 Ga Midcontinent Rift System, Journal of Geophysical Research, 98, B8, 13, 997-14013.

Palmer, A.R. and Repina, L.N., 1993, Through a glass darkly: Taxonomy, phylogeny, and biostratigraphy of the Olenellina, Univ. Kansas Paleo Contributions, 3, 1-35.

Parfenov, L.M., and Kuzmin, M.I., eds., 2001, Tectonics, Geodynamics and Metallogeny of the Sakha Republic (Yakutia), Moscow, MAIK Nauka/Interperiodica, 571 p. (in Russian).

Pavlov, V.E., Gallet, Y., Petrov, P.Yu., Zhuravlev, D.Z., and Shatsillo, A.V., 2002, Uy Group and late Riphean sills of the Uchur-Maya region: isotopic, paleomagnetic data and problems of Rodinia supercontinent reconstructions, Geotectonics, 4, 26–41 (in Russian).

Piqué, A., 2003, Evidence for an important extensional event during the Latest Proterozoic and Earliest Paleozoic in Morocco, C.R. Geoscience, 335, 865-868.

Prave, A.R., 1984, Stratigraphy, sedimentology, and petrography of the Lower Cambrian Zabriskie Quartzite in the Death Valley region, Southeastern California and Southwestern Nevada [PhD dissertation], Pennsylvania State University, 193 p.

Prave, A.R., 1999, Two diamictites, two cap carbonates, two delta (super 13) C excursions, two rifts; the Neoproterozoic Kingston Peak Formation, Death Valley, California, Geology (Boulder), 27, 4, 339-342.

Prave, A.R., Wright, L.A., 1986, Isopach pattern of the Lower Cambrian Zabriskie Quartzite, Death Valley region, California-Nevada; how useful in tectonic reconstructions?, Geology (Boulder), 14, 3, 251-254.

Price, R.A., and Sears, J.W., 2000, A preliminary palinspastic map of the Mesoproterozoic Belt-Purcell Supergroup, Canada and USA: Implications for the tectonic setting and structural evolution of the Purcell anticlinorium and Sullivan deposit, in Lydon, J.W., Høy, T., Slack, J.F., and Knapp, M., eds., The Sullivan deposit and its geological environment, Geological Association of Canada, Mineral Deposits Division Special Publication 1, 61–81.

Rainbird, R.H., Stern, R.A., Khudoley, A.K., Kropachev, A.P., Heaman, L.M., and Sukhorukov, V.I., 1998, U–Pb geochronology of Riphean sandstone and gabbro from southeast Siberia and its bearing on the Laurentia – Siberia connection, Earth and Planetary Science Letters, 164, 409–420.

Reed, V.S., 1976, Stratigraphy and depositional environment of the upper Precambrian Hakatai Shale, Grand Canyon, Arizona [M.S. thesis], Flagstaff, Northern Arizona University, 163 p.

Repina, L.N., 1981, Trilobite biostratigraphy of the Lower Cambrian Stages of Siberia, in Taylor, M.E. (Ed.), Short Papers for the Second International Symposium on the Cambrian System. U.S. Geological Survey, Open-File Report 81-743, 173–180.

Riding, R., Zhuravlev, A.Y., 1995, Structure and diversity of oldest sponge-microbe reefs: Lower Cambrian, Aldan River, Siberia, Geology, 23, 7, 649-652.

Roberts, M.T., 1982, Depositional environments and tectonic setting of the Crystal Spring Formation, Death Valley region, California: Geology of selected areas in the San Bernardino Mountains, western Mojave Desert, and southern Great Basin, California, Shoshone, CA.

Roberts, M.T., 1974, Stratigraphy and depositional environments of the Crystal Spring Formation, southern Death Valley region, California, Guidebook; Death Valley Region, California and Nevada, Shoshone, CA, Death Valley Publishing Co., 49-58.

Rosen, O.M., Condie, K.C., Natapov, L.M., and Nozhkin, A.D., 1994, Archean and early Proterozoic evolution of the Siberian craton: A preliminary assessment, in Condie, K.C., ed., Archean crustal evolution, Developments in Precambrian geology, 11, 411–459.

Ross, G.M., Eaton, D.W., Boerner, D.E., and Miles, W., 2000, Tectonic entrapment and its role in the evolution of continental lithosphere: An example from the Precambrian of Western Canada, Tectonics, 19, 116–134.

Rowland, S.M. and Shapiro, R.S., 2002, Reef patterns and environmental influences in the Cambrian and earliest Ordovician, Society of Economic Paleontology and Mineralogy Special Publication, 72, 95–128.

Rozanov A.Y. & Zhuravlev, A.Y., 1992, The Lower Cambrian fossil record of the Soviet Union, in Lipps, J.H. & Signor, P.W., eds., Origin and early evolution of the metazoan,Plenum Press, New York, 205-266.

Rushton, A.W.A. & Hughes, N.C., 1996, Biometry, systematics and biogeography of the late Cambrian trilobite Maladioidella, Transactions of the Royal Society of Edinburgh, Earth Sciences, 86, 247–256.

Russel, J., 1995, Direct Pb/Pb dating of Silurian macrofossils from Gotland, Sweden. In: Dunay, R.E., and Hailwood, E.A., (eds.), Non-biostratigraphic Methods of Dating and Correlation. Geological Society Special Publication 89, 175-200.

Saquaque, A., Beharref, M., Abia, H., Nrini, Z., Reuber, I., Karson, J.A., 1992, Evidence for a Pan-African volcanic arc and wrench fault tectonics in the Jbel Saghro, Anti-Atlas, Morocco, Geologische. Rundschau. 81, 1–13.

Sawyer, D.S., 2002, Discovering Plate Boundaries, a Data Rich Classroom Exercise [abstract], American Geophysical Union Abstracts with Programs.

Schwab, F.L., 1975, Framework mineralogy and chemical composition of continental margin-type sandstone, Geology, 3, 487-490.

Scott, D.J., Gauthier, G., 1996, Comparison of TIMS (U-Pb and laser ablation microprobe ICP-MS (Pb) techniques for age determination of detrital zircons from Paleoproterozoic metasedimentary rocks from northeastern Laurentia, Canada, with tectonic implications, Chemical Geology, 131, 127-142.

Sdzuy, K., The Precambrian–Cambrian boundary beds in Morocco (Preliminary report), Geological Magazine, 115, 2, 83–94. 1978.

Sears, J.W., 2007, Rift destabilization of a Proterozoic epicontinental pediment: A model for the Belt-Purcell Basin, North America, in Proterozoic Geology of Western North America and Siberia, SEPM Special Publication 86, 3-29, *in press*.

Sears, J.W., Khudoley, A.K., Prokopiev, A.V., 2005, Stratigraphic tests of the Proterozoic southeast Siberia – southwest Laurentia connection, Supercontinents and Earth Evolution Symposium Abstracts with Programs.

Sears, J.W., and Price, R.A., 2003, Tightening the Siberian connection to western Laurentia. Geologic Society of America Bulletin, 115, 943-953.

Sears, J.W., and Price, R.A., 2000, New look at the Siberian connection: No SWEAT, Geology, 28, 423-426.

Sears, J.W., and Price, R.A., 1978, The Siberian connection: A case for the Precambrian separation of the North American and Siberian cratons, Geology, 6, 267-270.

Sears, J.W. &Wright, J., 2005, Transforming the Siberian craton from SW Laurentia to the Ural Mountains and allochthonous terranes from the Appalachians to the Cordillera, Geological Society of America Abstracts with Programs, 37.

Seeland, D.A., 1968, Paleocurrents of the late Precambrian to Early Ordovician (basal Sauk) transgressive clastics of the western and northern United States [Ph.D. thesis], Salt Lake City, University of Utah, 276 p.

Semikhatov, M.A., Ovchinnikova, G.V., Gorokhov, I.M., Kuznetsov, A.B., Vasilieva, I.M., Gorokhovskii, B.M., and Podkovyrov, V.N., 2000, Isotopic age of boundary between middle and upper Riphean: Pb–Pb geochronology of carbonate rocks of the Lakhanda Group, east Siberia, Doklady, Russian Academy of Sciences, 372, 216–221 (in Russian).

Semikhatov, M.A., Serebryakov, S.N., 1983, Siberian Hypostratotype of Riphean, Nauka Press, Moscow (in Russian).

Signor, P.W., Mount, J.F. & Onken, B.R., 1987, A pre-trilobite shelly fauna from the White-Inyo region of eastern California and western Nevada, Journal of Paleontology, 61, 425-438.

Smelov, A.P., and Timofeev, V.F., 2003, Terrane analysis and geodynamic model of the formation of the North Asian craton in the Early Precambrian, Pacific Geology, 22, 6, 42–54 (in Russian).

Smith, P.E., and Farquhar, R.M., 1989, Direct dating of Phanerozoic sediments by the 238U/206Pb method, Nature, 341, 518-521.

Smith, P.E., Brand, U., and Farquhar, R.M., 1994, U-Pb systematics and alteration trends of Pennsylvanian-aged aragonite and calcite. Geochimica et Cosmochemica Acta, 58, 313-322.

Smith, P.E., Farquhar, R.M., and Hancock, R.G., 1991, Direct radiometric age determination of carbonate diagenesis using U-Pb in secondary calcite. Earth and Planetary Science Letters, 105, 474-491.

Soulaimani, A., Bouabdelli, M., Piqué, A , 2003, L extension continental au Ne´o-Prote´rozoı¨que supe´rieur-Cambrien infe´ieur dans l_Anti-Atlas (Maroc), Bulletin Socie´te´ Ge´ologique France, 174, 88–92.

Soulaimani, A., Piqué, A., 2004, The Tasrirt structure (Kerdous inlier, Western Anti-Atlas, Morocco): a late Pan-African transtensive dome, Journal of African Earth Sciences, 39, 247-255.

Stewart, J.H., Gehrels, G.E., Barth, A.P., Link, P.K., Christie-Blick, N., and Wrucke, C.T., 2001, Detrital zircon provenance of Mesoproterozoic to Cambrian arenites in the western United States and northwestern Mexico, Geological Society of America Bulletin, 113, 1343–1356.

Stewart, J.H., 1972, Initial deposition in the Cordilleran Geosyncline: Evidence of a Late Precambrian (>850 m.y.) continental separation, Geological Society of America Bulletin, 83, 1345-1360.

Stewart, J.H., 1970, Upper Precambrian and Lower Cambrian strata in the southern Great Basin, California and Nevada, U.S. Geological Survey Professional Paper 620, 205 p..

Thomas, R.J., Fekkak, A., Ennih, N., Errami, E., Loughlin, S.C., Gresse, P.G., Chevallier, L.P., Liégeois, J.-P., 2004, A new lithostratigraphic framework for the Anti-Atlas Orogen, Morocco, Journal of African Earth Sciences, 39, 217-226.

Thomas, R.J., Gresse, P.O., Harmer, R.E., Eglington, B.M., Armstrong, R.A., de Beer, C.H., Chevallier, L.C., Martini, J.E., de Kock, G.S., Pick, T., Macey, P.H., Ingram, B.A., 2002, Precambrian evolution of the Sirwa window, Anti-Atlas orogen, Morocco, Precambrian Research, 137, 1–57.

Thomas, W.A., 1991, The Appalachian – Ouachita rifted margin of southeastern North America, Geological Society of America Bulletin, 103, 3, 415-431.

Timmons, J.M., Karlstrom, K.E., Heizler, M.T., Bowring, S.A., Gehrels, G.E., Crossey, L.J., 2005, Tectonic inferences from the ca. 1255–1100 Ma Unkar Group and Nankoweap Formation, Grand Canyon: Intracratonic deformation and basin formation during protracted Grenville orogenesis, Geological Society of America Bulletin, 117, 11/12, 1573-1595.

Trompette, R., 1996, Temporal relationship between cratonization and glaciation; the Vendian-Early Cambrian glaciation in western Gondwana, Palaeogeography, Palaeoclimatology, Palaeoecology, 123, 1-4, 373-383.

Tucker, M.E., 1983, Diagenesis, geochemistry, and origin of a Precambrian dolomite; the Beck Spring Dolomite of eastern California, Journal of Sedimentary Petrology, 53, 4, 1097-1119.

Vermeesch, P., 2004, How many grains are needed for a provenance study?, Earth and Planetary Science Letters, 224, 441-451.

Vogel, M.B., 2004, Provenance and geochemistry of upper Proterozoic strata in California and other areas of the western United States: Paleogeographic and biogeochemical implications [PhD dissertation], Stanford University, 255 p.

Walsh, G.J., Aleinikoff, J.N., Benziane, F., Yazidi, A., Armstrong, T.R., 2002, U-Pb zircon geochronology of the Paleoproterozoic Tagragra de Tata inlier and its Neoproterozoic cover, western Anti-Atlas, Morocco, Precambrian Research, 117, 1-20.

Weil, A.B., Geissman, J.W., Heizler, M.T., and Van der Voo, R., 2003, Paleomagnetism of Middle Proterozoic mafic intrusions and Upper Proterozoic (Nankoweap) red beds from the Lower Grand Canyon Supergroup, Arizona, Tectonophysics, 375, 199–220.

Weil, A.B., Van der Voo, R., MacNiocaill, C., Meert, J.G., 1998, The Proterozoic supercontinent Rodinia; paleomagnetically derived reconstructions for 1100 to 800 Ma , Earth and Planetary Science Letters, 154, 1-4, 13-24.

Weislogel, A., Wooden, J., Gehrels, G., 2004, A comparison of detrital zircon provenance techniques; SHRIMP versus LA-ICP-MS, Abstracts with Programs - Geological Society of America, 36, 5, 264 p.

Wernicke, B., Axen, G.J., and Snow, J.K., 1988, Basin and Range extensional tectonics at the latitude of Las Vegas, Nevada, Geological Society of America Bulletin, 100, 1738-1757.

Wertz, W.E., 1983, The depositional environments and petrography of the Stirling Quartzite, Death Valley Region, California and Nevada [PhD dissertation], Pennsylvania State University, 192 p.

Wertz, W.E., 1982, Stratigraphy and sedimentology of the Stirling Quartzite, Death Valley area, California and Nevada, Geology of Selected Areas in the San Bernardino Mountains, Western Mojave Desert, and Southern Great Basin, California.

Williams I., 1998, U-Th-Pb geochronology by ion microprobe, in Applications of microanalytical techniques to understanding mineralizing processes, McKibben MA, Shanks III WC, Ridley WI (eds), Reviews in Economic Geology, 7, 1-35.

Williams, A., 1973, Distribution of Brachiopod Assemblages in Relation to Ordovician Palaeogeography, Special Papers in Palaeontology, 12, 241–269.

Wingate, M.T.D., Pisarevsky, S.A., and Evans, D.A.D., 2002, Rodinia connections between Australia and Laurentia: No SWEAT, no AUSWUS?, Terra Nova, 14, 121-128.

Winter, B.L., and Johnson, C.M., 1995, U-Pb dating of a carbonate subaerial exposure event, Earth and Planetary Science Letters, 131, 177-187.

Wright, L.A., Troxel, B.W., 1966, Strata of Late Precambrian-Cambrian Age, Death Valley Region, California-Nevada, AAPG Bulletin, 50, 846-857.

Wright, L.A., Troxel, B.W., Williams, E.G., Roberts, M.T., and Diehl, P.E., 1976, Precambrian sedimentary environments of the Death Valley region, eastern California, in Troxel, B.W., and Wright, L.A., eds., Geologic features of Death Valley, California, California Division of Mines and Geology Special Report 106, 7-15.

Zhuravlev, A.Y., 1986, Evolution of archaeocyaths and paleobiogeography of the Early Cambrian, Geological Magazine, 123, 377–385.

APPENDIX A

AN ATTEMPT TO ADDRESS THE GEOCHRONOLOGICALLY POORLY CONSTRAINED PROTEROZOIC DEATH VALLEY SEDIMENTARY SUCCESSION USING CARBONATE U-Pb GEOCHRONOLOGY

A.1 Introduction

In recent years, several researchers have used Pb-Pb and U-Pb geochronology techniques to date the sedimentation or early diagenesis of carbonates (Moorbath et al., 1987; Jahn, 1988; Smith and Farquhar, 1989; Jahn et al., 1990; DeWolf and Halliday, 1991; Smith et al., 1991; Jahn and Cuvellier, 1994; Smith et al., 1994; Babinski et al., 1995; 1999; Hoff et al., 1995; Russell, 1995; Jahn and Simonson, 1995; Winter and Johnson, 1995; Brannon et al., 1996; Israelson et al., 1996; Holt, 1998). The techniques are based on the highly radiogenic Pb isotopes commonly observed in marine carbonates (Jahn and Cuvellier, 1994). Equilibrium is assumed between seawater and newly forming carbonates. The long residence time of uranium and the short residence time of lead cause a high U:Pb ratio in seawater, and therefore carbonates. Although the mobilization of U and Pb from carbonates has decreased the U:Pb ratio in most ancient carbonates, many carbonates retain high enough radiogenic concentrations to be useful for geochronology techniques (Jahn and Cuvellier, 1994).

Carbonate geochronology is not yet a firmly established technique in part because carbonate rocks are capable of experiencing several stages of diagenesis that can reset the U-Pb system. Diagenesis often causes the expulsion of U and/or the incorporation of Pb during interaction with continental water. Continental water has a much lower U/Pb value (0.1-2) than that of marine water (~1500) (Broecker and Peng, 1982; Chester, 1990).

To address the problem that over 800 million years of possible sedimentation in the Death Valley region (between 1.4 Ga basement and 543 Ma Cambrian sediments) are constrained by only two dates (1087±3 and 1069±3 Ma, Heaman and Grotzinger, 1992) of intruded mafic sills, we performed U-Pb geochronology analyses on several carbonates. We performed geochemical analyses using the isotope dilution-thermal ionization mass spectrometer (ID-TIMS) at the University of Wyoming. We conducted thin-section analyses at the University of Montana to prioritize the most useful samples for isotopic analysis, based on the level of observable diagenetic alteration. Unfortunately, the analyses yielded results that could not be interpreted for geochronologic significance. Our methods and results are reported below.

A.2 Methods

We collected carbonate samples from several locations in the Death Valley region, including Saratoga Springs, Alexander Hills, and the Kingston Range (Figure A1). Samples were carefully selected to avoid obvious fractures and chemical alteration. However, the Precambrian rocks in the Death Valley region have undergone multiple phases of deformation, including Mesozoic compression and Cenozoic extension, making pristine carbonates difficult to find. We had 14 samples prepared for thin section analysis. Of these samples, five were selected for geochronologic analyses (Figure A2, Table A1), based on their apparently low levels of alteration.

We performed the sample preparation and geochronologic analyses at the clean laboratory and isotope dilution-mass spectrometer at the University of Wyoming. To prepare samples A5, A6, and K20, We sawed 3-4 small pieces off the thin section billets in an attempt to separate ~200-300 mg of carbonate. The sawed pieces were relatively homogeneous and crack-free. We washed the samples with deionized water in ultrasound, rinsed them three times, and transferred them to beakers to dry under a

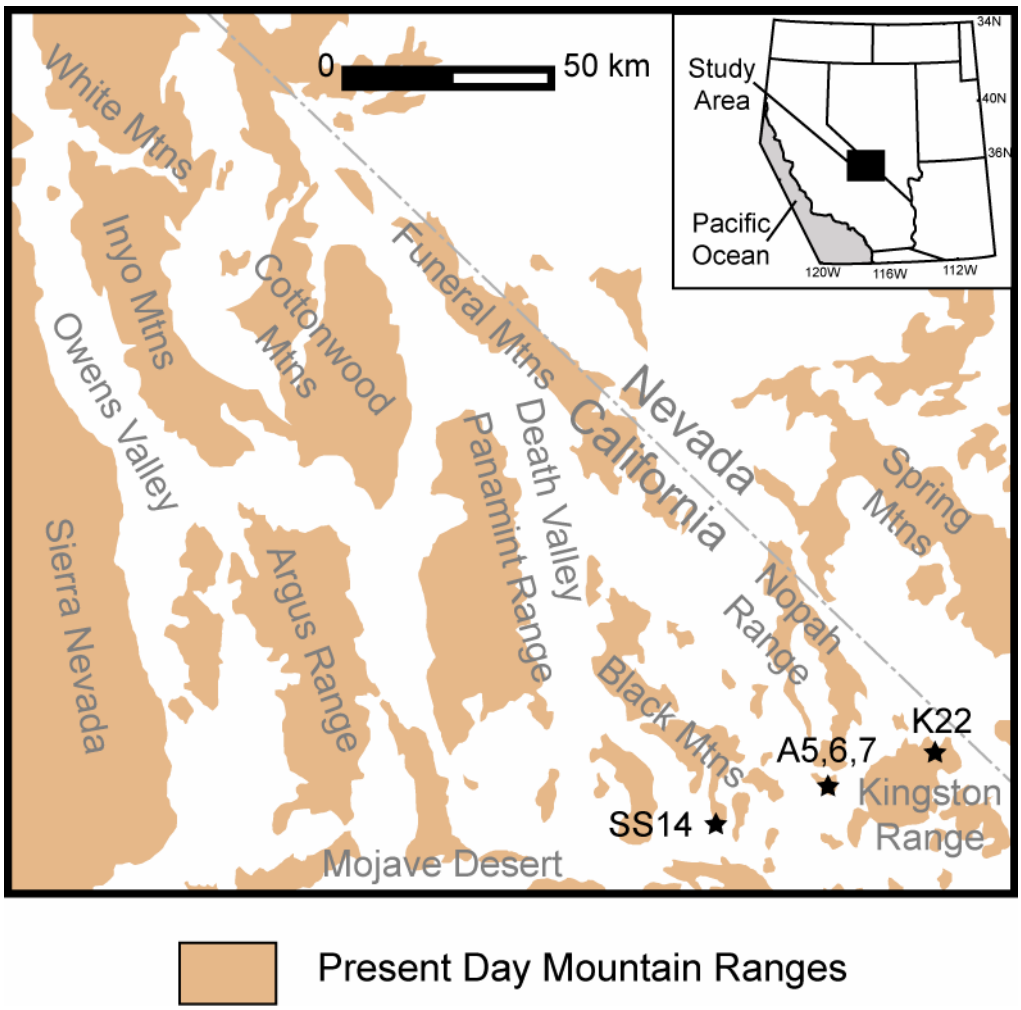

Figure A1. Location map of samples collected in Death Valley region.

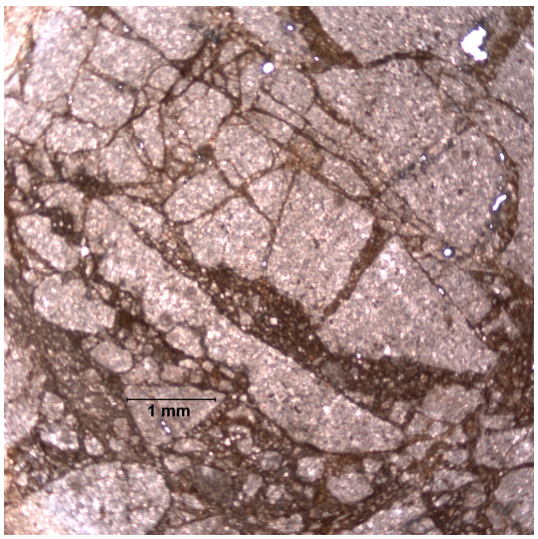

A5

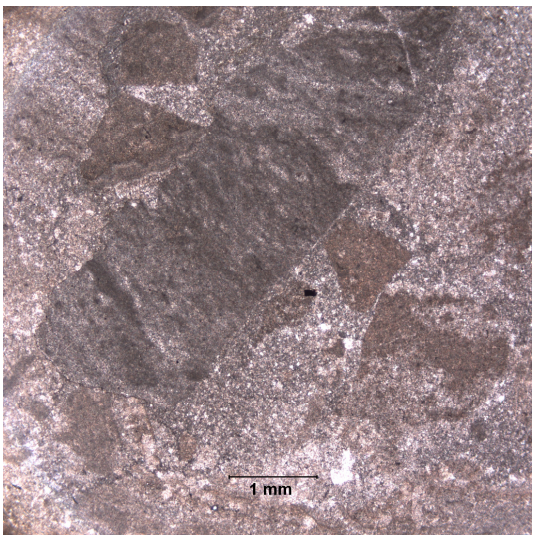

K22

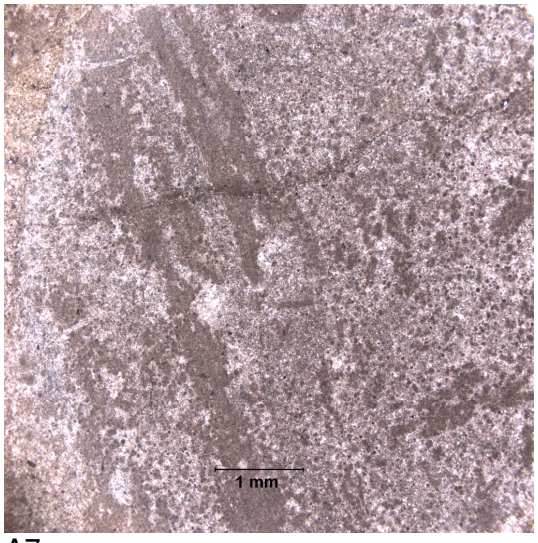

A7

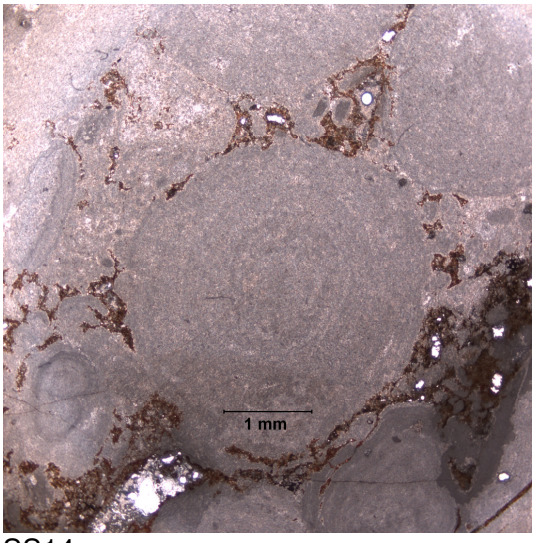

SS14

Figure A2. Photomicrographs of selected thin sections. Note breccia in A6, fenestral texture in A7, laminated clast in K22, and pisolite in SS14.

Table A1. Descriptions of thin sections of analyzed samples.

Sample #	*Location*	*Description*
A5	Alexander Hills	Dolomicrite with local silicification; relatively homogeneous; packed, rod-like filaments with preferred orientation; possible bedding
A6	Alexander Hills	Fractured dolomite with spherical cocoid algae and elongate filaments; possible secondary filling of organically caused cavities; clasts between fractures may be homogeneous
A7	Alexander Hills	Fenestral fabric in dolomite; primary algal mat texture; loosely constructed carbonate with spaces that were filled post-deposition with fine-grain carbonate matrix, organics, and/or trapped gas
K22	Kingston Range	Healed dolomite breccia; some brecciated clasts contain flat algal lamination
SS14	Saratoga Springs	Pisolitic dolomite with cavities, possibly from organic matter; original depositional structures are preserved

clean hood. We duplicated the process with a blank to record the level of Pb contamination that the sample preparation method introduced.

We weighed the samples and added ~1 mL of 0.6 N HBr for the first leach. After two hours, we emptied the solution into beakers, and we rinsed the leftover bits of samples. We dried and weighed the samples. Then we filled the beakers with 0.6 N HBr proportional to ~10 mL of HBr per ~400 mg of sample for the second leach, with the intention of dissolving the entire remaining sample. The amount of HBr was ~5 mL. The samples were left to dissolve overnight, but were not completely dissolved. We set the beakers onto a hotplate to speedup reactions, but after four hours the samples still had not completely dissolved. We emptied the second leach into beakers and weighed them, and we washed and dried the remaining bits again. To dissolve the remaining residue, we filled the beakers with ~5 mL of 7 N HCl and placed them onto a hotplate overnight. The chips were mostly dissolved in the morning. We emptied the third leach into beakers and weighed them. We separated the leaches into aliquot for isotopic spiking, and we attempted to make the quantity of spike ~10% of the quantity of estimated Pb load, (~250 µL of spike).

To prepare samples SS14, A7, A5 (again), and K20 (again), we replaced sawing chunks with micro-drilling in crack-free, homogeneous zones within the thin section billets. The remaining procedure was identical to the first attempt, except the second and third leaches were both performed with 7 N HCl on a hotplate overnight. We analyzed 1-3 sections of each sample. All isotopic measurements were made on the ID-TIMS at University of Wyoming. Samples A7, K20, and SS14 appeared to be the most homogeneous and least altered. After obtaining data from these samples that yielded meaningless dates, it was apparent that more analyses would likely be fruitless.

A.3 Results

Table A2 lists the isotopic results from the analyses. Note that the $^{206}Pb/^{204}Pb$ ratios ranged from 18.716 to 22.200, and the $^{207}Pb/^{204}Pb$ ratios ranged from 15.682 to 16.442. The U levels ranged from 0.12 ppm to 0.81 ppm, and the Pb levels ranged from 0.61 ppm to 7.70 ppm. Meaningful radiogenic ages could not be calculated (discussed below).

A.4 Discussion

The Pb isotopic compositions and the U and Pb concentrations observed for all samples fall into the Type II Pb category described by Babinski et al. (1999). According to their study, Type II Pb is nonradiogenic Pb that could represent seawater Pb or crustal Pb generated during deformation. A large amount of nonradiogenic Pb was introduced at some time, lowering the U/Pb ratio. The radiogenic Pb isotopic compositions cannot be discerned because of high levels of nonradiogenic Pb. Therefore, meaningful dates could not be obtained.

The carbonates in the Death Valley region could have experienced common Pb introduction due to seawater during the Cambrian transgression, or due to deformation during Mesozoic compression and/or Cenozoic extension. Our results show that even seemingly low levels of alteration in Precambrian carbonates may preclude meaningful isotopic geochronologic analyses due to various means of common Pb introduction. Despite these challenges, extending the emerging method of carbonate U-Pb geochronology to Precambrian rocks would provide immense help in constraining the timing of sedimentation in settings where fossil evidence is scarce or absent.

Table A2. Isotopic results from ID-TIMS analyses.

				Corrected Ratios								*Rho*	*Rho*	*Rho*	*Rho*
Sample	*Name*	*ppm U*	*ppm Pb*	*206Pb/ 204Pb*	*%err*	*207Pb/ 204Pb*	*%err*	*208Pb/ 204Pb*	*%err*	*238U/ 204Pb*	*%err*	*235U/ 204Pb*	*6/4- 7/4*	*6/4- 8/4*	*Alpha- Mu*	*Beta- Nu*
A7-1		0.38	0.89	21.870	(0.28)	15.828	(0.28)	39.936	(0.31)	28.86	(1.10)	0.209	0.888	0.879	0.612	0.256
A7-3		0.40	1.09	20.673	(0.20)	15.768	(0.22)	39.689	(0.26)	24.53	(0.91)	0.178	0.933	0.903	0.461	0.224
A7-4		0.22	0.61	20.787	(0.29)	15.778	(0.21)	39.986	(0.26)	24.18	(2.80)	0.175	0.675	0.749	0.715	0.137
K20-1 1st	leach	0.14	3.21	18.716	(0.11)	15.688	(0.20)	39.545	(0.29)	2.87	(0.61)	0.021	0.789	0.695	0.167	0.142
K20-1 2nd	leach	0.69	7.70	19.387	(0.11)	15.752	(0.16)	39.494	(0.21)	5.87	(4.40)	0.043	0.987	0.974	0.026	0.025
K20-1 3rd	leach	0.81	4.74	18.765	(0.10)	15.682	(0.15)	39.677	(0.20)	11.12	(2.30)	0.081	0.999	0.999	0.044	0.044
K20-2 2nd	leach	0.00	0.00	0.000	(0.00)	0.000	(0.00)	0.000	(0.00)	0.00	(0.00)	0.000	0.000	0.000	0.000	0.000
SS14-2		0.13	2.68	20.340	(0.14)	15.787	(0.18)	39.646	(0.22)	3.15	(2.22)	0.023	0.971	0.944	0.075	0.062
SS14-3		0.12	1.71	20.579	(0.17)	15.814	(0.20)	39.822	(0.24)	4.88	(1.08)	0.035	0.941	0.908	0.321	0.166
SS14-4		0.24	0.83	22.200	(0.81)	16.442	(0.81)	40.170	(0.82)	19.88	(1.51)	0.144	0.983	0.977	0.677	0.575

APPENDIX B

SHRIMP AND LAICPMS DATA TABLES

B.1 SHRIMP data

Spot Name	ppm U	ppm Th	232/ 238	206/ 238 Date (Ma) 204 corrected	1σ err	207/ 206 date (Ma) 204 corrected	1σ err	% Disc.	238/ 206 total	% err	207/ 206 total	% err	238/ 206* 204 corrected	% err	207/ 236* 204 corrected	% err	207*/ 235 204 corrected	% err	206* /238 204 corrected	% err	err corr
X0415-31	76	87	1.18	911	12	990	102	8.7	6.6169	1.3523	0.0680	2.3689	6.5853	1.4010	0.0722	5.0022	1.511	5.1947	0.1519	1.4010	0.27
X0415-37	219	188	0.88	1507	10	1421	27	-5.7	3.7861	0.7454	0.0924	0.9390	3.7978	0.7525	0.0898	1.4262	3.260	1.6125	0.2633	0.7525	0.47
X0415-23	219	75	0.36	1792	11	1798	14	0.3	3.1198	0.6928	0.1099	0.7572	3.1196	0.6928	0.1099	0.7583	4.858	1.0271	0.3206	0.6928	0.67
X0415-11	284	323	1.18	1935	10	1903	12	-1.6	2.8579	0.6067	0.1161	0.6296	2.8566	0.6080	0.1165	0.6890	5.624	0.9189	0.3501	0.6080	0.66
X0415-24	157	143	0.94	1934	13	1924	15	-0.5	2.8567	0.7835	0.1184	0.8116	2.8587	0.7839	0.1178	0.8388	5.684	1.1481	0.3498	0.7839	0.68
X0415-18	152	66	0.45	2003	15	1935	18	-3.4	2.7409	0.8548	0.1197	0.8821	2.7447	0.8577	0.1186	1.0243	5.957	1.3360	0.3643	0.8577	0.64
X0415-7	58	83	1.46	1854	22	1935	26	4.4	2.9952	1.3634	0.1201	1.4041	3.0005	1.3642	0.1186	1.4721	5.450	2.0071	0.3333	1.3642	0.68
X0415-27	307	29	0.10	1948	10	1939	12	-0.5	2.8313	0.5957	0.1195	0.6024	2.8336	0.5968	0.1188	0.6604	5.782	0.8901	0.3529	0.5968	0.67
X0415-26	67	37	0.57	1894	21	1948	24	2.8	2.9242	1.2743	0.1204	1.2894	2.9275	1.2745	0.1195	1.3156	5.627	1.8317	0.3416	1.2745	0.70
X0415-28	34	24	0.74	1915	28	1952	41	2.0	2.8819	1.6973	0.1225	1.7062	2.8915	1.7108	0.1197	2.3069	5.709	2.8720	0.3458	1.7108	0.60
X0415-15	63	30	0.50	2058	23	1961	24	-4.7	2.6570	1.3227	0.1209	1.2929	2.6590	1.3233	0.1203	1.3315	6.238	1.8772	0.3761	1.3233	0.70
X0415-9	130	79	0.63	2041	17	1962	25	-3.9	2.6809	0.9415	0.1217	0.9395	2.6853	0.9525	0.1204	1.3801	6.181	1.6769	0.3724	0.9525	0.57
X0415-33	121	95	0.81	2012	21	1972	20	-2.0	2.7279	1.2165	0.1218	0.9732	2.7305	1.2187	0.1210	1.1043	6.112	1.6446	0.3662	1.2187	0.74
X0415-30	214	225	1.09	2036	12	1975	19	-3.0	2.6926	0.7044	0.1213	1.0663	2.6926	0.7044	0.1213	1.0663	6.211	1.2780	0.3714	0.7044	0.55
X0415-40	104	52	0.52	1962	18	1984	20	1.1	2.8062	1.0371	0.1231	1.0777	2.8103	1.0381	0.1219	1.1401	5.980	1.5419	0.3558	1.0381	0.67
X0415-6	61	60	1.01	1881	22	1986	32	5.6	2.9493	1.3424	0.1227	1.3765	2.9517	1.3532	0.1220	1.8016	5.700	2.2532	0.3388	1.3532	0.60
X0415-16	89	39	0.45	2005	19	1989	20	-0.8	2.7395	1.1106	0.1226	1.0954	2.7408	1.1112	0.1222	1.1314	6.149	1.5858	0.3649	1.1112	0.70
X0415-29	180	201	1.16	2007	13	1991	13	-0.8	2.7383	0.7513	0.1225	0.7459	2.7385	0.7513	0.1224	0.7487	6.162	1.0607	0.3652	0.7513	0.71
X0415-20	94	49	0.54	2067	19	1992	19	-3.7	2.6438	1.0885	0.1228	1.0610	2.6452	1.0889	0.1224	1.0831	6.380	1.5359	0.3780	1.0889	0.71
X0415-38	223	99	0.46	2011	12	2007	13	-0.2	2.7333	0.7115	0.1229	0.6985	2.7314	0.7125	0.1235	0.7439	6.233	1.0301	0.3661	0.7125	0.69
X0415-3	93	49	0.54	1872	17	2008	20	7.3	2.9671	1.0645	0.1239	1.0779	2.9684	1.0657	0.1235	1.1330	5.739	1.5555	0.3369	1.0657	0.69
X0415-13	117	53	0.47	1980	16	2012	19	1.6	2.7810	0.9411	0.1239	0.9452	2.7813	0.9445	0.1238	1.0885	6.139	1.4412	0.3595	0.9445	0.66
X0415-19	139	59	0.43	2068	16	2024	16	-2.1	2.6404	0.8886	0.1257	0.8595	2.6437	0.8894	0.1247	0.9081	6.502	1.2711	0.3783	0.8894	0.70
X0415-4	93	61	0.68	1957	18	2027	19	3.6	2.8190	1.0869	0.1252	1.0614	2.8200	1.0877	0.1248	1.0987	6.104	1.5461	0.3546	1.0877	0.70
X0415-5	39	49	1.31	2021	30	2032	38	0.6	2.7131	1.6920	0.1261	1.6247	2.7159	1.7058	0.1252	2.1692	6.359	2.7596	0.3682	1.7058	0.62
X0415-34	142	248	1.80	2074	16	2044	15	-1.4	2.6359	0.8909	0.1258	0.8598	2.6349	0.8909	0.1261	0.8580	6.598	1.2369	0.3795	0.8909	0.72
X0415-32	167	131	0.81	2042	14	2089	19	2.3	2.6818	0.8132	0.1300	0.7800	2.6838	0.8218	0.1294	1.0854	6.646	1.3614	0.3726	0.8218	0.60
X0415-12	82	127	1.59	2059	20	2098	23	1.9	2.6632	1.1405	0.1283	1.0998	2.6574	1.1460	0.1300	1.3019	6.747	1.7345	0.3763	1.1460	0.66
X0415-36	136	87	0.66	2077	16	2113	15	1.8	2.6302	0.8897	0.1314	0.8520	2.6309	0.8904	0.1311	0.8801	6.873	1.2520	0.3801	0.8904	0.71
X0415-2	68	70	1.05	2010	22	2133	21	6.1	2.7347	1.2728	0.1323	1.2147	2.7339	1.2731	0.1326	1.2241	6.687	1.7661	0.3658	1.2731	0.72
X0415-22	212	74	0.36	2078	12	2152	11	3.6	2.6298	0.6798	0.1339	0.6365	2.6291	0.6802	0.1341	0.6499	7.033	0.9407	0.3804	0.6802	0.72
X0415-10	207	79	0.39	2420	14	2400	10	-0.8	2.1942	0.7153	0.1552	0.5814	2.1952	0.7154	0.1548	0.5881	9.726	0.9261	0.4555	0.7154	0.77

X0415-8	120	97	0.83	2834	21	2848	11	0.5	1.8081	0.9349	0.2039	0.6301	1.8111	0.9372	0.2027	0.6841	15.433	1.1603	0.5522	0.9372	0.81
culled																					
X0415-1	264	229	0.90	1829	10	2171	13	18.7	3.0466	0.6572	0.1361	0.6599	3.0487	0.6587	0.1355	0.7181	6.130	0.9744	0.3280	0.6587	0.68
X0415-25	544	254	0.48	1489	7	1777	21	19.3	3.8171	0.5475	0.1153	0.5036	3.8479	0.5552	0.1086	1.1625	3.892	1.2883	0.2599	0.5552	0.43
X0415-21	146	95	0.67	1620	14	1960	19	21.0	3.5048	0.9926	0.1192	0.9169	3.5002	0.9953	0.1202	1.0466	4.737	1.4443	0.2857	0.9953	0.69
X0415-14	414	243	0.61	1643	7	2143	11	30.4	3.4373	0.5052	0.1352	0.5200	3.4449	0.5080	0.1334	0.6422	5.338	0.8189	0.2903	0.5080	0.62
X0415-35	766	961	1.30	734	3	1532	34	108.8	8.2235	0.4471	0.1026	0.9128	8.2954	0.4676	0.0952	1.8236	1.582	1.8826	0.1205	0.4676	0.25
X0415-39	680	1328	2.02	704	3	1563	48	122.0	8.5351	0.4754	0.1097	0.7446	8.6675	0.5171	0.0968	2.5484	1.539	2.6003	0.1154	0.5171	0.20
X0415-17	294	401	1.41	581	4	506	64	-13.0	10.5641	0.7231	0.0606	1.5426	10.6026	0.7383	0.0574	2.8956	0.746	2.9883	0.0943	0.7383	0.25
X0416-17	2031	1459	0.74	645	2	606	14	-6.2	9.4929	0.2684	0.0605	0.5492	9.4979	0.2694	0.0601	0.6416	0.872	0.6959	0.1053	0.2694	0.39
X0416-34	339	200	0.61	705	4	656	38	-6.9	8.6529	0.6165	0.0617	1.2229	8.6555	0.6241	0.0615	1.7674	0.979	1.8743	0.1155	0.6241	0.33
X0416-30	303	300	1.02	714	5	687	39	-3.8	8.5188	0.7010	0.0637	1.3555	8.5325	0.7065	0.0624	1.8066	1.008	1.9398	0.1172	0.7065	0.36
X0416-23	99	110	1.16	1961	17	1863	21	-5.0	2.8078	1.0210	0.1154	1.0548	2.8131	1.0229	0.1139	1.1561	5.585	1.5436	0.3555	1.0229	0.66
X0416-5	215	219	1.05	1799	11	1929	17	7.2	3.0988	0.6749	0.1199	0.7177	3.1058	0.6813	0.1182	0.9579	5.248	1.1755	0.3220	0.6813	0.58
X0416-22	74	194	2.70	1918	19	1934	21	0.8	2.8858	1.1534	0.1185	1.1665	2.8857	1.1534	0.1185	1.1666	5.662	1.6405	0.3465	1.1534	0.70
X0416-32	154	261	1.75	1897	13	1940	18	2.3	2.9202	0.8078	0.1196	0.9447	2.9229	0.8101	0.1189	1.0280	5.609	1.3089	0.3421	0.8101	0.62
X0416-9	150	78	0.54	2034	18	1945	18	-4.4	2.6905	1.0454	0.1206	0.8446	2.6953	1.0484	0.1193	1.0018	6.101	1.4501	0.3710	1.0484	0.72
X0416-33	119	71	0.61	2112	19	1963	34	-7.1	2.5795	1.0399	0.1203	1.8952	2.5790	1.0401	0.1205	1.8956	6.442	2.1622	0.3878	1.0401	0.48
X0416-12	229	56	0.25	2047	12	1983	14	-3.2	2.6749	0.6955	0.1219	0.7479	2.6754	0.6966	0.1218	0.7860	6.276	1.0503	0.3738	0.6966	0.66
X0416-27	247	53	0.22	1893	11	1984	15	4.8	2.9253	0.6408	0.1232	0.6681	2.9306	0.6450	0.1219	0.8240	5.734	1.0464	0.3412	0.6450	0.62
X0416-24	291	198	0.70	2023	10	1989	10	-1.7	2.7117	0.5878	0.1224	0.5854	2.7122	0.5878	0.1222	0.5898	6.214	0.8327	0.3687	0.5878	0.71
X0416-8	358	77	0.22	1996	9	1993	10	-0.1	2.7548	0.5431	0.1228	0.5319	2.7560	0.5433	0.1225	0.5410	6.129	0.7667	0.3628	0.5433	0.71
X0416-4	55	17	0.33	2084	24	1998	38	-4.1	2.6050	1.3215	0.1273	1.2780	2.6206	1.3483	0.1229	2.1487	6.465	2.5367	0.3816	1.3483	0.53
X0416-29	198	43	0.23	2026	13	2006	13	-1.0	2.7098	0.7237	0.1230	0.7243	2.7082	0.7246	0.1234	0.7532	6.284	1.0451	0.3692	0.7246	0.69
X0416-13	351	30	0.09	2125	11	2010	10	-5.4	2.5607	0.5804	0.1239	0.5687	2.5613	0.5808	0.1237	0.5875	6.659	0.8261	0.3904	0.5808	0.70
X0416-19	123	112	0.94	2059	16	2030	16	-1.4	2.6492	0.8852	0.1274	0.8470	2.6577	0.8852	0.1251	0.9036	6.489	1.2650	0.3763	0.8852	0.70
X0416-7	130	26	0.21	2119	16	2037	15	-3.9	2.5655	0.8807	0.1266	0.8490	2.5690	0.8808	0.1256	0.8650	6.738	1.2345	0.3893	0.8808	0.71
X0416-18	333	150	0.47	2031	10	2044	10	0.7	2.6981	0.5482	0.1268	0.5353	2.7005	0.5487	0.1261	0.5620	6.439	0.7854	0.3703	0.5487	0.70
X0416-3	227	108	0.49	2054	12	2060	14	0.3	2.6620	0.6488	0.1279	0.6375	2.6645	0.6541	0.1272	0.8052	6.583	1.0374	0.3753	0.6541	0.63
X0416-10	255	124	0.50	2082	12	2065	11	-0.8	2.6229	0.6480	0.1278	0.6217	2.6237	0.6486	0.1276	0.6432	6.703	0.9135	0.3811	0.6486	0.71
X0416-16	120	69	0.59	2071	15	2075	15	0.2	2.6411	0.8563	0.1279	0.8265	2.6397	0.8572	0.1283	0.8549	6.701	1.2106	0.3788	0.8572	0.71
X0416-15	174	105	0.62	2079	14	2086	14	0.4	2.6298	0.7925	0.1286	0.7616	2.6281	0.7935	0.1291	0.7927	6.775	1.1216	0.3805	0.7935	0.71
X0416-21	122	357	3.01	2066	16	2097	16	1.5	2.6488	0.8883	0.1293	0.8592	2.6466	0.8898	0.1299	0.9051	6.770	1.2692	0.3778	0.8898	0.70
X0416-14	144	114	0.82	1979	16	2150	42	8.6	2.7579	0.8779	0.1404	1.4781	2.7827	0.9297	0.1339	2.3833	6.635	2.5582	0.3594	0.9297	0.36
X0416-6	105	40	0.39	2215	18	2171	18	-1.9	2.4374	0.9561	0.1362	0.9069	2.4394	0.9599	0.1356	1.0232	7.663	1.4030	0.4099	0.9599	0.68
X0416-35	98	71	0.75	2688	21	2678	18	-0.4	1.9322	0.9437	0.1829	1.0342	1.9327	0.9469	0.1827	1.0756	13.034	1.4331	0.5174	0.9469	0.66
X0416-28	71	94	1.36	2608	26	2708	16	3.8	2.0025	1.1905	0.1870	0.8903	2.0051	1.1932	0.1861	0.9454	12.797	1.5224	0.4987	1.1932	0.78
X0416-11	49	18	0.37	2714	31	2782	26	2.5	1.9060	1.4095	0.1962	1.4637	1.9104	1.4189	0.1947	1.5857	14.050	2.1278	0.5235	1.4189	0.67
culled																					
X0416-31	167	124	0.76	2504	16	2880	9	15.0	2.1047	0.7629	0.2073	0.5518	2.1063	0.7639	0.2068	0.5687	13.535	0.9523	0.4748	0.7639	0.80
X0416-20	322	631	2.03	1696	8	1963	17	15.7	3.3218	0.5636	0.1207	0.9402	3.3232	0.5651	0.1204	0.9770	4.997	1.1287	0.3009	0.5651	0.50
X0416-1	79	67	0.87	2686	24	3285	19	22.3	1.9322	1.0697	0.2671	1.1639	1.9347	1.0747	0.2664	1.1928	18.983	1.6055	0.5169	1.0747	0.67
X0416-2	128	174	1.41	1396	11	1908	20	36.7	4.1327	0.9070	0.1172	1.0805	4.1351	0.9079	0.1168	1.1137	3.895	1.4368	0.2418	0.9079	0.63
X0416-25	327	252	0.80	1349	8	1922	39	42.5	4.2272	0.5954	0.1299	0.6862	4.2974	0.6379	0.1177	2.1661	3.778	2.2581	0.2327	0.6379	0.28
X0416-26	510	857	1.74	939	5	1866	92	98.7	6.1972	0.5095	0.1350	3.3544	6.3746	0.5794	0.1141	5.1226	2.469	5.1553	0.1569	0.5794	0.11

X0423-38	82	74	0.93	1199	14	1084	46	-9.6	4.8689	1.2914	0.0791	1.8757	4.8909	1.2947	0.0756	2.2761	2.130	2.6185	0.2045	1.2947	0.49
X0423-4	2500	2483	1.03	1131	2	1115	9	-1.4	5.2076	0.2341	0.0779	0.3305	5.2154	0.2354	0.0768	0.4650	2.029	0.5212	0.1917	0.2354	0.45
X0423-9	134	104	0.80	1185	11	1124	59	-5.2	4.9441	1.0095	0.0786	2.8227	4.9539	1.0112	0.0771	2.9584	2.146	3.1265	0.2019	1.0112	0.32
X0423-11	51	38	0.77	1166	17	1139	48	-2.3	5.0435	1.6297	0.0777	2.3927	5.0435	1.6297	0.0777	2.3927	2.124	2.8950	0.1983	1.6297	0.56
X0423-14	318	224	0.73	1208	7	1144	19	-5.2	4.8530	0.6602	0.0779	0.9714	4.8530	0.6602	0.0779	0.9714	2.213	1.1745	0.2061	0.6602	0.56
X0423-32	66	45	0.71	1186	19	1151	54	-2.9	4.9377	1.7022	0.0805	2.0353	4.9526	1.7100	0.0782	2.6965	2.176	3.1930	0.2019	1.7100	0.54
X0423-36	302	484	1.66	1209	8	1151	21	-4.8	4.8435	0.6838	0.0786	0.9806	4.8463	0.6851	0.0782	1.0747	2.224	1.2745	0.2063	0.6851	0.54
X0423-29	381	384	1.04	1216	7	1159	18	-4.6	4.8155	0.6051	0.0790	0.8791	4.8187	0.6052	0.0785	0.8943	2.246	1.0798	0.2075	0.6052	0.56
X0423-19	153	155	1.05	1178	10	1180	32	0.1	4.9838	0.9694	0.0796	1.4066	4.9855	0.9724	0.0793	1.5977	2.194	1.8704	0.2006	0.9724	0.52
X0423-13	502	832	1.71	1157	6	1180	18	2.0	5.0856	0.5401	0.0796	0.7796	5.0872	0.5420	0.0793	0.9023	2.150	1.0526	0.1966	0.5420	0.51
X0423-34	386	579	1.55	1181	7	1189	18	0.6	4.9715	0.6122	0.0797	0.9060	4.9715	0.6122	0.0797	0.9060	2.209	1.0935	0.2011	0.6122	0.56
X0423-3	157	80	0.52	1177	10	1204	26	2.3	4.9990	0.9158	0.0793	1.3536	4.9925	0.9158	0.0803	1.3445	2.218	1.6268	0.2003	0.9158	0.56
X0423-6	234	81	0.36	1208	8	1215	28	0.6	4.8489	0.7568	0.0810	1.0678	4.8505	0.7626	0.0807	1.4074	2.295	1.6008	0.2062	0.7626	0.48
X0423-23	302	49	0.17	1337	8	1341	18	0.3	4.3376	0.6778	0.0861	0.9076	4.3376	0.6778	0.0861	0.9076	2.738	1.1327	0.2305	0.6778	0.60
X0423-17	218	131	0.62	1490	11	1470	19	-1.3	3.8435	0.7912	0.0924	0.9763	3.8450	0.7915	0.0921	0.9961	3.304	1.2723	0.2601	0.7915	0.62
X0423-31	1273	455	0.37	1375	4	1491	8	8.5	4.2048	0.3152	0.0935	0.4023	4.2066	0.3157	0.0932	0.4324	3.054	0.5354	0.2377	0.3157	0.59
X0423-30	569	209	0.38	1467	6	1496	11	2.0	3.9136	0.4530	0.0932	0.5695	3.9125	0.4534	0.0934	0.5910	3.292	0.7449	0.2556	0.4534	0.61
X0423-33	192	115	0.62	1539	11	1511	20	-1.8	3.7104	0.7978	0.0937	0.9696	3.7083	0.7992	0.0941	1.0399	3.501	1.3115	0.2697	0.7992	0.61
X0423-8	57	31	0.57	1520	20	1524	38	0.2	3.7521	1.4680	0.0964	1.7625	3.7602	1.4726	0.0948	2.0423	3.476	2.5179	0.2659	1.4726	0.58
X0423-22	162	113	0.72	1566	13	1568	22	0.1	3.6387	0.9084	0.0965	1.0925	3.6360	0.9105	0.0971	1.1894	3.681	1.4978	0.2750	0.9105	0.61
X0423-12	148	71	0.49	1657	14	1613	20	-2.7	3.4117	0.9288	0.0994	1.0649	3.4117	0.9288	0.0994	1.0649	4.018	1.4130	0.2931	0.9288	0.66
X0423-37	556	532	0.99	1585	7	1698	15	7.1	3.5790	0.4791	0.1059	0.5445	3.5877	0.4843	0.1041	0.7926	4.000	0.9288	0.2787	0.4843	0.52
X0423-35	363	233	0.66	1768	9	1746	13	-1.3	3.1669	0.5849	0.1072	0.6433	3.1687	0.5858	0.1068	0.6883	4.647	0.9039	0.3156	0.5858	0.65
X0423-25	297	205	0.71	1791	10	1751	13	-2.3	3.1210	0.6712	0.1073	0.7193	3.1218	0.6714	0.1071	0.7266	4.731	0.9893	0.3203	0.6714	0.68
X0423-10	78	21	0.28	1846	20	1792	24	-2.9	3.0118	1.2233	0.1106	1.2860	3.0159	1.2236	0.1095	1.3183	5.008	1.7986	0.3316	1.2236	0.68
X0423-18	133	73	0.57	1839	16	1806	19	-1.8	3.0282	0.9769	0.1104	1.0335	3.0282	0.9769	0.1104	1.0335	5.026	1.4221	0.3302	0.9769	0.69
X0423-16	572	127	0.23	1783	8	1819	9	2.0	3.1371	0.4820	0.1113	0.5000	3.1377	0.4822	0.1112	0.5091	4.885	0.7012	0.3187	0.4822	0.69
X0423-27	230	122	0.55	1856	11	1866	14	0.5	2.9958	0.7118	0.1144	0.7359	2.9970	0.7125	0.1141	0.7666	5.249	1.0466	0.3337	0.7125	0.68
X0423-28	343	189	0.57	1955	10	1937	11	-0.9	2.8208	0.5914	0.1193	0.5761	2.8228	0.5928	0.1187	0.6365	5.799	0.8699	0.3543	0.5928	0.68
X0423-40	245	120	0.51	1993	12	1945	13	-2.4	2.7590	0.7051	0.1196	0.6878	2.7601	0.7054	0.1193	0.7031	5.958	0.9959	0.3623	0.7054	0.71
X0423-21	29	15	0.53	2132	37	1982	40	-7.1	2.5443	2.0586	0.1237	1.9375	2.5510	2.0654	0.1217	2.2320	6.580	3.0410	0.3920	2.0654	0.68
X0423-15	167	159	0.98	1971	15	1984	15	0.7	2.7936	0.8621	0.1227	0.8337	2.7966	0.8621	0.1219	0.8446	6.011	1.2068	0.3576	0.8621	0.71
X0423-26	67	33	0.51	2047	23	2026	22	-1.0	2.6733	1.2962	0.1255	1.2216	2.6757	1.2962	0.1248	1.2313	6.432	1.7878	0.3737	1.2962	0.73
X0423-2	230	43	0.19	2067	13	2033	12	-1.6	2.6452	0.7072	0.1256	0.6688	2.6461	0.7075	0.1253	0.6813	6.530	0.9822	0.3779	0.7075	0.72
X0423-24	326	72	0.23	2041	11	2035	10	-0.3	2.6860	0.6245	0.1253	0.5862	2.6854	0.6245	0.1255	0.5856	6.442	0.8561	0.3724	0.6245	0.73
X0423-7	212	81	0.39	2066	13	2071	12	0.3	2.6474	0.7343	0.1280	0.6807	2.6474	0.7343	0.1280	0.6807	6.667	1.0013	0.3777	0.7343	0.73
X0423-20	48	30	0.65	2707	34	2706	19	0.0	1.9141	1.5317	0.1868	1.0935	1.9167	1.5335	0.1859	1.1355	13.373	1.9081	0.5217	1.5335	0.80
X0423-1	174	123	0.73	2756	17	2769	9	0.5	1.8745	0.7801	0.1931	0.5327	1.8745	0.7801	0.1931	0.5327	14.205	0.9446	0.5335	0.7801	0.83
X0423-39	93	25	0.28	2771	25	2781	12	0.4	1.8606	1.0885	0.1951	0.7369	1.8621	1.0894	0.1945	0.7565	14.403	1.3263	0.5370	1.0894	0.82
X0423-5	37	21	0.57	2740	38	2840	19	3.6	1.8868	1.6849	0.2021	1.1675	1.8878	1.6858	0.2017	1.1841	14.734	2.0601	0.5297	1.6858	0.82
X04_24-13	24	78	3.30	1918	44	1863	68	-2.9	2.8599	2.5954	0.1206	2.0817	2.8853	2.6331	0.1140	3.7529	5.446	4.5845	0.3466	2.6331	0.57
X04_24-11	395	167	0.44	1989	9	1964	9	-1.3	2.7673	0.5286	0.1204	0.5209	2.7667	0.5288	0.1205	0.5304	6.006	0.7490	0.3614	0.5288	0.71
X04_24-18	754	69	0.09	1969	8	2001	12	1.6	2.7951	0.4460	0.1241	0.6391	2.7990	0.4473	0.1231	0.6872	6.062	0.8200	0.3573	0.4473	0.55
X04_24-17	204	109	0.55	2001	13	2008	13	0.4	2.7492	0.7267	0.1232	0.7017	2.7476	0.7277	0.1236	0.7357	6.201	1.0348	0.3639	0.7277	0.70
X04_24-7	258	20	0.08	2092	12	2017	11	-3.6	2.6075	0.6527	0.1245	0.6191	2.6085	0.6531	0.1242	0.6347	6.563	0.9107	0.3834	0.6531	0.72
X04_24-20	349	35	0.10	2038	10	2018	9	-0.9	2.6898	0.5526	0.1244	0.5301	2.6902	0.5527	0.1243	0.5329	6.369	0.7677	0.3717	0.5527	0.72
X04_24-12	342	107	0.32	2069	10	2038	10	-1.5	2.6418	0.5840	0.1259	0.5494	2.6427	0.5848	0.1256	0.5805	6.555	0.8240	0.3784	0.5848	0.71
X04_24-5	123	67	0.56	2018	17	2041	19	1.1	2.7150	0.9677	0.1272	0.9114	2.7198	0.9724	0.1259	1.0865	6.381	1.4581	0.3677	0.9724	0.67
X04_24-14	348	63	0.19	1995	10	2041	10	2.3	2.7553	0.5539	0.1263	0.5327	2.7567	0.5539	0.1259	0.5383	6.297	0.7724	0.3627	0.5539	0.72
X04_24-15	74	40	0.56	2085	22	2044	21	-2.0	2.6178	1.2183	0.1263	1.1405	2.6187	1.2189	0.1261	1.1649	6.639	1.6860	0.3819	1.2189	0.72
X04_24-2	122	60	0.51	2056	17	2046	16	-0.5	2.6588	0.9481	0.1269	0.8861	2.6615	0.9486	0.1262	0.9145	6.538	1.3176	0.3757	0.9486	0.72

X04_24-16	212	98	0.48	2075	13	2056	13	-0.9	2.6330	0.7321	0.1271	0.6779	2.6337	0.7333	0.1269	0.7225	6.644	1.0295	0.3797	0.7333	0.71
X04_24-3	404	128	0.33	2077	9	2061	9	-0.8	2.6286	0.5277	0.1278	0.4874	2.6301	0.5282	0.1273	0.5065	6.675	0.7318	0.3802	0.5282	0.72
X04_24-1	138	137	1.02	2092	16	2068	16	-1.1	2.6059	0.8914	0.1287	0.8332	2.6090	0.8937	0.1278	0.9214	6.754	1.2836	0.3833	0.8937	0.70
X04_24-8	233	124	0.55	2081	12	2068	12	-0.6	2.6224	0.6981	0.1283	0.6427	2.6241	0.6992	0.1278	0.6831	6.717	0.9775	0.3811	0.6992	0.72
X04_24-10	27	7	0.25	2172	37	2120	33	-2.4	2.4978	1.9953	0.1310	1.8113	2.4956	1.9969	0.1317	1.8573	7.275	2.7271	0.4007	1.9969	0.73
X04_24-119	139	93	0.69	2229	16	2241	13	0.5	2.4202	0.8672	0.1413	0.7490	2.4208	0.8676	0.1411	0.7636	8.036	1.1558	0.4131	0.8676	0.75
culled																					
X04_24-9	1123	498	0.46	1630	5	1875	7	15.0	3.4741	0.3219	0.1151	0.3472	3.4761	0.3223	0.1147	0.3696	4.550	0.4904	0.2877	0.3223	0.66
X04_24-4	1467	1273	0.90	1478	4	1760	11	19.1	3.8795	0.2869	0.1081	0.5685	3.8818	0.2873	0.1077	0.5849	3.824	0.6516	0.2576	0.2873	0.44
X04_24-6	194	62	0.33	1390	12	1982	21	42.6	4.1460	0.9694	0.1237	0.9204	4.1568	0.9753	0.1217	1.1599	4.037	1.5154	0.2406	0.9753	0.64
X0432-11	256	158	0.64	1808	10	1886	20	4.4	3.0744	0.6205	0.1190	0.6552	3.0892	0.6330	0.1154	1.1372	5.151	1.3015	0.3237	0.6330	0.49
X0432-15	250	180	0.74	1935	10	1915	13	-1.1	2.8549	0.6263	0.1175	0.6411	2.8557	0.6278	0.1173	0.6984	5.662	0.9391	0.3502	0.6278	0.67
X0432-14	409	278	0.70	1436	7	1939	22	35.1	3.9720	0.4940	0.1256	0.5556	4.0083	0.5087	0.1189	1.2334	4.088	1.3342	0.2495	0.5087	0.38
X0432-16	39	37	0.99	2003	27	1943	33	-3.0	2.7383	1.5661	0.1207	1.6424	2.7441	1.5702	0.1191	1.8222	5.986	2.4054	0.3644	1.5702	0.65
X0432-2	166	81	0.50	1884	13	1965	26	4.3	2.9361	0.7606	0.1232	0.7812	2.9462	0.7841	0.1206	1.4486	5.644	1.6471	0.3394	0.7841	0.48
X0432-6	279	358	1.32	1454	8	1975	22	35.9	3.9240	0.6008	0.1269	0.6667	3.9539	0.6157	0.1213	1.2515	4.229	1.3948	0.2529	0.6157	0.44
X0432-7	221	105	0.49	2018	12	1975	12	-2.1	2.7194	0.6645	0.1215	0.6616	2.7200	0.6646	0.1213	0.6670	6.148	0.9416	0.3676	0.6646	0.71
X0432-13	84	54	0.66	1991	18	1976	20	-0.8	2.7577	1.0606	0.1227	1.0488	2.7628	1.0618	0.1213	1.1179	6.054	1.5418	0.3620	1.0618	0.69
X0432-12	97	53	0.57	2015	17	1989	19	-1.3	2.7246	1.0064	0.1223	0.9961	2.7248	1.0089	0.1223	1.0858	6.186	1.4822	0.3670	1.0089	0.68
X0432-1	169	102	0.62	1985	13	2012	14	1.4	2.7710	0.7487	0.1246	0.7500	2.7737	0.7503	0.1238	0.8133	6.156	1.1065	0.3605	0.7503	0.68
X0432-5	63	66	1.08	2071	22	2014	23	-2.8	2.6274	1.2160	0.1272	1.1833	2.6390	1.2160	0.1239	1.2716	6.475	1.7595	0.3789	1.2160	0.69
X0432-3	160	103	0.66	2522	19	2534	11	0.5	2.0877	0.9234	0.1680	0.5970	2.0888	0.9259	0.1676	0.6629	11.064	1.1388	0.4787	0.9259	0.81
X0432-8	319	162	0.53	2312	11	2680	13	15.9	2.2973	0.5346	0.1892	0.4255	2.3186	0.5455	0.1830	0.7848	10.881	0.9558	0.4313	0.5455	0.57
X0432-10	138	178	1.33	2826	19	2775	10	-1.8	1.8167	0.8141	0.1943	0.5757	1.8177	0.8147	0.1939	0.5871	14.707	1.0042	0.5501	0.8147	0.81
X0432-9	667	460	0.71	906	4	1948	55	115.0	6.4250	0.4228	0.1421	0.5597	6.6267	0.4807	0.1195	3.0674	2.486	3.1048	0.1509	0.4807	0.15
X0432-4	414	981	2.45	918	7	2037	247	122.0	5.6001	0.5302	0.2314	0.5278	6.5371	0.8703	0.1256	13.9734	2.649	14.0005	0.1530	0.8703	0.06
X0433-2	387	152	0.41	1835	8	1971	10	7.5	3.0357	0.5018	0.1215	0.5199	3.0375	0.5026	0.1210	0.5577	5.493	0.7508	0.3292	0.5026	0.67
X0433-21	327	296	0.93	1967	9	1985	10	0.9	2.8014	0.5429	0.1222	0.5391	2.8022	0.5439	0.1219	0.5847	5.999	0.7986	0.3569	0.5439	0.68
X0433-20	157	94	0.61	2026	13	1994	16	-1.6	2.7047	0.7590	0.1237	0.7584	2.7083	0.7620	0.1226	0.8989	6.239	1.1784	0.3692	0.7620	0.65
X0433-8	99	21	0.22	2042	22	1998	18	-2.2	2.6800	1.2279	0.1237	0.9947	2.6826	1.2283	0.1229	1.0253	6.316	1.5999	0.3728	1.2283	0.77
X0433-18	288	189	0.68	2084	10	2013	13	-3.4	2.6193	0.5876	0.1243	0.7141	2.6206	0.5884	0.1239	0.7462	6.519	0.9503	0.3816	0.5884	0.62
X0433-3	91	64	0.73	1934	17	2014	20	4.1	2.8500	1.0090	0.1262	1.0055	2.8577	1.0110	0.1240	1.1298	5.983	1.5161	0.3499	1.0110	0.67
X0433-9	185	103	0.57	1920	15	2023	13	5.4	2.8837	0.8863	0.1243	0.7312	2.8828	0.8863	0.1246	0.7299	5.959	1.1482	0.3469	0.8863	0.77
X0433-24	169	36	0.22	2070	13	2046	12	-1.2	2.6407	0.7330	0.1263	0.7014	2.6410	0.7332	0.1262	0.7071	6.588	1.0186	0.3786	0.7332	0.72
X0433-4	145	65	0.46	2061	14	2047	14	-0.6	2.6524	0.7961	0.1271	0.7649	2.6551	0.7965	0.1263	0.7922	6.559	1.1234	0.3766	0.7965	0.71
X0433-22	74	27	0.37	2031	20	2048	20	0.9	2.7008	1.1468	0.1264	1.1116	2.7008	1.1468	0.1264	1.1116	6.453	1.5971	0.3703	1.1468	0.72
X0433-14	242	145	0.62	1940	11	2049	12	5.6	2.8459	0.6376	0.1268	0.6331	2.8472	0.6383	0.1264	0.6669	6.122	0.9232	0.3512	0.6383	0.69
X0433-25	415	105	0.26	2135	9	2050	8	-4.0	2.5472	0.4798	0.1265	0.4582	2.5472	0.4799	0.1265	0.4619	6.847	0.6661	0.3926	0.4799	0.72
X0433-13	241	155	0.66	2025	11	2052	11	1.4	2.7103	0.6197	0.1266	0.5975	2.7102	0.6197	0.1266	0.5976	6.443	0.8609	0.3690	0.6197	0.72
X0433-31	134	117	0.90	2065	15	2053	16	-0.6	2.6467	0.8291	0.1274	0.7882	2.6489	0.8316	0.1267	0.8964	6.595	1.2227	0.3775	0.8316	0.68
X0433-19	194	133	0.71	2139	16	2053	12	-4.0	2.5409	0.8667	0.1270	0.6741	2.5418	0.8671	0.1267	0.6969	6.873	1.1124	0.3934	0.8671	0.78
X0433-15	63	41	0.67	2131	22	2054	21	-3.6	2.5528	1.2358	0.1268	1.1937	2.5528	1.2358	0.1268	1.1937	6.849	1.7182	0.3917	1.2358	0.72
X0433-7	85	40	0.48	2066	18	2057	18	-0.5	2.6462	1.0300	0.1270	0.9987	2.6462	1.0300	0.1270	0.9987	6.618	1.4347	0.3779	1.0300	0.72
X0433-26	86	62	0.74	2089	18	2058	19	-1.5	2.6147	1.0303	0.1265	0.9919	2.6128	1.0318	0.1271	1.0497	6.705	1.4719	0.3827	1.0318	0.70

X0433-30	109	71	0.67	2079	16	2070	16	-0.5	2.6256	0.9186	0.1283	0.8798	2.6270	0.9192	0.1279	0.9077	6.715	1.2918	0.3807	0.9192	0.71
X0433-27	214	104	0.50	2068	12	2070	11	0.1	2.6439	0.6733	0.1279	0.6470	2.6437	0.6733	0.1280	0.6467	6.675	0.9336	0.3783	0.6733	0.72
X0433-16	162	91	0.58	2039	14	2071	13	1.6	2.6901	0.7851	0.1274	0.7530	2.6880	0.7851	0.1280	0.7512	6.567	1.0866	0.3720	0.7851	0.72
X0433-23	162	100	0.64	2034	13	2073	15	1.9	2.6917	0.7432	0.1296	0.7083	2.6962	0.7460	0.1282	0.8343	6.555	1.1192	0.3709	0.7460	0.67
X0433-34	56	23	0.42	2029	21	2079	25	2.4	2.7003	1.2039	0.1295	1.1641	2.7032	1.2101	0.1286	1.4087	6.559	1.8570	0.3699	1.2101	0.65
X0433-29	143	92	0.66	2013	14	2084	15	3.6	2.7299	0.8062	0.1287	0.8465	2.7289	0.8067	0.1290	0.8642	6.518	1.1822	0.3664	0.8067	0.68
X0433-17	120	46	0.40	2112	17	2088	17	-1.1	2.5799	0.9309	0.1293	0.8621	2.5800	0.9339	0.1293	0.9840	6.910	1.3566	0.3876	0.9339	0.69
X0433-10	77	52	0.69	1977	19	2096	19	6.0	2.7877	1.1074	0.1295	1.0755	2.7865	1.1074	0.1299	1.0728	6.425	1.5418	0.3589	1.1074	0.72
X0433-5	156	131	0.87	2717	17	2704	9	-0.5	1.9085	0.7702	0.1853	0.5520	1.9076	0.7710	0.1857	0.5693	13.419	0.9584	0.5242	0.7710	0.80
culled																					
X0433-32	392	140	0.37	1792	7	2026	9	13.1	3.1191	0.4780	0.1249	0.4924	3.1196	0.4780	0.1248	0.4929	5.518	0.6866	0.3206	0.4780	0.70
X0433-12	200	105	0.54	1766	13	2007	14	13.7	3.1690	0.8502	0.1246	0.7027	3.1735	0.8517	0.1235	0.7926	5.365	1.1634	0.3151	0.8517	0.73
X0433-1	605	155	0.27	1675	6	1958	9	16.9	3.3682	0.4051	0.1209	0.4328	3.3714	0.4061	0.1201	0.4818	4.912	0.6301	0.2966	0.4061	0.64
X0433-6	216	180	0.86	1907	14	2298	182	20.5	2.9055	0.8317	0.1458	10.5663	2.9055	0.8317	0.1458	10.5663	6.921	10.5989	0.3442	0.8317	0.08
X0433-35	945	887	0.97	1270	4	1690	13	33.1	4.5736	0.3165	0.1070	0.3970	4.5919	0.3208	0.1036	0.7082	3.111	0.7775	0.2178	0.3208	0.41
X0433-28	836	310	0.38	1328	5	1795	11	35.1	4.3594	0.4203	0.1117	0.4132	4.3698	0.4227	0.1097	0.5861	3.462	0.7227	0.2288	0.4227	0.58
X0433-11	1858	1301	0.72	1087	3	1471	45	35.4	5.3476	0.2501	0.1077	0.3346	5.4467	0.2817	0.0922	2.3740	2.334	2.3907	0.1836	0.2817	0.12
X0433-33	146	161	1.14	1197	11	2030	19	69.6	4.8966	0.9717	0.1257	0.9741	4.9006	0.9746	0.1251	1.0998	3.519	1.4695	0.2041	0.9746	0.66
04KRIC-31	467	154	0.34	1044	5	1005	19	-3.7	5.6852	0.5351	0.0729	0.8543	5.6864	0.5361	0.0727	0.9329	1.763	1.0760	0.1759	0.5361	0.50
04KRIC-23	177	115	0.67	1566	12	1579	20	0.8	3.6379	0.8291	0.0972	0.9762	3.6357	0.8305	0.0976	1.0465	3.702	1.3360	0.2751	0.8305	0.62
04KRIC-30	340	219	0.67	1678	9	1726	12	2.9	3.3624	0.5780	0.1059	0.6503	3.3636	0.5780	0.1057	0.6531	4.331	0.8722	0.2973	0.5780	0.66
04KRIC-8	352	218	0.64	1740	9	1745	12	0.3	3.2282	0.5863	0.1068	0.6231	3.2283	0.5867	0.1067	0.6424	4.559	0.8700	0.3098	0.5867	0.67
04KRIC-7	408	164	0.41	1658	8	1747	17	5.4	3.3964	0.5411	0.1098	0.5863	3.4094	0.5479	0.1069	0.9287	4.324	1.0783	0.2933	0.5479	0.51
04KRIC-15	205	104	0.53	1838	12	1748	16	-4.9	3.0285	0.7463	0.1078	0.7903	3.0319	0.7475	0.1069	0.8616	4.863	1.1407	0.3298	0.7475	0.66
04KRIC-24	171	73	0.45	1793	13	1755	29	-2.1	3.1013	0.7987	0.1116	0.8556	3.1190	0.8171	0.1073	1.6029	4.745	1.7991	0.3206	0.8171	0.45
04KRIC-37	286	96	0.35	1835	10	1772	13	-3.4	3.0351	0.6365	0.1086	0.6762	3.0362	0.6370	0.1084	0.7033	4.921	0.9489	0.3294	0.6370	0.67
04KRIC-27	358	103	0.30	1790	9	1773	15	-0.9	3.1137	0.5707	0.1111	0.6068	3.1246	0.5745	0.1084	0.8420	4.785	1.0193	0.3200	0.5745	0.56
04KRIC-1	266	226	0.88	1775	10	1774	13	-0.1	3.1551	0.6504	0.1082	0.6947	3.1540	0.6509	0.1085	0.7192	4.742	0.9700	0.3171	0.6509	0.67
04KRIC-19	586	152	0.27	1719	7	1777	9	3.4	3.2725	0.4390	0.1086	0.4771	3.2725	0.4390	0.1086	0.4771	4.577	0.6484	0.3056	0.4390	0.68
04KRIC-39	109	114	1.08	1826	16	1779	21	-2.6	3.0515	1.0187	0.1093	1.0834	3.0538	1.0194	0.1088	1.1243	4.910	1.5177	0.3275	1.0194	0.67
04KRIC-14	237	76	0.33	1785	11	1784	14	-0.1	3.1345	0.7134	0.1091	0.7530	3.1345	0.7134	0.1091	0.7530	4.798	1.0373	0.3190	0.7134	0.69
04KRIC-10	276	105	0.39	1818	10	1784	13	-1.8	3.0692	0.6546	0.1093	0.6841	3.0702	0.6551	0.1091	0.7097	4.899	0.9658	0.3257	0.6551	0.68
04KRIC-5	63	106	1.73	1827	22	1785	32	-2.3	3.0457	1.3625	0.1108	1.4265	3.0526	1.3691	0.1091	1.7341	4.928	2.2094	0.3276	1.3691	0.62
04KRIC-22	177	209	1.22	1790	13	1785	16	-0.3	3.1239	0.8075	0.1091	0.8536	3.1239	0.8075	0.1091	0.8536	4.816	1.1750	0.3201	0.8075	0.69
04KRIC-18	346	71	0.21	1685	9	1785	19	6.0	3.3322	0.6025	0.1128	0.6432	3.3482	0.6101	0.1092	1.0416	4.495	1.2071	0.2987	0.6101	0.51
04KRIC-29	166	66	0.41	1722	12	1786	19	3.7	3.2610	0.7908	0.1102	0.8792	3.2654	0.7951	0.1092	1.0632	4.611	1.3276	0.3062	0.7951	0.60
04KRIC-17	252	67	0.27	1822	11	1787	14	-1.9	3.0596	0.6723	0.1098	0.7174	3.0619	0.6732	0.1093	0.7610	4.920	1.0160	0.3266	0.6732	0.66
04KRIC-38	266	120	0.47	1781	10	1787	14	0.4	3.1418	0.6415	0.1097	0.6916	3.1435	0.6435	0.1093	0.7776	4.793	1.0093	0.3181	0.6435	0.64
04KRIC-13	303	139	0.47	1811	10	1789	12	-1.2	3.0835	0.6085	0.1090	0.6450	3.0820	0.6092	0.1094	0.6716	4.893	0.9067	0.3245	0.6092	0.67
04KRIC-36	191	152	0.82	1937	13	1791	16	-7.6	2.8494	0.7856	0.1102	0.8418	2.8522	0.7856	0.1095	0.8532	5.293	1.1598	0.3506	0.7856	0.68
04KRIC-40	352	142	0.42	1830	9	1791	11	-2.1	3.0447	0.5639	0.1097	0.5996	3.0458	0.5640	0.1095	0.6053	4.957	0.8273	0.3283	0.5640	0.68
04KRIC-28	656	96	0.15	1862	7	1792	10	-3.8	2.9821	0.4273	0.1106	0.4384	2.9861	0.4291	0.1096	0.5321	5.058	0.6835	0.3349	0.4291	0.63
04KRIC-2	55	82	1.53	1816	23	1797	28	-1.0	3.0740	1.4305	0.1098	1.5238	3.0738	1.4305	0.1099	1.5232	4.929	2.0896	0.3253	1.4305	0.68
04KRIC-20	297	41	0.14	1791	10	1800	17	0.5	3.1112	0.6337	0.1126	0.6652	3.1220	0.6393	0.1100	0.9499	4.859	1.1450	0.3203	0.6393	0.56
04KRIC-4	376	411	1.13	1755	9	1803	26	2.7	3.1643	0.5650	0.1175	0.5872	3.1950	0.5813	0.1102	1.4331	4.757	1.5465	0.3130	0.5813	0.38
04KRIC-11	236	96	0.42	1809	11	1805	13	-0.2	3.0849	0.6930	0.1107	0.7292	3.0865	0.6932	0.1103	0.7396	4.928	1.0136	0.3240	0.6932	0.68
04KRIC-6	270	41	0.16	1807	10	1810	13	0.2	3.0928	0.6499	0.1103	0.6892	3.0917	0.6499	0.1106	0.6880	4.933	0.9464	0.3234	0.6499	0.69
04KRIC-21	229	107	0.48	1824	11	1815	14	-0.5	3.0600	0.6920	0.1104	0.7356	3.0578	0.6933	0.1110	0.7899	5.003	1.0510	0.3270	0.6933	0.66
04KRIC-25	221	96	0.45	1812	11	1818	15	0.3	3.0827	0.7174	0.1108	0.7591	3.0815	0.7183	0.1111	0.7991	4.972	1.0745	0.3245	0.7183	0.67
04KRIC-32	166	131	0.81	1820	13	1827	17	0.4	3.0611	0.8275	0.1128	0.8716	3.0656	0.8285	0.1117	0.9310	5.022	1.2462	0.3262	0.8285	0.66

04KRIC-34	280	102	0.38	1839	11	1838	54	0.0	2.9507	0.6389	0.1319	0.6261	3.0294	0.6850	0.1124	2.9896	5.114	3.0670	0.3301	0.6850	0.22
04KRIC-3	133	126	0.97	1917	15	1895	17	-1.1	2.8860	0.9070	0.1163	0.9236	2.8872	0.9072	0.1160	0.9387	5.539	1.3055	0.3464	0.9072	0.69
04KRIC-26	243	108	0.46	2047	12	2088	12	2.0	2.6755	0.6732	0.1292	0.7022	2.6755	0.6732	0.1292	0.7022	6.661	0.9728	0.3738	0.6732	0.69
04KRIC-16	290	193	0.69	2262	12	2480	13	9.7	2.3635	0.5995	0.1670	0.4825	2.3791	0.6078	0.1624	0.7741	9.410	0.9842	0.4203	0.6078	0.62
culled																					
04KRIC-35	327	204	0.64	1541	9	1699	56	10.2	3.6144	0.6048	0.1225	0.6611	3.7040	0.6506	0.1041	3.0595	3.875	3.1279	0.2700	0.6506	0.21
04KRIC-33	302	148	0.51	1584	9	1758	27	11.0	3.5588	0.6138	0.1139	0.6780	3.5892	0.6298	0.1075	1.4635	4.131	1.5933	0.2786	0.6298	0.40
04KRIC-9	374	542	1.50	1971	10	2666	57	35.2	2.6397	0.5328	0.2194	0.3981	2.7954	0.6054	0.1814	3.4652	8.947	3.5177	0.3577	0.6054	0.17
04KRIC-12	517	275	0.55	1181	6	1874	72	58.6	4.7795	0.4917	0.1436	0.5381	4.9716	0.5581	0.1146	3.9702	3.179	4.0092	0.2011	0.5581	0.14
JSMD03-01-11	182	87	0.49	1443	9	1428	20	-1.0	3.9866	0.6897	0.0902	0.8924	3.9871	0.6919	0.0901	1.0367	3.116	1.2464	0.2508	0.6919	0.56
JSMD03-01-14	336	75	0.23	1574	7	1694	15	7.6	3.6119	0.5294	0.1049	0.6288	3.6164	0.5324	0.1038	0.7893	3.959	0.9521	0.2765	0.5324	0.56
JSMD03-01-15	734	303	0.43	1601	6	1729	21	8.0	3.5372	0.4297	0.1081	0.8112	3.5465	0.4397	0.1058	1.1396	4.115	1.2215	0.2820	0.4397	0.36
JSMD03-01-4	929	171	0.19	1673	6	1761	9	5.2	3.3724	0.3764	0.1080	0.4473	3.3737	0.3770	0.1077	0.4770	4.402	0.6080	0.2964	0.3770	0.62
JSMD03-01-8	361	130	0.37	1802	8	1770	10	-1.8	3.1011	0.4857	0.1083	0.5356	3.1014	0.4858	0.1082	0.5436	4.812	0.7290	0.3224	0.4858	0.67
JSMD03-01-10	230	95	0.43	1839	10	1770	13	-3.8	3.0273	0.6266	0.1086	0.6878	3.0284	0.6266	0.1083	0.6909	4.929	0.9327	0.3302	0.6266	0.67
JSMD03-01-9	171	54	0.33	1796	11	1779	15	-1.0	3.1109	0.6899	0.1092	0.7580	3.1125	0.6912	0.1088	0.8285	4.818	1.0790	0.3213	0.6912	0.64
JSMD03-01-13	536	59	0.11	1800	6	1783	9	-0.9	3.1040	0.3946	0.1092	0.4284	3.1048	0.3953	0.1090	0.4668	4.841	0.6117	0.3221	0.3953	0.65
JSMD03-01-5	754	149	0.20	1802	6	1784	9	-1.0	3.1010	0.3976	0.1090	0.4652	3.1008	0.3977	0.1091	0.4674	4.849	0.6137	0.3225	0.3977	0.65
JSMD03-01-1	852	80	0.10	1816	7	1791	19	-1.4	3.0716	0.4272	0.1097	1.0468	3.0724	0.4274	0.1095	1.0546	4.915	1.1379	0.3255	0.4274	0.38
JSMD03-01-3	390	405	1.07	2502	9	2648	6	5.8	2.1062	0.4389	0.1802	0.3394	2.1083	0.4396	0.1794	0.3615	11.736	0.5692	0.4743	0.4396	0.77
culled																					
JSMD03-01-2	435	291	0.69	2253	10	2915	13	29.4	2.3881	0.5002	0.2120	0.7728	2.3903	0.5009	0.2113	0.7825	12.186	0.9291	0.4183	0.5009	0.54
JSMD03-01-7	566	375	0.69	1830	6	2517	14	37.5	3.0145	0.3627	0.1740	0.3564	3.0462	0.3741	0.1659	0.8552	7.509	0.9334	0.3283	0.3741	0.40
JSMD03-01-6	918	1884	2.12	1776	6	2701	7	52.1	3.1375	0.3662	0.1888	0.2645	3.1522	0.3686	0.1853	0.4080	8.105	0.5498	0.3172	0.3686	0.67
JSMD03-01-12	2200	1851	0.87	518	2	1029	193	98.5	11.1981	0.2460	0.1281	0.3800	11.9456	0.3414	0.0735	9.5286	0.849	9.5348	0.0837	0.3414	0.04
JSDV03-12	141	175	1.28	1356	11	1301	28	-4.1	4.2705	0.9135	0.0847	1.2299	4.2721	0.9165	0.0843	1.4444	2.722	1.7106	0.2341	0.9165	0.54
JSDV03-6	289	123	0.44	1305	7	1330	17	1.9	4.4547	0.5955	0.0857	0.8266	4.4549	0.5962	0.0856	0.8763	2.651	1.0598	0.2245	0.5962	0.56
JSDV03-34	280	74	0.27	1413	7	1373	16	-2.9	4.0767	0.5419	0.0883	0.7226	4.0801	0.5435	0.0876	0.8445	2.959	1.0042	0.2451	0.5435	0.54
JSDV03-39	178	113	0.66	1608	10	1676	16	4.2	3.5286	0.7228	0.1028	0.8519	3.5286	0.7228	0.1028	0.8552	4.018	1.1198	0.2834	0.7228	0.65
JSDV03-3	180	86	0.49	1747	11	1689	16	-3.3	3.2130	0.7476	0.1036	0.8444	3.2130	0.7476	0.1036	0.8444	4.444	1.1278	0.3112	0.7476	0.66
JSDV03-37	244	128	0.54	1728	9	1692	15	-2.1	3.2477	0.5953	0.1048	0.6795	3.2519	0.5974	0.1037	0.8050	4.398	1.0024	0.3075	0.5974	0.60
JSDV03-14	259	118	0.47	1726	9	1695	14	-1.8	3.2573	0.6250	0.1041	0.7022	3.2578	0.6257	0.1039	0.7399	4.399	0.9689	0.3070	0.6257	0.65
JSDV03-40	417	196	0.49	1645	8	1714	10	4.2	3.4397	0.5821	0.1051	0.5432	3.4401	0.5823	0.1050	0.5603	4.208	0.8081	0.2907	0.5823	0.72
JSDV03-31	276	116	0.43	1722	9	1718	14	-0.3	3.2645	0.6109	0.1055	0.6862	3.2655	0.6118	0.1052	0.7361	4.442	0.9571	0.3062	0.6118	0.64
JSDV03-2	254	122	0.50	1729	9	1720	13	-0.5	3.2510	0.6096	0.1055	0.6894	3.2517	0.6097	0.1053	0.6960	4.465	0.9253	0.3075	0.6097	0.66

JSDV03-22	496	211	0.44	1614	6	1733	10	7.4	3.5112	0.4329	0.1067	0.5002	3.5138	0.4338	0.1061	0.5519	4.163	0.7020	0.2846	0.4338	0.62
JSDV03-8	376	176	0.48	1652	8	1736	13	5.1	3.4190	0.5172	0.1074	0.5868	3.4236	0.5196	0.1063	0.7236	4.280	0.8909	0.2921	0.5196	0.58
JSDV03-33	449	238	0.55	1719	6	1737	9	1.0	3.2716	0.4243	0.1063	0.4739	3.2716	0.4243	0.1063	0.4739	4.481	0.6361	0.3057	0.4243	0.67
JSDV03-21	317	39	0.13	1709	8	1739	12	1.7	3.2935	0.5596	0.1064	0.6260	3.2936	0.5598	0.1064	0.6334	4.455	0.8453	0.3036	0.5598	0.66
JSDV03-19	194	22	0.12	1697	10	1748	14	3.0	3.3211	0.6513	0.1070	0.7436	3.3211	0.6513	0.1070	0.7436	4.441	0.9885	0.3011	0.6513	0.66
JSDV03-35	410	200	0.51	1704	7	1750	10	2.7	3.3034	0.4489	0.1074	0.5104	3.3045	0.4493	0.1071	0.5344	4.467	0.6982	0.3026	0.4493	0.64
JSDV03-17	178	112	0.65	1709	11	1762	17	3.1	3.2948	0.7628	0.1078	0.8444	3.2950	0.7639	0.1078	0.9052	4.509	1.1845	0.3035	0.7639	0.64
JSDV03-32	163	56	0.36	1768	9	1765	12	-0.2	3.1675	0.5730	0.1084	0.6408	3.1693	0.5733	0.1079	0.6645	4.696	0.8777	0.3155	0.5733	0.65
JSDV03-23	194	65	0.35	1696	10	1769	16	4.3	3.3185	0.6879	0.1091	0.7833	3.3222	0.6899	0.1082	0.8951	4.490	1.1301	0.3010	0.6899	0.61
JSDV03-11	291	152	0.54	1686	9	1799	12	6.7	3.3446	0.6084	0.1102	0.6618	3.3455	0.6088	0.1100	0.6846	4.533	0.9161	0.2989	0.6088	0.66
JSDV03-28	207	53	0.26	1836	11	1833	13	-0.2	3.0347	0.6854	0.1121	0.7366	3.0351	0.6855	0.1120	0.7434	5.090	1.0112	0.3295	0.6855	0.68
JSDV03-20	609	53	0.09	1953	7	1958	7	0.2	2.8252	0.3932	0.1202	0.4009	2.8256	0.3932	0.1201	0.4025	5.860	0.5627	0.3539	0.3932	0.70
JSDV03-24	607	36	0.06	2397	8	2474	31	3.2	2.2187	0.3834	0.1621	1.8562	2.2198	0.3838	0.1618	1.8636	10.048	1.9027	0.4505	0.3838	0.20
JSDV03-1	229	112	0.50	2664	16	2677	8	0.5	1.9531	0.7265	0.1829	0.4852	1.9539	0.7269	0.1826	0.4980	12.887	0.8811	0.5118	0.7269	0.82
JSDV03-9	46	269	6.06	2610	29	2697	17	3.3	2.0006	1.3565	0.1858	1.0017	2.0033	1.3583	0.1848	1.0509	12.720	1.7174	0.4992	1.3583	0.79
culled																					
JSDV03-25	441	202	0.47	1594	7	1756	11	10.1	3.5629	0.4725	0.1079	0.5470	3.5652	0.4733	0.1074	0.5969	4.153	0.7618	0.2805	0.4733	0.62
JSDV03-26	382	116	0.31	1523	7	1722	17	13.1	3.7424	0.5108	0.1079	0.6138	3.7534	0.5164	0.1054	0.9149	3.872	1.0506	0.2664	0.5164	0.49
JSDV03-5	306	108	0.36	1509	8	1712	14	13.4	3.7882	0.5804	0.1056	0.6922	3.7915	0.5811	0.1048	0.7371	3.813	0.9386	0.2638	0.5811	0.62
JSDV03-13	701	88	0.13	1534	7	1744	61	13.7	3.6603	0.4746	0.1206	1.9780	3.7219	0.5297	0.1067	3.3285	3.954	3.3704	0.2687	0.5297	0.16
JSDV03-38	426	213	0.52	1416	6	1683	16	18.8	4.0584	0.4658	0.1056	0.5722	4.0699	0.4705	0.1032	0.8437	3.496	0.9660	0.2457	0.4705	0.49
JSDV03-15	516	155	0.31	1324	6	1608	22	21.5	4.3601	0.4756	0.1042	0.5844	4.3863	0.4853	0.0991	1.1954	3.117	1.2902	0.2280	0.4853	0.38
JSDV03-7	289	102	0.36	1412	10	1762	20	24.9	4.0728	0.7440	0.1103	0.7138	4.0849	0.7498	0.1078	1.0676	3.638	1.3046	0.2448	0.7498	0.57
JSDV03-36	404	54	0.14	1731	9	2201	16	27.2	3.2447	0.5611	0.1383	0.9227	3.2460	0.5615	0.1379	0.9356	5.859	1.0912	0.3081	0.5615	0.51
JSDV03-30	580	154	0.27	1229	5	1690	27	37.6	4.7372	0.4508	0.1082	1.0726	4.7629	0.4596	0.1036	1.4396	3.000	1.5112	0.2100	0.4596	0.30
JSDV03-10	700	310	0.46	1090	5	1560	66	43.1	5.4189	0.4952	0.0980	3.4512	5.4277	0.4974	0.0966	3.5343	2.454	3.5691	0.1842	0.4974	0.14
JSDV03-29	584	125	0.22	1019	4	1692	24	66.0	5.8140	0.4134	0.1072	0.9301	5.8383	0.4246	0.1037	1.3085	2.450	1.3757	0.1713	0.4246	0.31
JSDV03-18	968	30	0.03	817	3	1444	14	76.8	7.3910	0.3348	0.0923	0.5345	7.4036	0.3378	0.0909	0.7153	1.692	0.7911	0.1351	0.3378	0.43
JSDV03-16	598	125	0.22	905	5	1604	31	77.1	6.5679	0.5451	0.1071	0.6411	6.6321	0.5614	0.0989	1.6698	2.056	1.7616	0.1508	0.5614	0.32
JSDV03-27	1713	2491	1.50	532	2	1091	124	105.2	11.1591	0.3718	0.1112	0.5012	11.6316	0.4353	0.0759	6.2042	0.899	6.2195	0.0860	0.4353	0.07
JSDV03-4	753	427	0.59	681	3	1423	33	108.8	8.8926	0.5189	0.0971	0.6997	8.9683	0.5347	0.0899	1.7283	1.382	1.8091	0.1115	0.5347	0.30
JSWI-37	265	83	0.33	1067	7	1016	31	-4.8	5.5439	0.6855	0.0745	1.0945	5.5531	0.6906	0.0731	1.5166	1.815	1.6665	0.1801	0.6906	0.41
JSWI-40	190	86	0.47	1421	9	1410	23	-0.8	4.0467	0.7402	0.0907	0.9828	4.0537	0.7433	0.0892	1.2098	3.036	1.4199	0.2467	0.7433	0.52
JSWI-38	198	124	0.65	1667	11	1666	16	-0.1	3.3904	0.7315	0.1017	0.8429	3.3882	0.7323	0.1023	0.8830	4.163	1.1471	0.2951	0.7323	0.64
JSWI-25	49	14	0.29	1714	22	1668	32	-2.7	3.2801	1.4703	0.1029	1.6734	3.2821	1.4709	0.1024	1.7171	4.302	2.2610	0.3047	1.4709	0.65
JSWI-13	91	27	0.30	1685	20	1676	31	-0.5	3.3433	1.3098	0.1041	1.2312	3.3484	1.3168	0.1029	1.6807	4.235	2.1351	0.2987	1.3168	0.62
JSWI-14	198	64	0.33	1741	14	1695	19	-2.6	3.2210	0.8909	0.1052	0.8276	3.2259	0.8935	0.1039	1.0173	4.442	1.3540	0.3100	0.8935	0.66
JSWI-8	266	60	0.23	1689	9	1696	15	0.4	3.3360	0.6215	0.1046	0.7045	3.3385	0.6233	0.1040	0.8108	4.295	1.0227	0.2995	0.6233	0.61
JSWI-3	376	284	0.78	1641	8	1698	13	3.5	3.4458	0.5471	0.1050	0.6218	3.4498	0.5487	0.1041	0.7186	4.159	0.9041	0.2899	0.5487	0.61
JSWI-17	184	46	0.26	1696	11	1703	19	0.4	3.3185	0.7628	0.1056	0.8625	3.3235	0.7658	0.1043	1.0404	4.329	1.2918	0.3009	0.7658	0.59
JSWI-24	235	52	0.23	1673	10	1734	15	3.7	3.3720	0.6757	0.1067	0.7404	3.3740	0.6768	0.1062	0.8058	4.338	1.0523	0.2964	0.6768	0.64
JSWI-29	277	79	0.30	1755	9	1737	13	-1.1	3.1938	0.6080	0.1066	0.6857	3.1950	0.6083	0.1063	0.7084	4.587	0.9338	0.3130	0.6083	0.65
JSWI-4	138	74	0.55	1700	13	1739	20	2.3	3.3128	0.8788	0.1069	0.9981	3.3148	0.8801	0.1064	1.0744	4.426	1.3889	0.3017	0.8801	0.63
JSWI-28	181	82	0.47	1767	11	1752	18	-0.8	3.1684	0.7392	0.1078	0.8164	3.1708	0.7420	0.1072	0.9682	4.661	1.2198	0.3154	0.7420	0.61
JSWI-36	76	120	1.63	1675	17	1754	37	4.7	3.3540	1.1255	0.1114	1.2764	3.3706	1.1409	0.1073	2.0291	4.389	2.3279	0.2967	1.1409	0.49
JSWI-35	430	32	0.08	1778	8	1765	10	-0.7	3.1478	0.4848	0.1082	0.5327	3.1490	0.4855	0.1079	0.5711	4.726	0.7495	0.3176	0.4855	0.65
JSWI-7	363	127	0.36	1775	8	1774	12	0.0	3.1525	0.5388	0.1091	0.5840	3.1547	0.5401	0.1085	0.6562	4.741	0.8499	0.3170	0.5401	0.64
JSWI-21	574	83	0.15	1763	7	1782	9	1.1	3.1783	0.4238	0.1092	0.4681	3.1794	0.4245	0.1089	0.5089	4.724	0.6627	0.3145	0.4245	0.64
JSWI-31	362	118	0.34	1761	8	1783	11	1.3	3.1834	0.5336	0.1090	0.5895	3.1834	0.5338	0.1090	0.5987	4.722	0.8021	0.3141	0.5338	0.67

JSWI-5	570	208	0.38	1765	6	1787	9	1.2	3.1732	0.4177	0.1096	0.4630	3.1747	0.4185	0.1092	0.5105	4.744	0.6601	0.3150	0.4185	0.63
JSWI-16	162	71	0.46	1801	13	1790	22	-0.6	3.1064	0.8175	0.1086	0.8907	3.1032	0.8247	0.1094	1.2139	4.862	1.4675	0.3222	0.8247	0.56
JSWI-22	323	162	0.52	1762	9	1793	12	1.7	3.1825	0.5763	0.1091	0.6228	3.1807	0.5773	0.1096	0.6714	4.751	0.8855	0.3144	0.5773	0.65
JSWI-19	87	39	0.47	1764	17	1805	21	2.4	3.1817	1.0914	0.1094	1.1890	3.1780	1.0914	0.1104	1.1819	4.788	1.6088	0.3147	1.0914	0.68
JSWI-12	418	146	0.36	1802	8	1839	11	2.1	3.0965	0.4908	0.1134	0.5365	3.1002	0.4921	0.1124	0.6143	5.001	0.7871	0.3226	0.4921	0.63
JSWI-20	284	128	0.47	1704	9	1852	15	8.7	3.3001	0.6003	0.1143	0.6642	3.3040	0.6036	0.1133	0.8221	4.727	1.0199	0.3027	0.6036	0.59
JSWI-32	87	78	0.93	1823	17	1860	21	2.0	3.0592	1.0910	0.1138	1.1668	3.0592	1.0910	0.1138	1.1668	5.127	1.5973	0.3269	1.0910	0.68
JSWI-1	337	146	0.45	1768	9	1869	12	5.7	3.1662	0.5780	0.1148	0.6297	3.1681	0.5783	0.1143	0.6488	4.975	0.8691	0.3156	0.5783	0.67
JSWI-6	62	22	0.37	1883	21	1880	24	-0.2	2.9505	1.2792	0.1144	1.3384	2.9482	1.2792	0.1150	1.3316	5.378	1.8465	0.3392	1.2792	0.69
JSWI-30	107	33	0.32	2282	18	2336	14	2.4	2.3514	0.9508	0.1502	0.8148	2.3544	0.9509	0.1491	0.8292	8.733	1.2617	0.4247	0.9509	0.75
JSWI-15	468	75	0.17	2426	9	2462	6	1.5	2.1892	0.4570	0.1605	0.3732	2.1888	0.4571	0.1606	0.3774	10.117	0.5928	0.4569	0.4571	0.77
JSWI-10	172	77	0.46	2553	16	2514	10	-1.5	2.0587	0.7458	0.1655	0.5823	2.0584	0.7458	0.1657	0.5842	11.096	0.9474	0.4858	0.7458	0.79
JSWI-18	782	209	0.28	2402	9	2538	5	5.7	2.2142	0.4333	0.1682	0.2828	2.2146	0.4334	0.1680	0.2862	10.463	0.5194	0.4516	0.4334	0.83
JSWI-23	261	136	0.54	2504	12	2675	8	6.8	2.1064	0.5973	0.1825	0.4543	2.1068	0.5980	0.1824	0.4691	11.935	0.7600	0.4746	0.5980	0.79
JSWI-34	270	166	0.63	2711	13	2757	7	1.7	1.9123	0.6045	0.1920	0.4271	1.9129	0.6046	0.1917	0.4299	13.821	0.7419	0.5228	0.6046	0.81
JSWI-26	370	393	1.10	2787	11	2797	6	0.3	1.8482	0.5017	0.1967	0.3526	1.8487	0.5021	0.1965	0.3619	14.652	0.6189	0.5409	0.5021	0.81
JSWI-11	54	32	0.61	2789	29	2809	14	0.7	1.8466	1.2658	0.1982	0.8791	1.8474	1.2660	0.1979	0.8866	14.767	1.5456	0.5413	1.2660	0.82
JSWI-2	135	135	1.03	2769	20	2878	10	4.0	1.8629	0.8814	0.2069	0.6020	1.8640	0.8815	0.2065	0.6051	15.276	1.0692	0.5365	0.8815	0.82
culled																					
JSWI-33	901	47	0.05	1578	5	1753	7	11.1	3.6048	0.3516	0.1073	0.4076	3.6054	0.3516	0.1072	0.4084	4.100	0.5389	0.2774	0.3516	0.65
JSWI-39	478	119	0.26	2494	9	2806	22	12.5	2.1161	0.4366	0.1978	1.3106	2.1169	0.4374	0.1976	1.3168	12.867	1.3875	0.4724	0.4374	0.32
JSWI-27	861	650	0.78	1910	5	2562	6	34.2	2.8955	0.3280	0.1717	0.2955	2.8998	0.3295	0.1705	0.3421	8.106	0.4750	0.3448	0.3295	0.69
JSWI-9	536	411	0.79	1206	5	1697	24	40.7	4.8244	0.4554	0.1101	0.5780	4.8595	0.4692	0.1040	1.3053	2.952	1.3870	0.2058	0.4692	0.34
MLS1-39	550	39	0.07	1083	4	1059	15	-2.2	5.4662	0.4241	0.0748	0.6783	5.4674	0.4247	0.0746	0.7297	1.882	0.8443	0.1829	0.4247	0.50
MLS-1-17	251	64	0.26	1150	7	1092	21	-5.1	5.1175	0.6474	0.0765	1.0020	5.1211	0.6479	0.0759	1.0540	2.043	1.2372	0.1953	0.6479	0.52
MLS-1-23	100	44	0.46	1142	10	1108	37	-3.0	5.1559	0.9632	0.0771	1.4806	5.1592	0.9681	0.0765	1.8628	2.045	2.0993	0.1938	0.9681	0.46
MLS-1-20	423	124	0.30	1177	5	1162	15	-1.2	4.9952	0.4888	0.0784	0.7350	4.9938	0.4891	0.0786	0.7504	2.170	0.8957	0.2002	0.4891	0.55
MLS-1-24	704	150	0.22	1192	4	1191	23	-0.1	4.9127	0.3603	0.0819	0.9236	4.9249	0.3645	0.0797	1.1677	2.233	1.2233	0.2030	0.3645	0.30
MLS-1-16	654	308	0.49	1192	4	1238	12	3.8	4.9207	0.3853	0.0820	0.5649	4.9226	0.3855	0.0817	0.5880	2.288	0.7031	0.2031	0.3855	0.55
MLS-1-15	139	50	0.37	1337	10	1268	33	-5.2	4.3287	0.8378	0.0853	1.1528	4.3404	0.8451	0.0829	1.6844	2.634	1.8845	0.2304	0.8451	0.45
MLS-1-1	110	39	0.37	1299	11	1281	33	-1.3	4.4766	0.8991	0.0844	1.2625	4.4810	0.9052	0.0835	1.6786	2.570	1.9071	0.2232	0.9052	0.47
MLS1-36	56	22	0.41	1350	16	1282	57	-5.0	4.2808	1.2568	0.0857	1.7161	4.2916	1.2771	0.0836	2.9478	2.685	3.2125	0.2330	1.2771	0.40
MLS-1-21	135	51	0.39	1370	10	1370	21	0.0	4.2183	0.8262	0.0881	1.1004	4.2216	0.8262	0.0874	1.1136	2.855	1.3866	0.2369	0.8262	0.60
MLS1-40	171	46	0.28	1400	9	1375	21	-1.8	4.1205	0.7230	0.0882	0.9834	4.1232	0.7248	0.0876	1.1162	2.931	1.3309	0.2425	0.7248	0.54
MLS1-28	226	73	0.34	1373	8	1381	17	0.6	4.2137	0.6524	0.0879	0.8722	4.2137	0.6529	0.0879	0.9060	2.878	1.1167	0.2373	0.6529	0.58
MLS1-29	108	54	0.51	1368	13	1385	66	1.3	4.1977	0.9729	0.0949	1.5999	4.2309	1.0162	0.0881	3.4595	2.872	3.6056	0.2364	1.0162	0.28
MLS-1-27	263	107	0.42	1380	10	1395	213	1.1	3.9141	0.6238	0.1450	3.6623	4.1898	0.7702	0.0886	11.1141	2.915	11.1407	0.2387	0.7702	0.07
MLS-1-6	69	22	0.34	1355	15	1401	104	3.4	4.1852	1.1747	0.1066	1.4701	4.2735	1.2653	0.0889	5.4268	2.867	5.5724	0.2340	1.2653	0.23
MLS-1-22	483	154	0.33	1338	6	1407	95	5.1	4.1720	0.4338	0.1211	0.5144	4.3335	0.4923	0.0891	4.9411	2.836	4.9656	0.2308	0.4923	0.10
MLS1-38	102	33	0.33	1436	12	1416	24	-1.4	4.0076	0.9340	0.0895	1.2326	4.0072	0.9341	0.0896	1.2371	3.082	1.5502	0.2496	0.9341	0.60
MLS1-37	381	144	0.39	1521	7	1457	12	-4.2	3.7557	0.4925	0.0918	0.6302	3.7571	0.4925	0.0915	0.6386	3.357	0.8065	0.2662	0.4925	0.61
MLS-1-12	313	81	0.27	1470	7	1480	15	0.7	3.9066	0.5493	0.0923	0.7131	3.9051	0.5501	0.0926	0.7657	3.270	0.9429	0.2561	0.5501	0.58
MLS-1-7	136	53	0.40	1479	11	1485	20	0.4	3.8779	0.8401	0.0928	1.0678	3.8776	0.8402	0.0929	1.0712	3.303	1.3614	0.2579	0.8402	0.62
MLS-1-2	85	42	0.50	1543	27	1527	639	-1.1	2.8731	1.2993	0.2847	1.8595	3.6978	1.9912	0.0949	33.8968	3.539	33.9553	0.2704	1.9912	0.06
MLS1-33	625	44	0.07	1485	7	1539	259	3.6	3.4230	0.3728	0.1918	0.3438	3.8599	0.5229	0.0955	13.7756	3.413	13.7856	0.2591	0.5229	0.04
MLS-1-19	504	275	0.56	1531	8	1600	68	4.5	3.6297	0.5248	0.1216	1.3515	3.7308	0.5526	0.0987	3.6197	3.647	3.6617	0.2680	0.5526	0.15
MLS-1-5	621	287	0.48	1562	6	1600	12	2.4	3.6397	0.4033	0.1003	0.4723	3.6468	0.4062	0.0987	0.6631	3.732	0.7776	0.2742	0.4062	0.52
MLS1-35	110	76	0.72	1675	13	1607	20	-4.1	3.3686	0.8915	0.0997	1.0424	3.3711	0.8916	0.0991	1.0588	4.052	1.3842	0.2966	0.8916	0.64
MLS-1-14	67	59	0.91	1607	17	1631	50	1.5	3.5197	1.1604	0.1036	1.3770	3.5330	1.1904	0.1004	2.6816	3.916	2.9340	0.2830	1.1904	0.41
MLS1-32.2	188	156	0.86	1683	10	1645	15	-2.3	3.3525	0.6985	0.1010	0.8164	3.3520	0.6986	0.1011	0.8233	4.159	1.0798	0.2983	0.6986	0.65

MLS1-32.1	80	43	0.55	1694	16	1663	24	-1.9	3.3263	1.0623	0.1023	1.2442	3.3271	1.0628	0.1021	1.2801	4.231	1.6638	0.3006	1.0628	0.64
MLS-1-3	244	118	0.50	1558	9	1676	25	7.6	3.6376	0.6362	0.1074	0.7409	3.6574	0.6466	0.1029	1.3361	3.877	1.4844	0.2734	0.6466	0.44
ML5-1-4	179	79	0.45	1766	12	1747	16	-1.1	3.1723	0.7478	0.1071	0.8309	3.1730	0.7482	0.1069	0.8506	4.645	1.1328	0.3152	0.7482	0.66
MLS-1-26	126	71	0.58	1818	14	1860	19	2.3	3.0719	0.8581	0.1128	0.9285	3.0684	0.8605	0.1137	1.0386	5.111	1.3488	0.3259	0.8605	0.64
MLS1-30	460	162	0.36	1929	7	1902	8	-1.4	2.8664	0.4394	0.1165	0.4544	2.8667	0.4395	0.1164	0.4603	5.598	0.6364	0.3488	0.4395	0.69
MLS-1-18	12	9	0.82	2008	49	2088	98	4.0	2.7198	2.7114	0.1343	2.6311	2.7365	2.8156	0.1293	5.5488	6.513	6.2223	0.3654	2.8156	0.45
MLS-1-10	132	58	0.45	2461	16	2500	11	1.6	2.1497	0.8065	0.1649	0.6595	2.1516	0.8065	0.1642	0.6655	10.525	1.0456	0.4648	0.8065	0.77
MLS1-34	147	93	0.66	2701	16	2713	9	0.5	1.9220	0.7292	0.1865	0.5287	1.9217	0.7292	0.1867	0.5283	13.392	0.9005	0.5204	0.7292	0.81
culled																					
MLS-1-11	579	145	0.26	983	4	1085	19	10.4	6.0604	0.4310	0.0767	0.6941	6.0681	0.4344	0.0756	0.9527	1.718	1.0471	0.1648	0.4344	0.41
MLS-1-8	38	13	0.36	1133	18	1309	94	15.6	5.2391	1.7093	0.0792	3.2104	5.2059	1.7482	0.0847	4.8309	2.244	5.1375	0.1921	1.7482	0.34
MLS-1-13	732	326	0.46	1001	6	1242	266	24.1	5.5942	0.3768	0.1336	5.5121	5.9505	0.6533	0.0819	13.5567	1.897	13.5725	0.1681	0.6533	0.05
MLS1-31	2479	913	0.38	445	1	608	137	36.5	13.5128	0.2945	0.0900	0.4478	13.9838	0.3387	0.0601	6.3376	0.593	6.3467	0.0715	0.3387	0.05
TT3-21	169	191	1.17	1884	11	1881	16	-0.1	2.9438	0.6986	0.1159	0.7289	2.9467	0.7023	0.1151	0.9056	5.385	1.1460	0.3394	0.7023	0.61
TT3-41	68	49	0.74	1874	21	1900	22	1.4	2.9613	1.3077	0.1171	1.1211	2.9641	1.3096	0.1163	1.2407	5.408	1.8040	0.3374	1.3096	0.73
TT3-15	84	81	0.99	1902	16	1903	25	0.0	2.9060	0.9935	0.1186	1.0265	2.9133	1.0013	0.1165	1.3933	5.513	1.7158	0.3433	1.0013	0.58
TT3-27	137	86	0.65	1928	13	1903	17	-1.3	2.8721	0.7588	0.1154	0.8016	2.8683	0.7623	0.1165	0.9563	5.599	1.2230	0.3486	0.7623	0.62
TT3-6	211	293	1.43	2025	13	1914	13	-5.5	2.7094	0.7262	0.1172	0.7234	2.7094	0.7262	0.1172	0.7234	5.964	1.0250	0.3691	0.7262	0.71
TT3-33	249	329	1.36	1883	10	1921	12	2.0	2.9492	0.5886	0.1171	0.6206	2.9472	0.5901	0.1177	0.6855	5.505	0.9045	0.3393	0.5901	0.65
TT3-36	110	111	1.04	1892	14	1924	16	1.7	2.9313	0.8490	0.1181	0.8885	2.9321	0.8494	0.1179	0.9113	5.543	1.2458	0.3410	0.8494	0.68
TT3-25	51	27	0.56	1964	22	1930	36	-1.7	2.7963	1.2709	0.1218	1.2712	2.8082	1.2891	0.1183	2.0357	5.806	2.4096	0.3561	1.2891	0.53
TT3-7	149	134	0.93	2027	15	1932	17	-4.7	2.7032	0.8619	0.1192	0.8456	2.7058	0.8637	0.1184	0.9395	6.034	1.2761	0.3696	0.8637	0.68
TT3-20	135	228	1.74	1911	13	1938	21	1.4	2.8998	0.7909	0.1182	0.8322	2.8977	0.7995	0.1188	1.1604	5.652	1.4091	0.3451	0.7995	0.57
TT3-2	208	536	2.66	1877	11	1942	14	3.5	2.9547	0.6901	0.1202	0.7371	2.9589	0.6902	0.1190	0.7556	5.547	1.0233	0.3380	0.6902	0.67
TT3-16	88	54	0.63	1926	16	1947	25	1.1	2.8660	0.9718	0.1208	1.0093	2.8711	0.9815	0.1194	1.4057	5.733	1.7145	0.3483	0.9815	0.57
TT3-37	101	104	1.07	1945	15	1949	25	0.2	2.8426	0.8706	0.1183	0.9086	2.8387	0.8849	0.1195	1.4219	5.804	1.6748	0.3523	0.8849	0.53
TT3-24	191	92	0.50	1874	10	1950	12	4.1	2.9640	0.6308	0.1198	0.6650	2.9649	0.6313	0.1196	0.6896	5.562	0.9349	0.3373	0.6313	0.68
TT3-38	85	105	1.27	1965	16	1955	20	-0.5	2.8041	0.9673	0.1204	1.0262	2.8057	0.9692	0.1199	1.1141	5.894	1.4767	0.3564	0.9692	0.66
TT3-4	77	58	0.78	2053	21	1957	25	-4.7	2.6621	1.1665	0.1215	1.1546	2.6670	1.1712	0.1200	1.3843	6.206	1.8133	0.3750	1.1712	0.65
TT3-26	176	94	0.55	1938	12	1957	17	1.0	2.8488	0.6866	0.1209	0.7017	2.8518	0.6933	0.1200	0.9730	5.804	1.1947	0.3507	0.6933	0.58
TT3-9	247	243	1.02	1905	12	1959	15	2.8	2.9072	0.7158	0.1205	0.7819	2.9083	0.7169	0.1202	0.8321	5.697	1.0984	0.3438	0.7169	0.65
TT3-17	99	66	0.69	1954	15	1959	18	0.2	2.8237	0.9086	0.1202	0.9310	2.8239	0.9103	0.1202	1.0065	5.869	1.3571	0.3541	0.9103	0.67
TT3-12	286	41	0.15	1890	9	1960	11	3.7	2.9365	0.5289	0.1198	0.5623	2.9350	0.5296	0.1202	0.5924	5.648	0.7947	0.3407	0.5296	0.67
TT3-35	300	232	0.80	1930	9	1963	10	1.7	2.8635	0.5141	0.1209	0.5284	2.8648	0.5143	0.1205	0.5413	5.799	0.7466	0.3491	0.5143	0.69
TT3-34	122	146	1.24	1903	14	1966	16	3.3	2.9116	0.8390	0.1207	0.8774	2.9116	0.8397	0.1207	0.9078	5.714	1.2366	0.3434	0.8397	0.68
TT3-29	149	90	0.62	1925	12	1968	14	2.2	2.8744	0.7502	0.1205	0.7518	2.8735	0.7506	0.1208	0.7699	5.796	1.0752	0.3480	0.7506	0.70
TT3-31	204	157	0.80	1911	11	1988	12	4.0	2.8975	0.6567	0.1223	0.6684	2.8981	0.6571	0.1221	0.6894	5.811	0.9524	0.3451	0.6571	0.69
TT3-32	106	86	0.84	1980	16	2002	20	1.1	2.7855	0.9069	0.1217	0.9041	2.7806	0.9130	0.1231	1.1457	6.105	1.4650	0.3596	0.9130	0.62
TT3-13	319	117	0.38	1926	9	2011	11	4.4	2.8712	0.5150	0.1237	0.5175	2.8712	0.5177	0.1237	0.6232	5.942	0.8102	0.3483	0.5177	0.64
TT3-5	83	47	0.58	2152	21	2014	20	-6.4	2.5229	1.1474	0.1240	1.1001	2.5231	1.1485	0.1240	1.1489	6.775	1.6245	0.3963	1.1485	0.71
TT3-1	93	76	0.85	2122	19	2018	18	-4.9	2.5634	1.0680	0.1246	1.0195	2.5647	1.0683	0.1242	1.0390	6.678	1.4902	0.3899	1.0683	0.72
TT3-11	42	22	0.55	2015	25	2023	35	0.4	2.7160	1.4126	0.1272	1.3763	2.7247	1.4278	0.1246	1.9839	6.305	2.4443	0.3670	1.4278	0.58
TT3-19	64	27	0.44	2058	20	2032	21	-1.3	2.6603	1.1415	0.1248	1.1186	2.6589	1.1428	0.1252	1.1697	6.494	1.6353	0.3761	1.1428	0.70
TT3-14	199	102	0.53	2115	12	2128	14	0.6	2.5721	0.6377	0.1331	0.6054	2.5750	0.6428	0.1322	0.7915	7.079	1.0196	0.3883	0.6428	0.63
TT3-10	311	100	0.33	2478	11	2564	7	3.5	2.1322	0.5200	0.1710	0.4024	2.1332	0.5217	0.1707	0.4450	11.031	0.6857	0.4688	0.5217	0.76
TT3-28	31	17	0.56	2399	31	2575	26	7.3	2.2200	1.5416	0.1711	1.2281	2.2183	1.5554	0.1717	1.5389	10.674	2.1881	0.4508	1.5554	0.71
TT3-3	63	72	1.18	2823	29	2700	16	-4.3	1.8150	1.2717	0.1873	0.9344	1.8200	1.2717	0.1852	0.9590	14.035	1.5928	0.5495	1.2717	0.80
TT3-18	87	77	0.92	2715	21	2715	14	0.0	1.9143	0.9492	0.1850	0.7034	1.9095	0.9563	0.1869	0.8504	13.498	1.2797	0.5237	0.9563	0.75
TT3-40	273	135	0.51	2727	12	2717	6	-0.4	1.8981	0.5220	0.1875	0.3852	1.8989	0.5221	0.1872	0.3888	13.590	0.6510	0.5266	0.5221	0.80
TT3-30	105	129	1.27	2724	19	2726	10	0.1	1.9017	0.8460	0.1880	0.6106	1.9014	0.8468	0.1882	0.6279	13.645	1.0542	0.5259	0.8468	0.80

TT3-39	77	49	0.66	2663	22	2736	12	2.7	1.9565	0.9896	0.1887	0.7194	1.9550	0.9909	0.1893	0.7467	13.352	1.2408	0.5115	0.9909	0.80
TT3-23	179	251	1.45	2645	18	2739	17	3.5	1.9695	0.8278	0.1902	0.9870	1.9711	0.8298	0.1896	1.0190	13.262	1.3141	0.5073	0.8298	0.63
culled																					
TT3-22	385	366	0.98	1351	7	1978	37	46.4	4.2099	0.5212	0.1367	0.5684	4.2892	0.5517	0.1215	2.0825	3.905	2.1544	0.2331	0.5517	0.26

B2 LAICPMS Data

Sample name	207/ 235	1σ abs err	206/ 238	1σ abs err	RHO	207/ 206	1σ abs err	% discord.	207/ 235 date (Ma)	1σ abs err	206/ 238 date (Ma)	1σ abs err	207/ 206 date (Ma)	1σ abs err
AKX0415_029	2.42	0.09	0.219	0.005	1.03	0.0801	0.0011	-7.1	1250	27	1278	27	1200	28
AKX0415_037	5.01	0.25	0.328	0.013	0.98	0.1107	0.0014	-1.3	1822	41	1831	65	1811	23
AKX0415_034	5.61	0.28	0.356	0.015	0.98	0.1142	0.0015	-6.0	1917	42	1964	69	1867	23
AKX0415_024	5.58	0.22	0.353	0.009	1.02	0.1149	0.0016	-4.3	1914	33	1947	41	1878	25
AKX0415_022	5.71	0.22	0.353	0.008	1.03	0.1173	0.0016	-2.0	1933	33	1948	38	1916	25
AKX0415_028	5.72	0.22	0.353	0.008	1.03	0.1175	0.0017	-1.9	1935	33	1949	38	1919	25
AKX0415_036	5.91	0.30	0.361	0.015	0.98	0.1186	0.0015	-3.2	1963	44	1989	72	1936	23
AKX0415_018	5.41	0.32	0.331	0.016	0.98	0.1188	0.0018	5.8	1887	50	1841	76	1938	27
AKX0415_026	5.90	0.23	0.360	0.008	1.03	0.1188	0.0017	-2.6	1961	33	1983	39	1939	25
AKX0415_039	5.89	0.30	0.359	0.015	0.98	0.1190	0.0015	-2.2	1960	43	1977	70	1941	23
AKX0415_033	5.95	0.30	0.361	0.015	0.98	0.1196	0.0015	-2.0	1968	43	1985	70	1951	23
AKX0415_027	6.00	0.23	0.363	0.009	1.02	0.1197	0.0017	-2.7	1975	33	1998	41	1952	25
AKX0415_016	5.69	0.35	0.344	0.017	0.98	0.1198	0.0019	2.7	1930	51	1908	80	1954	28
AKX0415_020	6.21	0.38	0.375	0.018	0.98	0.1201	0.0019	-5.8	2006	51	2054	84	1957	28
AKX0415_019	6.05	0.36	0.362	0.017	0.98	0.1214	0.0019	-0.8	1984	51	1990	82	1977	27
AKX0415_015	5.93	0.37	0.354	0.017	0.98	0.1215	0.0020	1.4	1966	52	1954	83	1978	28
AKX0415_017	6.21	0.37	0.370	0.018	0.98	0.1218	0.0019	-2.6	2006	51	2027	82	1983	27
AKX0415_040	6.38	0.32	0.366	0.015	0.98	0.1262	0.0016	1.9	2029	43	2013	71	2045	22
AKX0415_021	10.14	0.38	0.464	0.009	1.05	0.1586	0.0023	-0.7	2448	34	2456	41	2441	24
AKX0415_037b	12.55	0.63	0.498	0.021	0.98	0.1828	0.0023	3.3	2647	46	2606	88	2678	21

AKX0415_031	13.78	0.70	0.537	0.022	0.98	0.1862	0.0024	-2.7	2735	47	2770	93	2709	21
AKX0415_032	16.04	0.82	0.570	0.024	0.98	0.2042	0.0026	-2.0	2879	48	2906	98	2860	21
SHRIMPed														
AKX0415_001	5.72	0.31	0.313	0.014	0.99	0.1324	0.0017	20.0	1935	45	1757	67	2130	23
AKX0415_002	7.03	0.37	0.383	0.016	0.98	0.1331	0.0018	2.6	2116	46	2091	76	2139	23
AKX0415_003	4.72	0.27	0.322	0.015	0.98	0.1064	0.0015	-3.9	1770	46	1797	72	1738	26
AKX0415_004	5.91	0.37	0.344	0.018	0.98	0.1247	0.0019	6.9	1963	52	1904	85	2025	26
AKX0415_005	6.07	0.34	0.353	0.016	0.98	0.1245	0.0017	4.1	1986	48	1950	76	2022	24
AKX0415_006	8.48	0.48	0.399	0.019	0.98	0.1540	0.0020	11.1	2283	50	2165	85	2391	22
AKX0415_007	5.19	0.28	0.324	0.014	0.98	0.1162	0.0015	5.5	1850	45	1808	70	1898	23
AKX0415_010	5.86	0.33	0.351	0.016	0.98	0.1212	0.0017	2.1	1955	48	1938	78	1974	24
AKX0415_011	5.65	0.36	0.347	0.018	0.98	0.1182	0.0018	0.5	1924	54	1919	86	1928	28
AKX0415_012	5.93	0.39	0.351	0.019	0.98	0.1227	0.0019	3.3	1966	56	1938	91	1995	28
AKX0415_013	5.85	0.36	0.353	0.017	0.98	0.1203	0.0019	0.7	1955	52	1949	82	1960	28
AKX0415_014	4.38	0.29	0.264	0.015	0.98	0.1202	0.0019	25.7	1708	54	1510	76	1959	27
culled														
AKX0415_008	no data	no data	no data	no data	no data	-0.0380	-0.1092		no data	no data	no data	no data	0	786
AKX0415_009	no data	no data	no data	no data	no data	-2.3250	-1.3171		no data	no data	no data	no data	99	no data
AKX0415_038	6.74	0.35	0.421	0.018	0.98	0.1159	0.0015	-23.3	2077	45	2267	81	1894	23
AKX0415_025	6.30	0.27	0.387	0.011	1.00	0.1180	0.0017	-11.2	2018	37	2110	51	1926	25
AKX0415_035	4.71	0.26	0.288	0.013	0.98	0.1189	0.0015	18.1	1770	45	1629	67	1939	22
AKX0415_023	4.66	0.21	0.280	0.009	0.99	0.1206	0.0017	21.4	1760	36	1592	44	1965	25
AKX0415_030	2.21	0.15	0.118	0.007	0.99	0.1365	0.0019	70.8	1185	47	717	41	2183	24

AKX0416_008	0.80	0.02	0.097	0.003	0.97	0.0596	0.0004	-2.0	596	13	599	15	587	16
AKX0416_034	0.91	0.03	0.108	0.003	0.94	0.0613	0.0008	-1.7	658	15	660	16	649	26
AKX0416_011	0.82	0.03	0.097	0.003	0.95	0.0613	0.0007	8.6	609	15	597	15	651	23
AKX0416_015	1.02	0.03	0.114	0.003	0.96	0.0646	0.0005	8.9	712	14	697	15	761	16
AKX0416_027	5.63	0.14	0.342	0.007	0.97	0.1193	0.0009	2.9	1921	22	1898	35	1946	13
AKX0416_012	5.71	0.19	0.340	0.010	0.98	0.1217	0.0009	5.4	1933	28	1888	49	1981	13
AKX0416_001	6.36	0.36	0.379	0.020	0.99	0.1218	0.0010	-5.2	2027	48	2070	95	1983	15
AKX0416_006	6.05	0.24	0.358	0.013	0.98	0.1225	0.0010	1.1	1983	35	1973	64	1993	14

AKX0416_028	5.79	0.15	0.340	0.008	0.97	0.1234	0.0009	6.8	1945	22	1889	36	2006	12
AKX0416_009	5.87	0.30	0.343	0.017	0.99	0.1240	0.0010	6.4	1956	43	1902	79	2014	14
AKX0416_014	6.22	0.18	0.359	0.009	0.97	0.1258	0.0010	3.7	2007	25	1975	42	2040	14
AKX0416_019	6.17	0.22	0.355	0.011	0.98	0.1260	0.0009	4.7	2000	30	1959	54	2042	13
AKX0416_003	6.58	0.36	0.378	0.020	0.99	0.1264	0.0010	-1.0	2057	47	2065	91	2048	14
AKX0416_025	6.22	0.18	0.355	0.009	0.97	0.1270	0.0010	5.5	2008	25	1960	43	2058	14
AKX0416_004	6.72	0.35	0.382	0.019	0.99	0.1275	0.0010	-1.3	2075	46	2086	89	2063	14
AKX0416_029	6.30	0.17	0.358	0.008	0.96	0.1275	0.0010	5.0	2018	23	1975	38	2063	14
AKX0416_021	6.35	0.18	0.360	0.009	0.97	0.1277	0.0010	4.6	2025	25	1984	42	2067	14
AKX0416_040	6.44	0.16	0.366	0.008	0.97	0.1279	0.0008	3.4	2038	22	2008	38	2069	11
AKX0416_002	6.69	0.33	0.377	0.018	0.99	0.1285	0.0011	0.8	2071	43	2064	82	2078	15
AKX0416_033	6.39	0.19	0.355	0.009	0.96	0.1305	0.0012	8.1	2031	26	1959	42	2105	16
AKX0416_024	11.19	0.32	0.473	0.012	0.97	0.1717	0.0013	3.7	2539	26	2495	51	2575	12
culled														
AKX0416_032	5.43	0.14	0.321	0.007	0.97	0.1226	0.0008	11.3	1890	22	1797	36	1995	12
AKX0416_038	5.46	0.13	0.321	0.007	0.97	0.1233	0.0008	11.9	1894	21	1795	33	2004	12
AKX0416_020	9.41	0.31	0.416	0.012	0.97	0.1640	0.0014	12.1	2378	29	2242	54	2498	14
AKX0416_018	6.37	0.20	0.346	0.009	0.97	0.1333	0.0011	12.1	2028	27	1917	45	2142	15
AKX0416_026	0.89	0.03	0.102	0.002	0.96	0.0631	0.0006	12.6	644	13	625	14	711	19
AKX0416_036	5.73	0.15	0.325	0.007	0.97	0.1281	0.0009	14.4	1937	22	1812	36	2072	12
AKX0416_035	7.20	0.19	0.359	0.008	0.96	0.1455	0.0012	16.0	2137	23	1978	36	2293	14
AKX0416_017	5.15	0.21	0.305	0.012	0.98	0.1226	0.0009	16.0	1845	34	1715	57	1995	13
AKX0416_007	5.07	0.21	0.301	0.012	0.98	0.1220	0.0010	16.5	1831	34	1697	57	1986	15
AKX0416_022	5.01	0.17	0.295	0.009	0.97	0.1229	0.0010	18.7	1821	28	1669	44	1999	15
AKX0416_023	1.00	0.03	0.109	0.003	0.93	0.0664	0.0009	19.2	704	16	669	15	819	27
AKX0416_039	5.05	0.14	0.293	0.007	0.97	0.1250	0.0009	20.7	1828	23	1657	35	2028	12
AKX0416_037	5.27	0.18	0.294	0.009	0.98	0.1301	0.0009	23.7	1864	29	1661	47	2099	13
AKX0416_030	0.98	0.03	0.105	0.003	0.92	0.0673	0.0009	24.8	692	17	646	15	846	29
AKX0416_013	11.46	0.31	0.412	0.009	0.97	0.2019	0.0015	25.7	2561	25	2222	43	2842	12
AKX0416_010	4.70	0.20	0.268	0.011	0.98	0.1272	0.0010	28.8	1767	36	1531	55	2060	14
AKX0416_005	3.73	0.15	0.225	0.008	0.98	0.1203	0.0009	36.7	1578	31	1309	43	1960	14
AKX0416_031	2.54	0.11	0.132	0.006	0.99	0.1397	0.0009	68.0	1284	32	799	32	2224	11
AKX0416_016	3.03	0.10	0.109	0.003	0.96	0.2017	0.0020	80.3	1415	25	666	18	2840	16

AKX0418_002	6.10	0.29	0.367	0.015	0.97	0.1206	0.0016	-2.9	1991	41	2015	68	1966	23
AKX0418_016	5.97	0.27	0.358	0.013	0.97	0.1209	0.0015	-0.1	1971	39	1972	63	1970	22
AKX0418_027	5.68	0.22	0.340	0.012	0.98	0.1210	0.0010	4.9	1928	33	1888	59	1971	14
AKX0418_009	6.20	0.29	0.371	0.015	0.97	0.1211	0.0016	-3.7	2004	40	2035	68	1972	23
AKX0418_030	6.48	0.17	0.388	0.009	0.97	0.1211	0.0009	-8.4	2043	23	2114	41	1973	13
AKX0418_006	6.13	0.28	0.366	0.014	0.97	0.1216	0.0015	-1.6	1995	39	2008	65	1980	22
AKX0418_003	6.03	0.28	0.359	0.014	0.97	0.1217	0.0015	0.1	1980	40	1979	67	1981	22
AKX0418_8_031	5.61	0.31	0.332	0.017	0.98	0.1224	0.0014	8.2	1917	47	1850	82	1991	20
AKX0418_018	5.95	0.30	0.353	0.015	0.97	0.1224	0.0016	2.6	1969	43	1947	72	1992	22
AKX0418_012	5.71	0.26	0.338	0.013	0.97	0.1224	0.0015	6.6	1933	39	1878	62	1992	22
AKX0418_024	6.50	0.18	0.384	0.009	0.97	0.1226	0.0009	-6.0	2046	25	2097	44	1995	13
AKX0418_026	6.59	0.20	0.389	0.010	0.97	0.1229	0.0009	-6.9	2058	26	2117	47	1999	14
AKX0418_010	5.67	0.27	0.331	0.013	0.97	0.1241	0.0015	9.9	1926	40	1843	63	2017	22
AKX0418_025	6.43	0.18	0.373	0.009	0.97	0.1249	0.0009	-1.0	2037	24	2046	42	2028	13
AKX0418_020	6.51	0.29	0.377	0.014	0.97	0.1254	0.0016	-1.4	2048	39	2060	65	2035	22
AKX0418_023b	5.84	0.19	0.337	0.010	0.97	0.1255	0.0010	9.1	1953	27	1875	46	2036	14
AKX0418_021	6.74	0.20	0.387	0.010	0.97	0.1262	0.0010	-3.7	2077	26	2110	47	2045	14
AKX0418_029	6.65	0.19	0.381	0.009	0.97	0.1264	0.0009	-1.9	2065	24	2082	43	2049	13
AKX0418_015	7.08	0.33	0.406	0.016	0.97	0.1265	0.0016	-8.5	2121	40	2196	71	2050	22
AKX0418_011	6.79	0.30	0.389	0.014	0.97	0.1267	0.0015	-3.8	2085	38	2118	65	2052	21
AKX0418_014	6.64	0.30	0.380	0.014	0.97	0.1268	0.0016	-1.3	2065	40	2076	67	2054	22
AKX0418_005	6.48	0.31	0.370	0.015	0.97	0.1271	0.0016	1.6	2043	41	2029	68	2058	22
AKX0418_022	6.90	0.20	0.394	0.010	0.97	0.1271	0.0010	-4.7	2099	26	2140	47	2059	13
AKX0418_019	6.89	0.30	0.393	0.014	0.97	0.1271	0.0016	-4.4	2097	38	2137	65	2059	22
AKX0418_013	7.08	0.33	0.403	0.016	0.97	0.1275	0.0016	-6.7	2122	41	2182	72	2064	22
AKX0418_8_032	6.17	0.34	0.350	0.018	0.98	0.1277	0.0014	7.3	2000	47	1935	85	2066	19
AKX0418_8_037	6.14	0.34	0.348	0.018	0.98	0.1281	0.0015	8.3	1996	48	1923	85	2072	20
AKX0418_001	6.80	0.31	0.383	0.014	0.97	0.1289	0.0016	-0.3	2086	39	2088	66	2083	22
AKX0418_028	7.01	0.19	0.394	0.009	0.97	0.1290	0.0009	-3.1	2112	24	2140	43	2085	12

culled

AKX0418_8_034	10.81	0.71	0.445	0.027	0.98	0.1760	0.0026	11.0	2507	59	2374	118	2616	24
AKX0418_8_033	5.61	0.31	0.327	0.017	0.98	0.1243	0.0014	11.0	1918	47	1825	80	2019	19
AKX0418_8_036	5.00	0.28	0.309	0.016	0.98	0.1176	0.0012	11.1	1820	46	1733	77	1920	19
AKX0418_8_040	5.31	0.30	0.318	0.016	0.98	0.1212	0.0014	11.3	1871	47	1779	79	1975	20
AKX0418_8_039	5.99	0.34	0.338	0.017	0.98	0.1287	0.0015	11.4	1975	48	1875	84	2081	21
AKX0418_008	5.53	0.25	0.312	0.012	0.97	0.1286	0.0016	18.0	1905	38	1750	57	2078	21
AKX0418_017	16.91	0.98	0.507	0.026	0.97	0.2419	0.0034	19.0	2929	54	2643	109	3132	22
AKX0418_004	23.02	2.31	0.551	0.052	0.98	0.3030	0.0056	23.2	3228	93	2829	213	3485	29
AKX0418_023	4.42	0.15	0.262	0.008	0.97	0.1224	0.0011	27.6	1717	28	1500	41	1992	16
AKX0418_8_038	3.78	0.21	0.229	0.012	0.98	0.1196	0.0014	35.0	1589	44	1331	62	1950	21
AKX0418_8_035	1.28	0.09	0.077	0.005	0.99	0.1194	0.0013	78.0	835	38	481	29	1948	19
AKX0418_007	7.58	0.34	0.432	0.016	0.97	0.1272	0.0015	-14.9	2183	40	2316	73	2059	21
AKX0419_001	5.88	0.18	0.352	0.010	0.97	0.1213	0.0009	1.9	1959	27	1943	48	1975	13
AKX0419_027	5.66	0.14	0.337	0.008	0.97	0.1217	0.0007	6.4	1925	21	1872	36	1982	10
AKX0419_031	6.04	0.16	0.360	0.009	0.98	0.1218	0.0006	0.1	1982	23	1982	43	1983	8
AKX0419_036	5.88	0.16	0.350	0.009	0.98	0.1219	0.0007	3.0	1958	23	1933	42	1984	10
AKX0419_016	5.97	0.15	0.355	0.008	0.97	0.1221	0.0008	1.8	1972	22	1957	39	1988	11
AKX0419_028	5.67	0.17	0.336	0.009	0.98	0.1222	0.0007	6.9	1927	25	1870	45	1989	11
AKX0419_039	5.92	0.16	0.351	0.009	0.98	0.1223	0.0006	2.9	1964	23	1939	43	1990	8
AKX0419_038	5.90	0.19	0.350	0.010	0.97	0.1224	0.0010	3.4	1961	27	1933	49	1991	14
AKX0419_015	5.92	0.16	0.351	0.008	0.97	0.1224	0.0009	3.1	1964	23	1939	40	1991	12
AKX0419_024	5.61	0.14	0.332	0.007	0.96	0.1225	0.0009	8.4	1917	21	1848	35	1993	13
AKX0419_019	5.98	0.13	0.352	0.007	0.97	0.1230	0.0007	3.2	1973	19	1946	33	2001	10
AKX0419_040	6.03	0.16	0.355	0.009	0.97	0.1231	0.0008	2.4	1980	23	1959	42	2001	11
AKX0419_012	5.98	0.20	0.352	0.010	0.96	0.1233	0.0011	3.6	1972	28	1942	50	2004	16
AKX0419_013	6.25	0.14	0.361	0.007	0.96	0.1256	0.0008	3.0	2011	20	1986	35	2038	12
AKX0419_005	6.25	0.20	0.360	0.011	0.98	0.1260	0.0008	3.4	2012	27	1982	50	2043	11
AKX0419_035	6.29	0.17	0.358	0.009	0.98	0.1273	0.0007	4.8	2017	23	1975	43	2061	9
AKX0419_029	6.49	0.14	0.369	0.007	0.97	0.1274	0.0007	2.0	2044	19	2026	34	2062	9
AKX0419_008	6.56	0.21	0.373	0.011	0.98	0.1275	0.0009	1.1	2054	28	2044	52	2064	13
AKX0419_033	6.63	0.17	0.377	0.009	0.98	0.1275	0.0007	0.1	2063	22	2062	42	2064	10

AKX0419_010	6.46	0.22	0.367	0.012	0.98	0.1277	0.0009	2.9	2040	30	2015	56	2067	12
AKX0419_006	6.62	0.21	0.376	0.011	0.97	0.1278	0.0010	0.6	2062	28	2057	51	2068	14
AKX0419_023	6.90	0.16	0.391	0.008	0.96	0.1279	0.0008	-3.4	2098	20	2129	36	2069	11
AKX0419_037	6.65	0.17	0.377	0.009	0.98	0.1280	0.0007	0.5	2066	23	2062	44	2071	9
AKX0419_011	6.83	0.14	0.387	0.007	0.97	0.1281	0.0007	-2.0	2090	18	2108	34	2072	10
AKX0419_004	6.25	0.20	0.352	0.010	0.98	0.1288	0.0008	7.6	2012	27	1945	49	2081	12
culled														
AKX0419_007	7.37	0.24	0.440	0.014	0.98	0.1215	0.0009	-22.5	2157	29	2350	60	1978	13
AKX0419_021	6.03	0.19	0.338	0.010	0.98	0.1295	0.0008	11.8	1980	27	1877	48	2091	11
AKX0419_032	5.15	0.13	0.308	0.008	0.98	0.1211	0.0006	13.9	1845	22	1733	37	1973	8
AKX0419_018	6.27	0.20	0.338	0.010	0.98	0.1344	0.0008	14.8	2014	27	1879	49	2156	10
AKX0419_002	5.64	0.19	0.320	0.010	0.98	0.1279	0.0009	15.5	1923	29	1790	49	2070	13
AKX0419_022	5.14	0.13	0.296	0.007	0.97	0.1260	0.0007	20.7	1842	21	1670	34	2043	10
AKX0419_034	4.54	0.14	0.267	0.008	0.99	0.1237	0.0006	27.1	1739	25	1523	39	2010	9
AKX0419_020	4.70	0.12	0.263	0.006	0.98	0.1294	0.0007	31.3	1767	21	1506	31	2090	9
AKX0419_025	3.85	0.09	0.232	0.005	0.97	0.1203	0.0007	34.6	1604	19	1347	27	1960	10
AKX0419_017	4.22	0.13	0.239	0.007	0.98	0.1282	0.0009	37.1	1678	24	1380	35	2073	12
AKX0419_030	3.22	0.07	0.187	0.004	0.97	0.1248	0.0007	49.4	1462	18	1105	21	2026	10
AKX0419_026	1.90	0.07	0.115	0.004	0.99	0.1194	0.0007	67.3	1080	26	703	25	1947	11
AKX0419_009	1.56	0.15	0.093	0.009	1.00	0.1217	0.0008	74.1	955	60	574	54	1981	11
AKX0419_014	0.49	0.05	0.032	0.004	1.00	0.1109	0.0007	90.2	403	37	202	22	1815	12
AKX0419_003	no data	no data	no data	no data	no data	-0.4019	-0.1157	no data	no data	no data	no data	no data	-1979	no data
AKX0421_041	4.36	0.19	0.305	0.011	0.97	0.1038	0.0013	-1.4	1705	35	1714	53	1694	23
AKX0421_059	4.51	0.24	0.314	0.014	0.97	0.1040	0.0015	-4.3	1732	44	1761	70	1697	26
AKX0421_060	4.51	0.23	0.314	0.014	0.97	0.1041	0.0014	-4.3	1733	41	1762	66	1699	24
AKX0421_008	5.64	0.29	0.353	0.017	0.99	0.1160	0.0009	-3.1	1923	43	1947	81	1896	13
AKX0421_070	5.09	0.54	0.313	0.032	0.99	0.1178	0.0020	9.9	1834	86	1757	154	1923	30
AKX0421_066	5.88	0.49	0.356	0.028	0.99	0.1197	0.0016	-0.7	1958	70	1963	134	1952	24
AKX0421_065	5.61	0.29	0.340	0.015	0.98	0.1198	0.0015	4.1	1918	43	1885	72	1954	22
AKX0421_053	5.85	0.26	0.353	0.013	0.97	0.1202	0.0015	0.6	1954	38	1949	61	1960	22

AKX0421_017	5.79	0.26	0.348	0.015	0.99	0.1205	0.0009	2.2	1945	39	1927	70	1964	13
AKX0421_047	5.60	0.32	0.333	0.017	0.98	0.1219	0.0015	7.5	1916	48	1853	81	1984	22
AKX0421_073	6.46	0.42	0.381	0.023	0.98	0.1229	0.0014	-4.8	2041	56	2082	107	1999	21
AKX0421_042	6.62	0.30	0.389	0.015	0.97	0.1234	0.0015	-6.4	2062	40	2117	68	2007	21
AKX0421_050	6.33	0.29	0.371	0.015	0.97	0.1237	0.0015	-1.6	2023	40	2036	68	2010	21
AKX0421_033	6.36	0.28	0.373	0.013	0.97	0.1239	0.0015	-1.7	2027	37	2041	62	2013	21
AKX0421_069	6.65	0.51	0.387	0.028	0.99	0.1246	0.0015	-5.0	2066	65	2109	130	2023	21
AKX0421_013	6.65	0.30	0.384	0.016	0.99	0.1254	0.0009	-3.5	2066	39	2096	75	2035	12
AKX0421_064	6.58	0.29	0.380	0.014	0.97	0.1255	0.0015	-2.4	2056	38	2077	64	2036	21
AKX0421_024	6.24	0.27	0.359	0.014	0.98	0.1259	0.0011	3.5	2010	38	1979	67	2041	16
AKX0421_022	5.93	0.27	0.340	0.014	0.98	0.1264	0.0012	9.0	1965	39	1888	68	2048	17
AKX0421_049	6.46	0.29	0.370	0.014	0.97	0.1264	0.0015	1.0	2040	38	2031	64	2048	21
AKX0421_018	6.58	0.31	0.377	0.017	0.99	0.1265	0.0009	-0.8	2056	40	2063	77	2050	12
AKX0421_063	6.72	0.30	0.384	0.014	0.97	0.1269	0.0015	-2.3	2075	38	2095	65	2055	21
AKX0421_027	6.70	0.27	0.382	0.013	0.98	0.1271	0.0012	-1.6	2073	35	2088	62	2059	17
AKX0421_039	7.05	0.30	0.402	0.014	0.98	0.1272	0.0014	-6.8	2118	37	2179	66	2060	19
AKX0421_032	6.46	0.27	0.368	0.013	0.98	0.1273	0.0014	2.3	2041	37	2021	61	2061	19
AKX0421_068	7.09	0.49	0.403	0.026	0.99	0.1275	0.0015	-6.9	2123	60	2185	120	2063	21
AKX0421_054	6.33	0.35	0.360	0.017	0.98	0.1277	0.0016	4.8	2023	47	1981	82	2066	23
AKX0421_057	7.05	0.36	0.400	0.018	0.98	0.1278	0.0016	-5.8	2118	45	2170	82	2068	22
AKX0421_071	6.77	0.44	0.384	0.023	0.98	0.1278	0.0015	-1.5	2081	56	2094	108	2068	21
AKX0421_072	6.98	0.49	0.396	0.026	0.98	0.1278	0.0016	-4.7	2109	60	2151	119	2069	22
AKX0421_048	6.75	0.32	0.375	0.015	0.97	0.1306	0.0016	3.1	2079	41	2051	69	2107	22
AKX0421_004	7.47	0.43	0.410	0.022	0.98	0.1321	0.0017	-5.1	2170	51	2217	98	2126	22
AKX0421_067	8.65	0.56	0.424	0.026	0.99	0.1479	0.0017	2.1	2302	57	2280	115	2321	19
AKX0421_038	9.64	0.42	0.469	0.017	0.97	0.1491	0.0018	-7.4	2401	39	2479	74	2336	21
AKX0421_009	9.94	0.51	0.456	0.022	0.99	0.1579	0.0011	0.5	2429	46	2424	98	2433	12
AKX0421_001	12.91	0.73	0.500	0.027	0.99	0.1872	0.0013	4.7	2673	52	2614	115	2718	12
AKX0421_040	16.22	0.74	0.589	0.023	0.98	0.1998	0.0023	-7.1	2890	43	2984	92	2824	18
AKX0421_002	14.69	0.84	0.528	0.029	0.99	0.2017	0.0015	4.6	2796	53	2734	121	2840	12
AKX0421_061	15.59	0.68	0.558	0.020	0.97	0.2025	0.0024	-0.6	2852	41	2859	81	2846	19
culled														
AKX0421_062	5.58	0.25	0.328	0.012	0.97	0.1233	0.0015	10.0	1913	38	1830	58	2005	21

AKX0421_012b	5.39	0.27	0.322	0.015	0.99	0.1213	0.0009	10.1	1883	42	1801	73	1975	13
AKX0421_003	5.36	0.33	0.321	0.019	0.99	0.1210	0.0010	10.1	1878	51	1796	91	1970	14
AKX0421_052	5.32	0.29	0.319	0.015	0.98	0.1208	0.0015	10.5	1872	46	1787	75	1968	22
AKX0421_030	6.47	0.27	0.347	0.012	0.97	0.1354	0.0016	13.4	2042	36	1918	58	2169	20
AKX0421_029	5.48	0.21	0.318	0.011	0.98	0.1252	0.0010	14.3	1898	32	1778	52	2032	14
AKX0421_026	3.97	0.22	0.268	0.014	0.98	0.1076	0.0012	14.7	1628	44	1528	69	1759	20
AKX0421_011	5.18	0.27	0.308	0.015	0.99	0.1221	0.0009	14.7	1850	43	1730	74	1987	13
AKX0421_012	5.05	0.23	0.303	0.013	0.99	0.1209	0.0008	15.3	1828	38	1706	65	1970	12
AKX0421_044	5.07	0.27	0.302	0.014	0.98	0.1220	0.0015	16.4	1832	44	1699	69	1986	22
AKX0421_006	5.08	0.28	0.301	0.016	0.99	0.1224	0.0009	16.9	1832	46	1696	78	1991	13
AKX0421_051	18.23	1.16	0.520	0.030	0.98	0.2545	0.0037	19.6	3002	60	2697	125	3213	23
AKX0421_028	4.55	0.20	0.279	0.011	0.98	0.1182	0.0010	20.0	1740	37	1588	57	1929	15
AKX0421_021	4.35	0.30	0.261	0.017	0.99	0.1210	0.0013	27.1	1703	56	1494	88	1971	19
AKX0421_016	2.95	0.19	0.207	0.012	0.99	0.1033	0.0010	30.8	1394	47	1211	66	1685	18
AKX0421_014	3.96	0.21	0.231	0.012	0.99	0.1240	0.0009	36.9	1625	43	1342	62	2015	14
AKX0421_037	3.64	0.24	0.215	0.013	0.99	0.1226	0.0014	40.6	1558	50	1257	69	1994	20
AKX0421_015	6.58	1.74	0.277	0.073	1.00	0.1724	0.0014	43.8	2056	210	1574	357	2582	14
AKX0421_007	33.30	3.16	0.500	0.046	0.99	0.4827	0.0057	45.3	3589	89	2615	194	4189	17
AKX0421_019	44.83	3.16	0.508	0.034	0.99	0.6404	0.0078	51.3	3884	68	2647	142	4602	17
AKX0421_036	13.29	0.68	0.279	0.013	0.98	0.3454	0.0040	63.9	2700	48	1586	64	3687	18
AKX0421_031	2.09	0.45	0.122	0.026	1.00	0.1243	0.0015	66.9	1144	139	740	149	2018	22
AKX0421_043	23.77	1.89	0.034	0.002	0.97	5.0729	0.1073	98.4	3259	75	215	15	7439	28
AKX0421_025	-2.62	-3.07	-0.106	-0.123	1.00	0.1801	0.0023	120.8	no data	no data	-720	-952	2654	21
AKX0421_055	no data	no data	no data	no data	no data	0.5598	0.0229	no data	no data	no data	no data	no data	4407	58
AKX0421_046	no data	no data	no data	no data	no data	2.1238	0.7639	no data	no data	no data	no data	no data	6276	414
AKX0421_045	no data	no data	no data	no data	no data	0.5579	0.0140	no data	no data	no data	no data	no data	4402	36
AKX0421_035	no data	no data	no data	no data	no data	-0.1873	-0.0778	no data	no data	no data	no data	no data	99	617
AKX0421_010	no data	no data	no data	no data	no data	0.1484	0.0027	no data	no data	no data	no data	no data	2327	31
AKX0421_007b	no data	no data	no data	no data	no data	0.5141	0.0066	no data	no data	no data	no data	no data	4282	19
AKX0421_034	4.10	0.60	0.314	0.045	1.00	0.0946	0.0012	-18.2	1654	113	1762	218	1520	23
AKX0421_074	7.09	0.48	0.422	0.026	0.98	0.1218	0.0018	-17.2	2123	59	2270	119	1983	25
AKX0421_020	3.39	0.18	0.277	0.013	0.98	0.0885	0.0010	-14.9	1502	40	1579	66	1394	21
AKX0421_075	6.57	0.42	0.399	0.024	0.98	0.1195	0.0016	-13.0	2056	55	2164	109	1948	23
AKX0421_023	6.55	0.26	0.398	0.014	0.98	0.1195	0.0010	-12.6	2053	34	2158	63	1949	15

AKX0421_058	6.33	0.54	0.387	0.030	0.98	0.1186	0.0021	-10.6	2023	72	2110	139	1936	32
AKX0421_046b	7.48	0.32	0.421	0.015	0.97	0.1288	0.0016	-10.4	2170	38	2265	67	2082	21
AKX0421_005	6.32	0.43	0.386	0.025	0.99	0.1186	0.0014	-10.3	2021	58	2106	114	1936	21
AKX0421_056	15.73	0.94	0.591	0.031	0.98	0.1932	0.0026	-10.0	2861	55	2992	126	2770	22
AKX0423_025	2.29	0.09	0.211	0.008	0.98	0.0785	0.0006	-7.3	1208	27	1236	40	1159	16
AKX0423_011	2.26	0.12	0.206	0.010	0.98	0.0794	0.0010	-2.5	1200	37	1210	52	1183	25
AKX0423_044	2.20	0.07	0.200	0.005	0.97	0.0798	0.0008	1.3	1182	22	1177	27	1191	19
AKX0423_023	2.28	0.09	0.205	0.008	0.98	0.0806	0.0006	0.8	1207	29	1204	42	1212	15
AKX0423_033	2.15	0.04	0.192	0.003	0.96	0.0812	0.0005	8.3	1165	14	1133	18	1227	11
AKX0423_042	2.33	0.08	0.207	0.005	0.97	0.0817	0.0008	2.4	1222	23	1212	28	1239	20
AKX0423_035	2.55	0.07	0.212	0.005	0.98	0.0870	0.0004	9.6	1285	19	1241	28	1360	9
AKX0423_020	3.52	0.20	0.273	0.013	0.98	0.0932	0.0012	-5.0	1531	43	1558	68	1493	24
AKX0423_014	3.41	0.18	0.263	0.012	0.98	0.0939	0.0012	-0.1	1507	41	1507	63	1506	24
AKX0423_027	3.53	0.14	0.265	0.010	0.98	0.0966	0.0007	3.2	1534	31	1515	50	1560	14
AKX0423_016	4.15	0.22	0.302	0.014	0.98	0.0997	0.0012	-5.9	1665	43	1702	69	1618	23
AKX0423_036	4.83	0.11	0.328	0.007	0.98	0.1066	0.0005	-5.9	1789	19	1831	33	1741	9
AKX0423_026	4.96	0.19	0.331	0.012	0.99	0.1086	0.0008	-4.4	1812	32	1844	57	1776	13
AKX0423_019	5.48	0.32	0.356	0.018	0.97	0.1117	0.0016	-8.5	1897	49	1961	86	1827	26
AKX0423_045	5.63	0.19	0.362	0.010	0.97	0.1127	0.0011	-9.4	1921	29	1994	48	1844	17
AKX0423_049	5.09	0.20	0.321	0.011	0.97	0.1150	0.0011	5.1	1835	32	1796	53	1879	17
AKX0423_040	6.00	0.18	0.372	0.010	0.97	0.1171	0.0008	-7.7	1976	26	2038	48	1912	13
AKX0423_034	5.89	0.11	0.347	0.006	0.97	0.1232	0.0006	4.9	1960	17	1919	28	2004	9
AKX0423_024	5.96	0.25	0.347	0.013	0.98	0.1246	0.0010	5.9	1970	35	1920	63	2024	14
AKX0423_022	6.17	0.26	0.357	0.014	0.99	0.1253	0.0009	3.7	2000	36	1968	66	2033	13
AKX0423_041	6.46	0.23	0.368	0.011	0.97	0.1273	0.0012	2.2	2041	30	2022	51	2061	17
AKX0423_012	7.26	0.39	0.412	0.019	0.98	0.1279	0.0016	-8.8	2143	46	2222	87	2069	22
AKX0423_038	6.65	0.17	0.377	0.009	0.98	0.1280	0.0006	0.4	2066	22	2062	42	2070	9
AKX0423_032	13.84	0.29	0.535	0.010	0.98	0.1874	0.0009	-2.0	2739	20	2764	43	2720	8
AKX0423_037	13.69	0.26	0.529	0.009	0.97	0.1877	0.0009	-0.6	2728	18	2736	38	2723	8
AKX0423_046	13.80	0.45	0.532	0.014	0.97	0.1882	0.0017	-1.0	2736	30	2749	59	2727	15

SHRMIPed

AKX0423_001	1.87	0.14	0.173	0.012	0.99	0.0782	0.0009	11.4	1070	47	1030	65	1152	23
AKX0423_001b	1.81	0.13	0.160	0.011	0.98	0.0821	0.0012	25.0	1050	48	958	61	1248	28
AKX0423_002	2.07	0.15	0.193	0.013	0.99	0.0780	0.0010	1.1	1139	49	1135	70	1147	25
AKX0423_003	6.29	0.45	0.363	0.025	0.99	0.1257	0.0015	2.5	2016	61	1995	115	2038	21
AKX0423_004	6.46	0.47	0.367	0.025	0.99	0.1275	0.0015	2.6	2040	62	2017	118	2063	21
AKX0423_005	3.26	0.24	0.255	0.018	0.99	0.0928	0.0012	1.5	1471	56	1463	90	1483	25
AKX0423_006	2.13	0.16	0.188	0.013	0.98	0.0818	0.0011	11.4	1157	49	1112	69	1242	26
AKX0423_007	3.94	0.29	0.279	0.019	0.99	0.1025	0.0013	5.7	1622	57	1585	95	1669	23
AKX0423_008	4.98	0.37	0.324	0.023	0.99	0.1115	0.0014	1.1	1815	61	1807	109	1825	22
AKX0423_009	3.16	0.23	0.247	0.017	0.99	0.0927	0.0011	4.3	1448	55	1425	87	1482	22
AKX0423_010	6.04	0.44	0.358	0.025	0.99	0.1223	0.0015	0.9	1982	62	1974	117	1990	21
culled														
AKX0423_039	2.02	0.04	0.183	0.004	0.97	0.0800	0.0004	10.4	1121	14	1083	20	1197	10
AKX0423_029	5.59	0.26	0.326	0.014	0.99	0.1243	0.0009	11.2	1915	39	1821	69	2018	12
AKX0423_050	2.29	0.07	0.197	0.005	0.97	0.0845	0.0008	12.3	1210	23	1158	27	1305	19
AKX0423_047	3.06	0.12	0.230	0.008	0.97	0.0964	0.0010	15.6	1422	31	1336	43	1555	20
AKX0423_043	2.23	0.11	0.190	0.008	0.97	0.0851	0.0012	16.2	1192	35	1123	46	1319	26
AKX0423_048	4.18	0.16	0.269	0.009	0.98	0.1127	0.0011	18.7	1671	32	1537	47	1843	17
AKW0423_031	2.47	0.17	0.197	0.012	0.98	0.0912	0.0014	22.1	1264	48	1157	64	1451	30
AKX0423_017	4.06	0.40	0.256	0.024	0.99	0.1151	0.0015	24.5	1647	77	1470	124	1882	24
AKX0423_018	1.73	0.12	0.156	0.010	0.98	0.0806	0.0012	24.6	1021	45	934	57	1212	28
AKX0423_015	2.46	0.22	0.159	0.013	0.99	0.1124	0.0015	51.9	1261	62	950	74	1839	24
AKX0423_030	4.40	0.58	0.173	0.021	0.98	0.1842	0.0054	66.6	1712	103	1030	116	2691	47
AKX0423_021	4.80	0.20	0.340	0.013	0.98	0.1024	0.0009	-15.2	1785	35	1887	63	1668	15
AKX0423_028	7.29	0.29	0.419	0.016	0.98	0.1263	0.0009	-12.0	2148	35	2255	71	2048	13
AKX0423_013	17.21	0.93	0.615	0.029	0.98	0.2029	0.0026	-10.7	2947	51	3091	116	2850	21

AKX0426_032	3.65	0.17	0.280	0.009	0.97	0.0947	0.0016	-5.2	1562	37	1591	47	1521	31
AKX0426_028	5.45	0.29	0.333	0.014	0.97	0.1186	0.0020	4.8	1893	45	1855	67	1936	30
AKX0426_027	6.30	0.30	0.369	0.013	0.97	0.1239	0.0020	-0.7	2019	41	2025	61	2013	29
AKX0426_029	6.60	0.45	0.380	0.022	0.97	0.1259	0.0023	-2.0	2059	58	2077	103	2042	31
AKX0426_024	6.11	0.34	0.351	0.016	0.97	0.1263	0.0020	6.0	1992	47	1940	75	2047	28

AKX0426_036	6.63	0.31	0.380	0.013	0.97	0.1265	0.0020	-1.6	2064	40	2078	60	2049	28
AKX0426_033	6.61	0.32	0.379	0.014	0.97	0.1266	0.0020	-1.1	2061	42	2071	64	2051	28
AKX0426_034	6.59	0.33	0.377	0.014	0.97	0.1269	0.0021	-0.3	2058	43	2060	67	2055	29
AKX0426_030	6.48	0.37	0.370	0.018	0.97	0.1269	0.0021	1.4	2043	50	2031	82	2056	29
AKX0426_012	7.15	0.39	0.407	0.017	0.97	0.1272	0.0021	-8.3	2130	47	2203	80	2059	29
AKX0426_037	6.17	0.31	0.351	0.014	0.97	0.1275	0.0021	7.1	2000	43	1938	65	2064	28
AKX0426_026	7.20	0.35	0.409	0.015	0.97	0.1276	0.0021	-8.4	2137	42	2212	66	2066	28
AKX0426_019	6.51	0.33	0.369	0.014	0.97	0.1280	0.0021	2.5	2048	44	2025	68	2070	29
AKX0426_025	6.69	0.40	0.377	0.019	0.97	0.1288	0.0023	1.1	2072	52	2061	87	2082	31
AKX0426_010	6.16	0.33	0.347	0.015	0.97	0.1290	0.0022	9.2	1999	46	1918	71	2084	29
AKX0426_041	6.92	0.32	0.389	0.013	0.97	0.1291	0.0021	-1.7	2102	40	2117	58	2086	28
AKX0426_039	6.75	0.31	0.379	0.012	0.97	0.1292	0.0021	1.0	2079	39	2070	56	2087	28
AKX0426_005	6.79	0.44	0.380	0.021	0.97	0.1295	0.0022	0.7	2085	56	2078	98	2091	29
AKX0426_040	6.88	0.33	0.385	0.013	0.97	0.1297	0.0022	-0.2	2096	41	2098	62	2094	29
AKX0426_043	6.62	0.32	0.370	0.013	0.97	0.1297	0.0022	3.6	2062	41	2029	59	2094	29
AKX0426_004	6.78	0.37	0.375	0.017	0.97	0.1312	0.0021	3.4	2084	48	2053	78	2114	28
AKX0426_017	7.15	0.47	0.384	0.022	0.97	0.1351	0.0022	3.8	2131	57	2095	102	2165	28
AKX0426_035	7.26	0.48	0.385	0.021	0.96	0.1366	0.0029	4.4	2144	57	2102	96	2185	36
AKX0426_031	15.37	0.89	0.545	0.026	0.97	0.2046	0.0034	2.6	2838	54	2803	108	2863	27
culled														
AKX0426_023	9.18	0.71	0.538	0.037	0.97	0.1238	0.0024	-46.9	2356	69	2775	153	2011	34
AKX0426_014	7.87	0.55	0.456	0.027	0.96	0.1252	0.0026	-23.2	2216	61	2422	119	2031	36
AKX0426_042	7.54	0.41	0.433	0.018	0.96	0.1263	0.0023	-15.8	2178	48	2318	82	2047	31
AKX0426_021	5.74	0.81	0.333	0.045	0.99	0.1252	0.0026	10.2	1937	115	1851	215	2032	36
AKX0426_020	5.86	0.76	0.333	0.041	0.98	0.1276	0.0029	11.9	1955	106	1852	195	2066	40
AKX0426_015	5.58	0.34	0.323	0.017	0.97	0.1253	0.0020	12.8	1914	51	1806	81	2032	28
AKX0426_044	5.99	0.27	0.334	0.011	0.97	0.1300	0.0020	13.0	1975	39	1860	52	2097	27
AKX0426_011	12.52	0.66	0.464	0.019	0.97	0.1956	0.0031	14.3	2644	48	2458	84	2790	26
AKX0426_013	5.14	0.26	0.301	0.012	0.97	0.1237	0.0020	17.7	1843	42	1698	57	2011	28
AKX0426_002	4.04	0.27	0.260	0.015	0.97	0.1125	0.0020	21.3	1641	52	1491	75	1840	32
AKX0426_022	4.88	0.38	0.287	0.020	0.98	0.1235	0.0021	21.6	1798	64	1624	101	2007	30
AKX0426_001	3.84	0.25	0.248	0.014	0.97	0.1123	0.0019	24.7	1602	52	1429	73	1837	30
AKX0426_016	4.25	0.54	0.237	0.029	0.99	0.1297	0.0024	38.1	1683	100	1373	151	2094	32

AKX0426_009	3.94	0.39	0.228	0.021	0.98	0.1256	0.0026	38.8	1622	76	1321	108	2037	36
AKX0426_038	no data	no data	no data	no data	no data	0.4725	0.0160	no data	no data	no data	no data	no data	4158	49
AKX0426_018	no data	no data	no data	no data	no data	0.1896	0.0043	no data	no data	no data	no data	no data	2739	36
AKX0426_008	no data	no data	no data	no data	no data	0.0779	0.2173	no data	no data	no data	no data	no data	1144	2301
AKX0426_007	no data	no data	no data	no data	no data	0.2321	0.1506	no data	no data	no data	no data	no data	3067	776
AKX0426_006	no data	no data	no data	no data	no data	0.0597	0.0751	no data	no data	no data	no data	no data	594	1568
AKX0426_003	no data	no data	no data	no data	no data	0.1343	0.0047	no data	no data	no data	no data	no data	2155	59
AKX0433_008	5.79	0.43	0.348	0.021	0.98	0.1207	0.0023	2.5	1945	63	1924	102	1967	34
AKX0433_024	6.01	0.29	0.361	0.012	0.98	0.1209	0.0019	-0.9	1977	41	1985	58	1969	28
AKX0433_006	6.01	0.45	0.351	0.022	0.98	0.1241	0.0024	4.5	1977	64	1939	103	2016	33
AKX0433_030	6.65	0.32	0.389	0.013	0.98	0.1242	0.0020	-5.8	2066	41	2116	61	2017	28
AKX0433_025	6.66	0.32	0.387	0.013	0.98	0.1247	0.0019	-5.0	2067	42	2111	62	2025	27
AKX0433_017	6.02	0.44	0.349	0.024	0.99	0.1250	0.0012	5.6	1978	62	1930	116	2028	17
AKX0433_010	6.17	0.47	0.358	0.022	0.98	0.1250	0.0024	3.3	2001	64	1972	105	2029	34
AKX0433_020	6.15	0.45	0.355	0.025	0.99	0.1255	0.0012	4.4	1997	62	1959	117	2036	17
AKX0433_019	6.11	0.45	0.352	0.025	0.99	0.1257	0.0013	5.4	1991	62	1945	117	2039	18
AKX0433_012	6.21	0.45	0.357	0.025	0.99	0.1261	0.0012	4.2	2006	62	1970	117	2044	17
AKX0433_021	6.58	0.31	0.378	0.013	0.98	0.1261	0.0020	-1.3	2056	41	2068	59	2045	27
AKX0433_022	6.47	0.31	0.372	0.013	0.98	0.1263	0.0020	0.5	2042	41	2038	59	2047	27
AKX0433_002	6.41	0.48	0.367	0.023	0.98	0.1267	0.0024	2.2	2034	64	2014	106	2053	33
AKX0433_014	6.14	0.45	0.351	0.025	0.99	0.1268	0.0012	6.4	1995	62	1940	116	2053	17
AKX0433_028	6.31	0.30	0.361	0.012	0.98	0.1268	0.0020	3.8	2020	41	1987	59	2054	27
AKX0433_029	6.41	0.30	0.367	0.012	0.98	0.1269	0.0020	2.3	2034	41	2013	58	2055	27
AKX0433_011	6.42	0.47	0.366	0.026	0.99	0.1270	0.0012	2.5	2034	63	2012	121	2056	17
AKX0433_026	6.79	0.34	0.386	0.014	0.98	0.1277	0.0020	-2.1	2085	43	2104	66	2067	28
AKX0433_018	6.44	0.48	0.362	0.026	0.99	0.1288	0.0013	4.9	2037	63	1993	120	2082	18
AKX0433_015	6.56	0.48	0.364	0.025	0.99	0.1306	0.0013	5.8	2054	62	2002	119	2106	17
culled														
AKX0433_016	5.56	0.41	0.325	0.023	0.99	0.1241	0.0012	11.4	1910	61	1814	110	2015	17
AKX0433_005	5.62	0.43	0.326	0.021	0.98	0.1250	0.0025	11.9	1919	64	1818	99	2029	34

AKX0433_001	5.26	0.42	0.303	0.020	0.98	0.1257	0.0024	18.5	1862	66	1707	100	2038	34
AKX0433_009	4.83	0.37	0.283	0.018	0.98	0.1238	0.0024	22.8	1790	63	1605	91	2012	34
AKX0433_027	4.59	0.23	0.273	0.010	0.98	0.1220	0.0019	24.4	1747	41	1555	51	1986	27
AKX0433_007	4.15	0.32	0.250	0.016	0.98	0.1203	0.0023	29.7	1664	60	1438	80	1961	34
AKX0433_004	3.66	0.28	0.234	0.015	0.98	0.1134	0.0022	29.9	1562	59	1354	76	1855	34
AKX0433_013	4.06	0.30	0.240	0.017	0.99	0.1225	0.0012	33.6	1647	58	1389	87	1993	17
AKX0433_003	4.94	0.38	0.247	0.015	0.98	0.1449	0.0030	41.9	1809	63	1424	79	2286	36
AKX0433_023	2.82	0.14	0.179	0.007	0.98	0.1144	0.0018	47.0	1360	38	1059	38	1871	28

AKX0434_009	5.39	0.12	0.340	0.006	0.97	0.1149	0.0007	-0.6	1884	18	1888	31	1879	10
AKX0434_044	4.92	0.19	0.310	0.009	0.97	0.1153	0.0015	8.9	1806	32	1738	46	1885	23
AKX0434_007	5.75	0.13	0.348	0.007	0.96	0.1201	0.0008	2.0	1939	20	1923	33	1957	11
AKX0434_021	5.54	0.13	0.332	0.008	0.98	0.1212	0.0006	7.3	1908	21	1848	36	1974	8
AKX0434_001	6.08	0.15	0.363	0.008	0.97	0.1213	0.0007	-1.4	1987	21	1999	37	1975	10
AKX0434_043	6.50	0.25	0.387	0.011	0.96	0.1216	0.0016	-7.8	2045	33	2111	52	1979	23
AKX0434_018	6.45	0.19	0.377	0.010	0.98	0.1241	0.0007	-2.8	2039	25	2063	48	2015	10
AKX0434_026	6.02	0.24	0.351	0.013	0.98	0.1244	0.0009	4.7	1979	34	1940	63	2021	13
AKX0434_011	6.36	0.20	0.370	0.011	0.98	0.1247	0.0008	-0.2	2027	28	2029	52	2025	11
AKX0434_005	6.41	0.13	0.371	0.007	0.97	0.1253	0.0007	0.0	2033	18	2033	31	2033	10
AKX0434_010	5.93	0.17	0.341	0.009	0.97	0.1261	0.0008	8.5	1966	24	1893	42	2044	11
AKX0434_040	6.49	0.21	0.373	0.011	0.98	0.1262	0.0007	0.1	2045	27	2044	52	2045	10
AKX0434_031	6.89	0.21	0.396	0.011	0.98	0.1263	0.0009	-5.9	2098	27	2150	52	2047	12
AKX0434_030	6.53	0.19	0.375	0.010	0.97	0.1264	0.0008	-0.1	2050	25	2051	47	2049	12
AKX0434_035	6.21	0.21	0.356	0.011	0.98	0.1265	0.0008	5.0	2005	29	1962	53	2050	12
AKX0434_008	6.62	0.16	0.379	0.008	0.97	0.1269	0.0008	-0.8	2063	21	2070	38	2055	11
AKX0434_038	6.74	0.20	0.385	0.011	0.98	0.1270	0.0008	-2.3	2077	26	2098	49	2057	12
AKX0434_017	6.55	0.19	0.373	0.010	0.99	0.1273	0.0006	1.1	2052	26	2043	49	2062	9
AKX0434_046	6.29	0.24	0.357	0.010	0.97	0.1277	0.0016	5.6	2017	33	1967	48	2067	22
AKX0434_020	6.31	0.24	0.358	0.013	0.98	0.1278	0.0009	5.4	2020	33	1973	62	2068	12
AKX0434_050	6.18	0.27	0.350	0.013	0.97	0.1279	0.0017	7.5	2002	38	1936	60	2070	23
AKX0434_033	6.39	0.21	0.359	0.011	0.98	0.1290	0.0008	6.0	2030	29	1977	54	2085	11
AKX0434_019	7.04	0.24	0.380	0.013	0.99	0.1343	0.0007	4.2	2116	30	2077	59	2154	10

AKX0434_024	10.56	0.30	0.467	0.013	0.99	0.1641	0.0008	1.4	2485	26	2470	55	2498	8
AKX0434_012	11.76	0.35	0.497	0.014	0.98	0.1716	0.0009	-1.4	2585	28	2601	60	2573	9
AKX0434_039	11.65	0.42	0.469	0.016	0.99	0.1800	0.0011	7.8	2576	33	2481	71	2653	11
AKX0434_016b	12.52	0.38	0.492	0.014	0.99	0.1847	0.0010	5.2	2645	28	2579	62	2695	9
AKX0434_027	14.15	0.40	0.543	0.015	0.98	0.1890	0.0010	-2.8	2760	27	2796	61	2734	9
AKX0434_002	13.29	0.37	0.509	0.013	0.97	0.1892	0.0012	3.6	2700	26	2654	55	2735	11
AKX0434_047	13.41	0.53	0.514	0.015	0.96	0.1894	0.0025	2.9	2709	37	2672	65	2737	22
AKX0434_041	15.63	0.64	0.569	0.018	0.97	0.1991	0.0026	-3.8	2854	38	2905	75	2819	21
AKX0434_022	15.81	0.46	0.572	0.016	0.98	0.2006	0.0012	-3.6	2865	27	2914	63	2831	10
AKX0434_048	14.37	0.57	0.510	0.016	0.97	0.2041	0.0026	8.6	2774	37	2658	67	2860	20
AKX0434_034	17.10	0.50	0.581	0.016	0.98	0.2133	0.0012	-1.0	2940	28	2955	65	2931	9
culled														
AKX0434_045	10.90	0.43	0.446	0.014	0.97	0.1771	0.0023	11.2	2515	36	2379	61	2626	21
AKX0434_014	5.98	0.22	0.337	0.012	0.99	0.1287	0.0007	11.6	1973	31	1871	56	2081	10
AKX0434_025	11.72	0.50	0.449	0.019	0.99	0.1896	0.0010	15.3	2583	39	2389	82	2738	9
AKX0434_029	5.54	0.21	0.314	0.011	0.99	0.1279	0.0007	17.1	1906	32	1759	56	2070	10
AKX0434_004	5.13	0.13	0.300	0.007	0.97	0.1237	0.0007	17.9	1840	21	1693	33	2011	10
AKX0434_015	5.14	0.22	0.297	0.012	0.98	0.1255	0.0009	20.0	1843	35	1677	59	2036	13
AKX0434_016a	10.37	0.40	0.410	0.015	0.99	0.1833	0.0010	20.6	2468	35	2215	70	2683	9
AKX0434_006	4.32	0.10	0.262	0.006	0.97	0.1195	0.0007	25.6	1698	20	1503	29	1948	10
AKX0434_037	4.63	0.13	0.268	0.007	0.98	0.1253	0.0007	27.7	1754	23	1531	34	2033	10
AKX0434_013	4.39	0.19	0.258	0.011	0.99	0.1234	0.0008	29.3	1710	35	1480	55	2006	11
AKX0434_032	7.98	0.28	0.339	0.011	0.99	0.1710	0.0010	30.8	2229	31	1880	54	2567	10
AKX0434_042	4.25	0.16	0.251	0.007	0.97	0.1228	0.0015	31.0	1683	30	1442	35	1998	22
AKX0434_049	8.31	0.33	0.342	0.010	0.97	0.1765	0.0022	31.9	2266	35	1894	50	2621	21
AKX0434_036	3.77	0.11	0.220	0.006	0.98	0.1244	0.0008	40.3	1587	24	1281	33	2021	11
AKX0434_023	no data	no data	no data	no data	no data	0.1805	0.0021	no data	no data	no data	no data	no data	2658	19
AKX0434_028	6.85	0.22	0.414	0.012	0.97	0.1199	0.0009	-17.0	2092	28	2235	56	1954	14
AKX0434_003	6.74	0.15	0.409	0.008	0.97	0.1196	0.0007	-15.7	2078	20	2209	38	1950	10
JS04KR1c_033	3.69	0.10	0.277	0.007	0.98	0.0968	0.0006	-0.8	1570	22	1575	36	1563	12

JS04KR1c_012	4.27	0.25	0.292	0.013	0.97	0.1059	0.0019	4.9	1687	47	1654	66	1729	32
JS04KR1c_036	5.03	0.14	0.331	0.008	0.98	0.1101	0.0007	-2.8	1824	24	1844	41	1801	11
JS04KR1c_032	4.83	0.14	0.318	0.008	0.97	0.1103	0.0008	1.6	1790	24	1778	40	1804	14
JS04KR1c_038	5.06	0.15	0.332	0.009	0.98	0.1105	0.0007	-2.6	1829	24	1848	42	1807	12
JS04KR1c_013	4.86	0.28	0.319	0.014	0.98	0.1105	0.0019	1.6	1795	47	1783	68	1808	31
JS04KR1c_031	4.88	0.14	0.320	0.008	0.98	0.1107	0.0007	1.3	1799	23	1790	39	1810	11
JS04KR1c_004	4.84	0.25	0.314	0.014	0.98	0.1118	0.0013	4.3	1793	42	1761	70	1830	21
JS04KR1c_023	4.98	0.30	0.321	0.016	0.97	0.1126	0.0020	3.0	1816	50	1793	76	1841	31
JS04KR1c_024	4.74	0.19	0.304	0.006	1.09	0.1133	0.0020	8.9	1775	33	1709	29	1853	31
JS04KR1c_039	8.34	0.39	0.407	0.018	0.99	0.1486	0.0011	6.5	2269	42	2201	83	2330	13
culled														
JS04KR1c_014	4.44	0.26	0.291	0.014	0.97	0.1105	0.0019	10.0	1720	48	1648	68	1808	31
JS04KR1c_026	5.77	0.36	0.332	0.016	0.96	0.1262	0.0026	11.2	1942	52	1846	76	2045	36
JS04KR1c_034	4.48	0.15	0.291	0.009	0.98	0.1118	0.0007	11.4	1727	27	1644	44	1828	11
JS04KR1c_007	4.50	0.24	0.291	0.014	0.98	0.1123	0.0012	11.9	1731	43	1644	69	1837	20
JS04KR1c_027	4.68	0.18	0.294	0.005	1.18	0.1155	0.0019	13.6	1763	32	1660	24	1887	30
JS04KR1c_001	4.47	0.26	0.285	0.015	0.98	0.1138	0.0014	14.9	1725	47	1616	75	1861	22
JS04KR1c_028	5.71	0.29	0.321	0.010	0.98	0.1288	0.0027	15.7	1933	43	1797	48	2082	36
JS04KR1c_008	4.96	0.28	0.299	0.016	0.98	0.1202	0.0014	15.7	1812	47	1688	76	1959	21
JS04KR1c_019	5.57	0.35	0.317	0.015	0.96	0.1275	0.0027	16.0	1912	52	1775	72	2064	37
JS04KR1c_029	4.48	0.27	0.283	0.014	0.97	0.1147	0.0021	16.2	1727	49	1607	68	1875	32
JS04KR1c_017	3.97	0.28	0.260	0.016	0.98	0.1107	0.0019	19.7	1629	56	1492	81	1810	31
JS04KR1c_021	5.29	0.22	0.301	0.006	1.09	0.1274	0.0023	20.1	1867	35	1697	29	2062	32
JS04KR1c_030	5.04	0.22	0.291	0.007	1.05	0.1254	0.0023	21.5	1826	36	1648	33	2035	32
JS04KR1c_020	4.89	0.29	0.286	0.013	0.97	0.1241	0.0022	22.1	1801	49	1621	66	2016	32
JS04KR1c_035	3.85	0.19	0.252	0.012	0.99	0.1111	0.0007	22.8	1604	38	1446	60	1818	11
JS04KR1c_015	4.50	0.29	0.267	0.014	0.97	0.1223	0.0023	26.3	1730	53	1524	72	1990	33
JS04KR1c_009	4.16	0.23	0.256	0.012	0.97	0.1179	0.0017	26.4	1667	44	1469	63	1925	25
JS04KR1c_010	4.11	0.24	0.240	0.013	0.98	0.1245	0.0016	35.0	1657	47	1384	67	2021	22
JS04KR1c_005	3.42	0.22	0.217	0.013	0.99	0.1142	0.0013	35.3	1510	49	1269	69	1867	20
JS04KR1c_022	2.92	0.16	0.197	0.008	0.98	0.1075	0.0018	37.1	1388	39	1160	42	1757	30
JS04KR1c_011	3.75	0.21	0.217	0.009	0.98	0.1253	0.0021	41.5	1582	44	1266	48	2034	30
JS04KR1c_040	5.19	0.19	0.249	0.007	0.94	0.1512	0.0019	43.7	1851	30	1433	38	2359	22

JS04KR1c_006	5.68	0.29	0.259	0.012	0.98	0.1590	0.0018	43.8	1929	42	1486	59	2445	19
JS04KR1c_002	5.42	0.36	0.233	0.014	0.98	0.1688	0.0021	52.0	1887	55	1348	75	2546	21
JS04KR1c_003	2.63	0.19	0.149	0.010	0.99	0.1279	0.0014	60.6	1309	52	896	58	2069	20
JS04KR1c_016	3.59	0.24	0.173	0.010	0.97	0.1504	0.0027	60.6	1548	52	1030	54	2351	30
JS04KR1c_037	3.44	0.80	0.162	0.038	1.00	0.1535	0.0017	63.7	1513	169	970	206	2385	19
JS04KR1c_018	4.14	0.30	0.165	0.010	0.97	0.1821	0.0035	67.9	1662	58	984	57	2672	31
JS04KR1c_025	9.31	0.51	0.567	0.022	0.97	0.1192	0.0022	-60.9	2369	49	2893	91	1944	33
JSDV0301_006	8.33	0.19	0.408	0.009	0.98	0.1481	0.0008	6.0	2268	21	2206	40	2324	9
culled														
JSDV0301_010	4.87	0.11	0.303	0.007	0.98	0.1166	0.0006	12.0	1797	20	1705	33	1905	9
JSDV0301_009	5.85	0.13	0.380	0.008	0.96	0.1118	0.0007	-15.9	1954	19	2076	36	1828	11
JSDV0301_008	3.75	0.12	0.261	0.008	0.98	0.1042	0.0006	13.5	1583	25	1496	41	1701	10
JSDV0301_007	3.52	0.09	0.239	0.006	0.98	0.1069	0.0006	23.3	1532	20	1381	29	1748	10
JSDV0301_005	1.96	0.06	0.166	0.005	0.95	0.0857	0.0009	27.5	1103	21	991	25	1330	19
JSDV0301_004	1.16	0.10	0.075	0.007	1.00	0.1123	0.0009	77.3	781	47	465	39	1836	14
JSDV0301_003	3.28	0.07	0.229	0.004	0.98	0.1042	0.0005	24.2	1477	16	1327	23	1699	9
JSDV0301_002	9.31	0.19	0.388	0.007	0.98	0.1742	0.0008	21.9	2369	19	2112	34	2599	7
JSDV0301_001	1.69	0.05	0.119	0.004	0.99	0.1025	0.0005	59.6	1004	21	728	21	1671	9
JSMD03_002	0.97	0.06	0.111	0.006	0.96	0.0636	0.0013	7.6	689	32	677	35	730	41
JSMD03_020	2.68	0.15	0.221	0.011	0.98	0.0878	0.0009	7.0	1323	41	1290	60	1378	20
JSMD03_019	2.68	0.16	0.221	0.012	0.98	0.0880	0.0010	7.7	1324	43	1287	64	1383	21
JSMD03_033	2.81	0.16	0.226	0.012	0.99	0.0903	0.0009	9.3	1359	42	1312	63	1433	20
JSMD03_027	4.16	0.24	0.286	0.015	0.98	0.1053	0.0011	6.3	1666	45	1623	74	1719	20
JSMD03_012	4.53	0.26	0.303	0.016	0.98	0.1083	0.0012	4.2	1736	46	1707	78	1772	20
JSMD03_040	4.32	0.28	0.288	0.017	0.98	0.1087	0.0013	9.3	1697	52	1632	86	1778	22
JSMD03_021	4.50	0.25	0.299	0.016	0.98	0.1090	0.0011	6.1	1731	46	1688	77	1783	19
JSMD03_009	4.60	0.26	0.306	0.016	0.98	0.1092	0.0012	4.3	1749	46	1719	78	1786	19

JSMD03_035	4.59	0.26	0.303	0.016	0.98	0.1100	0.0012	6.0	1748	46	1705	78	1800	19
JSMD03_032	4.55	0.25	0.299	0.015	0.98	0.1103	0.0012	7.3	1741	45	1688	76	1804	19
JSMD03_016	4.74	0.28	0.310	0.017	0.98	0.1108	0.0013	4.4	1774	48	1742	81	1812	21
JSMD03_005	4.80	0.28	0.310	0.017	0.98	0.1123	0.0012	6.1	1784	49	1739	83	1837	19
JSMD03_036	5.05	0.29	0.326	0.017	0.98	0.1125	0.0013	1.3	1828	48	1818	84	1840	20
JSMD03_022	4.69	0.26	0.301	0.016	0.98	0.1130	0.0012	9.4	1766	46	1696	77	1849	19
JSMD03_003	5.11	0.29	0.326	0.017	0.98	0.1136	0.0012	2.3	1839	47	1821	83	1858	19
JSMD03_028	11.38	0.64	0.462	0.024	0.98	0.1786	0.0019	8.7	2554	51	2448	105	2640	17
JSMD03_015	12.16	0.74	0.482	0.027	0.98	0.1828	0.0021	6.3	2617	55	2538	117	2678	19
JSMD03_006	12.99	0.74	0.511	0.027	0.98	0.1843	0.0020	1.4	2679	53	2661	115	2692	18
culled														
JSMD03_037	4.35	0.25	0.288	0.015	0.99	0.1096	0.0011	10.2	1702	46	1630	76	1792	19
JSMD03_025	2.83	0.17	0.226	0.013	0.98	0.0911	0.0010	10.5	1364	44	1311	66	1448	21
JSMD03_024	4.52	0.26	0.292	0.016	0.98	0.1121	0.0012	11.2	1734	47	1652	78	1833	20
JSMD03_014	4.21	0.30	0.279	0.019	0.99	0.1096	0.0012	13.1	1676	56	1585	93	1793	20
JSMD03_010	4.21	0.27	0.278	0.017	0.98	0.1099	0.0013	13.7	1675	52	1579	84	1798	22
JSMD03_018	2.77	0.16	0.219	0.012	0.98	0.0919	0.0010	14.3	1348	43	1275	63	1466	21
JSMD03_034	3.99	0.24	0.267	0.015	0.99	0.1084	0.0011	15.6	1632	47	1526	74	1772	19
JSMD03_038	4.05	0.26	0.268	0.016	0.99	0.1098	0.0012	16.7	1645	51	1529	82	1796	20
JSMD03_030	3.78	0.21	0.255	0.013	0.98	0.1076	0.0011	18.8	1589	45	1463	68	1760	19
JSMD03_031	3.77	0.23	0.254	0.014	0.98	0.1075	0.0012	18.9	1586	47	1460	72	1757	20
JSMD03_023	3.48	0.20	0.243	0.013	0.98	0.1039	0.0011	19.2	1523	44	1402	66	1696	19
JSMD03_039	3.72	0.21	0.248	0.013	0.98	0.1086	0.0011	21.7	1576	45	1430	67	1776	19
JSMD03_013	3.07	0.19	0.210	0.012	0.99	0.1061	0.0011	31.9	1426	47	1229	66	1734	20
JSMD03_011	8.28	0.51	0.338	0.019	0.99	0.1777	0.0019	33.0	2263	54	1877	93	2632	17
JSMD03_004	3.13	0.19	0.211	0.012	0.99	0.1077	0.0011	33.0	1440	45	1232	62	1762	19
JSMD03_008	2.68	0.16	0.188	0.010	0.99	0.1036	0.0011	37.4	1323	43	1108	56	1689	19
JSMD03_029	1.98	0.14	0.143	0.009	0.99	0.1003	0.0011	50.3	1108	46	861	53	1630	21
JSMD03_017	28.80	3.43	0.357	0.041	0.99	0.5848	0.0108	64.3	3447	111	1968	192	4471	27
JSMD03_001	0.93	0.43	0.039	0.018	1.00	0.1735	0.0020	92.1	670	202	247	110	2592	19
JSMD03_026	no data	no data	no data	no data	no data	-0.1446	-0.3737	no data	no data	no data	no data	no data	765	no data
JSMD03_007	no data	no data	no data	no data	no data	0.9220	0.0520	no data	no data	no data	no data	no data	5123	77

JSPR0301_039	1.71	0.06	0.167	0.004	0.99	0.0742	0.0010	5.3	1013	23	996	22	1048	26
JSPR0301_011	1.77	0.04	0.172	0.003	0.96	0.0744	0.0005	2.8	1033	15	1025	17	1052	14
JSPR0301_021	1.84	0.07	0.178	0.005	0.97	0.0748	0.0011	0.7	1059	26	1057	27	1063	28
JSPR0301_016	1.93	0.05	0.184	0.004	0.96	0.0761	0.0006	1.1	1091	17	1087	21	1098	16
JSPR0301_020	2.17	0.05	0.199	0.003	0.97	0.0791	0.0005	0.4	1172	15	1171	18	1175	13
JSPR0301_009	2.36	0.06	0.208	0.005	0.98	0.0824	0.0005	3.3	1231	18	1217	24	1255	11
JSPR0301_028	2.65	0.10	0.222	0.006	0.98	0.0868	0.0011	5.3	1315	28	1291	31	1356	25
JSPR0301_001	2.86	0.11	0.232	0.008	0.98	0.0893	0.0008	5.0	1372	29	1347	43	1411	17
JSPR0301_026	3.02	0.12	0.243	0.007	0.97	0.0902	0.0013	1.9	1414	30	1404	35	1429	27
JSPR0301_007	3.36	0.09	0.263	0.006	0.97	0.0925	0.0006	-2.1	1495	20	1506	31	1478	12
JSPR0301_013	3.12	0.08	0.243	0.006	0.97	0.0931	0.0007	6.5	1438	20	1403	29	1491	14
JSPR0301_022	4.08	0.17	0.287	0.009	0.97	0.1032	0.0014	3.7	1651	33	1627	43	1682	24
JSPR0301_015	4.34	0.10	0.303	0.006	0.97	0.1038	0.0007	-0.9	1701	19	1707	29	1694	13
JSPR0301_031	4.10	0.15	0.286	0.007	0.99	0.1040	0.0014	4.9	1655	30	1623	36	1696	24
JSPR0301_019	4.75	0.11	0.321	0.006	0.96	0.1071	0.0008	-3.0	1776	19	1797	28	1751	14
JSPR0301_038	4.52	0.16	0.303	0.007	0.99	0.1082	0.0014	4.2	1735	30	1705	36	1770	23
JSPR0301_023	4.49	0.18	0.298	0.009	0.97	0.1092	0.0014	6.5	1729	33	1683	44	1785	24
JSPR0301_002	5.29	0.15	0.331	0.009	0.97	0.1159	0.0008	3.1	1868	24	1844	42	1894	12
JSPR0301_014	11.49	0.27	0.464	0.009	0.97	0.1795	0.0012	8.6	2564	22	2458	40	2648	11
JSPR0301_004	13.15	0.37	0.530	0.013	0.97	0.1798	0.0012	-4.3	2690	26	2743	56	2651	11
JSPR0301_006	12.71	0.31	0.511	0.011	0.98	0.1802	0.0010	-0.4	2658	23	2663	48	2655	10
JSPR0301_025	12.97	0.48	0.506	0.013	0.98	0.1858	0.0024	2.9	2677	35	2641	56	2705	21
JSPR0301_033	12.70	0.74	0.481	0.021	0.94	0.1916	0.0043	9.9	2658	53	2531	90	2756	36

culled

JSPR0301_018	1.99	0.05	0.181	0.004	0.97	0.0797	0.0005	10.6	1112	18	1073	22	1189	14
JSPR0301_024	4.27	0.19	0.282	0.010	0.97	0.1099	0.0015	12.4	1687	36	1600	49	1798	24
JSPR0301_032	1.84	0.07	0.171	0.005	0.98	0.0783	0.0010	13.0	1061	25	1016	26	1154	26
JSPR0301_005	1.80	0.07	0.167	0.006	0.98	0.0780	0.0006	14.0	1045	24	998	32	1146	14
JSPR0301_034	1.94	0.07	0.175	0.004	0.99	0.0802	0.0011	14.4	1095	25	1042	23	1202	28
JSPR0301_030	2.03	0.08	0.181	0.005	0.97	0.0816	0.0012	14.6	1126	27	1070	28	1236	28
JSPR0301_035	2.77	0.10	0.218	0.005	0.99	0.0920	0.0012	14.6	1347	27	1273	28	1468	25

JSPR0301_037	2.30	0.08	0.195	0.005	0.99	0.0855	0.0011	14.7	1212	26	1149	26	1328	25
JSPR0301_003	1.85	0.07	0.168	0.006	0.95	0.0799	0.0011	17.5	1065	26	1002	32	1195	26
JSPR0301_029	1.68	0.07	0.157	0.005	0.97	0.0778	0.0010	19.0	1002	27	940	29	1141	26
JSPR0301_036	1.65	0.06	0.154	0.004	0.99	0.0779	0.0010	20.9	989	23	921	20	1144	26
JSPR0301_040	1.79	0.07	0.161	0.004	0.97	0.0803	0.0012	21.4	1041	26	965	24	1204	29
JSPR0301_027	1.79	0.08	0.161	0.005	0.97	0.0809	0.0011	22.8	1042	28	960	29	1218	26
JSPR0301_008	2.43	0.09	0.179	0.006	0.97	0.0981	0.0010	35.8	1250	27	1063	33	1588	19
JSPR0301_017	3.54	0.24	0.151	0.009	0.95	0.1704	0.0036	69.1	1536	52	904	49	2561	35
JSPR0301_012	no data	no data	no data	no data	no data	0.0973	0.0032	no data	no data	no data	no data	no data	1574	60
JSPR0301_010	5.64	0.17	0.383	0.010	0.96	0.1067	0.0009	-23.4	1923	25	2093	46	1745	15
JSPR0303_041	1.98	0.05	0.184	0.004	0.96	0.0781	0.0006	5.8	1108	17	1088	22	1149	16
JSPR0303_031	2.68	0.06	0.223	0.005	0.96	0.0872	0.0006	5.3	1323	17	1298	24	1364	12
JSPR0303_026	3.08	0.07	0.245	0.005	0.97	0.0911	0.0005	2.9	1427	16	1412	24	1449	10
JSPR0303_033	3.13	0.09	0.247	0.006	0.97	0.0922	0.0006	3.8	1441	21	1421	32	1471	12
JSPR0303_037	3.19	0.09	0.249	0.006	0.95	0.0929	0.0008	4.0	1454	22	1432	31	1485	17
JSPR0303_028	4.08	0.09	0.284	0.006	0.97	0.1040	0.0006	5.6	1650	18	1613	29	1697	11
JSPR0303_008	4.05	0.13	0.279	0.005	1.07	0.1051	0.0014	8.4	1644	26	1589	23	1716	24
JSPR0303_004	4.39	0.14	0.299	0.005	1.05	0.1066	0.0014	3.6	1711	27	1686	26	1741	24
JSPR0303_018	4.66	0.15	0.310	0.006	0.99	0.1090	0.0013	2.7	1760	26	1741	31	1783	21
JSPR0303_021	4.51	0.15	0.295	0.007	0.98	0.1109	0.0013	9.3	1733	27	1665	32	1815	21
JSPR0303_038	5.33	0.12	0.340	0.007	0.97	0.1135	0.0007	-2.1	1873	20	1889	34	1856	11
JSPR0303_020	12.29	0.37	0.505	0.010	1.00	0.1765	0.0020	-0.7	2627	28	2635	41	2621	19
JSPR0303_042	13.59	0.30	0.534	0.011	0.97	0.1845	0.0010	-3.0	2721	21	2759	44	2694	9
culled														
JSPR0303_005	4.00	0.15	0.275	0.007	0.99	0.1057	0.0014	10.6	1635	29	1564	33	1727	24
JSPR0303_016	3.20	0.12	0.240	0.007	0.97	0.0968	0.0013	12.5	1458	29	1388	35	1563	25
JSPR0303_025	1.90	0.05	0.174	0.004	0.96	0.0790	0.0006	12.6	1080	19	1035	24	1171	15
JSPR0303_009	4.18	0.15	0.278	0.006	1.00	0.1090	0.0014	12.8	1669	28	1581	31	1782	24
JSPR0303_043	3.18	0.11	0.238	0.008	0.97	0.0967	0.0008	13.0	1451	27	1378	41	1561	15
JSPR0303_012	2.52	0.10	0.208	0.006	0.98	0.0881	0.0012	13.2	1279	28	1217	31	1384	26

JSPR0303_010	10.17	0.38	0.426	0.011	0.99	0.1730	0.0023	13.6	2451	34	2290	47	2587	22
JSPR0303_040	3.37	0.09	0.245	0.005	0.95	0.0998	0.0009	14.3	1497	21	1412	28	1620	17
JSPR0303_027	4.77	0.11	0.293	0.006	0.98	0.1178	0.0006	15.6	1779	18	1659	30	1924	9
JSPR0303_034	2.88	0.08	0.221	0.006	0.98	0.0944	0.0006	16.5	1376	22	1288	31	1516	11
JSPR0303_013	2.81	0.11	0.216	0.006	0.97	0.0941	0.0013	18.0	1357	30	1263	34	1509	26
JSPR0303_015	2.00	0.07	0.175	0.004	0.97	0.0829	0.0011	19.2	1117	23	1042	22	1266	27
JSPR0303_023	2.69	0.10	0.209	0.006	0.97	0.0932	0.0012	19.8	1324	28	1223	31	1493	24
JSPR0303_002	1.96	0.09	0.171	0.006	0.97	0.0833	0.0013	22.1	1102	30	1016	32	1277	29
JSPR0303_011	1.47	0.08	0.141	0.006	0.98	0.0757	0.0010	23.5	917	32	848	36	1087	27
JSPR0303_029	3.61	0.20	0.238	0.012	0.97	0.1098	0.0015	25.9	1551	43	1378	63	1796	25
JSPR0303_022	3.09	0.14	0.217	0.009	0.98	0.1029	0.0012	26.8	1429	35	1268	46	1677	22
JSPR0303_039	3.44	0.09	0.230	0.005	0.98	0.1085	0.0006	27.4	1514	20	1335	29	1775	10
JSPR0303_014	2.90	0.12	0.200	0.007	0.97	0.1050	0.0013	34.4	1381	31	1175	36	1715	23
JSPR0303_003	1.42	0.06	0.129	0.004	0.98	0.0797	0.0011	36.4	897	24	783	22	1191	26
JSPR0303_001	2.19	0.09	0.167	0.004	0.98	0.0951	0.0016	37.7	1178	27	995	22	1530	32
JSPR0303_007	7.33	0.36	0.291	0.012	0.98	0.1825	0.0024	43.4	2153	43	1649	59	2676	21
JSPR0303_036	2.76	0.22	0.173	0.014	1.00	0.1155	0.0006	49.0	1345	59	1031	76	1888	10
JSPR0303_032	2.15	0.10	0.144	0.007	0.99	0.1085	0.0006	54.7	1165	33	865	38	1775	10
JSPR0303_035	1.45	0.09	0.105	0.006	0.99	0.0998	0.0010	63.1	909	35	645	35	1620	19
JSPR0303_030	no data	no data	no data	no data	no data	2.9397	0.6716	no data	no data	no data	no data	no data	6714	275
JSPR0303_024	no data	no data	no data	no data	no data	0.2699	0.0757	no data	no data	no data	no data	no data	3305	383
JSPR0303_006	no data	no data	no data	no data	no data	-0.0001	-0.1746	no data	no data	no data	no data	no data	0	-474
JSPR0303_017	6.16	0.20	0.392	0.008	0.99	0.1140	0.0014	-16.9	1999	28	2133	38	1864	22
JSPR0303_019	4.63	0.14	0.327	0.006	1.00	0.1027	0.0012	-10.1	1754	25	1822	29	1674	22

JSWI0301_023	1.58	0.15	0.159	0.014	0.99	0.0723	0.0009	4.6	964	57	951	79	993	25
JSWI0301_011	2.24	0.18	0.200	0.016	0.99	0.0814	0.0008	4.9	1195	56	1175	85	1230	18
JSWI0301_030	2.60	0.24	0.220	0.020	0.99	0.0860	0.0011	4.8	1302	67	1280	104	1338	24
JSWI0301_025	4.04	0.38	0.280	0.025	0.99	0.1048	0.0012	7.9	1643	73	1590	126	1711	21
JSWI0301_029	4.47	0.42	0.308	0.028	0.99	0.1051	0.0013	-1.1	1725	76	1732	137	1716	22
JSWI0301_020	4.60	0.38	0.315	0.025	1.00	0.1060	0.0008	-2.2	1749	66	1764	122	1731	15
JSWI0301_018	4.53	0.37	0.303	0.024	0.99	0.1084	0.0009	4.3	1736	66	1705	120	1773	16

JSWI0301_016	4.41	0.37	0.292	0.024	1.00	0.1095	0.0009	8.7	1715	67	1653	118	1791	15
JSWI0301_028	4.76	0.45	0.312	0.028	0.99	0.1105	0.0013	3.6	1778	76	1752	137	1808	21
JSWI0301_022	4.83	0.45	0.314	0.028	0.99	0.1115	0.0013	3.9	1790	76	1761	137	1824	20
JSWI0301_026	5.02	0.47	0.320	0.029	0.99	0.1139	0.0014	4.5	1823	77	1789	140	1862	22
JSWI0301_027	5.80	0.55	0.342	0.031	0.99	0.1230	0.0015	6.1	1946	78	1895	147	2000	21
JSWI0301_021	9.62	0.90	0.439	0.039	0.99	0.1589	0.0018	4.8	2399	82	2346	174	2444	19
JSWI0301_013	12.67	1.03	0.518	0.041	1.00	0.1774	0.0014	-2.9	2655	74	2691	173	2629	13
JSWI0301_017	11.65	0.95	0.475	0.038	0.99	0.1778	0.0015	5.8	2576	73	2505	163	2633	14
JSWI0301_019	15.54	1.27	0.544	0.043	1.00	0.2071	0.0016	3.5	2849	75	2801	179	2883	13
JSWI0301_014	17.62	1.44	0.587	0.047	1.00	0.2178	0.0018	-0.5	2969	76	2976	187	2965	13
SHRIMPed														
JSWI0301_001	4.01	0.25	0.260	0.013	0.98	0.1120	0.0019	21.0	1637	49	1489	66	1833	31
JSWI0301_002	16.00	0.82	0.561	0.020	0.98	0.2069	0.0036	0.5	2877	48	2870	82	2882	28
JSWI0301_003	5.33	0.26	0.336	0.011	0.99	0.1151	0.0020	0.8	1874	41	1868	54	1881	31
JSWI0301_004	4.40	0.21	0.304	0.010	0.99	0.1051	0.0018	0.3	1712	39	1710	48	1715	31
JSWI0301_005	4.41	0.21	0.306	0.010	0.99	0.1045	0.0018	-0.9	1713	39	1720	47	1706	31
JSWI0301_006	4.55	0.22	0.304	0.010	0.99	0.1086	0.0018	4.1	1741	40	1712	48	1776	31
JSWI0301_007	4.25	0.21	0.297	0.010	0.99	0.1038	0.0018	1.2	1683	39	1675	48	1694	31
JSWI0301_008	11.62	0.58	0.449	0.015	0.99	0.1879	0.0032	14.7	2575	45	2389	68	2724	28
JSWI0301_009	4.46	0.23	0.281	0.010	0.98	0.1154	0.0020	17.4	1724	42	1594	51	1885	31
JSWI0301_009b	5.00	0.41	0.331	0.027	0.99	0.1096	0.0009	-3.3	1820	68	1844	128	1792	16
JSWI0301_010	3.07	0.15	0.245	0.008	0.99	0.0908	0.0016	2.3	1425	37	1413	41	1443	32
culled														
JSWI0301_024	3.72	0.35	0.242	0.022	0.99	0.1114	0.0013	25.9	1575	72	1397	112	1822	21
JSWI0301_015	15.42	10.84	0.065	0.045	0.99	1.7225	0.1406	95.8	2841	515	405	266	5991	107
JSWI0301_012	no data	no data	no data	no data	no data	0.8097	0.0083	no data	no data	no data	no data	no data	4939	15
C3_030	1.48	0.09	0.149	0.008	0.98	0.0719	0.0008	9.8	921	34	895	44	984	23
C3_007	1.78	0.10	0.178	0.010	0.98	0.0723	0.0008	-7.1	1037	38	1058	53	993	23
C3_033	1.57	0.09	0.157	0.008	0.98	0.0725	0.0008	6.6	957	35	938	46	1000	23
C3_006	1.84	0.12	0.173	0.010	0.98	0.0769	0.0010	8.4	1060	41	1031	55	1118	26
C3_027	2.18	0.13	0.196	0.011	0.98	0.0809	0.0010	5.9	1176	41	1153	58	1219	23

C3_029	2.45	0.15	0.216	0.012	0.97	0.0824	0.0011	-0.3	1258	42	1259	61	1256	27
C3_004	2.55	0.27	0.214	0.021	0.98	0.0864	0.0018	7.9	1287	74	1251	113	1347	39
C3_032	2.82	0.16	0.231	0.012	0.98	0.0887	0.0010	4.7	1362	42	1339	63	1398	21
C3_037	3.11	0.22	0.251	0.017	0.98	0.0896	0.0012	-2.2	1434	54	1445	87	1417	26
C3_018	3.18	0.25	0.255	0.019	0.98	0.0905	0.0013	-2.2	1453	60	1464	97	1436	27
C3_028	2.98	0.21	0.237	0.016	0.99	0.0912	0.0011	6.1	1402	53	1370	84	1450	24
C3_024	3.96	0.24	0.290	0.016	0.98	0.0990	0.0011	-2.6	1625	48	1641	81	1605	21
C3_023	4.15	0.37	0.297	0.026	0.99	0.1014	0.0013	-1.8	1664	71	1676	126	1650	23
C3_036	4.34	0.35	0.305	0.023	0.98	0.1032	0.0015	-2.3	1701	64	1715	112	1682	27
C3_010	3.94	0.35	0.274	0.023	0.99	0.1044	0.0016	9.4	1622	70	1561	117	1703	28
C3_026	4.26	0.25	0.296	0.016	0.98	0.1044	0.0012	2.2	1686	47	1672	79	1704	21
C3_005	4.89	0.31	0.309	0.018	0.98	0.1147	0.0015	8.4	1801	52	1737	88	1875	23
culled														
C3_031	1.69	0.11	0.162	0.010	0.97	0.0754	0.0012	10.9	1004	41	969	54	1079	32
C3_002	1.48	0.13	0.147	0.012	0.99	0.0730	0.0009	13.5	922	50	885	67	1013	26
C3_009	2.84	0.19	0.216	0.013	0.97	0.0957	0.0015	20.2	1367	49	1259	69	1542	29
C3_034	1.58	0.11	0.149	0.010	0.98	0.0765	0.0009	20.3	960	42	898	54	1107	24
C3_025	2.31	0.17	0.189	0.013	0.99	0.0885	0.0011	21.6	1214	50	1116	69	1392	24
C3_013	3.14	0.30	0.226	0.021	0.99	0.1009	0.0013	22.2	1443	71	1312	109	1641	24
C3_001	1.76	0.20	0.159	0.018	0.99	0.0802	0.0012	22.3	1032	71	953	98	1203	29
C3_015	1.57	0.13	0.141	0.011	0.99	0.0811	0.0011	32.7	960	48	848	60	1224	27
C3_019	2.11	0.19	0.166	0.014	0.98	0.0919	0.0015	34.9	1150	60	991	78	1465	30
C3_012	1.35	0.17	0.119	0.015	0.99	0.0825	0.0014	44.9	868	71	723	83	1257	33
C3_017	0.21	0.05	0.018	0.004	1.00	0.0825	0.0010	91.6	191	40	116	27	1258	24
C3_022	no data	no data	no data	no data	no data	-0.1677	-0.2914	no data	no data	no data	no data	no data	-450	no data
C3_021	no data	no data	no data	no data	no data	-0.7634	-0.3851	no data	no data	no data	no data	no data	99	no data
C3_011	no data	no data	no data	no data	no data	1.2553	0.3255	no data	no data	no data	no data	no data	5555	318
C3_035	2.58	0.17	0.266	0.016	0.97	0.0703	0.0011	-70.2	1295	46	1521	79	937	31
C3_008	4.78	0.34	0.358	0.024	0.98	0.0968	0.0015	-30.5	1781	58	1972	111	1562	29
C3_016	4.34	0.27	0.320	0.018	0.98	0.0985	0.0013	-13.8	1702	50	1789	88	1596	25
C3_020	2.94	0.31	0.251	0.026	0.99	0.0847	0.0014	-11.7	1391	77	1446	131	1309	32
C3_014	1.89	0.11	0.189	0.010	0.98	0.0728	0.0009	-11.4	1079	39	1114	56	1008	24
C3_003	7.18	0.45	0.413	0.024	0.98	0.1262	0.0014	-10.5	2135	54	2228	109	2046	20

TT4_035	4.97	0.26	0.328	0.013	0.96	0.1097	0.0020	-2.3	1814	43	1831	62	1795	32
TT4_002	5.23	0.22	0.338	0.009	0.99	0.1123	0.0018	-2.4	1858	35	1876	44	1837	28
TT4_045	5.05	0.26	0.324	0.013	0.96	0.1131	0.0019	2.5	1828	43	1809	63	1849	31
TT1_020	4.87	0.21	0.312	0.009	0.98	0.1132	0.0018	6.3	1797	36	1750	45	1851	29
TT4_010	5.14	0.22	0.329	0.010	0.98	0.1133	0.0018	1.1	1843	36	1835	47	1853	28
TT4_038	5.04	0.26	0.322	0.013	0.96	0.1136	0.0020	3.7	1826	43	1798	62	1858	31
TT4_004	5.38	0.23	0.343	0.009	0.99	0.1136	0.0018	-2.8	1881	35	1902	45	1858	28
TT4_028	5.13	0.23	0.327	0.010	0.98	0.1136	0.0018	2.1	1841	37	1825	47	1858	29
TT4_044	5.37	0.27	0.343	0.013	0.97	0.1137	0.0018	-2.5	1880	42	1899	63	1859	29
TT1_011	5.30	0.22	0.337	0.009	0.99	0.1139	0.0018	-0.7	1869	35	1875	44	1863	28
TT4_007	5.51	0.24	0.348	0.010	0.98	0.1149	0.0018	-2.9	1903	36	1925	47	1878	29
TT4_021	5.13	0.22	0.323	0.010	0.98	0.1152	0.0018	4.8	1841	36	1804	46	1883	28
TT4_005	5.36	0.23	0.337	0.010	0.98	0.1154	0.0018	0.9	1878	36	1871	46	1886	28
TT1_013	5.42	0.23	0.340	0.009	0.99	0.1158	0.0018	0.5	1889	36	1885	45	1893	28
TT4_036	5.68	0.32	0.351	0.015	0.96	0.1172	0.0023	-1.5	1928	48	1940	73	1915	34
TT4_034	5.21	0.25	0.322	0.011	0.97	0.1174	0.0020	7.0	1855	40	1800	54	1917	31
TT4_047	5.51	0.25	0.340	0.011	0.98	0.1176	0.0019	2.1	1901	38	1885	51	1919	28
TT4_041	5.40	0.31	0.332	0.015	0.96	0.1178	0.0022	4.5	1885	48	1849	71	1924	34
TT4_049	5.78	0.30	0.354	0.014	0.97	0.1184	0.0019	-1.3	1944	44	1954	68	1933	28
TT4_008	6.05	0.25	0.364	0.010	0.99	0.1205	0.0019	-2.2	1983	36	2001	46	1964	27
TT4_022	5.75	0.24	0.344	0.009	0.99	0.1214	0.0019	4.2	1939	36	1905	45	1977	28
TT4_048	6.21	0.34	0.356	0.015	0.97	0.1263	0.0021	4.7	2005	46	1965	73	2047	29
TT1_012	7.76	0.33	0.400	0.011	0.98	0.1409	0.0022	3.8	2204	37	2167	52	2239	27
TT4_033	9.75	0.66	0.460	0.027	0.97	0.1537	0.0029	-2.7	2412	61	2441	117	2387	32
TT4_050	11.52	0.60	0.498	0.020	0.97	0.1676	0.0028	-3.5	2566	48	2607	87	2534	28
TT4_042	12.22	0.60	0.498	0.018	0.97	0.1779	0.0029	1.3	2621	45	2605	79	2634	27
TT4_009	13.51	0.57	0.537	0.015	0.99	0.1825	0.0028	-4.3	2716	39	2770	61	2676	25
TT4_031	13.21	0.65	0.515	0.019	0.97	0.1862	0.0031	1.5	2695	46	2676	80	2709	27
TT4_043	15.43	0.72	0.566	0.019	0.97	0.1976	0.0031	-3.8	2842	44	2893	79	2806	26
TT4_024	16.76	0.72	0.542	0.016	0.98	0.2243	0.0034	9.0	2921	41	2791	67	3012	24
TT4_027	21.88	0.95	0.600	0.018	0.98	0.2642	0.0041	9.2	3178	41	3032	72	3272	24

culled														
TT1_018	3.67	0.16	0.262	0.008	0.98	0.1017	0.0016	10.6	1565	34	1498	39	1655	29
TT4_037	4.53	0.30	0.293	0.016	0.96	0.1121	0.0023	11.0	1737	54	1657	81	1834	37
TT4_040	5.04	0.24	0.309	0.011	0.97	0.1181	0.0020	11.2	1826	40	1738	54	1927	29
TT4_003	4.61	0.30	0.290	0.016	0.97	0.1155	0.0019	14.9	1751	53	1639	80	1887	29
TT1_015	5.10	0.22	0.298	0.008	0.99	0.1239	0.0019	18.6	1836	35	1683	41	2013	27
TT4_029	15.58	0.68	0.477	0.014	0.98	0.2369	0.0036	22.8	2851	41	2513	63	3099	24
TT4_046	13.98	0.69	0.454	0.017	0.97	0.2232	0.0035	23.5	2749	45	2415	75	3004	25
TT1_017	4.08	0.19	0.254	0.009	0.97	0.1164	0.0018	26.0	1650	38	1459	46	1902	28
TT4_032	8.12	0.44	0.331	0.014	0.97	0.1779	0.0028	34.4	2245	48	1844	69	2633	26
TT4_001	5.18	0.22	0.269	0.008	0.98	0.1398	0.0022	34.8	1850	36	1535	39	2224	27
TT4_030	3.18	0.14	0.198	0.006	0.98	0.1164	0.0018	42.2	1453	32	1167	30	1901	27
TT4_025	3.02	0.13	0.185	0.005	0.98	0.1183	0.0018	46.9	1413	32	1096	29	1931	27
TT1_016	2.09	0.10	0.149	0.005	0.97	0.1018	0.0016	49.3	1145	31	893	28	1658	28
TT1_014	1.26	0.06	0.094	0.003	0.98	0.0976	0.0015	66.2	830	25	579	18	1580	29
TT4_039	no data	no data	no data	no data	no data	0.1850	0.0035	no data	no data	no data	no data	no data	2698	31
TT4_026	no data	no data	no data	no data	no data	0.9142	0.0156	no data	no data	no data	no data	no data	5111	24
TT4_023	no data	no data	no data	no data	no data	0.9016	0.0149	no data	no data	no data	no data	no data	5091	23
TT1_019	no data	no data	no data	no data	no data	0.0756	0.1107	no data	no data	no data	no data	no data	1083	1626
TT4_006	no data	no data	no data	no data	no data	0.1324	0.0040	no data	no data	no data	no data	no data	2130	52

APPENDIX C

SHRIMP AND LAICPMS CONCORDIA DIAGRAMS

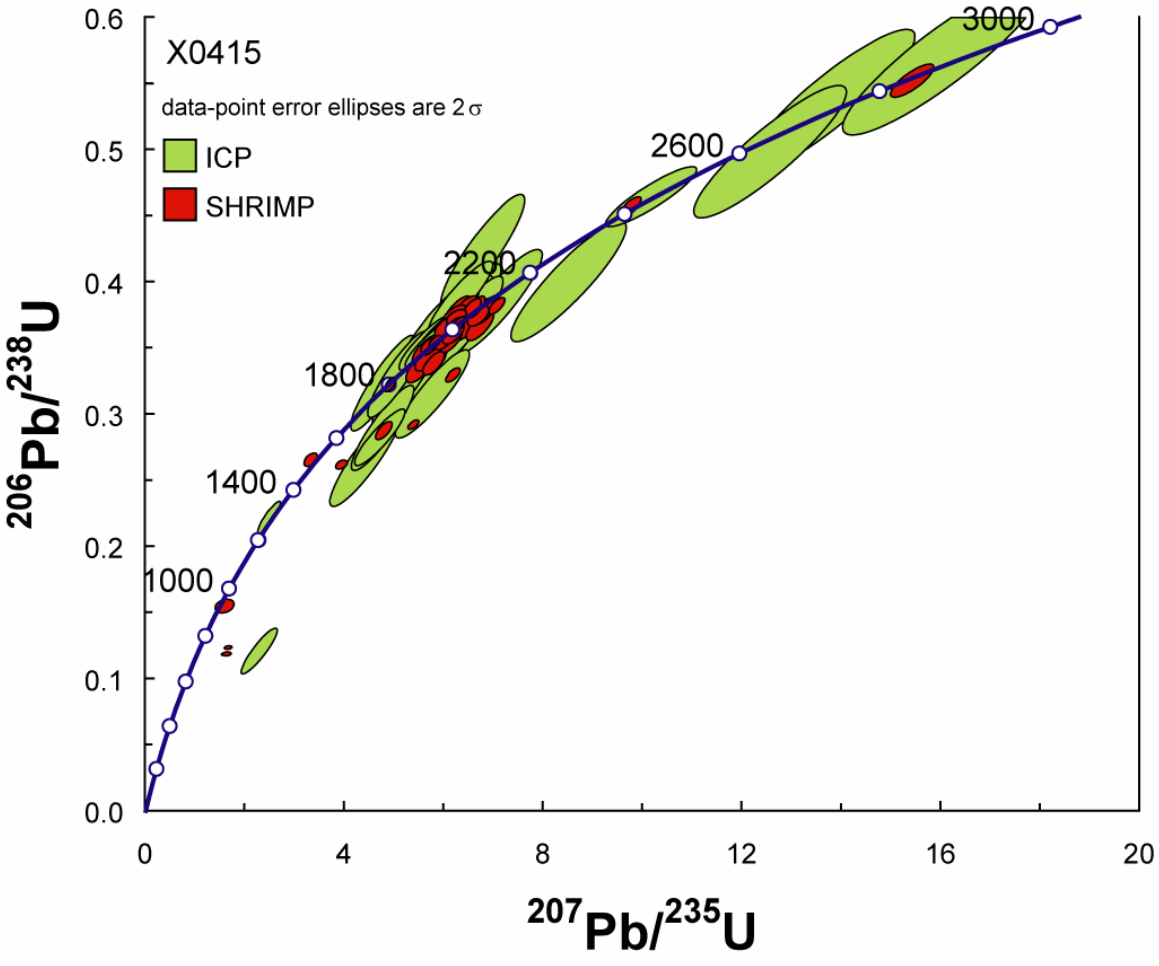

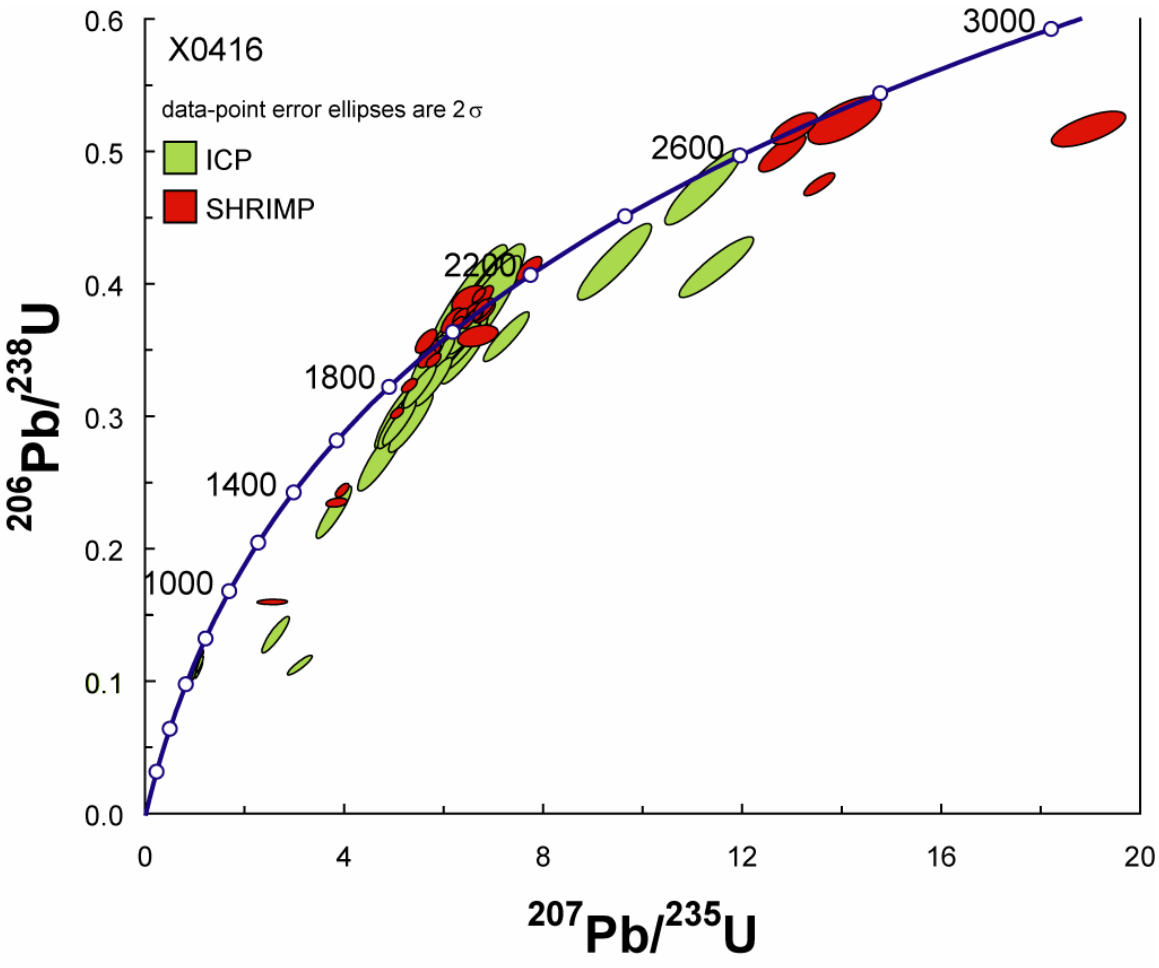
X0416
data-point error ellipses are 2σ
ICP
SHRIMP
3000
2600
2200
1800
1400
1000
0.6
0.5
0.4
0.3
0.2
0.1
0.0
0
4
8
12
16
20
206Pb/238U
207Pb/235U

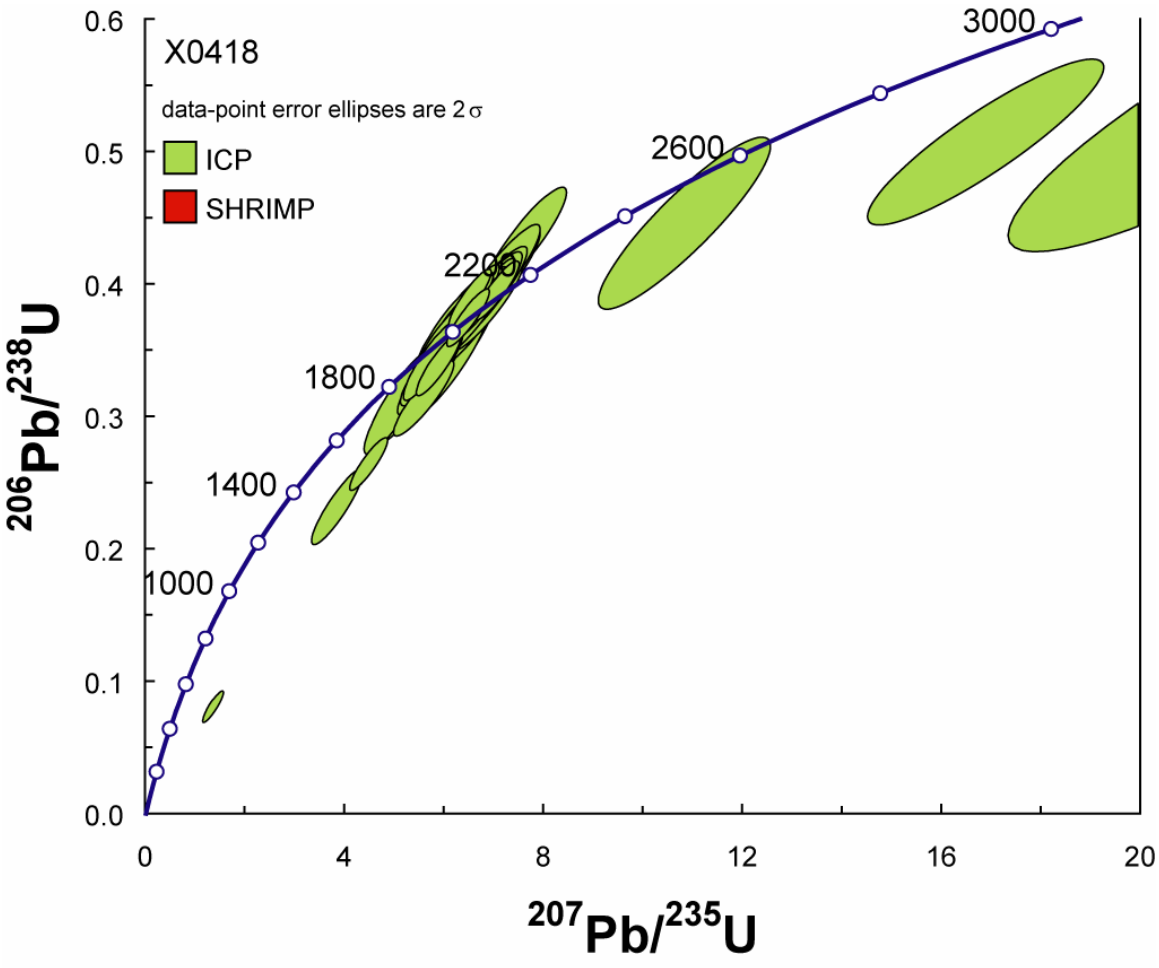
X0418
data-point error ellipses are 2σ
ICP
SHRIMP
3000
2600
2200
1800
1400
1000
0.6
0.5
0.4
0.3
0.2
0.1
0.0
0
4
8
12
16
20
206Pb/238U
207Pb/235U

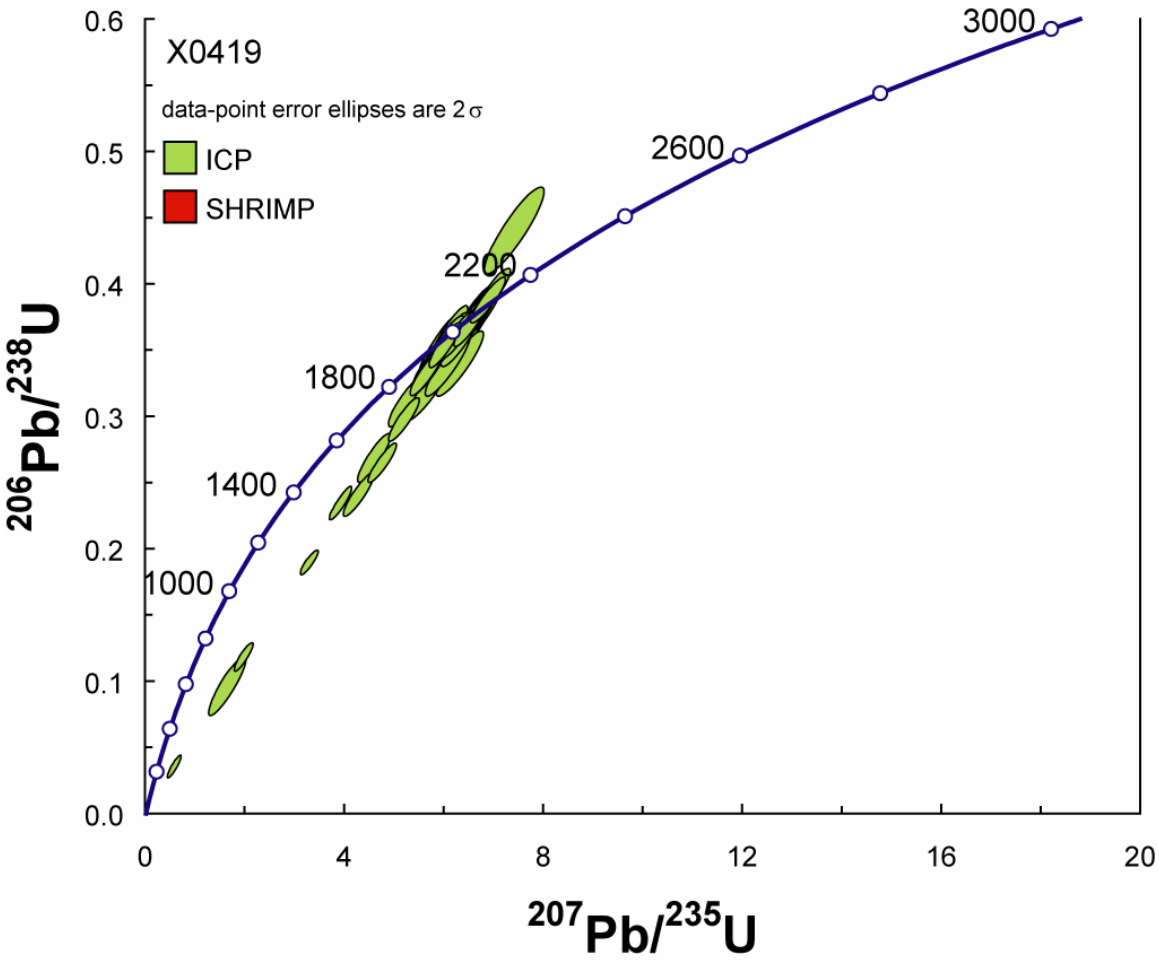
X0419
data-point error ellipses are 2σ
ICP
SHRIMP
3000
2600
2200
1800
1400
1000
0.6
0.5
0.4
0.3
0.2
0.1
0.0
0
4
8
12
16
20
206Pb/238U
207Pb/235U

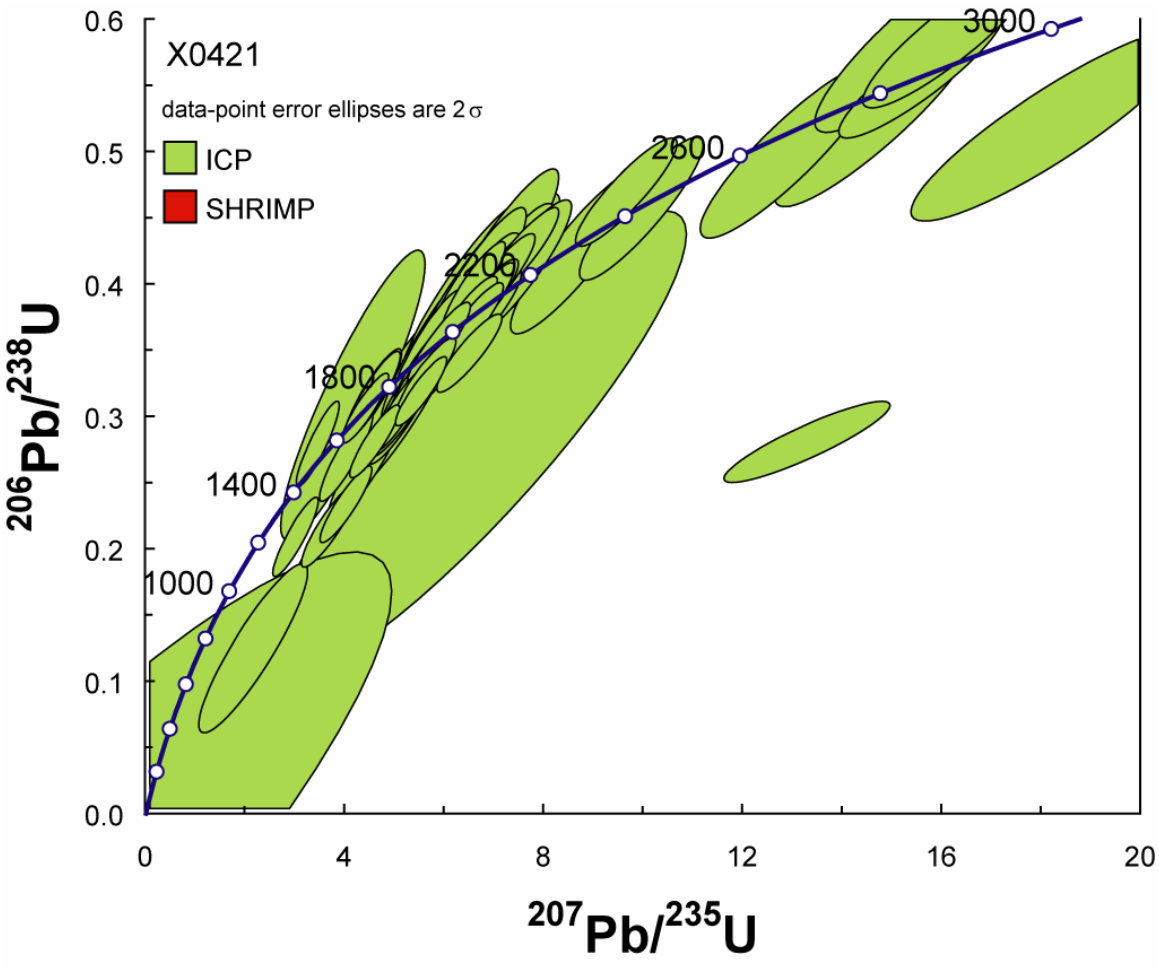
X0421
data-point error ellipses are 2σ
ICP
SHRIMP
1000
1400
1800
2200
2600
3000
0.0
0.1
0.2
0.3
0.4
0.5
0.6
0
4
8
12
16
20
206Pb/238U
207Pb/235U

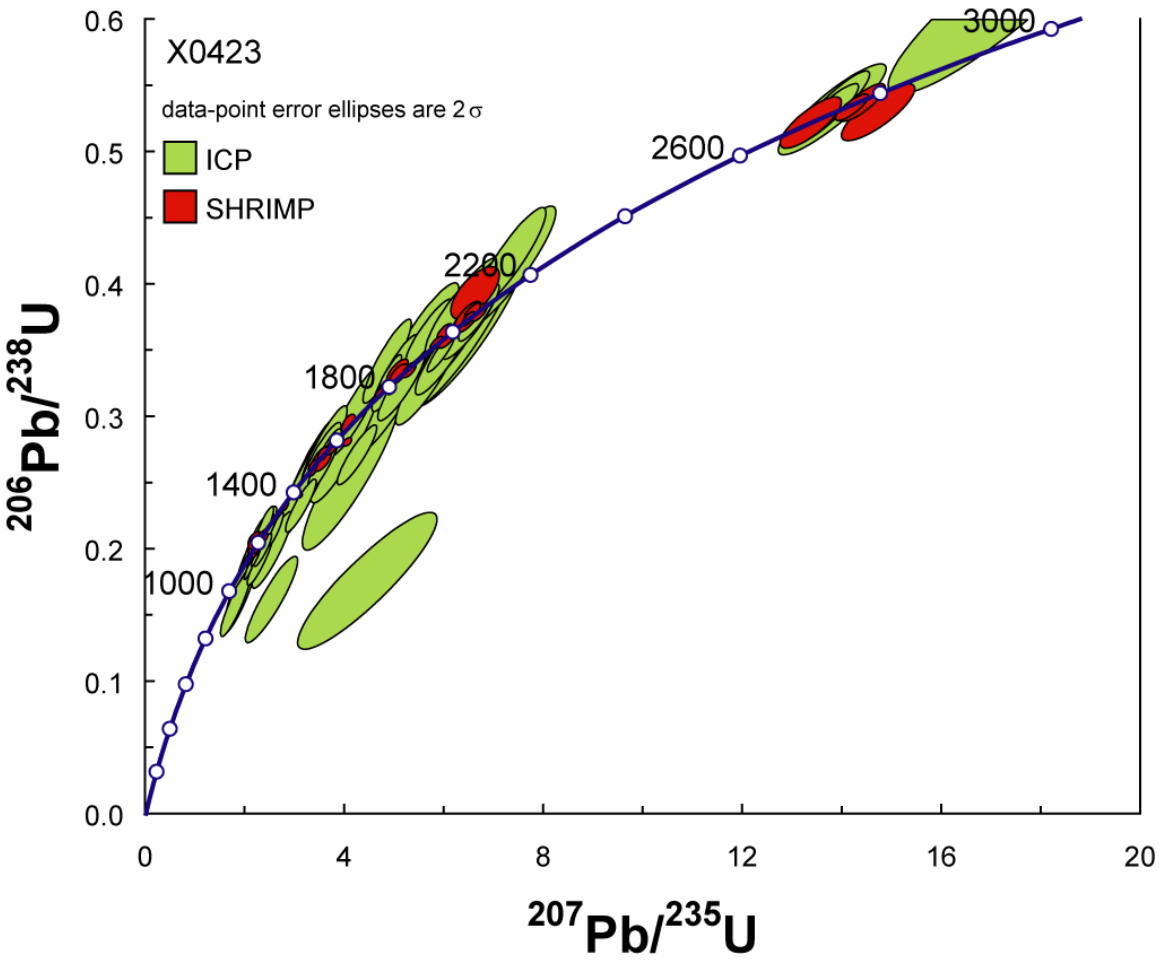
X0423
data-point error ellipses are 2σ
ICP
SHRIMP
1000
1400
1800
2200
2600
3000
0.0
0.1
0.2
0.3
0.4
0.5
0.6
0
4
8
12
16
20
206Pb/238U
207Pb/235U

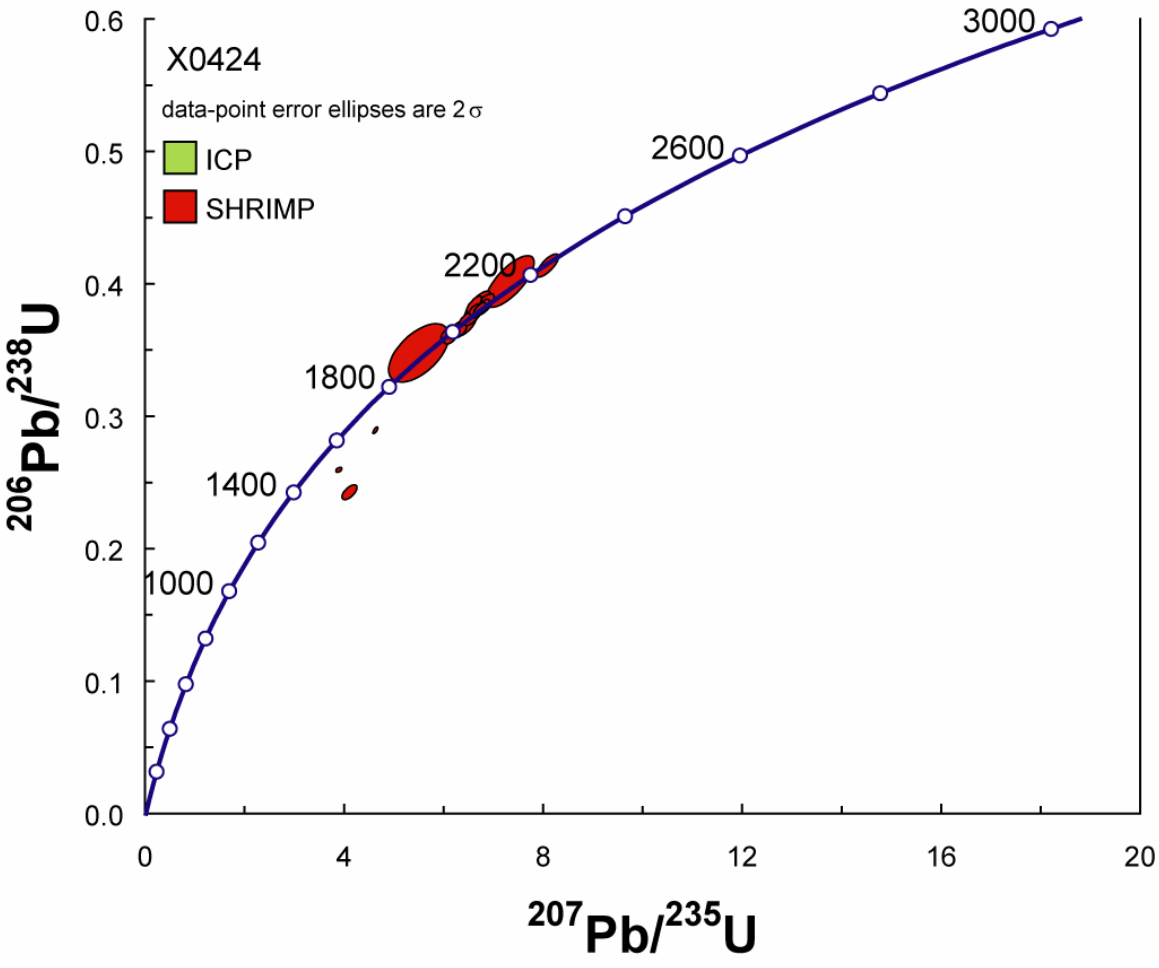
X0424
data-point error ellipses are 2σ
ICP
SHRIMP
3000
2600
2200
1800
1400
1000
0.6
0.5
0.4
0.3
0.2
0.1
0.0
0
4
8
12
16
20
206Pb/238U
207Pb/235U

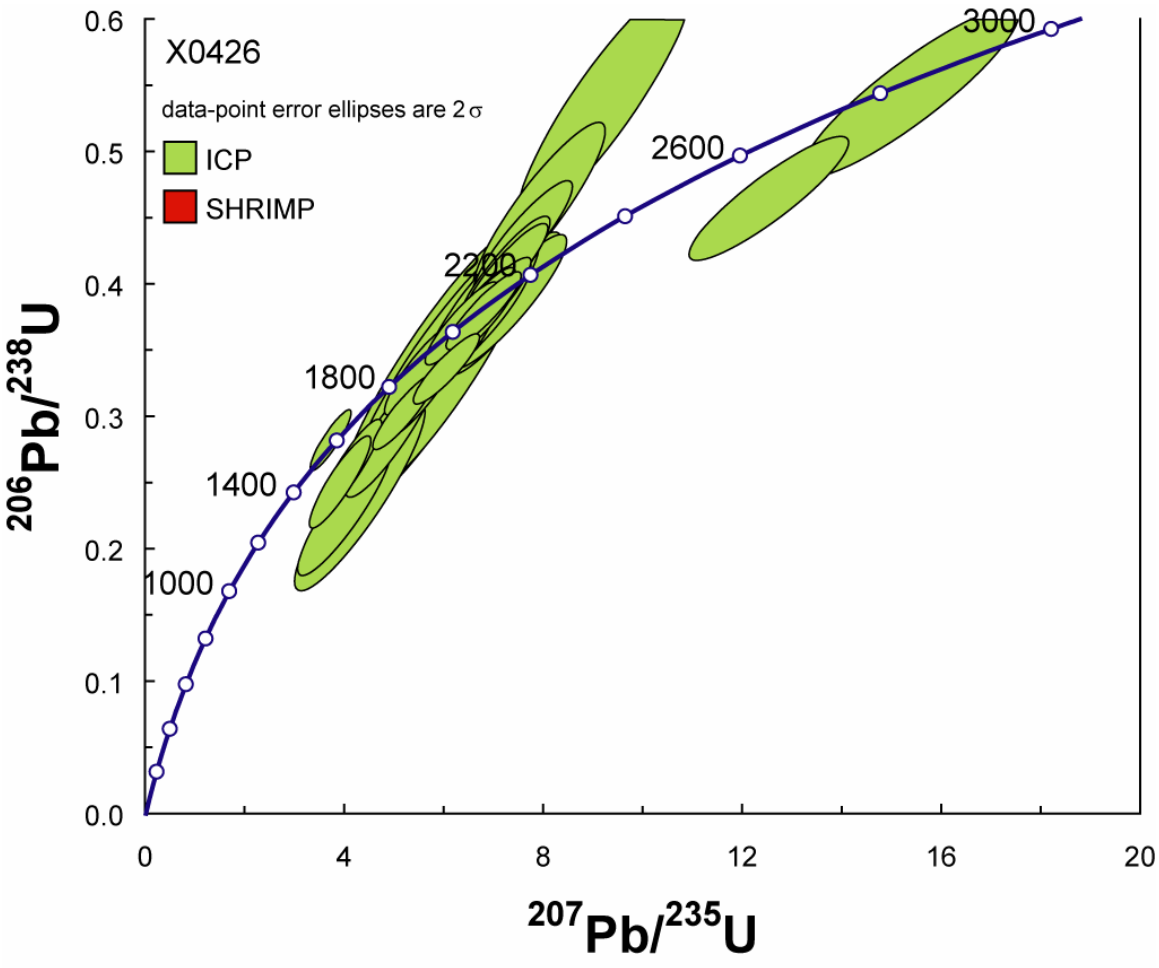
X0426
data-point error ellipses are 2σ
ICP
SHRIMP
1000
1400
1800
2200
2600
3000
0.0
0.1
0.2
0.3
0.4
0.5
0.6
0
4
8
12
16
20
206Pb/238U
207Pb/235U

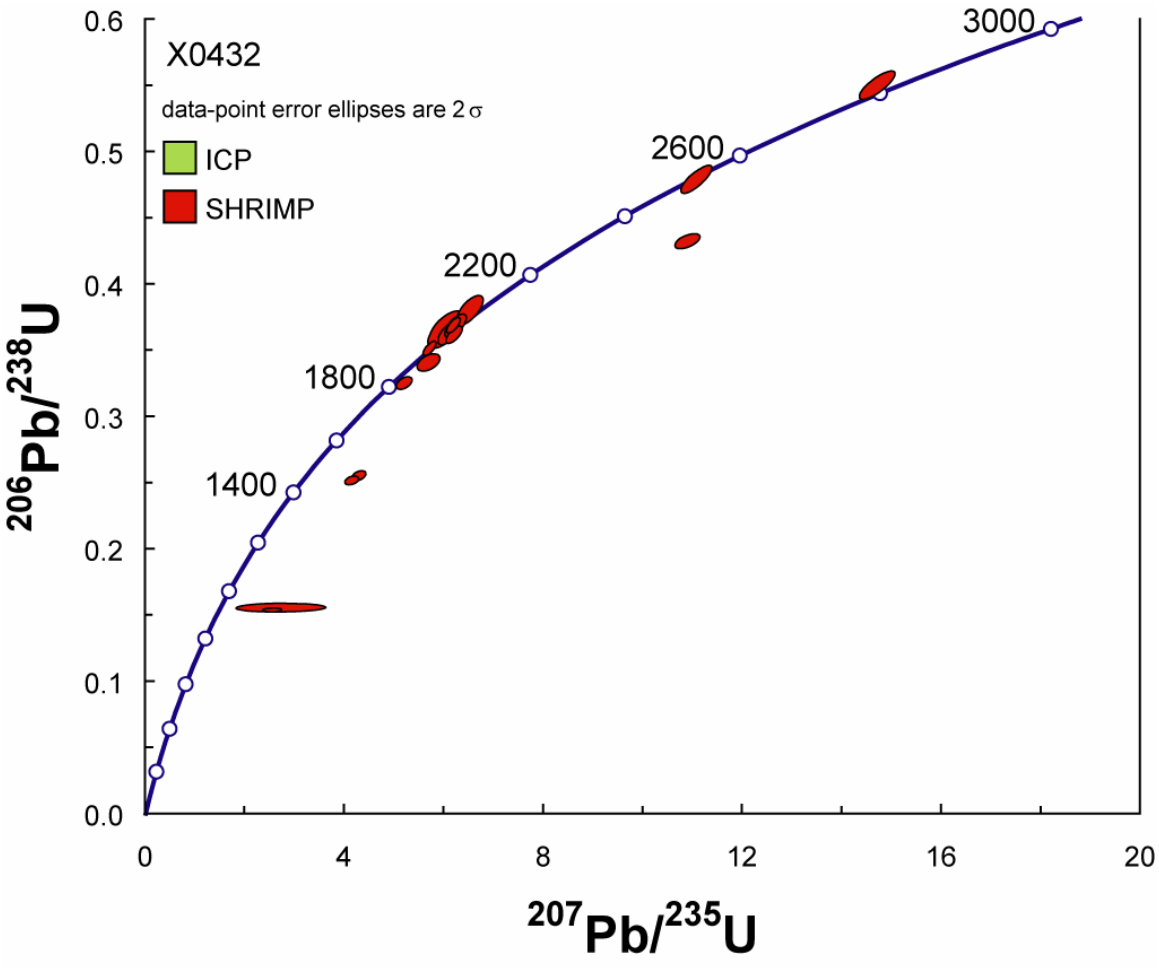
X0432
data-point error ellipses are 2 σ
ICP
SHRIMP
3000
2600
2200
1800
1400
0.6
0.5
0.4
0.3
0.2
0.1
0.0
0
4
8
12
16
20
206Pb/238U
207Pb/235U

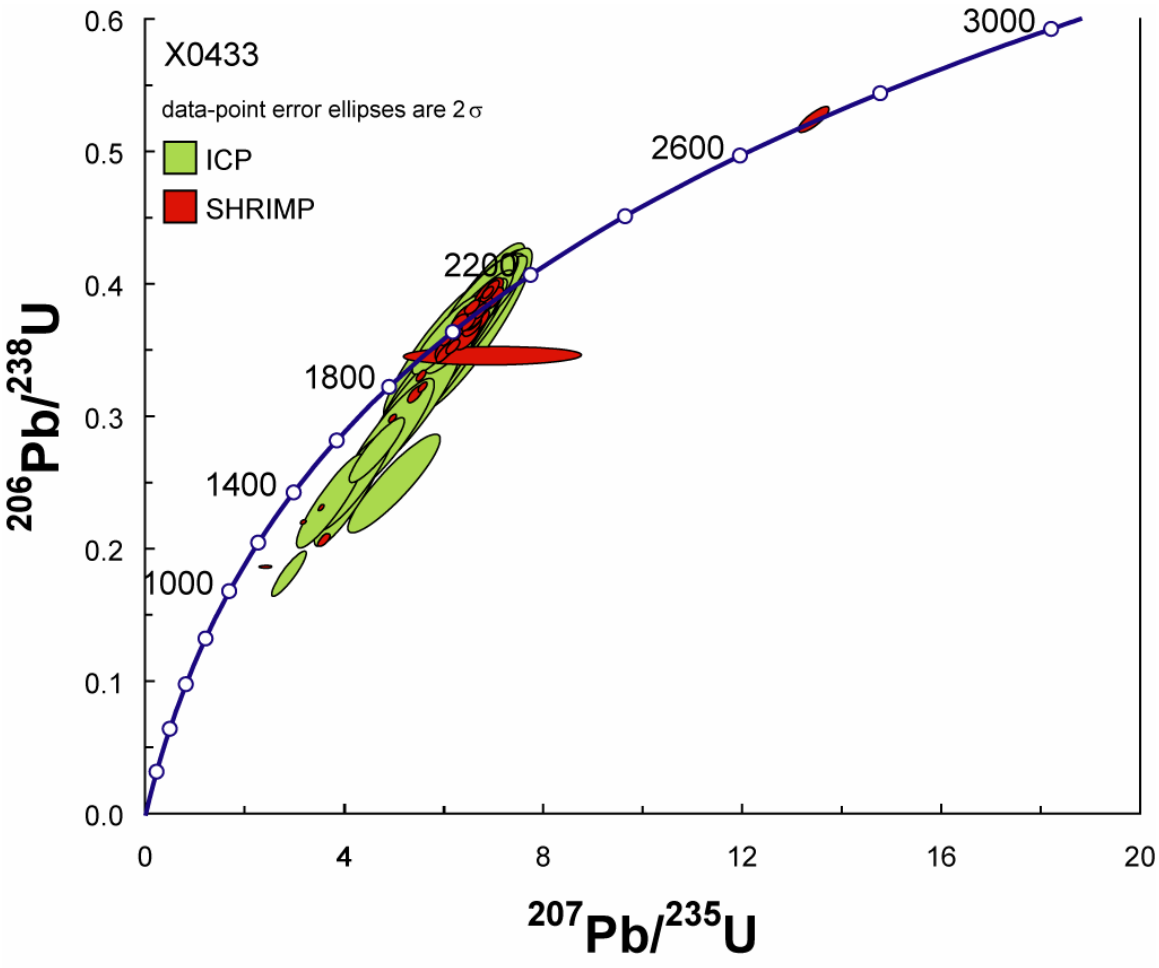
X0433
data-point error ellipses are 2σ
ICP
SHRIMP
3000
2600
2200
1800
1400
1000
0.6
0.5
0.4
0.3
0.2
0.1
0.0
0
4
8
12
16
20
206Pb/238U
207Pb/235U

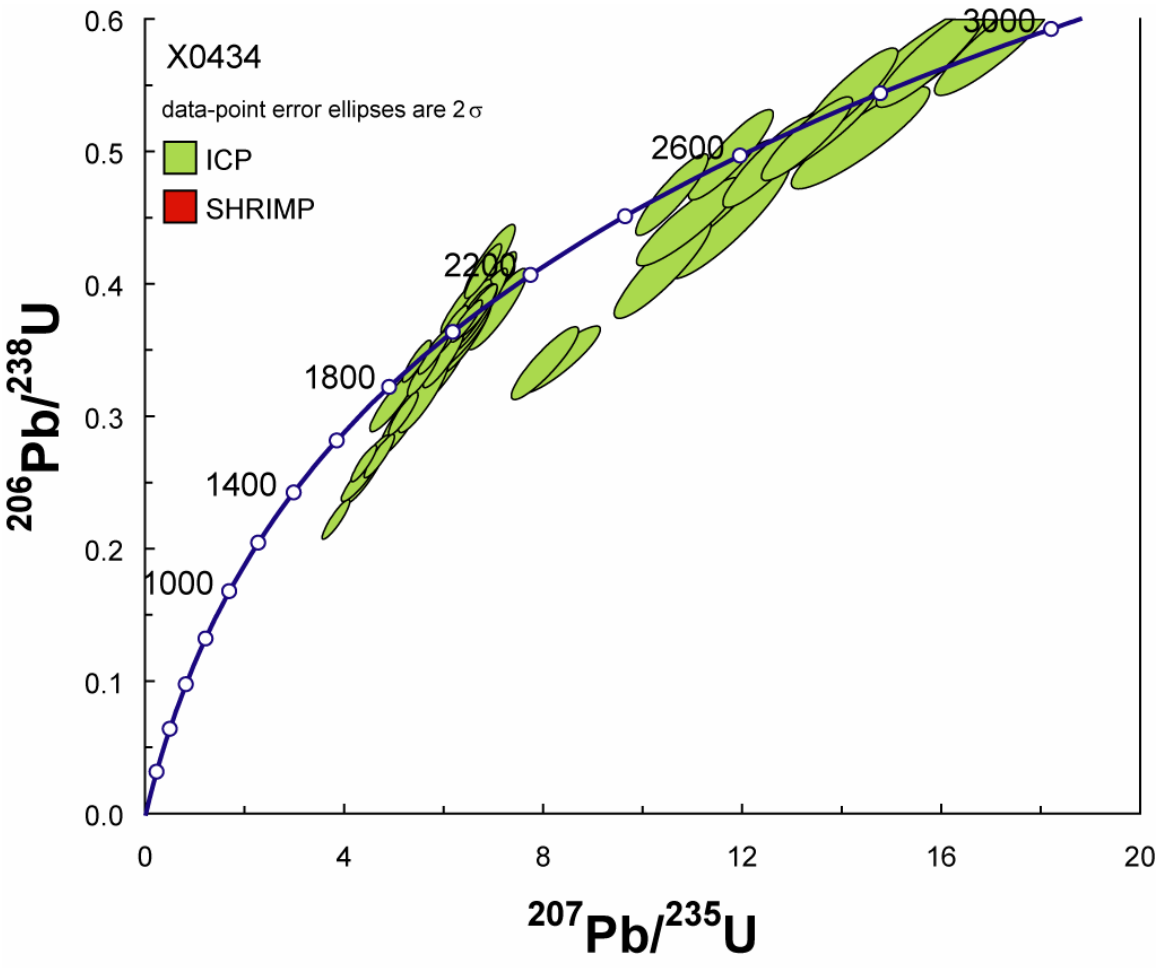
X0434
data-point error ellipses are 2σ
ICP
SHRIMP
1000
1400
1800
2200
2600
3000
0.0
0.1
0.2
0.3
0.4
0.5
0.6
0
4
8
12
16
20
206Pb/238U
207Pb/235U

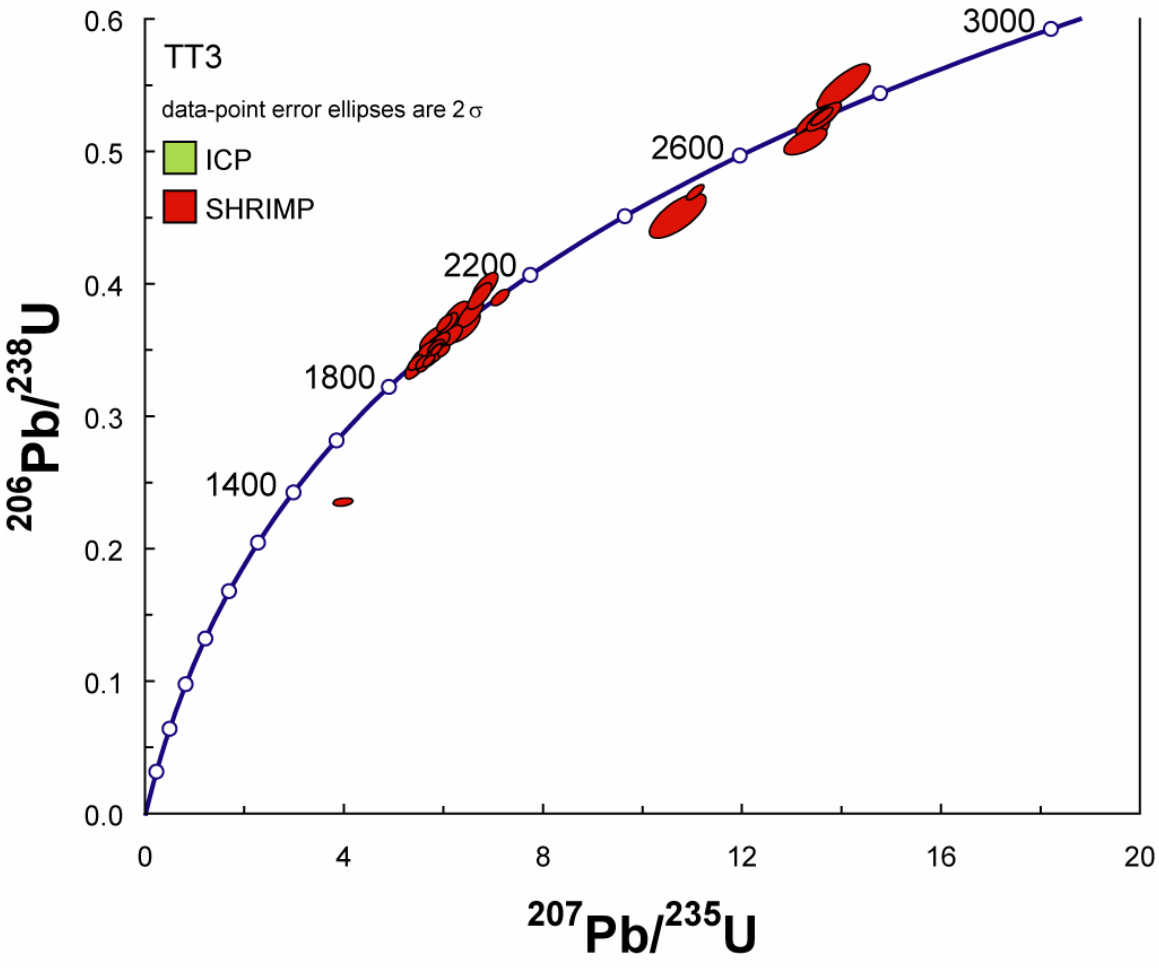
TT3
data-point error ellipses are 2 σ
ICP
SHRIMP
3000
2600
2200
1800
1400
0.6
0.5
0.4
0.3
0.2
0.1
0.0
0
4
8
12
16
20
206Pb/238U
207Pb/235U

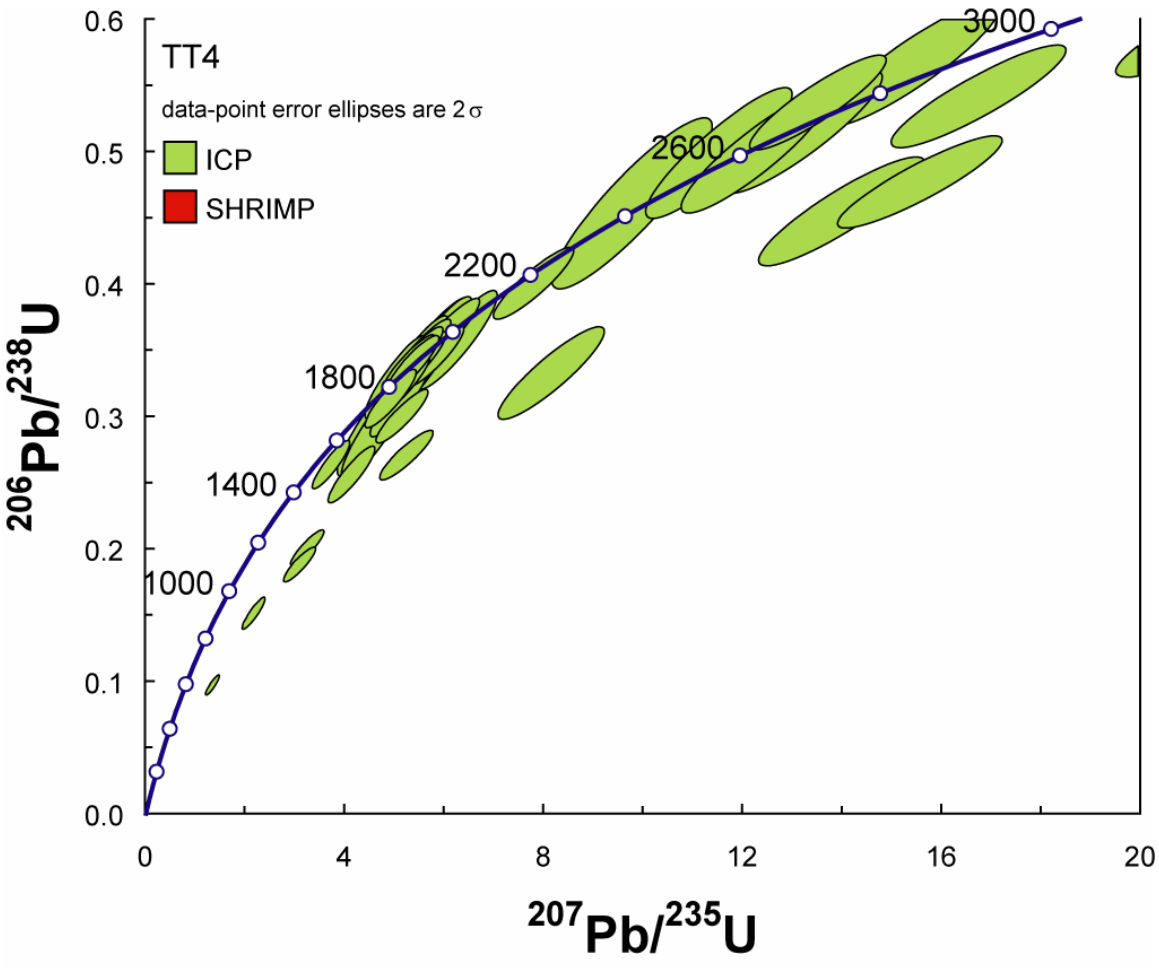
TT4
data-point error ellipses are 2σ
ICP
SHRIMP
1000
1400
1800
2200
2600
3000
0.0
0.1
0.2
0.3
0.4
0.5
0.6
0
4
8
12
16
20
206Pb/238U
207Pb/235U

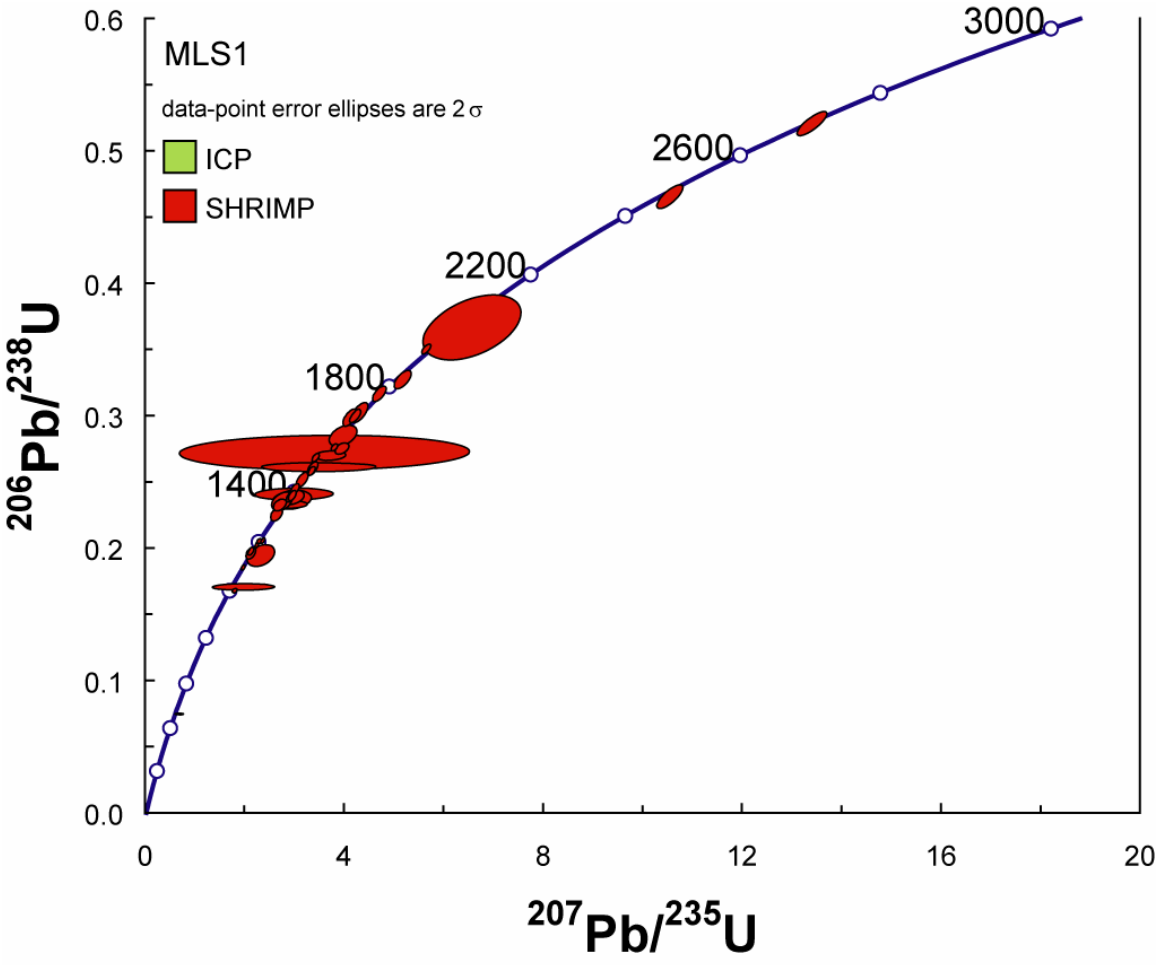
MLS1
data-point error ellipses are 2 σ
ICP
SHRIMP
3000
2600
2200
1800
1400
0.6
0.5
0.4
0.3
0.2
0.1
0.0
0
4
8
12
16
20
206Pb/238U
207Pb/235U

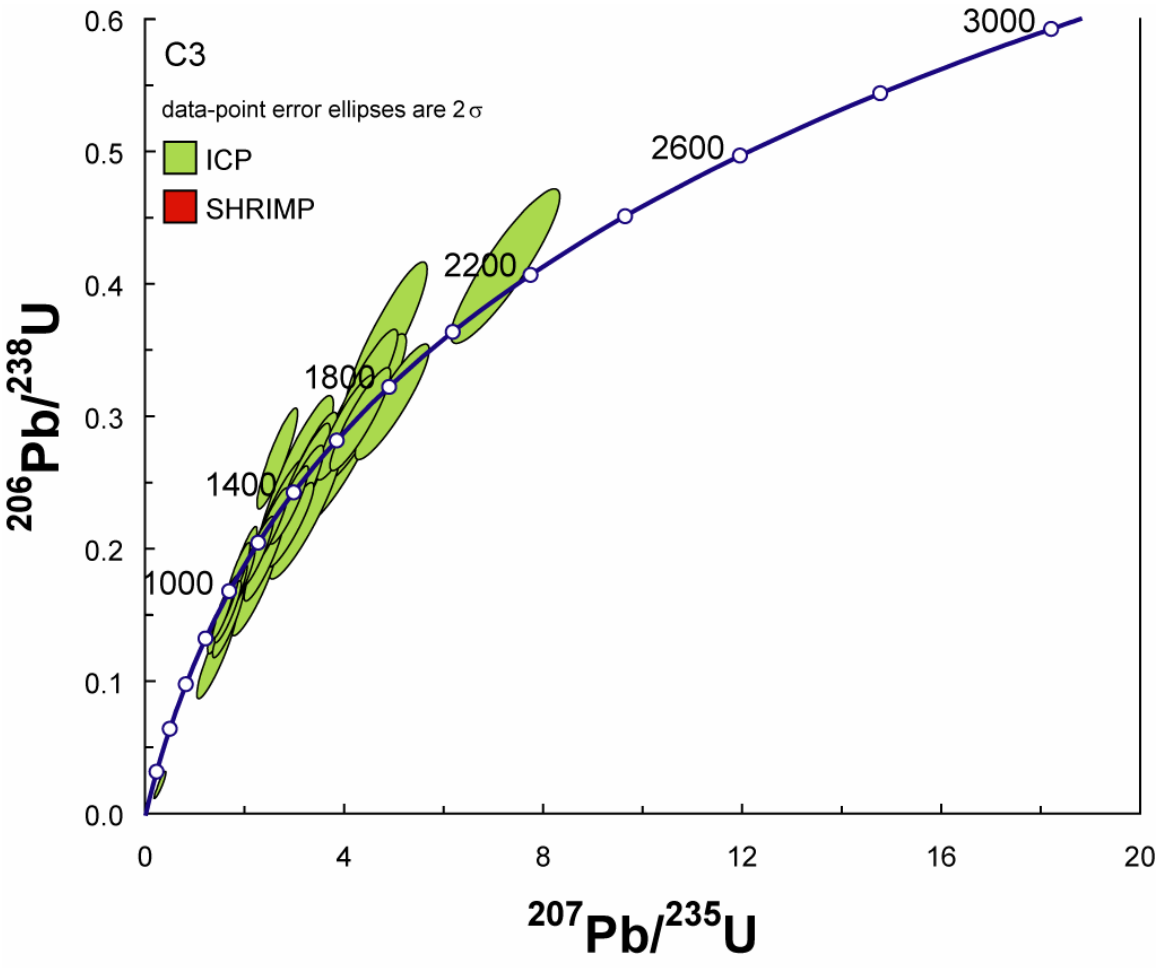
C3
data-point error ellipses are 2σ
ICP
SHRIMP
1000
1400
1800
2200
2600
3000
0.0
0.1
0.2
0.3
0.4
0.5
0.6
0
4
8
12
16
20
206Pb/238U
207Pb/235U

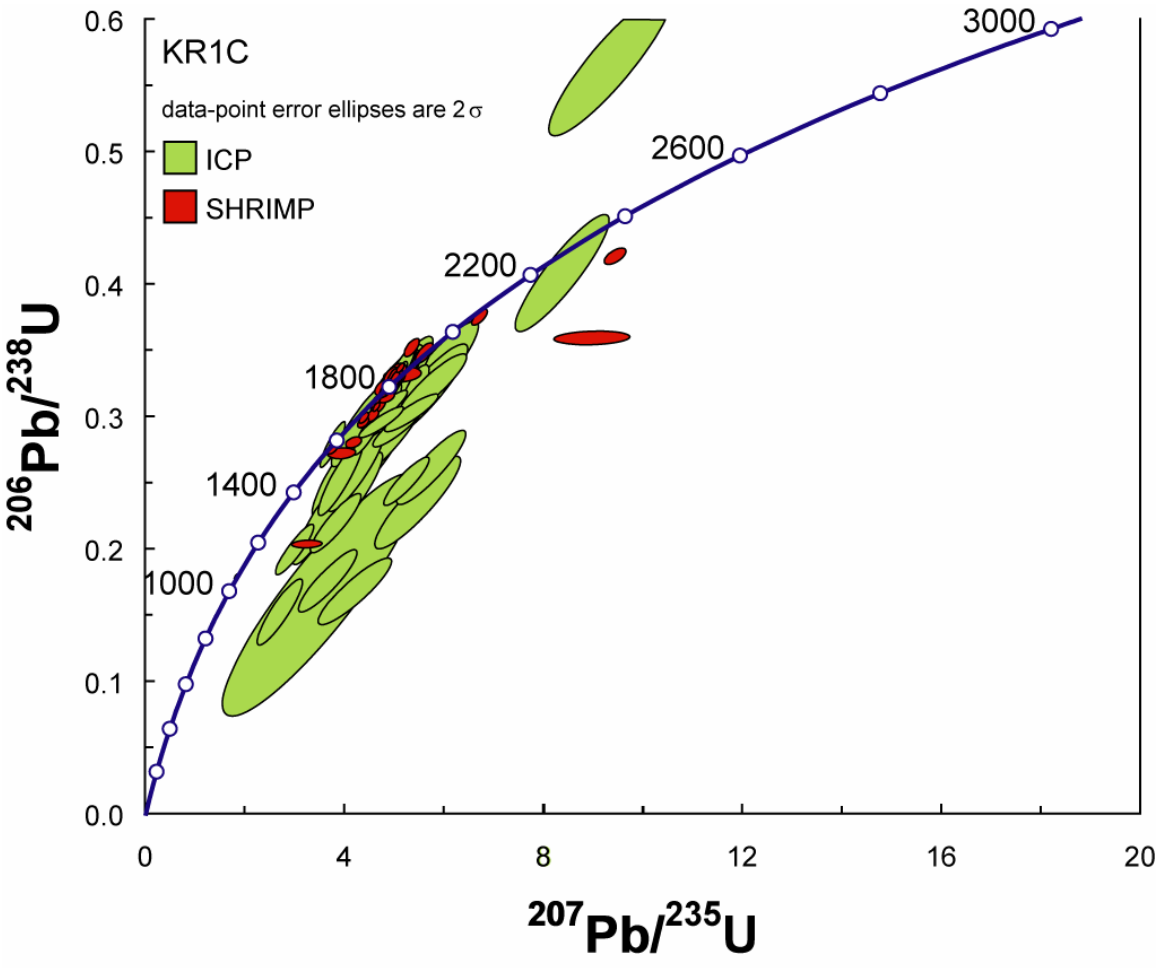
KR1C
data-point error ellipses are 2σ
ICP
SHRIMP
3000
2600
2200
1800
1400
1000
0.6
0.5
0.4
0.3
0.2
0.1
0.0
0
4
8
12
16
20
206Pb/238U
207Pb/235U

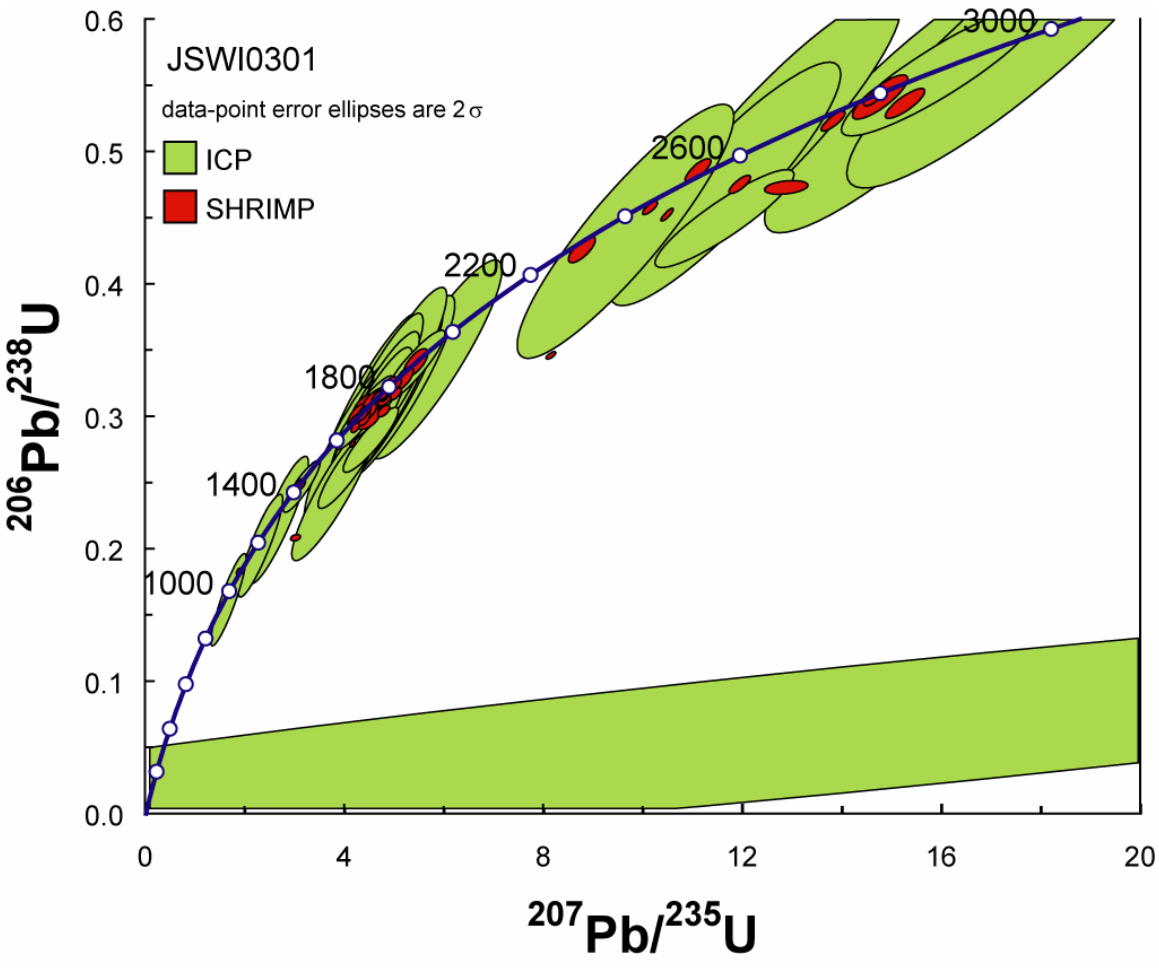
JSWI0301
data-point error ellipses are 2σ
ICP
SHRIMP
1000
1400
1800
2200
2600
3000
0.0
0.1
0.2
0.3
0.4
0.5
0.6
0
4
8
12
16
20
206Pb/238U
207Pb/235U

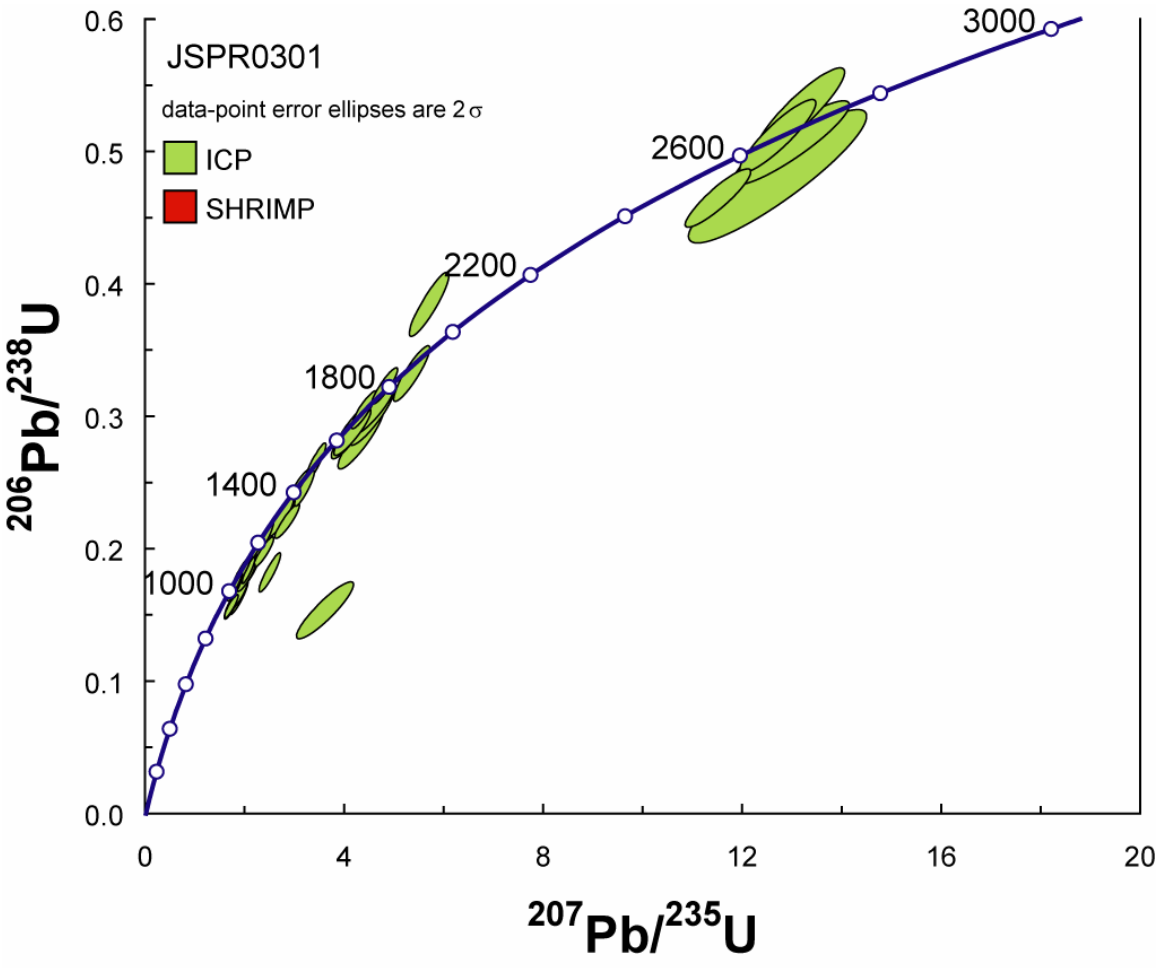
JSPR0301
data-point error ellipses are 2σ
ICP
SHRIMP
3000
2600
2200
1800
1400
1000
0.6
0.5
0.4
0.3
0.2
0.1
0.0
0
4
8
12
16
20
206Pb/238U
207Pb/235U

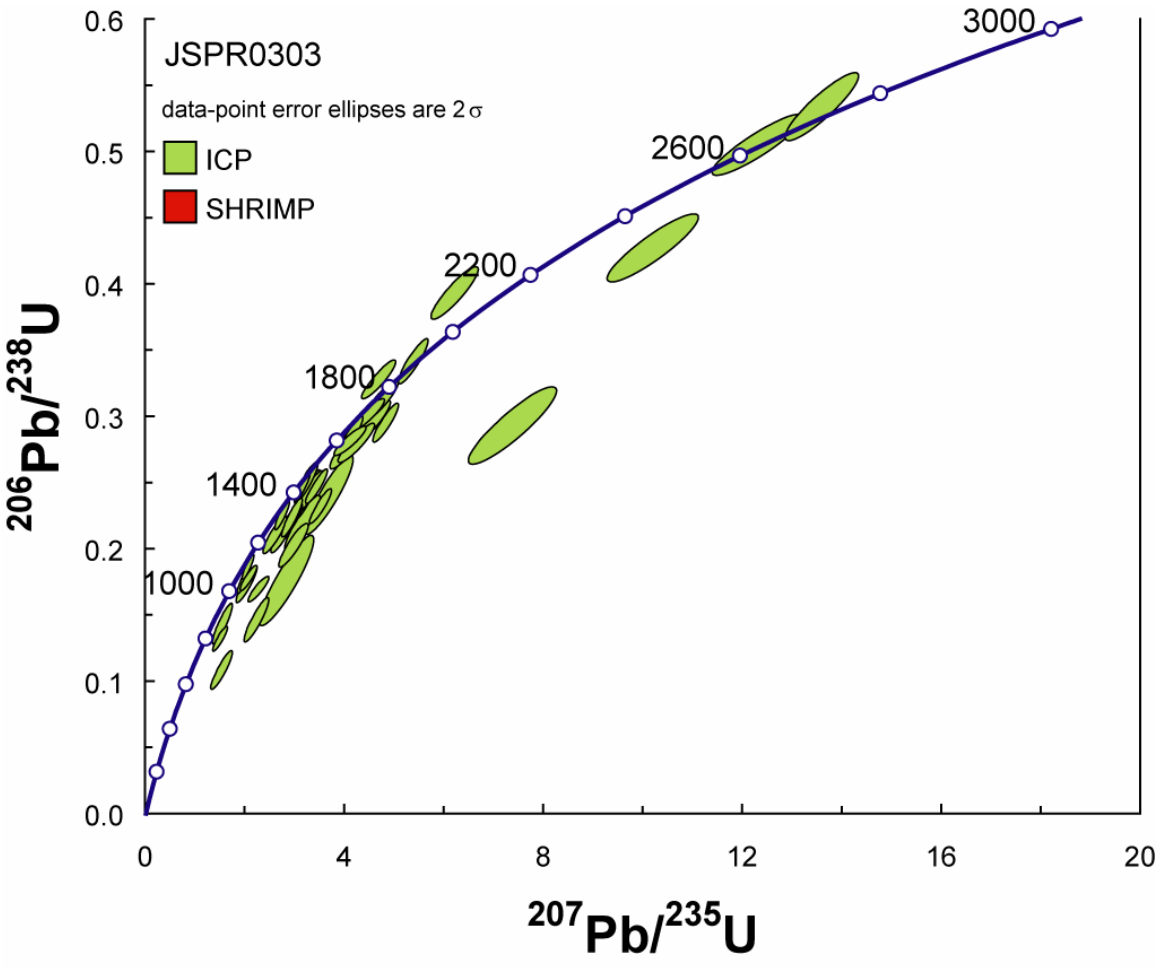
JSPR0303
data-point error ellipses are 2σ
ICP
SHRIMP
1000
1400
1800
2200
2600
3000
0.0
0.1
0.2
0.3
0.4
0.5
0.6
0
4
8
12
16
20
206Pb/238U
207Pb/235U

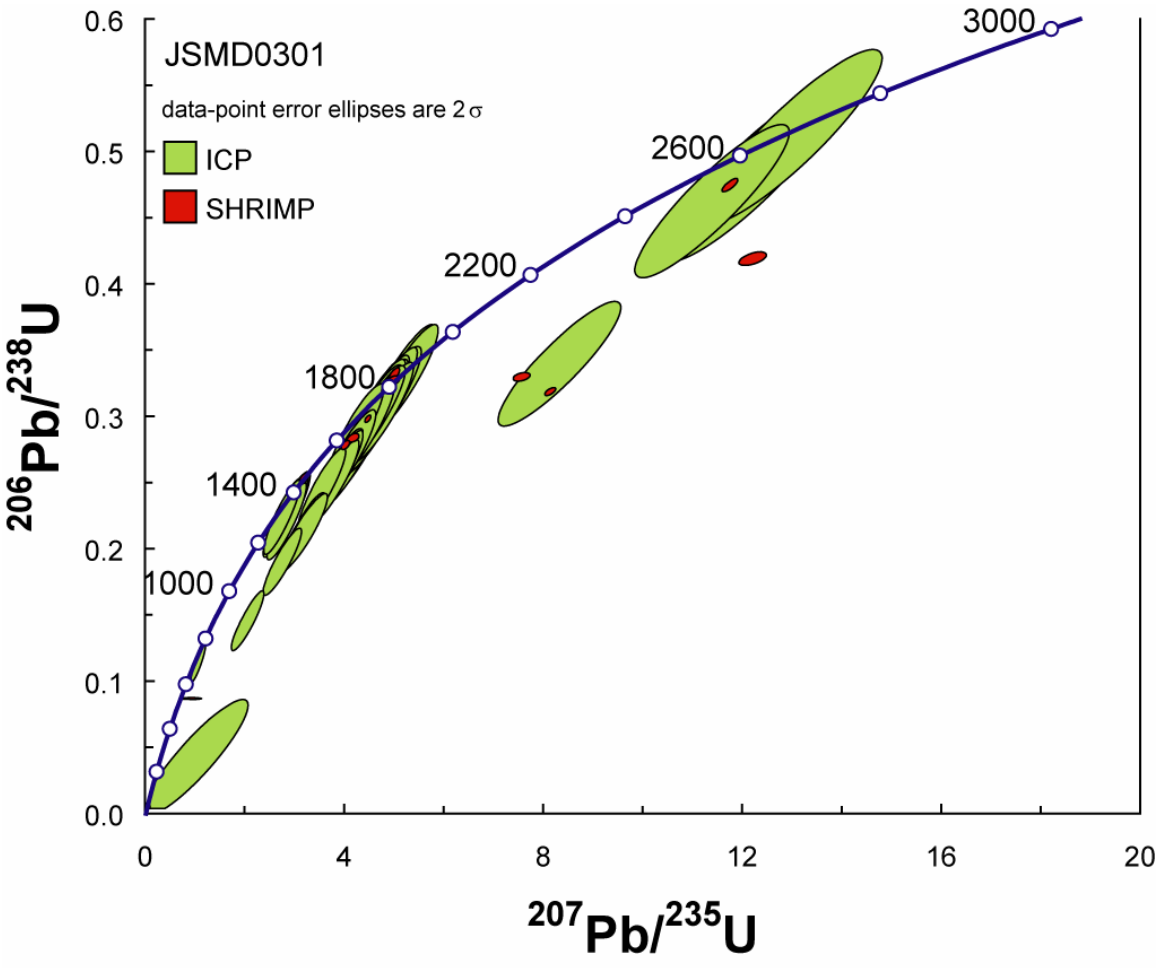
JSMD0301
data-point error ellipses are 2σ
ICP
SHRIMP
3000
2600
2200
1800
1400
1000
0.6
0.5
0.4
0.3
0.2
0.1
0.0
0
4
8
12
16
20
206Pb/238U
207Pb/235U

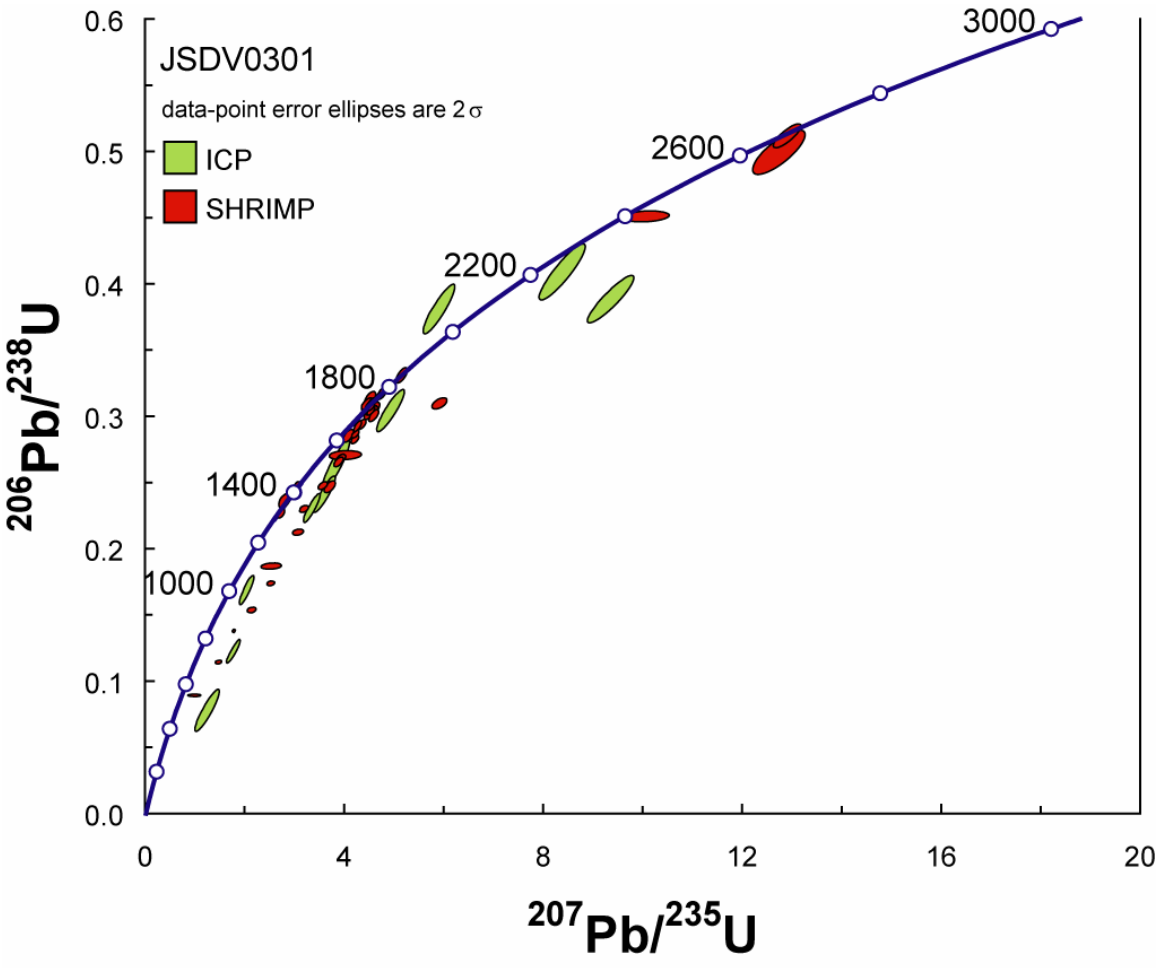
JSDV0301
data-point error ellipses are 2σ
ICP
SHRIMP
3000
2600
2200
1800
1400
1000
0.6
0.5
0.4
0.3
0.2
0.1
0.0
0
4
8
12
16
20
206Pb/238U
207Pb/235U